6.7. Post-EECO Changes at Possagno

Several small CIEs appear in the $\delta^{13}C$ record at Possagno during polarity chrons C22n, C21r and C21n. Some of these post-EECO excursions coincide with planktic foraminiferal assemblage changes similar to those recorded in lower strata. Specifically, there are marked

increases in *Acarinina* (Fig. 6). These "post-EECO" CIEs are concomitant with $\delta^{18}O$ excursions and coupled to distinct modifications in the planktic foraminiferal assemblages comparable to those recorded across known hyperthermals in Tethyan settings (Luciani et al., 2007; Agnini et al., 2009; D'Onofrio et al., 2014). Additional hyperthermals, although of less intensity and magnitude, may extend through the entirety of the early and middle Eocene, as suggested previously (Sexton et al., 2006, 2011; Kirtland-Turner et al., 2014). Whether these imply different forcing and feedback mechanisms compared to the PETM remains an open question.

7 Summary and Conclusions

The symbiont-bearing planktic foraminiferal genera *Morozovella* and *Acarinina* were among the most important calcifiers of the early Paleogene tropical and subtropical oceans. However, a remarkable and permanent switch in the relative abundance of these genera happened in the early Eocene, an evolutionary change accompanied by species reduction in *Morozovella* and species diversification of *Acarinina*. We show here that this switch probably coincided with a carbon isotope excursion presently coined J. Although the Early Eocene Climatic Optimum (EECO), a multi-million-year interval of extreme Earth surface warmth, lacks an accepted definition, we propose that the EECO is best defined as the duration of time between the J event and the base of *D. sublodoensis* (about 53 to 49 Ma on the 2012 GTS).

Our conclusion that the planktic foraminiferal switch coincides with the start of the EECO derives from the generation of new records and collation of old records concerning bulk sediment stable isotopes and planktic foraminiferal abundances at three sections. These sections span a wide longitude range of the low-latitude Paleogene world: the Possagno section from the western Tethys, DSDP Site 577 from the central Pacific Ocean and ODP Site 1051 from the western Atlantic Ocean. Importantly, these locations have robust calcareous nannofossils and polarity chron age markers, although the stratigraphy required amendment at Sites 577 and 1051.

An overarching problem is that global carbon cycling was probably very dynamic during the EECO. The interval appears to have been characterized not only by numerous CIEs but also by a major switch in the timing and magnitude of these perturbations. Furthermore, there was a rapid shoaling of carbonate dissolution horizons in the middle of the EECO. A key finding of our study is that the major switch in planktic foraminiferal assemblages happened at the start of the EECO. Significant, though ephemeral, modifications in planktic foraminiferal assemblages coincide with numerous short-term CIEs, before, during and after the EECO. Often, there are marked increases in the relative abundance of *Acarinina*, similar to what happened permanently across the start of the EECO.

Although we show for the first time that the critical turnover in planktic foraminifera clearly coincided with the start of the EECO, the exact cause for the switch (a.k.a. the decline in *Morozovella*) remains elusive. Possible causes are manifold and may include temperature effects on photosymbiont-bearing planktic foraminifera, changes in ocean chemistry or even interaction with other microplankton groups such as radiolarians, diatoms or dinoflagellates that represented possible competitors in the use of symbionts or as symbiont providers. For some reason, a critical threshold was surpassed at the start the EECO, and this induced an unfavourable habitat for continued *Morozovella* diversification and proliferation but a favourable habitat for the genus *Acarinina*.

Appendix A: Taxonomic list of planktic foraminiferal species cited in text and figures

Globanomalina australiformis (Jenkins, 1965)

Morozovella aequa (Cushman and Renz, 1942)

Morozovella gracilis (Bolli, 1957)

Morozovella lensiformis (Subbotina, 1953),

Morozovella marginodentata (Subbotina, 1953)

Morozovella subbotinae (Morozova, 1939)

Parasubbotina eoclava Coxall, Huber and Pearson, 2003

Parasubbotina griffinae (Blow, 1979)

Parasubbotina pseudowilsoni Olsson and Pearson, 2006

Subbotina corpulenta (Subbotina, 1953)

Subbotina eocaena (Gümbel, 1868)

Subbotina hagni (Gohrbandt, 1967)

Subbotina senni (Beckmann, 1953)

Subbotina yeguanesis (Weinzierl and Applin, 1929)

Planoglobanomalina pseudoalgeriana Olsson and Hemleben, 2006

Appendix B: Taxonomic list of calcareous nannofossil taxa cited in text and figures

Discoaster diastypus Bramlette and Sullivan, 1961

Discoaster lodoensis Bramlette and Sullivan, 1961

Discoaster sublodoensis Bramlette and Sullivan, 1961

Fasciculithus Bramlette and Sullivan, 1961

Fasciculithus tympaniformis Hay and Mohler in Hay et al., 1967

Sphenolithus radians Deflandre in Grassé, 1952

Toweius Hay and Mohler, 1967

Tribrachiatus contortus (Stradner, 1958); Bukry, 1972

Tribrachiatus orthostylus (Bramlette and Riedel, 1954);

References

Abels, H. A., W. C. Clyde, P. D. Gingerich, F. J. Hilgen, H. C. Fricke, G. J. Bowen, and L. J. Lourens (2012), Terrestrial carbon isotope excursions and biotic change during Palaeogene hyperthermals, Nat. Geosci., 5(5), 326–329, doi:10.1038/ngeo1427.

Agnini, C., G. Muttoni, D. V. Kent, and D. Rio (2006), Eocene biostratigraphy and magnetic stratigraphy from Possagno, Italy: the calcareous nannofossils response to climate variability, Earth Planet. Sc. Lett., 241, 815–830.

Agnini, C., P. Macrì, J. Backman, H. Brinkhuis, E. Fornaciari, L. Giusberti, V. Luciani, D. Rio, A. Sluijs, and F. Speranza (2009), An early Eocene carbon cycle perturbation at ~52.5 Ma in the Southern Alps: chronology and biotic response, Paleoceanography, 24, PA2209, doi:10.1029/2008PA001649.

Agnini, C., E. Fornaciari, I. Raffi, R. Catanzariti, H. Pälike, J. Backman, and D. Rio (2014), Biozonation and biochronology of Paleogene calcareous nannofossils from low to middle latitudes, Newsl. Strat., 47, 131–181.

Agnini, C., D. J. A. Spofforth, G. R. Dickens, D. Rio, H. Pälike, J. Backman, G. Muttoni, and E. Dallanave (2016), Stable isotope and calcareous nannofossil assemblage record of the late Paleocene and early Eocene (Cicogna section), Clim. Past, 12, 883–909, doi:10.5194/cp-12-883-2016.

Anderson, T. F. and S. A. Cole (1975), The stable isotope geochemistry of marine coccoliths: a preliminary comparison with planktonic foraminifera, J. Foramin. Res., 5, 188–192.

Arenillas, I., E. Molina, and B. Schmitz (1999), Planktic foraminiferal and $\delta^{13}C$ isotopic changes across the Paleocene/Eocene boundary at Possagno (Italy), Int. J. Earth Sci., 88, 352–364.

Arthur, M. A., W. E. Dean, D. Bottjer, and P. A. Schole (1984), Rhythmic bedding in Mesozoic-Cenozoic pelagic carbonate sequences: the primary and diagenetic origin of Milankovitch like cycles, in Milankovitch and Climate, edited by Berger, A., J. Imbrie, J. Hays, G. Kucla, and B. Satzman, 191–222, D. Reidel Publ. Company, Dordrecht, Holland.

Aze, T., T. H. G. Ezard, A. Purvis, H. K. Coxall, D. R. M Stewart, B. S. Wade, and P. N. Pearson (2011), A phylogeny of Cenozoic macroperforate planktonic foraminifera from fossil data, Biol. Rev., 86, 900–927, doi:10.1111/j.1469-185X.2011.00178.x.

Backman, J. (1986), Late Paleocene to middle Eocene calcareous nannofossil biochronology from the Shatsky Rise, Walvis Ridge and Italy, Palaeogeogr. Palaeocl., 57, 43–59.

Bé, A.W. H. (1982), Biology of planktonic foraminifera, in Foraminifera: notes for a short course, Broadhead T., Stud. Geol., 6, Univ. Knoxville, Tenn., 51–92.

Bé, A. W. H., W. M. John, and M. H. Stanley (1975), Progressive dissolution and ultrastructural breakdown of planktic foraminifera, Cushman Foundation for Foraminiferal Research Special Publication, 13, 27–55.

Bé, A.W. H., H. J. Spero, and O. R. Anderson (1982), Effects of symbiont elimination and reinfection on the life processes of the planktonic foraminifer *Globigerinoides sacculifer*, Mar. Biol., 70, 73–86.

Bemis, B. E., H. J. Spero, J. Bijma, and D. W. Lea (1998), Reevaluation of the oxygen isotopic composition of planktonic foraminifera: Experimental results and revised paleotemperature equations, Paleoceanography, 13, 150–160.

Berger, W. H. (1967), Foraminiferal ooze: Solution at depth, Science, 156, 383–385.

Berger, W. H. (1970), Planktonic foraminifera – selective solution and lysocline, Mar. Geol., 8, 111–138.

Berger, W. H., M.-C. Bonneau, and F. L. Parker (1982), Foraminifera on the deep-sea floor: lysocline and dissolution rate, Oceanol. Acta, 5, 249–258.

Berggren, W. A. and R. D. Norris (1997), Biostratigraphy, phylogeny and systematics of Paleocene trochospiral planktic foraminifera, Micropaleontology, 43 (Suppl. 1), 1–116.

Berggren,W. A. and P. N. Pearson (2005), A revised tropical to subtropical Paleogene planktic foraminiferal zonation, J. Foramin. Res., 35, 279–298.

Berggren, W. A., D. V. Kent, C. C. Swisher III, and M.-P. Aubry (1995), A revised Cenozoic geochronology and chronostratigraphy, in Geochronology, time scales and global stratigraphic correlation, edited by Berggren, W. A, D. V. Kent, M.-P. Aubry, and J. Hardenbol, SEPM Special Publication, 54, 129–212.

Bijl, P. K., S. Schouten, A. Sluijs, G.-J. Reichart, J. C. Zachos, and H. Brinkhuis (2009), Early Paleogene temperature evolution of the southwest Pacific Ocean, Nature, 461, 776–779, doi:10.1038/nature08399.

Bijl, P. K., J. A. Bendle, S. M. Bohaty, J. Pross, S. Schouten, L. Tauxe, C. E. Stickley, R. M. McKay, U. Röhl, M. Olney, A. Sluijs, Escutia C. Dotti, H. Brinkhuis, and Expedition 318 Scientists (2013), Eocene cooling linked to early flow across the Tasmanian Gateway, P. Natl. Acad. Sci. USA, 110, 9645–9650, doi:10.1073/pnas.1220872110.

Bleil, U. (1985), The magnetostratigraphy of northwest Pacific sediments, Deep Sea Drilling Project Leg 86, Initial Rep. Deep Sea, 86, 441–458.

Boersma, A. and I. Premoli Silva (1983), Paleocene planktonic foraminiferal biogeography and the paleoceanography of the Atlantic-Ocean, Micropaleontology, 29, 355–381.

Boersma, A., Premoli I. Silva, and N. Shackleton (1987), Atlantic Eocene planktonic foraminiferal biogeography and stable isotopic paleoceanography, Paleoceanography, 2, 287–331.

Bohaty, S. M., J. C. Zachos, F. Florindo, and M. L. Delaney (2009), Coupled greenhouse warming and deep-sea acidification in the middle Eocene, Paleoceanography, 24, PA2207, doi:10.1029/2008PA001676.

Bolli, H. M. (1975), Monografia micropaleontologica sul Paleocene e sull'Eocene di Possagno, Provincia di Treviso, Italia, Mémoires Suisses de Paléontologie, 97, 222 pp..

Borre, M. and I. L. Fabricus (1998), Chemical and mechanical processes during burial diagenesis of chalk: an interpretation based on specific surface data of deep-sea sediments, Sedimentology, 45, 755–769.

Bosellini, A. (1989), Dynamics of Tethyan carbonate platform, in Controls on Carbonate Platform and Basin Platform, edited by Crevello, P. D., J. L. Wilson, J. F. Sarg, and J. F. Read, SEPM Spec. Publ., 44, 3–13.

Bowen, G. J., T. J. Bralower, M. R. Delaney, G. R. Dickens, D. C. Kelly, P. L. Koch, L. R. Kump, J. Meng, L. C. Sloan, E. Thomas, S. L. Wing, and J. C. Zachos (2006), Eocene Hyperthermal Event Offers Insight Into Greenhouse Warming, EOS, 87, 165–169, doi:10.1029/2006EO170002.

Braga G. (1970), L'assetto tettonico dei dintorni di Possagno (Trevigiano occidentale), Rendiconti dell'Accademia Nazionale dei Lincei, 8/48, 451–455.

Bramlette, M. N. and W. R. Riedel (1954), Stratigraphic value of discoasters and some other microfossils related to recent coccolithophores, J. Paleontol., 28, 385–403.

Broecker, W. S., E. Clark, D. C. McCorkle, T.-H. Peng, I. Hajadas, and G. Bonani (1999), Evidence of a reduction in the carbonate ion content of the deep see during the course of the Holocene, Paleoceanography, 14, 744–752.

Brown, J. H., J. F. Gillooly, A. P. Allen, V. M. Savage, and G. B. West (2004), Toward a metabolic theory of ecology, Ecology, 85, 1771–1789.

Cita, M. B. (1975), Stratigrafia della Sezione di Possagno, in Monografia Micropaleontologica sul Paleocene e l'Eocene di Possagno, edited by Bolli, H. M., Provincia di Treviso, Italia, Schweiz, Palaeontol. Abhandl., 97, 9–33.

Clyde, W. C., P. D. Gingerich, S. L. Wing, U. Röhl, T. Westerhold, G. Bowen, K. Johnson, A. A. Baczynski, A. Diefendorf, F. McInerney, D. Schnurrenberger, A. Noren, K. Brady, and the BBCP Science Team (2013), Bighorn Basin Coring Project (BBCP): a continental perspective on early Paleogene hyperthermals, Sci. Dril., 16, 21–31, doi:10.5194/sd-16-21-2013.

Coccioni, R., G. Bancalà, R. Catanzariti, E. Fornaciari, F.Frontalini, L. Giusberti, L. Jovane, V. Luciani, J. Savian, and M. Sprovieri (2012), An integrated stratigraphic record of the Palaeocene–lower Eocene at Gubbio (Italy): new insights into the early Palaeogene hyperthermals and carbon isotope excursions, Terra Nova, 24, 380–386.

Coxall, H. K., Pearson, P. N. Shackleton, N. J. and Hall M. A. (2000), Hantkeninid depth adaptation: An evolving life strategy in a changing ocean, Geology, 28, 87–90, doi:10.1130/0091-7613(2000)28<87:HDAAEL>2.0.CO;2.

Coxall, H. K., B. T. Huber, and P. N. Pearson (2003), Origin and morphology of the Eocene planktic foraminifera Hantkenina, J. Foramin. Res., 33, 237–261.

Cramer, B. S., J. D. Wright, D. V. Kent, and M.-P. Aubry (2003), Orbital climate forcing of 13C excursions in the late Paleocene–early Eocene (chrons C24n–C25n), Paleoceanography, 18, 1097, doi:10.1029/2003PA000909.

Cramer, B. S., J. R. Toggweiler, M. E. Wright, J. D. Katz, and K. G. Miller (2009), Ocean overturning since the Late Cretaceous: Inferences from a new benthic foraminiferal isotope compilation, Paleoceanography, 24, PA4216, doi:10.1029/2008PA001683.

Crouch, E. M., C. Heilmann-Clausen, H. Brinkhuis, H. E. G. Morgans, K. M. Rogers, H. Egger, and B. Schmitz (2001), Global dinoflagellate event associated with the late Paleocene thermal maximum, Geology, 29, 315–318,.

Dallanave, E., C., Agnini, V. Bachtadse, G. Muttoni, J. S. Crampton, C. P. Strong, B. H. Hines, C. J. Hollis, and B. S. Slotnick (2015), Early to middle Eocene magneto-biochronology of the southwest Pacific Ocean and climate influence on sedimentation: Insights from the Mead Stream section, New Zealand, Geol. Soc. Am. Bull., 127, 643–660.

DeConto, R. M., S. Galeotti, M. Pagani, D. Tracy, K. Schaefer, T. Zhang, D. Pollard, and D. J. Beerling (2012), Past extreme warming events linked to massive carbon re-lease from thawing permafrost, Nature, 484, 87–92, doi:10.1038/nature10929.

Demicco, R. V. (2004), Modeling seafloor-spreading rates through time, Geology, 32, 485–488.

Dickens, G. R. (2000), Methane oxidation during the Late Palaeocene Thermal Maximum, B. Soc. Geol. Fr., 171, 37–49.

Dickens, G. R. (2011), Down the Rabbit Hole: toward appropriate discussion of methane release from gas hydrate systems during the Paleocene-Eocene thermal maximum and other past hyperthermal events, Clim. Past, 7, 831–846, doi:10.5194/cp-7-831-2011.

Dickens, G. R., and J. Backman (2013), Core alignment and composite depth scale for the lower Paleogene through uppermost Cretaceous interval at Deep Sea Drilling Project Site 577, Newsl. Stratigr., 46, 47–68.

Dickens, G. R., J. R. O'Neil, D. K. Rea, and R. M. Owen (1995), Dissociation of oceanic methane hydrate as a cause of the carbon isotope excursion at the end of the Paleocene, Paleoceanography, 10, 965–971, doi:10.1029/95PA02087.

Dickens, G. R., M. M. Castillo, and J. C. G. Walker (1997), A blast of gas in the latest Paleocene: simulating first-order effects of massive dissociation of oceanic methane hydrate, Geology, 25, 259–262.

D'Onofrio, R., V. Luciani, L. Giusberti, E. Fornaciari, and M. Sprovieri (2014), Tethyan planktic foraminiferal record of the early Eocene hyperthermal events ETM2, H2 and I1 (Terche section, northeastern Italy), Rendiconti Online della Società Geologica Italiana, 31, 66–67, doi:10.3301/ROL.2014.48.

Douglas, A. E. (2003), Coral bleaching – how and why?, Marine Pollut. Bull., 46, 385–392, doi:10.1016/S0025-326X(03)00037-7.

Dunkley Jones, T., D. J. Lunt, D. N. Schmidt, A. Ridgwell, A. Sluijs, P. J. Valdez, and M. A. Maslin (2013), Climate model and proxy data constraints on ocean warming across the Paleocene–Eocene Thermal Maximum, Earth Sci. Rev., 125, 123–145.

Edgar, K. M., S. M. Bohaty, S. J. Gibbs, P. F. Sexton, R. D. Norris, and P. A. Wilson (2012), Symbiont "bleaching" in planktic foraminifera during the Middle Eocene Climatic Optimum, Geology, 41, 15–18, doi:10.1130/G33388.1.

Ernst, S. R., E. Guasti, C. Dupuis, and R. P. Speijer (2006), Environmental perturbation in the southern Tethys across the Paleocene/Eocene boundary (Dababiya, Egypt): foraminiferal and clay mineral records, Mar. Micropaleontol., 60, 89–111.

Ezard, T. H. G., T. Aze, P. N. Pearson, and A. Purvis (2011), Interplay between changing climate and species' ecology drives macroevolutionary dynamics, Science, 332, 349–351.

Falkowski, P. G., M. E. Katz, A. J. Milligan, K. Fennel, B. S. Cramer, M. P. Aubry, R. A. Berner, M. J. Novacek, and W. M. Zapol (2005), Mammals evolved, radiated, and grew in size as the concentration of oxygen in Earth's atmosphere increased during the past 100 million years, Science, 309, 2202–2204.

Figueirido, B., C. M. Janis, J. A. Pérez-Claros, M. De Renzi, and P. Palmqvist (2012), Cenozoic climate change influences mammalian evolutionary dynamics, P. Natl. Acad. Sci. USA, 109, 722–727.

Fletcher, B. J., S. J. Brentnall, C. W. Anderson, R. A. Berner, and D. J. Beerling (2008), Atmospheric carbon dioxide linked with Mesozoic and early Cenozoic climate change, Nat. Geosci., 1, 43–48.

Fornaciari, E., L. Giusberti, V. Luciani, F. Tateo, C. Agnini, J. Backman, M. Oddone, and D. Rio (2007), An expanded Cretaceous Tertiary transition in a pelagic setting of the Southern Alps (central-western Tethys), Palaeogeor. Palaeoclimatol. Palaeoecol., 255, 98–131, doi:10.1016/j.palaeo.2007.02.044.

Fraass, A. J., D. K. Kelly, and S. E. Peters (2015), Macroevolutionary history of the planktic foraminifera, Annu. Rev. Earth Pl. Sc., 43, 139–66, doi:10.1146/annurev-earth-060614-105059.

Frank, T. D., M. A. Arthur, and W. E. Dean (1999), Diagenesis of Lower Cretaceous pelagic carbonates, North Atlantic: paleoceanographic signals obscured, J. Foramin. Res., 29, 340–351.

Galeotti, S., S. Krishnan, M. Pagani, L. Lanci, A. Gaudio, J. C. Zachos, S. Monechi, G. Morelli, and L. J. Lourens (2010), Orbital chronology of Early Eocene hyperthermals from the Contessa Road section, central Italy, Earth Planet. Sci. Lett., 290(1–2), 192–200, doi:10.1016/j.epsl.2009.12.021.

Gingerich, P. D. (2001), Rates of evolution on the time scale of the evolutionary process, Genetica, 112–113, 127–144.

Gingerich, P. D. (2003), Mammalian response to climate change at the Paleocene–Eocene boundary, Polecat Bench record in the northern Bighorn Basin, Wyoming, Geol. Soc. Am. Spec. Pap., 369, 463–478.

Giusberti, L., D. Rio, C. Agnini, J. Backman, E. Fornaciari, F. Tateo, and M. Oddone (2007), Mode and tempo of the Paleocene–Eocene thermal maximum in an expanded section from the Venetian pre-Alps, Geol. Soc. Am. Bull., 119, 391–412, doi:10.1130/B25994.1.

Guasti, E., and Speijer R. P. (2007), The Paleocene–Eocene thermal maximum in Egypt and Jordan: an overview of the planktic foraminiferal record, Geol. Soc. Spec. Pap., 424, 53–67.

Hallock, P. (1987), Fluctuations in the trophic resource continuum: a factor in global diversity cycles?, Paleoceanography, 2, 457–471.

Hancock, H. J. L., and G. R. Dickens (2005), Carbonate dissolution episodes in Paleocene and Eocene sediment, Shatsky Rise, west-central Pacific, in Proceedings of the Ocean Drilling Program, Scientific Results, edited by T. J. Bralower, I. Premoli Silva, and M. J. Malone, Texas A&M Univ., College Station, 198, 1–24, doi:10.2973/odp.proc.sr.198.116.2005.

Hemleben, C., M. Spindler, and O. R. Anderson (1989), Modern planktonic foraminifera, edited by Hemleben, C., M. Spindler, and O. R. Anderson, Springer-Verlag, New York, ISBN-13: 9780387968155, 1–363.

Hilgen, F. J., H. A. Abels, K. F. Kuiper, L. J. Lourens, and M. Wolthers (2015), Towards a stable astronomical time scale for the Paleocene: aligning Shatsky Rise with the Zumaia – WalvisRidge ODP Site 1262 composite, Newsl. Stratigr., 48, 91–110, doi:10.1127/nos/2014/0054.

Hollis, C. J., K. W. R. Taylor, L. Handley, R. D. Pancost, M. Huber, J. B. Creech, B. R. Hines, E. M. Crouch, H. E. G. Morgans, J. S. Crampton, S. Gibbs, P. N. Pearson, and J. C. Zachos (2012), Early Paleogene temperature history of the Southwest Pacific Ocean: Reconciling proxies and models, Earth Planet. Sc. Lett., 349–350, 53–66, doi:10.1016/j.epsl.2012.06.024.

Huber, M., and R. Caballero (2011), The early Eocene equable climate problem revisited, Clim. Past, 7, 603–633, doi:10.5194/cp-7-603-2011.

Hyland, E. G., and N. D. Sheldon (2013), Coupled CO_2-climate response during the Early Eocene Climatic Optimum, Palaeogeogr., Palaeocl., Palaeoecol., 369, 125–135.

Hyland, E. G., N. D. Sheldon, and M. Fan (2013), Terrestrial paleoenvironmental reconstructions indicate transient peak warming during the early Eocene climatic optimum, Geol. Soc. Am. Bull., 125, 1338–1348.

IPCC, (2014), Climate Change 2014: Synthesis Report, Contribution of Working Groups I, II and III to the Fifth Assessment Report of the Intergovernmental Panel on Climate Change, edited by Core Writing Team, Pachauri, R. K., and Meyer, L. A., IPCC, Geneva, Switzerland, 151 pp..

Inglis, G. N., A. Farnsworth, D. Lunt, G. L. Foster, C. J. Hollis, M. Pagani, P. E. Jardine, P. N. Pearson, P. Markwick, A. M. J. Galsworthy, L. Raynham, K. W. R. Taylor, and R. D. Pancost (2015), Descent toward the icehouse: Eocene sea surface cooling inferred from GDGT distributions, Paleoceanography, 30, 100–1020, doi:10.1002/2014PA002723.

Ito, G., and P. D. Clift (1998), Subsidence and growth of Pacific Cretaceous plateaus, Earth Plant. Sc. Lett., 161, 85–100.

John, E. H., P. N. Pearson, H. K., Coxall, H. Birch, B. S. Wade, and G. L. Foster (2013), Warm ocean processes and carbon cyclingin the Eocene, Philos. T. R. Soc., A, 371, 20130099,doi:10.1098/rsta.2013.0099.

John, E. H., J. D. Wilson, P. N. Pearson, and A. Ridgwell (2014), Temperature-dependent remineralization and carbon cycling in the warm Eocene oceans, Palaeogeogr., Palaeocl., Palaeoecol., 413, 158–166.

Kelly, D. C., T. J. Bralower, J. C. Zachos, I. Premoli Silva, and E. Thomas (1996), Rapid diversification of planktonic foraminifera in the tropical Pacific (ODP Site 865) during the late Paleocene Thermal Maximum, Geology, 24, 423–426.

Kelly, D. C., T. J. Bralower, and J. C. Zachos (1998), Evolutionaryconsequences of the latest Paleocene thermal maximum for tropical planktonic foraminifera, Palaeogeogr., Palaeoclimatol.,Palaeoecol., 141, 139–161.

Kelly, D. C. (2002), Response of Antartic (ODP) planktonic foraminifera to the Paleocene-Eocene Thermal Maximum: faunal evidence for ocean/climate change, Paleoceanography, 17, 1071,doi:10.1029/2002PA000761.

Kennett, J. P., and L. D. Stott (1991), Abrupt deep-sea warming, palaeoceanographic changes and benthic extinctions at the end of the Palaeocene, Nature, 353, 225–229.

Kirtland-Turner, S., P. F. Sexton, C. D. Charles, and R. D. Norris (2014), Persistence of carbon release events through the peak of early Eocene global warmth, Nat. Geosci., 12, 1–17, doi:10.1038/ngeo2240.

Komar, N., R. E. Zeebe, and G. R. Dickens (2013), Understandinglong-term carbon cycle trends: the late Paleocene through the early Eocene, Paleoceanography, 28, 650–662,doi:10.1002/palo.20060.

Kroenke, L. W., W. H. Berger, T. R. Janecek, J. Backman, F. Bassinot, R. M. Corfield, M. L. Delaney, R. Hagen, E. Jansen, L. A. Krissek, C. Lange, R. M. Leckie, I. Lykke Lind, M. W. Lyle, J. J. Mahoney, J. C. Marsters, L. Mayer, D. C. Mosher, R. Musgrave, M. L. Prentice, J. M. Resig, H. Schmidt, R. Stax, M. Storey, K. Takahashi, T. Takayama, J. A. Tarduno, R. H. Wilkens, G. Wu, and Barbu, E. M. (1991), Ontong Java Plateau, Leg 130: synopsis of major drilling results, in Proceedings of the Ocean Drilling Program, Initial Reports, 130, 497–537.

Kurtz, A. C., L. R. Kump, M. A. Arthur, J. C. Zachos, and A. Paytan (2003), Early Cenozoic decoupling of the global carbon and sulfur cycles, Paleoceanography, 18, 1090,doi:10.1029/2003PA000908.

Lauretano, V., K. Littler, M. Polling, and J. C. Zachos (2015), Frequency, magnitude and character of hyperthermal events at the onset of the Early Eocene Climatic Optimum, Clim. Past, 11(3), 1795–1820, doi:10.5194/cpd-11-1795-2015.

Lee, C. T., B. Shen, B. S. Slotnick, K. Liao, G. R. Dickens, Y. Yokoyama, A. Lenardic, R. Dasgupta, M. Jellinek, J. S. Lackey, T. Schneider, and M. M. Tice (2013), Continental arc-island arc fluctuations, growth of crustal carbonates, and long-term climate change, Geosphere, 9, 21–36.

LeGrande, A. N. and G. A. Schmidt (2006), Global gridded data set of the oxygen isotopic composition in sea-water, Geophys. Res. Lett., 33, L12604, doi:10.1029/2006GL026011.

Leon-Rodriguez, L., and G. R. Dickens (2010), Constraints on ocean acidification associated with rapid and massive carbon injections: The early Paleogene record at ocean drilling program site 1215, equatorial Pacific Ocean, Palaeogeogr. Palaeoclimatol. Palaeoecol., 298(3–4), 409–420, doi:10.1016/j.palaeo.2010.10.029.

Lirer, F. (2000), A new technique for retrieving calcareous microfossils from lithified lime deposits, Micropaleontology, 46, 365–369.

Littler, K., U. Röhl, T. Westerhold, and J. C. Zachos (2014), A high-resolution benthic stable isotope record for the South Atlantic: Implications for orbital-scale changes in late Paleocene–early Eocene climate and carbon cycling, Earth Planet. Sc. Lett., 401, 18–30, doi:10.1016/j.epsl.2014.05.054.

Lourens, L. J., A. Sluijs, D. Kroon, J. C. Zachos, E. Thomas, U. Röhl, J. Bowles, and I. Raffi (2005), Astronomical pacing of late Palaeocene to early Eocene global warming events, Nature, 435, 1083–1087.

Lowenstein, T. K., and R. V. Demicco (2006), Elevated Eocene atmospheric CO_2 and its subsequent decline, Science, 313, 1928, doi:10.1126/science.1129555.

Lu, G. (1995), Paleocene-Eocene transitional events in the ocean: Faunal and isotopic analyses of planktic foraminifera, PhD Thesis, Princeton University, Princeton, 1–284.

Lu, G. and G. Keller (1995), Planktic foraminiferal faunal turnovers in the subtropical Pacific during the late Paleocene to early Eocene, J. Foramin. Res., 25, 97–116.

Lu, G., G. Keller, and A. Pardo (1998), Stability and change in Tethyan planktic foraminifera across the Paleocene-Eocene transition, Mar. Micropaleontol., 35, 203–233.

Luciani, V., L. Giusberti, C. Agnini, J. Backman, E. Fornaciari, and D. Rio (2007), The Paleocene–Eocene Thermal Maximum as recorded by Tethyan planktonic foraminifera in the Forada section (northern Italy), Mar. Micropaleontol., 64(3), 189–214, doi:10.1016/j.marmicro.2007.05.001.

Luciani, V., L. Giusberti, C. Agnini, E. Fornaciari, D. Rio, D. J. A. Spofforth, and H. Pälike (2010), Ecological and evolutionary response of Tethyan planktonic foraminifera to the middle Eocene climatic optimum (MECO) from the Alano section (NE Italy), Palaeogeogr. Palaeocl., 292, 82–95, doi:10.1016/j.palaeo.2010.03.029.

Luciani, V., and L. Giusberti (2014), Reassessment of the early–middle Eocene planktic foraminiferal biomagnetochronology: new evidence from the Tethyan Possagno section (NE Italy) and Western North Atlantic Ocean ODP Site 1051, J. Foramin. Res., 44, 187–201.

Lunt, D. J., A. Ridgwell, A. Sluijs, J. C. Zachos, S. Hunter, and A. Haywood (2011), A model for orbital pacing of methan hydrate destabilization during the Paleogene, Nat. Geosci., 4, 775–778, doi:10.1038/ngeo1266.

Marshall, J. D. (1992), Climatic and oceanographic isotopic signals from the carbonate rock record and their preservation, Geol. Mag., 129(02), 143–160.

Martini, E. (1971), Standard Tertiary and Quaternary calcareous nannoplankton zonation, in Proceedings of the Second Planktonic Conference, vol. 1970, edited by A. Farinacci, pp. 739–785, Tecnoscienza, Roma.

Matter, A., R. G. Douglas, and K. Perch-Nielsen (1975), Fossil preservation, geochemistry and diagenesis of pelagic carbonates from Shatsky Rise, northwest Pacific, Initial Rep. Deep Sea, 32, 891–922, doi:10.2973/dsdp.proc.32.137.1975.

McInerney, F. A., and S. L. Wing (2011), The Paleocene-Eocene Thermal Maximum: A perturbation of carbon cycle, climate, and biosphere with implications for the future, Annu. Rev. Earth Planet. Sci., 39(1), 489–516, doi:10.1146/annurev-earth-040610-133431.

Mita, I. (2001), Data Report: Early to late Eocene calcareous nannofossil assemblages of Sites 1051 and 1052, Blake Nose, Northwestern Atlantic Ocean, Proc. Ocean Drill. Progr., Sci. Results, 171B, 1–28.

Molina, E., I. Arenillas, and A. Pardo (1999), High resolution planktic foraminiferal biostratigraphy and correlation across the Palaeocene/Eocene boundary in the Tethys, B. Soc. Géol. Fr., 170, 521–530.

Monechi, L., U. Bleil, and J. Backman (1985), Magnetobiochronology of Late Cretaceous-Paleogene and late Cenozoic pelagic sedimentary sequences from the northwest Pacific, Deep Sea Drilling Project, Leg 86, Site 577, Proceedings of the Ocean Drilling Program 86, Initial Reports, Ocean Drilling Program, College Station, TX, doi:10.2973/dsdp.proc.86.137.1985.

Nguyen, T. M. P., M.-R. Petrizzo, and R. P. Speijer (2009), Experimental dissolution of a fossil foraminiferal assemblage (Paleocene–Eocene Thermal Maximum, Dababiya, Egypt): Implications for paleoenvironmental reconstructions, Mar. Micropaleontol., 73(3–4), 241–258, doi:10.1016/j.marmicro.2009.10.005.

Nguyen, T. M. P., M.-R. Petrizzo, P. Stassen, and R. P. Speijer (2011), Dissolution susceptibility of Paleocene–Eocene planktic foraminifera: Implications for palaeoceanographic reconstructions, Mar. Micropaleontol., 81(1–2), 1–21.

Nicolo, M. J., G. R. Dickens, C. J. Hollis, and J. C. Zachos (2007), Multiple early Eocene hyperthermals: Their sedimentary expression on the New Zealand continental margin and in the deep sea, Geology, 35(8), 699–702.

Norris, R. D. (1991), Biased extinction and evolutionary trends, Paleobiology, 17, 388–399.

Norris, R. D. (1996), Symbiosis as an evolutionary innovation in the radiation of Paleocene planktic foraminifera, Paleobiology, 22, 461–480.

Norris, R. D., D. Kroon, and A. Klaus (1998), Proceedings of the Ocean Drilling Program, Initial Reports, Proc. Ocean Drill. Progr., Sci. Results, 171B, 1–749.

O'Connor, M., M. F. Piehler, D. M. Leech, A. Anton, and J. F. Bruno (2009), Warming and resource availability shift food web structure and metabolism, PLOS Biol., 7, 1–6, doi:10.1371/journal.pbio.1000178.

Ogg, J. G. and L. Bardot (2001), Aptian through Eocene magnetostratigraphic correlation of the Blake Nose Transect (Leg 171B), Florida continental margin, Proc. Ocean Drill. Progr., Sci. Results, 171B, 1–58, doi:10.2973/odp.proc.sr.171B.104.2001.

Okada, H., and D. Bukry (1980), Supplementary modification and introduction of code numbers to the low latitude coccolith biostratigraphy zonation (Bukry, 1973, 1975), Mar. Micropaleontol., 51, 321–325.

Olivarez Lyle, A., and M. W. Lyle (2006), Missing organic carbon in Eocene marine sediments: Is metabolism the biological feedback that maintains end-member climates?, Paleoceanography, 21, PA2007, doi:10.1029/2005PA001230.

Oreshkina, T. V. (2012), Evidence of late Paleocene–early Eocene hyperthermalevents in biosiliceous sediments of Western Siberia andadjacent areas, Aust. J. Earth Sci., 105, 145–153.

Pälike, H., M. W. Lyle, H. Nishi, I. Raffi, A. Ridgwell, K. Gamage, A. Klaus, G. Acton, L. Anderson, J. Backman, J. Baldauf, C. Beltran, S. M. Bohaty, P. Bown, W. Busch, J. E. T. Channell, C. O. J. Chun, M.

Delaney, P. Dewangan, T. DunkleyJones, K. M. Edgar, H. Evans, P. L. Fitch, G. L. Foster, N. Gussone, H. Hasegawa, E. C. Hathorne, H. Hayashi, J. O. Herrle, A. Holbourn, S. Hovan, K. Hyeong, K. Iijima, T. Ito, S. Kamikuri, K. Kimoto, J. Kuroda, L. Leon-Rodriguez, A. Malinverno, T. C. Moore, H. Brandon, D. P. Murphy, H. Nakamura, K. Ogane, C. Ohneiser, C. Richter, R. Robinson, E. J. Rohling, O. Romero, K. Sawada, H. Scher, L. Schneider, A. Sluijs, H. Takata, J. Tian, A. Tsujimoto, B. S. Wade, T. Westerhold, R. Wilkens, T. Williams, P. A. Wilson, Y. Yamamoto, S. Yamamoto, T. Yamazaki, and R. E. Zeebe (2012), Cenozoic record of the equatorial Pacific carbonate compensation depth, Nature, 488, 609–614, doi:10.1038/nature11360.

Pearson P. N., and H. K. Coxall (2014), Origin of the Eocene planktonic foraminifer Hantkenina by gradual evolution, Palaeontology, 57,243–267.

Pearson, P. N., and M. R. Palmer (2000), Atmospheric carbon dioxide concentrations over the past 60 million years, Nature, 406, 695–699,doi:10.1038/35021000.

Pearson, P. N., N. J. Shackleton, and M. A. Hall (1993), Stable isotope paleoecology of middle Eocene planktonic foraminifera and multi species isotope stratigraphy, DSDP Site 523, south Atlantic, J. Foramin. Res., 23, 123–140.

Pearson, P. N., P. W Ditchfield, J. Singano, K. G. Harcourt-Brown, C. J. Nicholas, R. K. Olsson, N. J. Shackleton, and M. A. Hall (2001), Warm tropical sea surface temperatures in the Late Cretaceous and Eocene epochs, Nature, 413, 481–487, doi:10.1038/35097000.

Pearson, P. N., R. K. Olsson, C. Hemblen, B. T. Huber, and W. A. Berggren (Eds.) (2006), Atlas of Eocene Planktonic Foraminifera, Cushman Special Publication, 41, pp. 513, Department of Geology East Carolina Univ., Greenville.

Pearson, P. N., B. E. Van Dongen, C. J. Nicholas, R. D. Pancost, S. Schouten, J. M. Singano, and B. S. Wade (2007), Stable warm tropical climate through the Eocene Epoch, Geology, 35, 211–214.

Petrizzo, M. R. (2007), The onset of the Paleocene–Eocene Thermal Maximum (PETM) at Sites 1209 and 1210 (Shatsky Rise, Pacific Ocean) as recorded by planktonic foraminifera, Mar. Micropaleontol., 63, 187–200.

Petrizzo, M.-R., G. Leoni, R. P. Speijer, B. De Bernardi, and F. Felletti (2008), Dissolution susceptibility of some Paleogene planktonic foraminifera from ODP Site 1209 (Shatsky Rise, Pacific Ocean), J. Foraminiferal Res., 38(4), 357–371.

Pross, J., L. Contreras, P. K. Bijl, D. R. Greenwood, S. M. Bohaty, S. Schouten, J. A. Bendle, U. Röhl, L. Tauxe, J. I. Raine, E. Claire, C. E. Huck, T. van de Flierdt, S. R. Stewart, S. S. R. Jamieson, C. E. Stickley, B. van de Schootbrugge, C. Escutia, and H. Brinkhuis (2012), Persistent near-tropical warmth on the Antarcticcontinent during the early Eocene Epoch, Nature, 488, 73–77, doi:10.1038 /nature11300.

Pujalte, V., J. I. Baceta, and B. Schmitz (2015), A massive input of coarse-grained siliciclastics in the Pyrenean Basin during the PETM: the missing ingredient in a coeval abrupt change in hydrological regime, Clim. Past, 11, 1653–1672, doi:10.5194/cp-11-1653-2015.

Quillévéré, F., R. D. Norris, I. Moussa, and W. A. Berggren (2001), Role of photosymbiosis and biogeography in the diversification of early Paleogene acarininids (planktonic foraminifera), Paleobiology, 27(2), 311–326, doi:10.1666/0094-8373(2001)027<0311:ROPABI>2.0.CO;2.

Raffi, I., and B. De Bernardi (2008), Response of calcareous nannofossils to the Paleocene–Eocene Thermal Maximum: Observations on composition, preservation and calcification in sediments from ODP Site 1263 (Walvis Ridge—SW Atlantic), Marine Micropaleontology, 69(2), 119-138.

Raymo, M. E., and W. F. Ruddiman (1992), Tectonic forcing of late Cenozoic climate, Nature, 359, 117–122.

Reghellin, D., H. K. Coxall, G. R. Dickens, and J. Backman, (2015), Carbon and oxygen isotopes of bulk carbonate in sediment deposited beneath the eastern equatorial Pacific over the last 8 million years, Paleoceanography, 30(10), 1261-1286.

Röhl, U., T. Westerhold, S. Monechi, E. Thomas, J. C. Zachos, and B. Donner (2005), The third and final early Eocene Thermal Maximum: Characteristics, timing, and mechanisms of the "X" event, Geol. Soc. Am. Abstr. Program, 37 (7), 264.

Scheibner, C., and R. P. Speijer (2008), Late Paleocene–early Eocene Tethyan carbonate platform evolution—a response to long-and short-term paleoclimatic change, Earth-Science Reviews, 90 (3), 71-102.

Schlanger, S. O., and R. G. Douglas (1974), The pelagic ooze-chalk limestone transition and its implications for marine stratigraphy, in Pelagic Sediments: on Land and under the Sea, edited by Hsü, K. J. and Jenkyns, H. C., Sp. Publ. Int., 1, 117–148.

Schmidt, D. N., H. R. Thierstein, and J. Bollmann (2004), The evolutionaryhistory of size variation of planktic foraminiferal assemblagesin the Cenozoic, Palaeogeogr. Palaeocl., 212, 159–180,doi:10.1016/j.palaeo.2004.06.002.

Schmitz, B., and V. Pujalte (2007), Abrupt increase in seasonal extreme precipitation at the Paleocene-Eocene boundary, Geology, 35, 215–218.

Schneider, L. J., T. J. Bralower, and L. J. Kump (2011), Response ofnannoplankton to early Eocene ocean destratification, Palaeogeogr.Palaeocl., 310, 152–162.

Scholle, P. A., and M. A. Arthur (1980), Carbon isotope fluctuations in Cretaceous pelagic limestones: potential stratigraphic and petroleum exploration tool, American Association of Petroleum Geologists Bulletin, 64, 67–87.

Schulte, P., C. Scheibner, and R. C. Speijer (2011), Fluvial discharge and sea-level changes controlling black shale deposition during the Paleocene–Eocene Thermal Maximum in the Dababiya Quarry section, Egypt, Chem. Geol., 285, 167–183, doi:10.1016/j.chemgeo.2011.04.004.

Schrag, D. P., D. J. Depaolo, and F. M. Richter (1995), Reconstructing past sea surface temperatures: Correcting for diagenesis of bulk marine carbonate, Geochim. Cosmochim. Acta, 59, 2265–2278, doi:10.1016/0016-7037(95)00105-9.

Schmitz, B., R. P. Speijer, and M.-P. Aubry (1996), Latest Paleocene benthic extinction event on the southern Tethyan shelf (Egypt), Foraminiferal stable isotopic ($\delta^{13}C$, $\delta^{18}O$) records, Geology, 24,347–350.

Self-Trail, J. M., D. S. Powars, D. K. Watkins, and G. A. Wandless (2012), Calcareous nannofossil assemblage changes across thePaleocene–Eocene Thermal Maximum: Evidence from a shelfsetting, Mar. Micropaleontol., 92–93, 61–80.

Sexton, P. F., P. A. Wilson, and P. N. Pearson (2006), Microstructural and geochemical perspectives on planktic foraminiferal preservation: 'Glassy' versus 'Frosty', Geochemistry Geophysics Geosystems, v. 7, Q12P19, doi:10.1029/2006GC001291.

Sexton, P. F., R. D. Norris, P. A. Wilson, H. Pälike, T. Westerhold, U. Röhl, C. T. Bolton, and S. Gibbs (2011), Eocene global warming events driven by ventilation of oceanic dissolved organic carbon, Nature, 471, 349–353, doi:10.1038/nature09826.

Shackleton, N. J. (1986), Paleogene stable isotope events, Palaeogeogr. Palaeocl., 57, 91–102.

Shackleton, N. J., and M. A. Hall (1984), Carbon isotope data from Leg 74 sediments, Initial Rep. Deep Sea, 74, 613–619.

Shackleton, N. J. and M. A. Hall (1995), Stable isotope records in bulk sediments (Leg 138), Proc. Ocean Drill. Progr., Sci. Results, 138, 797–805, doi:10.2973/odp.proc.sr.171B.104.2001.

Shamrock, J. L., D. K. Watkins, and K. W. Johnston (2012), Eocene biogeochronology of ODP Leg 122 Hole 762C, Exmouth Plateau (northwest Australian Shelf), Stratigraphy, 9, 55–76.

Shipboard Scientific Party, (1985), Site 577: Initial Rep., Deep Sea, 86, edited by Heath, G. R., L. H. Burckle, G. R. Heath, L. H. Burckle, A. E. D'Agostino, U. Bleil, K. Horai, R. D. Jacobi, T. R. Janecek, I. Koizumi, L. A. Krissek, S. Monechi, N. Lenotre, J. J. Morley, P. J. Schultheiss, A. A. Wright, and K. L. Turner, US Government Printing Office, Washington, 91–137, doi:10.2973/dsdp.proc.86.104.1985, 1985.

Shipboard Scientific Party, (1998), Site 1051, in Proceeding Ocean Drilling Program, Initial Reports, 171B, edited by Norris, R. D., D. Kroon, A. Klaus, I. T. Alexander, L. P. Bardot, C. E. Barker, J.-P. Bellier, C. D. Blome, L. J. Clarke, J. Erbacher, K. L. Faul, B. T. Holmes, M. Huber, M. E. Katz, K. G. MacLeod, S. Marca, F. C. Martinez-Ruiz, I. Mita, M. Nakai, J. G. Ogg, D. K. Pak, T. K. Pletsch, J. M. Self-Trail, N. J. Shackleton, J. Smit, W. Ussler III, D. K. Watkins, J. Widmark, P. A. Wilson, L. A. Baez, and E. Kapitan-White, Ocean Drilling Program, College Station,TX, 171–239, doi:10.2973/odp.proc.ir.171b.105.1998, 1998.

Sims, P. A., D. G. Mann, and L. K. Medlin (2006), Evolution of the diatoms: insights from fossil, biological and molecular data, Phycologia,45, 361–402.

Sinton, C. W., and R. A. Duncan (1998), 40Ar-39Ar ages of lavas from the southeast Greenland margin, ODP Leg 152, and the Rockall Plateau, DSDP Leg 81, Ocean Drill. Progr., Sci. Res., 152, 387–402, doi:10.2973/odp.proc.sr.152.234.1998.

Slotnick, B. S., Dickens, G. R., Nicolo, M. J., Hollis, C. J., Crampton,J. S., Zachos, J. C., and Sluijs, A.: Large-amplitude variationsin carbon cycling and terrestrial weathering during the latestPaleocene and earliest Eocene: The Record at Mead Stream,New Zealand, J. Geol., 120, 487–505, 2012.

Slotnick, B. S., G. R. Dickens, M. J. Nicolo, C. J. Hollis, J. S. Crampton, and J. C. Zachos (2012), Large-amplitude variations in carbon cycling and terrestrial weathering during the latest Paleocene and earliest Eocene: The record at Mead Stream, New Zealand, J. Geol., 120(5), 487–505, doi:10.1086/666743.

Slotnick, B. S., G. R. Dickens, C. J. Hollis, J. S. Crampton, P. S. Strong, and A. Phillips (2015a), The onset of the Early Eocene Climatic Optimum at Branch Stream, Clarence River valley, New Zealand, New Zeal. J. Geol. Geop., 58, 1–19, doi:10.1080/00288306.2015.1063514.

Slotnick, B. S., V. Lauretano, J. Backman, G. R. Dickens, A. Sluijs, and L. Lourens (2015b), Early Paleogene variations in the calcite compensation depth: new constraints using old borehole sediments from across Ninety east Ridge, central Indian Ocean, Clim. Past, 11, 473–493, doi:10.5194/cp-11-473-2015.

Sluijs, A., and G. R. Dickens (2012), Assessing offsets between the ^{13}C of sedimentary components and the global exogenic carbon pool across early Paleogene carbon cycle perturbations, Global Biogeochem. Cy., 26, GB4019, doi:10.1029/2011GB004094.

Sluijs, A., S. Schouten, M. Pagani, M. Woltering, H. Brinkhuis, J. S. Sinninghe Damsté, G. R. Dickens, M. Huber, G. Reichart, R. Stein, J. Matthiessen, L. J. Lourens, N. Pedentchouk, J. Backman, K. Moran, and the Expedition 302 Scientists (2006), Subtropical Arctic Ocean temperatures during the Palaeocene/Eocene thermal maximum, Nature, 441, 610–613,doi:10.1038/nature04668.

Sluijs, A., G. J. Bowen, H. Brinkhuis, L. J. Lourens, and E. Thomas (2007), The Paleocene–Eocene thermal maximum super greenhouse: biotic and geochemical signatures, age models and mechanisms of global change, in Deep-Time Perspectives on Climate Change, edited by Williams, M., A. M. Haywood, F. J. Gregory, and D. N. Schmidt, Micropalaeont. Soc. Spec. Publ., Geological Society, London, 323–350.

Smith, R. Y., D. R. Greenwood, and J. F. Basinger (2010), Estimating paleoatmospheric pCO_2 during the Early Eocene Climatic Optimum from stomatal frequency of Ginkgo, Okanagan Highlands, British Columbia, Canada, Palaeogeogr. Palaeocl., 293, 120–131.

Stap, L., A. Sluijs, E. Thomas, and L. J. Lourens (2009), Patterns and magnitude of deep sea carbonate dissolution during Eocene Thermal Maximum 2 and H2, Walvis Ridge, Southeastern Atlantic Ocean, Paleoceanography, 24, PA1211, doi:10.1029/2008PA001655.

Thomas, E. (1998), Biogeography of the late Paleocene benthic foraminiferal extinction, in Late Paleocene-early Eocene climatic and biotic events in the marine and terrestrial Records, edited by Aubry, M.-P., S. Lucas, and W. A. Berggren, Columbia University Press, New York, 214–243.

Thomas, E., H. Brinkhuis, M. Huber, and U. Röhl (2006), An ocean view of the early Cenozoic Greenhouse world, Oceanography, 19, 94–103.

Thunell R. C. and S. Honjo (1981), Calcite dissolution and the modification of planktonic foraminiferal assemblages, Mar. Micropaleontol., 6, 169–182.

Vandenberghe, N., F. J. Hilgen, R. P. Speijer, J. G. Ogg, F. M. Gradstein, O. Hammer, C. J. Hollis, and J. J. Hooker (2012) The Paleogene Period, in The Geologic Time Scale 2012, edited by Gradstein, F., J. G. Ogg, M. D. Schmitz, and G. M. Ogg, 855–921, Elsevier, Amsterdam.

Van Hinsbergen, D. J. J., L. V. de Groot, S. J. van Schaik, W. Spakman, P. K. Bijl, A. Sluijs, C. G. Langereis, and H. Brinkhuis (2015), A Paleolatitude Calculator for Paleoclimate Studies, PLoSONE, 10, e0126946, doi:10.1371/journal.pone.0126946.

Vincent, E. and W. H. Berger (1981), Planktonic foraminifera and their use in paleoceanography; in The Sea, edited by Emiliani, C., NewYork, 7, 1025–1119.

Vogt, P. R. (1979), Global magmatic episodes: New evidence and implications for the steady state mid-oceanic ridge, Geology, 7, 93–98.

Wade, B. S. (2004), Planktonic foraminiferal biostratigraphy and mechanisms in the extinction of *Morozovella* in the late Middle Eocene, Mar. Micropaleontol., 51, 23–38.

Wade, B. S., N. Al-Sabouni, C. Hemleben, and D. Kroon (2008), Symbiont bleaching in fossil planktonic foraminifera, Evol. Ecol., 22, 253–265, doi:10.1007/s10682-007-9176-6.

Wade, B. S., P. N. Pearson, W. A. Berggren, and H. Pälike (2011), Review and revision of Cenozoic tropical planktonic foraminiferal biostratigraphy and calibration to the geomagnetic polarity and astronomical time scale, Earth Sci. Rev., 104, 111–142, doi:10.1016/j.earscirev.2010.09.003.

Westerhold, T., U. Röhl, T. Frederichs, S. M. Bohaty, and J. C. Zachos (2015), Astronomical calibration of the geological timescale: closing the middle Eocene gap, Clim. Past, 11, 1181–1195, doi:10.5194/cp-11-1181-2015.

Wilf, P., R. N. Cúneo, K. R. Johnson, J. F. Hicks, S. L. Wing, and J. D. Obradovich (2003), High plant diversity in Eocene South America:evidence from Patagonia, Science, 300, 122–125.

Wing, S. L., T. M. Bown, and J. D. Obradovich (1991), Early Eocene biotic and climatic change in interior western North America, Geology, 19, 1189–1192.

Woodburne, M. O., G. F. Gunnell, and R. K. Stucky (2009), Climate directly influences Eocene mammal faunal dynamics in North America, P. Natl. Acad. Sci. USA, 106, 13399–13403.

Yamaguchi, T., and R. D. Norris (2012), Deep-sea ostracode turnovers through the Paleocene-Eocene thermal maximum in DSDP Site 401, Bay of Biscay, North Atlantic, Mar. Micropaleontol., 86–87, 32–44.

Yapp, C. J. (2004), $Fe(CO_3)OH$ in goethite from a mid-latitude North American Oxisol: Estimate of atmospheric CO_2 concentration in the early Eocene "climatic optimum", Geochim. Cosmochim. Ac., 68, 935–947, doi:10.1016/j.gca.2003.09.002.

Zachos, J. C., M. Pagani, L. Sloan, E. Thomas, and K. Billups (2001), Trends, rhythms, and aberrations in global climate 65Ma toPresent, Science, 292, 686–693.

Zachos, J. C., U. Röhl, S. A. Schellenberg, A. Sluijs, D. A. Hodell, D. C. Kelly, E. Thomas, M. Nicolo, I. Raffi, L. J. Lourens, H. McCarren, and D. Kroon (2005), Rapid acidification of the ocean during the Paleocene–Eocene thermal maximum, Science, 308,1611–1615.

Zachos, J. C., G. R. Dickens, and R. E. Zeebe (2008), An early Cenozoic perspective on greenhouse warming and carbon-cycle dynamics, Nature, 451, 279–283.

Zachos, J. C., H. McCarren, B. Murphy, U. Röhl, and T. Westerhold (2010), Tempo and scale of late Paleocene and earlyEocene carbon isotope cycles: Implications for the originof hyperthermals, Earth Planet. Sc. Lett., 299, 242–249, doi:10.1016/j.epsl.2010.09.004.

Zeebe, R. E., J. C. Zachos, and G. R. Dickens (2009), Carbon dioxide forcing alone insufficient to explain Palaeocene–Eocene Thermal Maximum warming, Nat. Geosci., 2, 576–580, doi:10.1038/ngeo578.

Zonneveld, J. P., G. F.Gunnell, and W. S. Bartels (2000), Early Eocenefossil vertebrates from the southwestern Green River Basin, Lincolnand Uinta Counties, Wyoming, J. Vertebr. Paleontol., 20, 369–386.

CHAPTER IV

Testing photosymbiont bleaching in planktic foraminifera at the start of the Early Eocene Climatic Optimum

To be submitted

Abstract

The symbiont-bearing planktic foraminiferal genera *Morozovella* and *Acarinina* were among the most important calcifiers of early Paleogene tropical-subtropical oceans. A marked and permanent switch in the abundance of these genera occurred at low-latitude sites at the beginning of the Early Eocene Climatic Optimum (EECO), when the relative abundance of *Morozovella* permanently decreased by at least two thirds across the J event, along with a progressive decrease in the number of species. Concomitantly, the genus *Acarinina* almost doubled its abundance and diversified within the EECO. Here we examine sediment at ODP Site 1051 to refine the timing of this biotic event, to document its details at the species level, and to test a possible cause: the loss of photosymbionts **(**bleaching). We measure the stable isotope composition of bulk carbonate to obtain an accurate age model, the *Morozovella* assemblages to understand changes in species composition, and the size and stable isotope composition of selected specimens to evaluate potential loss of photosymbionts. The switch in *Morozovella* and *Acarinina* abundance clearly happened rapidly across a negative carbon isotope excursion known as the J event, which marks the start of the EECO. The actual change occurred because of major declines in the presence of multiple morphologically defined species. Furthermore, our results demonstrate a significant reduction of morozovellid test-size at the J event, thus supporting the concept of bleaching. However, the recorded bleaching was a transitory effect and it involves the acarininids as well that increase their abundance concomitantly. The sudden switch in planktic foraminiferal genera during the early Eocene was a significant evolutionary change in the marine realm, but a loss of photosymbionts cannot be suggested as the complete cause.

1. Introduction

A striking biotic change happened within planktic foraminifera during the early Eocene (Luciani et al, 2016). The genera *Morozovella* and *Acarinina* were amongst the most important calcifiers of early Paleogene tropical and subtropical oceans (e.g., Berggren, 1978; Boersma et al., 1987; Premoli Silva and Boersma, 1988; Pearson et al., 2006; Aze et al., 2011). However, at multiple low-latitude sites (Fig. 1), a marked and permanent switch in the abundance of these genera occurred close to the start of the Early Eocene Climatic Optimum (EECO), the time of peak Cenozoic warmth (Zachos et al., 2008; Bijl et al., 2009; Huber and Caballero, 2011; Hollis et al., 2012; Pross et al., 2012; Inglis et al., 2015; Luciani et al, 2016;

Frontalini et al., 2016). Specifically, *Morozovella* abundances decreased by at least two thirds across the J event, while *Acarinina* abundances almost doubled. This major turnover further relates to taxonomic diversity, consisting of species reduction among *Morozovella* and species diversification among *Acarinina* (Pearson et al., 2006; Aze et al., 2011).

The major switch in planktic foraminifera appears to have happened near a negative carbon isotope excursion (CIE) called the J event (cf. Cramer et al., 2003; Luciani et al. 2016). This event, which occurred near the boundary between polarity chrons C24n.2r and C24n.3n, and thus ~53 Ma (Slotnick et al., 2015; Lauretano et al., 2015) seems to be one of a series of CIEs that transpired during the early Paleogene (e.g., Kennett and Stott 1991; Cramer et al., 2003; Zachos et al., 2010; Coccioni et al., 2012; Kirtland-Turner et al., 2014; Littler et al., 2014; Lauretano et al., 2016). In general, the CIEs appear to mark "hyperthermals", short-term (~40-200 kyr) global warming events associated with net input of organic carbon, deep sea carbonate dissolution, and biotic turnovers (e.g., Thomas, 1998; Gingerich 2003; Lourens et al., 2005; Zachos et al., 2005; Raffi and De Bernardi, 2008; Scheibner and Speijer, 2008; Leon-Rodriguez and Dickens, 2010; Sexton et al., 2011; Clyde et al., 2013; Hönisch et al., 2012; Yamaguchi and Norris, 2012; Agnini et al., 2014; Kirtland-Turner et al., 2014; D'Onofrio et al., 2016). Notably, the J event coincides with the beginning of the Early Eocene Climatic Optimum (EECO) (Slotnick et al., 2012, 2015; Lauretano et al., 2015; Luciani et al., 2016). A temporal relationship therefore might connect the onset of the EECO, a significant change in carbon cycling, and the *Morozovella-Acaranina* switch.

We refine here the timing and direct cause for the outstanding foraminifera turnover in terms of morozovellid species variance, and then explore a possible reason: the loss of photosymbionts. The symbiotic relationship with photosynthetic algae is a key strategy adopted by many modern planktic forminiferal species (e.g., Be´ 1982; Be´ et al. 1982; Hemleben et al. 1989). The endosymbiosis is thought to be advantageous to certain foraminifera as it provides energy, including for calcification, allowing the host to succeed in low-nutrient environments (e.g., Be´ 1982; Be´ et al. 1982; Hemleben et al., 1989). One might therefore, expect detrimental consequences for photosymbiotic-bearing foraminifera populations if environmental changes affect algal endosymbiosis. Even though photosymbionts are not preserved in the fossil record, we have indirect evidence on their presence in past foraminifera, notably including the morozovellids, because photosymbionts modify the chemistry of the microenvironment where a foraminifer calcifies. Specifically, algal symbionts preferentially remove the lighter ^{12}C isotope during photosynthesis, leaving water enriched in ^{13}C (e.g., Spero and DeNiro 1987). A characteristic increase in $\delta^{13}C$ with

increasing test size thus occurs because larger specimens support greater symbiont density and enhanced photosynthetic. Factors such as depth habitat/light penetration will also influence photoysmbiotic activity and the $\delta^{13}C$ signature (Spero and DeNiro, 1987; Spero and Williams 1988; Spero et al. 1991; Spero 1992; Spero and Lea 1993; D'Hondt et al. 1994). The geochemical signature recorded in the stable isotope ratios of the fossil planktic foraminifera has been therefore used as a proxy for symbiotic activity in extinct taxa (e.g., Pearson et al. 1993; D'Hondt et al. 1994; Norris 1996; Quillévéré et al. 2001; Elderfield et al. 2002; Bornemann and Norris, 2007; Birch et al., 2012; Wendler et al., 2013; Takagi et al., 2015). Bleaching of photosymbionts has been documented in many modern organisms including giant clams, anemones, and especially corals (e.g, Peters 1993; Glynn 1996; Addessi 2001; Suzuki et al. 2003; Grottoli et al. 2004). The loss of symbiont algae in corals result in extensive reduced calcification, degradation and mortality (Glynn 1996; Suzuki et al. 2003; Grottoli et al. 2004). Bleaching episodes also have been documented in modern benthic foraminifera from tropical oceans (e.g., Hallock and Peebles, 1993, Hallock et al., 1995; Hallock 2000; Talge and Hallock 1995, 2003; Williams and Hallock, 2004). The exact causes of bleaching can be manifold and may include elevated sea surface temperature, increased pCO_2 (and consequence decrease in pH), and several other stressors, such as changes in nutrient availability, salinity or increased ultraviolet radiation (e.g., Douglas 2003 and references therein).

Earth scientists have the peculiar possibility to examine whether past changes in the environment (e.g., ocean temperatures, pH, etc.) impacted biotic diversity and calcification processes. Bleaching events in the fossil record are relatively poorly documented. A temporary bleaching has been suggested for large species of *Acarinina* and the genus *Morozovelloides* (morphologically and ecologically comparable with *Morozovella*) during the Middle Eocene Climatic Optimum, MECO (Edgar et al., 2012), an intense warming event centered at ~40Ma (e.g., Bohaty et al., 2009). The postulated loss of the photosymbionts relationship involved an extinction of *Morozovelloides* in the late middle Eocene (Wade et al., 2008). Since endosymbiosis relates to calcification and foraminiferal longevity, the loss of such a relationship should result in the reduction of abundance and a decrease in test-size for the affected foraminiferal population (e.g., Bé et al., 1982; Caron et al., 1982). Such observations are recorded in the middle Eocene (Wade et al., 2008; Edgar et al., 2012).

For this study, we generate key records across the EECO at Ocean Drilling Program (ODP) Site 1051 in the northwest Atlantic. This is one of the sites (Fig. 1) where the morozovellid decline has been documented (Luciani et al., 2016), although not in fine detail.

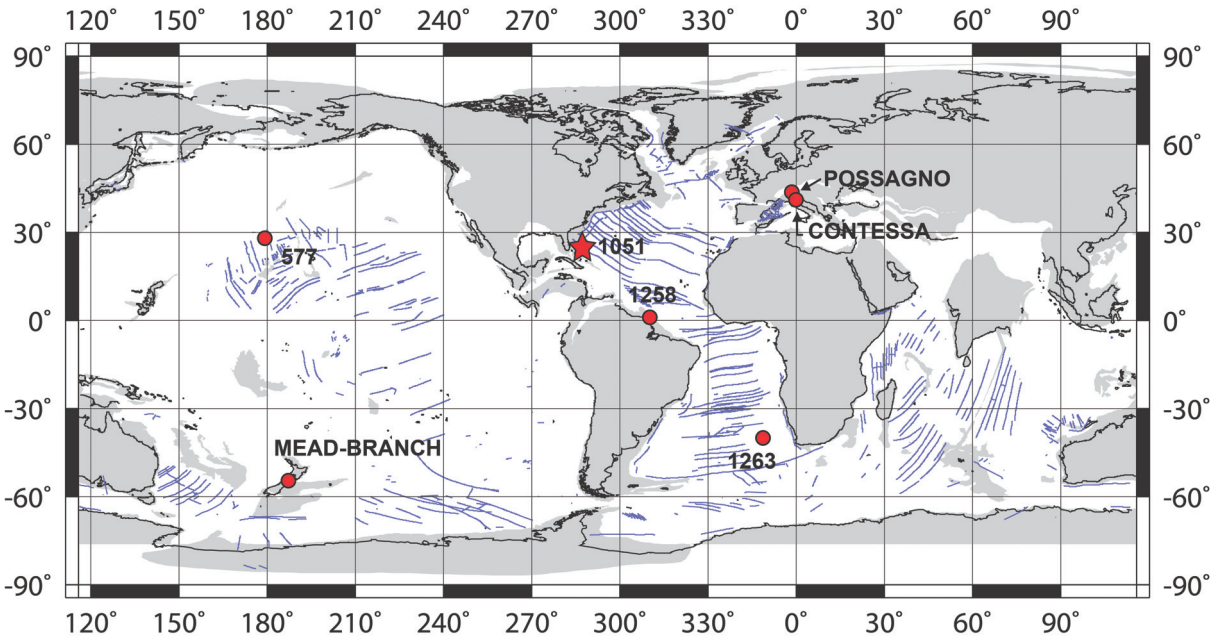

Figure 1. Earth at ~50 Ma showing the approximate locations of the studied site (star) during the early Eocene. Also shown are the other successions with planktic foraminiferal changes or $\delta^{13}C$ record across the EECO. Base map is from http://www.odsn/de/services/paleomap.html with paleolatitudes modified for Sites 577, 1051, 1258 and 1263, Branche and Mead Stream sections according to www.paleolatitude.org model version 1.2 (Van Hinsbergen et al., 2015). Possagno and Contessa paleolatitudes are based on the http://www.odsn.de/odsn/services/paleomap/adv_map.html model since are not yet available at www.paleolatitude.org.

Specifically, we provide stable carbon and oxygen isotope curves from bulk carbonate and tetraether lipid analysis (TEX_{86}) to determine the detailed stratigraphy and evidence for extreme warmth. We then document the changes in morozovellid species abundance, and for selected samples, the record of their variations in maximum test-size and stable isotope composition. We show here that the planktic foraminiferal turnover definitely corresponds to the J event and involves major declines in multiple morozovellid species. We further suggest that this change, which marks the start of the EECO, may relate to variations in photosymbiont activity.

2. ODP Site 1051, Northwest Atlantic

The succession selected for this study comes from ODP Site 1051 on Blake Nose (NW Atlantic, Fig. 1). Blake Nose is a gently sloping ramp that extends eastward from the Florida continental slope between 1000 and 2700 m water depth (Norris et al., 1998). Across Blake Nose, seismic reflection profiles and ODP Leg 171B drilling indicate a relatively thick early Paleogene sediment sequence buried at modest depths below the seafloor (Norris et al., 1998).

Site 1051, which comprises two holes (A and B) is located at 30° 03.2' N, 76° 21.5' W and ~1980 m water depth (Norris et al., 1998). However, during the early Eocene, the position was slightly to the south (Ogg and Bardot, 2001; Van Hinsbergen et al., 2015) and in shallower water (see below). Multiple characteristics make the lower Eocene sedimentary record at Site 1051 appropriate for understanding the major switch in planktic foraminifera. The succession predominantly consists of siliceous nannofossil ooze. Calcareous plankton biostratigraphy (Norris et al., 1998; Mita, 2001; Luciani and Giusberti, 2014**)** and polarity chrons, once recalibrated (Cramer et al., 2003; Luciani et al., 2016), show this depth interval to span from ~53.5 to ~47.5 Ma according to the Westerhold and Röhl (2009) and Westerhold et al. (2015) calibration. This implies a relatively high sedimentation rate (~2.7 cm/kyr) for much of the early Eocene. Moreover, sediment recovery was very good except for the depth interval between 382 and 390 mbsf, which contains significant chert and a hiatus (Shipboard Scientific Party, 1998; Cramer et al., 2003; Luciani et al., 2016).

Planktic foraminifera are well preserved and readily recognizable throughout the studied interval (Norris et al., 1998) and allowed for the identification of the *Morozovella/Acarinina* switch (Luciani et al., 2016). Such preservation is consistent with deposition at relatively shallow water depths, well above the lysocline, and modest burial. Indeed, water depths have been estimated as lower bathyal (1000–2000 m) during the entire late Paleocene through middle Eocene interval using benthic foraminiferal assemblages (Norris et al., 1998), or ~2200 m at ~50 Ma through subsidence and sedimentation rate calculations (Bohaty et al., 2009). Previous work at Site 1051 thus suggests a very good location for examining foraminiferal assemblages through the onset of the EECO.

We focused on the depth interval between 452.3 and 353.1 meters below sea floor (mbsf) at Hole 1051A. Within this interval, we analyzed a total of 227 samples (of nominally 20-30 cm^3) in order to provide new stable-isotope data and to improve the resolution of foraminifera aseemblages, especially across the J event. Samples were used for various analyses, at different spacing, as specified in paragraphs below.

3. Methods

3.1 Stable Isotope Measurements

Bulk carbon and oxygen stable isotope data were generated on 226 samples (Fig. 2). The sampling resolution is 40 cm for the lower (459.26-430.78 mbsf) and upper intervals

(425.182-369.9 mbsf), but is greater, between 5 cm and 20 cm, across the J event (Table S1). Samples were firstly freeze-dried and then pulverized manually in a mortar. Amounts of ~0.5g of powdered samples were acidified at 50°C to be analysed. Bulk isotope analyses for the lower and upper intervals were performed at the UCL Bloomsbury Environmental Isotope Facility using the Gas Bench II and Cardiff University (UK) using a Thermo Finnigan MAT 252 mass spectrometer coupled with a Kiel III carbonate preparation device. Analytical precision for both instruments was within 0.04 and 0.08‰ for $\delta^{13}C$ and $\delta^{18}O$ respectively. The higher resolution samples across the J event were analysed at Padua University with a Thermo Scientific Delta V Advantage Isotope Ratio Mass Spectrometer coupled with a Gas Bench II automated preparation device. Results are reported in conventional delta notation ($\delta^{13}C$ and $\delta^{18}O$) and referred to the Vienna Pee Dee Belemnite standard (VPDB). An internal standard (with $\delta^{18}O$= –2.43‰ and $\delta^{13}C$=2.43‰ versus VPDB) was measured every six samples. A total of 11 duplicate analyses were conducted on selected samples giving reproducibility better than 0.1 for carbon and 0.2‰ for oxygen isotopes. As the records align across the three laboratories, we consider laboratory offsets minimal.

Stable isotopes were also measured on size-constrained planktic foraminifera derived from five samples specifically selected to span the onset of the EECO, for a total of 111 analyses. The samples are alphabetically ordered from lower to higher depth below the seafloor as follows: A (443.58 mbsf), B (433.5 mbsf), C (425.4 mbsf), D (411.8 mbsf) and E (395.65 mbsf) (Fig. 3, Table S1). Analyses were conducted at Padua University as discussed above. Planktic foraminiferal specimens were selected as specified below (section 3.3).

3.2. Tetraether Lipid Analysis

Because significantly higher sea-surface temperature (SST) can lead to photosymbiont bleaching (e.g., Douglas, 2003; Edgar et al., 2012), it is important to reconstruct SSTs across the studied interval. Although SSTs generally reached their Cenozoic maximum during the EECO (e.g., Zachos et al., 2001, 2008; Huber and Caballero, 2011; Hollis et al., 2012; Pross et al., 2012), proxy data for early Paleogene SSTs at Site 1051 are lacking.

The TEX_{86} proxy has been developed and used extensively over the last decade to reconstruct Cenozoic paleotemperatures. The approach has been explained in multiple papers (e.g., Schouten et al., 2013). In brief, marine *Thaumarcheota* produce isoprenoid glycerol dialkyl glycerol tetraethers (GDGTs) and the distribution of these compounds changes with temperature (e.g. Uda et al., 2001; Boyd et al., 2011). Considering that marine *Thaumarcheota* live primarily at water depths of 0-200 metres, the TEX_{86} index (tetraethers

consisting of 86 carbons) has been developed to reconstruct SST based on the relative abundance of isoprenoid GDGTs (Schouten et al., 2002).

To verify the reliability of the TEX_{86} proxy at the Atlantic Site 1051 a preliminary test was performed at the Utrecht University GeoLab on ten samples selected across the interval 433.78-409.19 mbsf with a spacing variable from ~50 cm across the J event CIE peak (at 428.5 mbsf) to ~3-4 m below and above. Due to the general scarcity of lipids in our samples, an additional multi-sample analysis was obtained by combining four samples, 4 cm-spaced, at the J CIE peak (428.40 mbsf-428.52 mbsf). We followed the methods for samples preparations in Schouten et al. (2002, 2013) and present this in Supplementary Information. TEX_{86} values were obtained from the abundance of isoprenoid GDGTs according to the equation of Schouten et al. (2002):

TEX_{86}= [GDGT2+GDGT3+cren′]/[GDGT1+GDGT2+GDGT3+cren′]

where GDGTs 1–3 indicate compounds containing 1–3 cyclopentyl moieties, and cren′ refer to the regioisomer of crenarchaeol.

There is an ongoing debate on which is the temperature calibration deriving from the TEX_{86} proxy most appropriate for the warm climate of early Paleogene (Liu et al., 2009; Keating-Bitonti et al., 2011; Hollis et al., 2012; Bijl et al., 2013; Schouten et al., 2013). The most recent TEX_{86} calibration from Kim et al. (2010) invokes two separate indices, the TEX_{86}^{L} and TEX_{86}^{H}. Precisely, TEX_{86}^{L} was calibrated on a global data-set whereas TEX_{86}^{H} was calibrated excluding the polar oceans that present GDGT distributions systematically different. Kim et al. (2010) recommend the use of TEX_{86}^{H} in regions with SSTs >15°. The TEX_{86}^{H} calibration from Kim et al. (2010) should be, therefore, the best available choice for the early Paleogene low-latitude sites where SSTs is expected to be relatively high (Hollis et al., 2012; Schouten et al., 2013; Taylor et al., 2013), as in our case. On other hands, Hollis et al. (2012) noted that SSTs from carbonate sediments with TEX_{86} values >0.85 are better approximated by the Liu et al. (2009) calibration. We decided therefore to convert our TEX_{86} datum from the J event CIE-peak using both the logarithmic equation from Kim et al., (2010):

$$SST=68.4\times\log(TEX_{86})+38.6 \quad (R2 = 0.87;\ \text{standard error} \pm 2.5\ ^{\circ}C)$$

and the non-linear relationship from Liu et al. (2009):

$$SST=50.475-16.332(1/TEX_{86})$$

The BIT (branched isoprenoid tetraether) index can be considered as a proxy to evaluate in marine sediments the fluvially transported soil organic matter versus in situ produced marine organic matter (Schouten et al. 2013). We calculated the BIT index for the multi-sample at the J event CIE-peak, in order to evaluate the influence of terrestrial organic matter

input that could bias the marine SST estimation. This proxy is based on the relative proportion of marine (isoprenoid) GDGTs and terrestrial (branched) GDGTs, according to the following equation from Hopmans et al., 2004:

BIT=[GDGT I]+[GDGT II]+[GDGT III]/[GDGT I]+[GDGT II]+[GDGT III]+[Crenarchaeol]

3.3. Planktic Foraminifera

3.3.1. Samples

Planktic foraminifera were studied on washed residues using a stereomicroscope with an incident light beam. The residues were prepared by immersing previously freeze-dried samples in deionized water. Disaggregation occurred over times varying from a few hours to 3 days, depending on the compactness of sediments. When disaggregated, samples were washed over a >63 micron sieve. Sieves were immersed in a methylene blue bath after each washing in order to colour planktic foraminifera potentially trapped in the sieve mesh. This is an easy method to exclude possible contamination of successive samples. Washed residues were dried at <50 °C. The taxonomic criteria adopted in this study follow Olsson et al. (1999) and Pearson et al. (2006). Planktic foraminiferal biostratigraphy comes from Luciani et al. (2016), who applied the zonal scheme of Wade et al. (2011) and included the modification provided by Luciani and Giusberti (2014). Specifically, Zone E6 is invalid as defined by Wade et al. (2011) due to diachronous first appearance of the marker *Acarinina cuneicamerata* thus *Astrorotalia palmerae* has been tentatively proposed as the new marker for Zone E6 (Luciani and Giusberti, 2014). Actually *A. palmerae* is absent at Site 1051 therefore Zones E6/E7a have been combined.

3.3.2. Planktic Foraminiferal and Radiolarian Abundances

Relative abundances of planktic foraminiferal genera, *Morozovella* species and radiolarians were determined by counting at least 300 specimens in the >63μm size-fraction from random splits but were generated at different resolution.

Sixty-two new samples were analysed to refine records of planktic foraminiferal genera *Morozovella*, *Acarinina* and subbotinids presented in Luciani et al. (2016) (Table S2) with the primary aims to verify the link between the planktic foraminiferal switch and the J event and to establish whether other changes in abundance occurred across other early Eocene CIEs. Specifically, ten samples were studied across the J event at spacing between 5 cm and 20 cm

and the remaining samples at spacing from 40 cm to 1.0 m (Table S2). Within the "*Subbotina* group" are included representatives of both *Subbotina* and *Parasubbotina*, as these genera are suspected of having strong paleoecological affinities (Pearson et al., 2006, and references therein).

Quantitative data on various *Morozovella* species were not presented in the work by Luciani et al (2016), but this aspect is important for a more comprehensive documentation of the early Eocene morozovellid decline and potentially useful to understanding possible causes for the planktic foraminiferal shift. We selected therefore 50 representative samples throughout the entire investigated succession to document variations in the relative abundances of different *Morozovella* species (Table S3). Ten of these samples are the same as those examined for high-resolution changes in genera abundance across the J event; the remaining samples come from below or above, and are at lower resolution (Table S3). The abundance of the *Morozovella* species was estimated as the number of each species over the total planktic foraminiferal assemblage.

Radiolarian abundances were determined on at least 300 specimens with respect to foraminifera on the same 50 samples selected for the *Morozovella* species.

3.3.3. Maximum Size of the *Morozovella* Species

To examine variations in morozovellid test-size across the EECO, we measured the maximum linear length perpendicular to the coiling axis of all specimens present in the >300μm size-fraction (generally 100 specimens) from five samples (Fig. 3). This fraction was obtained through dry sieving the selected >63μm size-fraction residues. Measurements were taken using the stereomicroscope at 80 magnification using the Zeiss ZEN-Core software with instrumental error of ±1μm (Table S4). We calculated, for each of the five samples, the mean value of this parameter and the relative standard deviation (1σ) for each morphologically defined morozovellid species (Table S4).

3.3.4. Size-Restricted $\delta^{13}C$ Analyses

As bleaching is suspected to affect foraminiferal abundance, test-size and stable carbon isotope composition (e.g., Bé et al., 1982; Caron et al., 1982; Wade et al., 2008; Edgar et al., 2012), we generated $\delta^{13}C$ data from planktic foraminiferal specimens of different sizes. The samples selected for this exercise are the same five as noted above (Figs. 3, 4). The species examined were *Morozovella aragonensis*, *M. crater*, *M. subbotinae*, *M. gracilis* and *M.*

marginodentata. However, we also examined samples of *Acarinina* spp. and of the asymbiotic genus *Subbotina* (e.g., Pearson et al., 2006 and reference therein). We mainly focused on *Acarinina esnaensis* and *A. interposita* in samples A, B and C, and on *A. quetra* in samples D and E to limit interspecific variability. This is because the relative abundance and preservation of these species changes with depth/time. For the subbotinids, analysis mainly includes samples of *S. roesnaensis* and *S. patagonica*.

Specimens were picked from restricted size fractions, separated by dry sieving of the previously obtained washed residues >63 μm fraction. The size fractions include from 150 to 200μm, from 200 to 250μm, from 250 to 300μm, from 300 to 350μm, and from 350 to 400μm. In order to generate a reliable $\delta^{13}C$ record, the picked specimens were carefully checked for good preservation, and heavily recrystallized or infilled tests were removed (as they would probably have isotope signals heavily modified by diagenesis (e.g., Pearson et al. 2001; Sexton et al. 2006; Pearson, 2012). Between 10 and 50 individuals, depending on availability, were analysed from each size fraction to reach at least 250 μg. Notably, while morozovellids were present in the >350μm fraction, they were generally too scarce or too poorly preserved for selecting a quantity amenable for our stable isotope analysis. Furthermore, we were not able to analyse *Morozovella formosa* in such a manner, as its scarce abundance throughout did not allow to sufficient specimens in the different size fractions. The scarcity of *M. marginodentata* in sample D also did not permit collection of an adequate number of specimens. Lastly, we avoided analysing specimens of *M. aequa* and *M. lensiformis*, because tests of these species frequently present evidence of significant recrystallization (Fig. S2).

4. Results

4.1. Bulk Carbon Isotope Records

Bulk carbonate carbon isotope values at Site 1051 range between ~0.00 and ~1.50‰, with an average of 0.85‰ (Fig. 2, Table S1). The fairly high-resolution $\delta^{13}C$ record shows both trends and excursions. From a broad perspective, $\delta^{13}C$ decreases from the base of the studied interval toward at prominent low at 417.3 mbsf and increases above.

Nine negative CIEs, with magnitudes between ~0.20‰ and ~0.70‰, can be identified in our record at Site 1051. These are labelled for convenience as CIE1–CIE9 (Fig. 2). The CIE1, which occurs at 452.73 mbsf, is the most prominent, with a ~0.70‰ shift from background

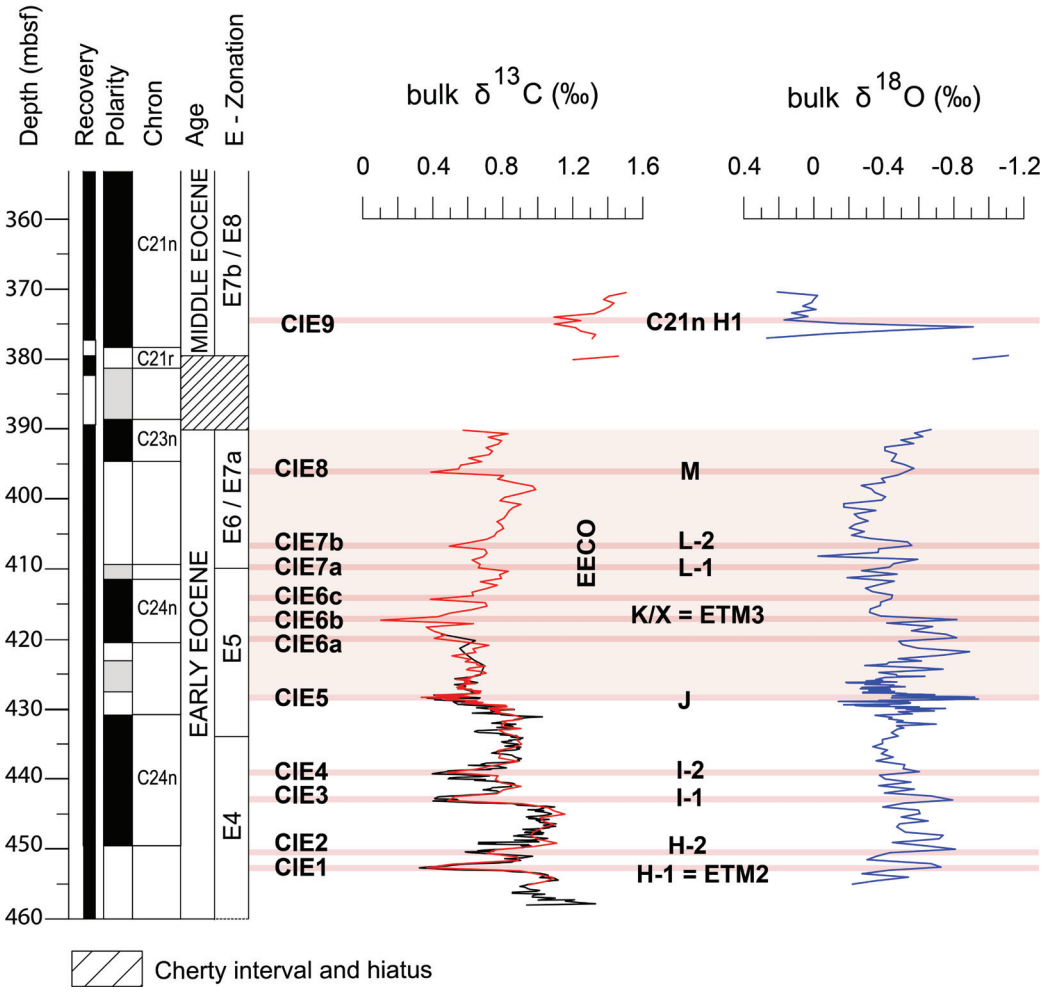

Figure 2. Bulk sediment carbon and oxygen stable isotope curves plotted against depth across the early Eocene at Ocean Drilling Program (ODP) Site 1051. The black $\delta^{13}C$ curve is from Cramer et al. (2003). The foraminiferal zonation scheme follows that presented by Wade et al. (2011), but as modified by Luciani and Giusberti (2014). Magnetostratigraphy comes from Ogg and Bardot (2001), but with an important modification to polarity chron labelling as discussed in subsequent literature (Cramer et al., 2003; Luciani et al., 2016). The thin light-red bands highlight significant negative carbon isotope excursions (CIEs). The pink shaded band defines the Early Eocene Climatic Optimum (EECO) interval, although the end cannot be shown at Site 1051 because of the interval with missing core and chert.

values. Other pronounced CIEs are CIE3 (443.13 mbsf), CIE5 (428.34 mbsf), CIE6b (417.30 mbsf) and CIE8 (396.10 mbsf), with negative shifts of 0.61‰, 0.56‰, 0.53‰ and 0.40‰, respectively. Smaller CIEs (<0.40‰) occur both in the early Eocene and earlier middle Eocene. These are CIE2 (450.67 mbsf), CIE4 (439.08 mbsf), CIE6a (419.90 mbsf), CIE6c (414.30 mbsf), CIE7a (409.80 mbsf), CIE7b (406.70 mbsf), and CIE9 (374.90 mbsf) (Fig. 2, Table S1).

Cramer et al. (2003) generated a high-resolution $\delta^{13}C$ bulk record for Site 1051 that partially covers the interval of interest (from the base up to ~420 mbsf). The trend of their bulk-carbon profile and the main excursions compliment our $\delta^{13}C$ bulk record although with

slight differences. Specifically, our CIE1 and CIE2 are ~0.1‰ and ~0.2‰, respectively, lower and our CIE6a is ~0.1‰ higher. Such differences can be expected, given reported analytical errors and different sampling depths.

The comparison of $\delta^{13}C$ changes to bio- and magneto-stratigraphy is crucial to the correlation of early Paleogene records from different locations. Most of the CIEs recorded in the early Eocene at Site 1051 occurred during Chron C24. Precisely, CIE1 and CIE2 fall in upper Chron C24r (Zone E4), CIE3 and CIE4 fall in the middle of Sub-Chron C24n.3n (upper Zone E4), CIE5 falls at the transition of Sub-Chron C24n.2r and C24n.2n (lower Zone E5), and CIE6a–CIE6c fall within Sub-Chron C24n.1n (middle-upper Zone E5). Above, CIE7a, CIE7b and CIE8 occurred during Chron C23r and lie within the merged foraminiferal Zone E6/E7a, and CIE9 occurred during the base of Chron C21n and lies within the merged foraminiferal Zone E7b/E8.

4.2. Bulk Oxygen Isotope Records

Bulk carbonate oxygen isotope values at Site 1051 vary between 0.14‰ and –0.95‰ in the early Eocene, and from 0.00‰ and –1.11‰ in the earlier middle Eocene, with a mean value of –0.45‰ (Fig. 2, Table S1). Two intervals with trends to lower $\delta^{18}O$ values are found within the main phase of the EECO. The lower interval occurs between 428.78 and 417.30 mbsf, and spans CIE5–CIE6b. The most negative values within this interval approach –0.9‰. The upper interval occurs between 408.68 and 390.10 mbsf, which corresponds to the base of the unrecovered interval, and where $\delta^{18}O$ values reach ~ –0.70‰. Samples above the missing section (377.0–370.4 mbsf) display a mean $\delta^{18}O$ value of ~0‰ that includes two single-sample shifts to ~ –1‰. The mean values of $\delta^{18}O$ for the earlier middle Eocene, therefore, are significantly ”heavier” (~0.5‰) with respect to those of the early Eocene.

Similar to $\delta^{13}C$, several negative $\delta^{18}O$ excursions punctuate the overall $\delta^{18}O$ trends at Site 1051. Interestingly, these show a clear correspondence to the CIEs (Fig. 2). The two most prominent $\delta^{18}O$ negative shifts are of ~0.8‰ (428.68 mbsf) and ~0.5‰ (406.70 mbsf) and coincide respectively with CIE5 and CIE7b. Other negative shifts coinciding with the CIEs are of ~0.3–0.4‰ and occur at 452.73 (CIE1), 450.17 (CIE2), 443.13 (CIE3), 439.08 (CIE4), 419.9 (CIE6a), 417.3 (CIE6b), and 408.68 (CIE7a).

4.3. TEX_{86} Record and BIT Index

Isoprenoidal GDGTs containing cyclopentane rings are very scarce throughout the studied interval. All the 10 individual samples analysed have concentrations below the detection limit (Schouten et al., 2002; 2013). The sole valuable datum comes from the combined sample at the peak of CIE-5. Despite analyzing a large amount of sediment (~60 g) for this sample, concentrations of some GDGTs, such as the GDGT-1 and GDGT-3, remain only close to the detection limit. On other hand, crenarcheol and its regioisomer, GDGT-4 and GDGT-4′, are particularly abundant. The BIT-value obtained for this combined sample is very low (0.126).

4.4. Abundance Changes in *Acarinina, Morozovella,* Subbotinids and Radiolarians

Abundant and diverse planktic foraminifera characterize the studied succession. The population is distinctive of open-ocean assemblages, and washed residues also include significant numbers of radiolarians throughout (Shipboard Scientific Party, 1998; Luciani et al., 2016). Planktic foraminifera generally show a 'frosty' preservation (*sensu* Sexton et al., 2006), and probably have a certain amount of recrystallization. However, they are generally free of infilling (Fig. S2).

Overall trends in planktic foraminiferal genera *Acarinina*, *Morozovella* and subbotinids basically resemble those determined at lower sample resolution (Luciani et al., 2016). The most noticeable refinement is that the marked and permanent decline in *Morozovella* abundance precisely coincides with CIE5. *Morozovella* percentages in samples decrease from a mean value of 43% to 12% across this short interval (Fig. 3, Table S2**).** This decline was counterbalanced by a prominent increase in *Acarinina* abundance, from a mean value of 37% below CIE5 to 62% above. The thermocline-dwelling *Subbotina* group slightly and gradually increase their abundance upward, from a mean value of ~15% in the early Eocene to ~25% in the middle Eocene.

Beyond the major switch, several transient variations in the abundance of planktic foraminiferal genera relate to the identified CIEs (Fig. 3). This is best realized in the record of *Acarinina* abundance, which has marked peaks generally corresponding to CIEs. Peaks in the abundance of *Morozovella* are mainly out of phase with those of *Acarinina*.

The mean abundance of radiolarian tests across the studied interval is 27.3% (Fig. 3). However, this abundance increases significantly within the EECO, where it averages 43.7%

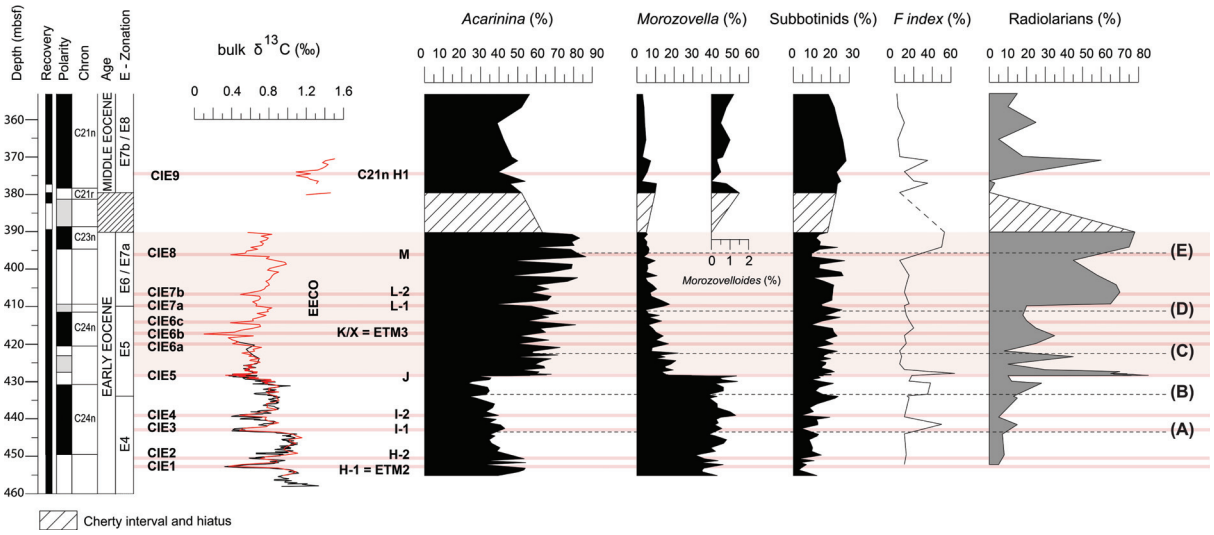

Figure 3. Stratigraphy, bulk sediment $\delta^{13}C$ composition, fragmentation index (*F index*, from Luciani et al. (2016), and relative abundances of primary planktic foraminiferal genera and radiolarians for the early Eocene interval at ODP Site 1051. Subbotinids include the ecologically similar genera *Subbotina* and *Parasubbotina*. Note that the major switch in *Morozovella* and *Acarinina* abundances precisely coincides with CIE-5, which corresponds to the J event and the onset of the EECO. (A) through (E) indicate the position of the five samples used to examine the size and stable isotope composition of *Morozovella* species. (A) and (B) are from the pre EECO interval, (C) is at the beginning of EECO, just after the J event, and (D) and (E) are from within the main EECO phase. Dashed lines help to identify the position of these samples, and other information is consistent with Figure 2.

and has a peak of 78.0%. The first prominent increase in radiolaria abundance (65-70%) corresponds to the marked morozovellid decline, and the maximum occurs just before the mostly unrecovered chert interval.

4.5. Variations in *Morozovella* Species

The distribution of *Morozovella* species within samples changes significantly with depth and time (Fig. 4). Preceding CIE5, *M. crater* and *M. marginodentata* are the most abundant forms (mean abundance of 8.6% and 10.4%, respectively). After this event, *M. crater*, *M. aragonensis* and *M. lensiformis* are the most common species (mean abundances of 5%, 3% and 2%, respectively).

The major switchover in planktic foraminifera is complex at the species level (Fig. 4). Coincident with CIE5, *M. marginodentata* and *M. gracilis* exhibit large reductions in mean abundance from 11.0% to 2.5% (former) and from 7.0% to 2.0% (latter); *M. subbotinae* and *M. crater* also display a drop in average abundance from 5.0% to 1.5% and from 9.1% to 4.3% respectively. The abundance of *M. aequa* decreases from mean values of 3.5% to 0.5%, but this reduction started between CIE4 and CIE5. By contrast, *M. formosa* remains rare (~1%) and *M. aragonensis* gradually increases upward across the interval investigated. The

abundance of *M. lensiformis* remains almost constant, except for a slight decrease in abundance (of ~2%) between CIE5 and CIE6c. As a consequence of the turnover, *M. crater* and *M. aragonensis* are the sole species that contribute significantly to the *Morozovella* population in middle Eocene sediment at Site 1051 (Fig. 4). Transient oscillations in the abundance of different *Morozovella* species are generally in phase, with the exception of *M. marginodentata*.

In summary, the pre-EECO interval at Site 1051 has a diverse *Morozovella* population with all early Eocene species (e.g. Pearson et al., 2006; Aze et al., 2011) represented (Fig. 4). Moreover, key *Morozovella* events are readily identified and include the following. The top (T) of *M. marginodentata* is recorded at 409. 80 mbsf (base C23r) at the upper boundary of Zone E5. The T of *M. gracilis* and T of *M. aequa* are recorded at 401.68 mbsf (middle C23r) and 394.10 mbsf (basal C23n), respectively, and within Zone E6/E7a. The base (B) of *M. caucasica* occurs at 397.65 mbsf (middle C23r) and within Zone E6/E7a, although this taxon is quite rare and unevenly distributed above its first appearance. Clear identification of the T of *M. formosa* and T of *M. lensiformis* are prevented by the occurrence of the unrecovered interval between 382 and 390 mbsf.

Most of the *Morozovella* species at Site 1051 became rare to very rare below the level of their definitive disappearances (Fig. 4). One can distinguish in some cases, therefore, a top of common occurrence (T_c), which occurs below the aforementioned horizons. As an example, the T_c of *M. marginodentata* is found at ~422.4 mbsf, and well below its T at 409.8 mbsf. This is important for stratigraphic reasons because rare specimens might be missed. The position of the T_c of *M. marginodentata* at Site 1051 is in perfect agreement with the T of this species in the Tethyan Possagno section (Luciani and Giusberti, 2014), whereas the true T of *M. marginodentata* is more consistent with stratigraphic concepts presented by Berggren and Pearson (2005). Due to our detailed counting in samples collected at fairly high spatial resolution, our record of lowest and highest occurrences of *Morozovella* species differs from that reported by the Shipboard Scientific Party (1998).

4.6. Variations in Test-Size of *Morozovella* across the Early Eocene

Measurements of the largest *Morozovella* species test-size, i.e., the maximum diameter of the morozovellids from the ≥300μm size-fraction, are shown in Fig. 4 as converted to a mean value for each species. From such record it emerges that at Site 1051 the most significant change is a test-size reduction involving almost all the *Morozovella* species at the sample C,

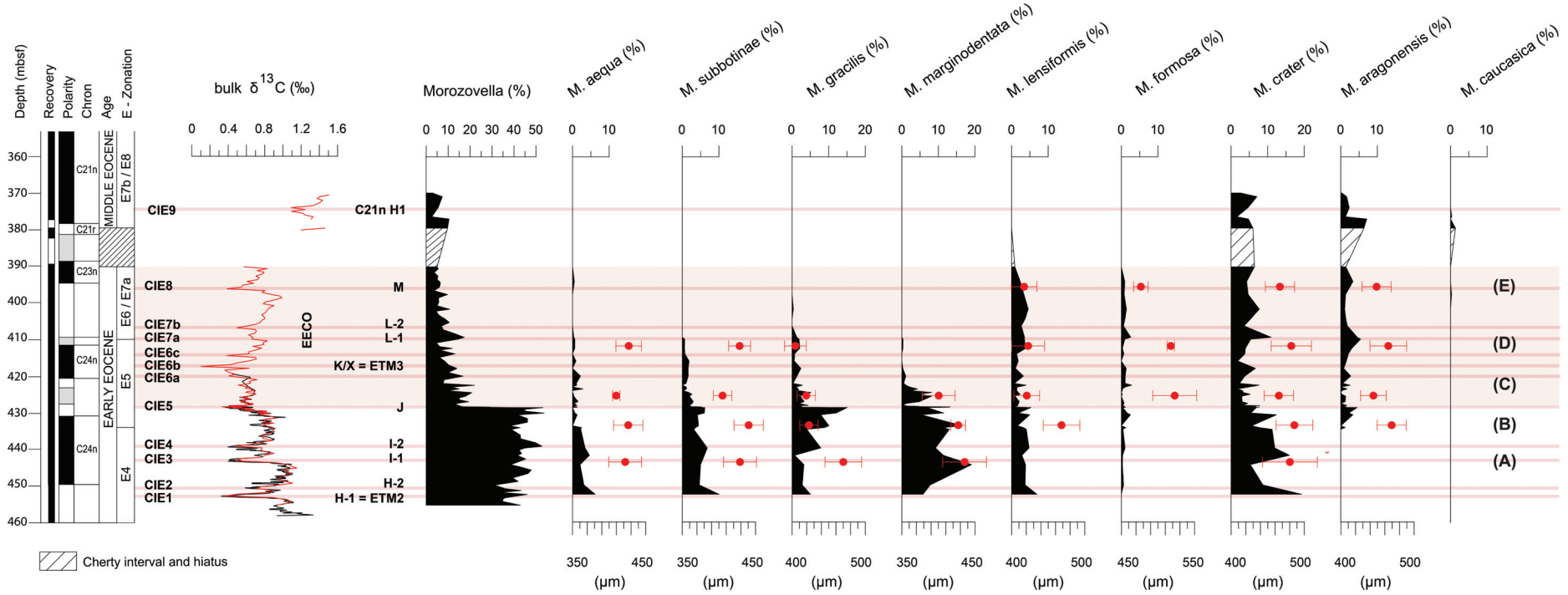

Figure 4. The bulk sediment $\delta^{13}C$ curve across the early Eocene interval at ODP Site 1051 along with relative abundances of *Morozovella* species. Note that the major permanent decline in *Morozovella* at the EECO onset mainly happens because of reductions in *M. gracilis* and *M. marginodentata* abundances and, to a lesser extent, *M. crater* and *M. subbotinae* abundances. Red symbols for each *Morozovella* species indicate the mean values (box) and standard deviation (bar) for the size of tests present in the ≥300µm fraction (generally ~100). Note the drop in test-size for almost all *Morozovella* species in sample C. The thin light-red bands highlight the main carbon isotope excursions (CIEs). Other information is the same as in previous figures.

during the initial EECO interval (Figs. 4, 5). This reduction is particularly marked for *M. lensiformis* (~50 μm), *M. marginodentata* (~30 μm) and *M. subbotinae* (~35 μm) while it is less evident for *M. aequa* (~15 μm), *M. aragonensis* (~20 μm) and *M. crater* (~20 μm). The *M. lensiformis* test-size does not recover above the sample C since this species stabilizes its largest size at mean values of 420 μm instead of 470 μm. *Morozovella marginodentata* decreases its size from the base upward, passing from 435 μm at sample A to 400 μm at sample C. This species further reduces its size resulting absent in the ≥300μm fraction at sample D (Figure 4). The species *M. aequa, M. aragonensis, M. crater* and *M. subbotinae*, almost recover their largest size above the CIE5, in samples D and E, reaching the values of 430 μm, 465 μm, 480 μm and 430 μm respectively. *Morozovella formosa* records a drop of ~40μm in test-size only at sample E. The test-size of *M. gracilis* shows a significant and permanent drop moving from a mean value of 470 μm to 410 μm starting from the pre-EECO interval (sample B).

4.7. Stable Isotopes and Test-Size

The typical isotopic signature of symbionts-bearing foraminifera presents a distinct gradient of $\delta^{13}C$ increase with increasing in test-size (e.g. Spero and DeNiro, 1987; Spero and Lea 1993; D'Hondt et al. 1994; Norris 1996; Wade et al., 2008). To test whether morozovellids maintained this signal across the EECO we analysed for theirs size-constrained $\delta^{13}C$ composition *Morozovella* species along with specimens of *Acarinina* spp. and *Subbotina* spp., as a comparison with other symbiotic and asymbiotic genera (e.g., Shackleton et al., 1985; Pearson et al. 2006, and references therein).

The test-size affects the stable isotope composition of certain planktic foraminifera at Site 1051 (Fig. 6). For most of the examined samples, there is indeed a clear increase in the $\delta^{13}C$ composition of *Morozovella* species with respect to size (i.e. exist a gradient). This is also true for the mixed *Acarinina* species whereas *Subbotina* does not display any clear variation in $\delta^{13}C$ with respect to different test-sizes. The $\delta^{13}C$ gradient among the examined size-fractions of *Morozovella* species and *Acarinina* spp. generally exceed the 0.7‰. Nonetheless, *M. marginodentata* and *M. subbotinae* recorded a significant decline of ~0.5‰ in the $\delta^{13}C$ gradients in the sample C at the initial EECO (Fig. 6). This reduction is paralleled with a decrease in their test-size (section 4.6, Figs. 4, 5). The variation in size-$\delta^{13}C$ gradients recorded by *M. subbotinae* is however transient since this species exhibits a complete restored

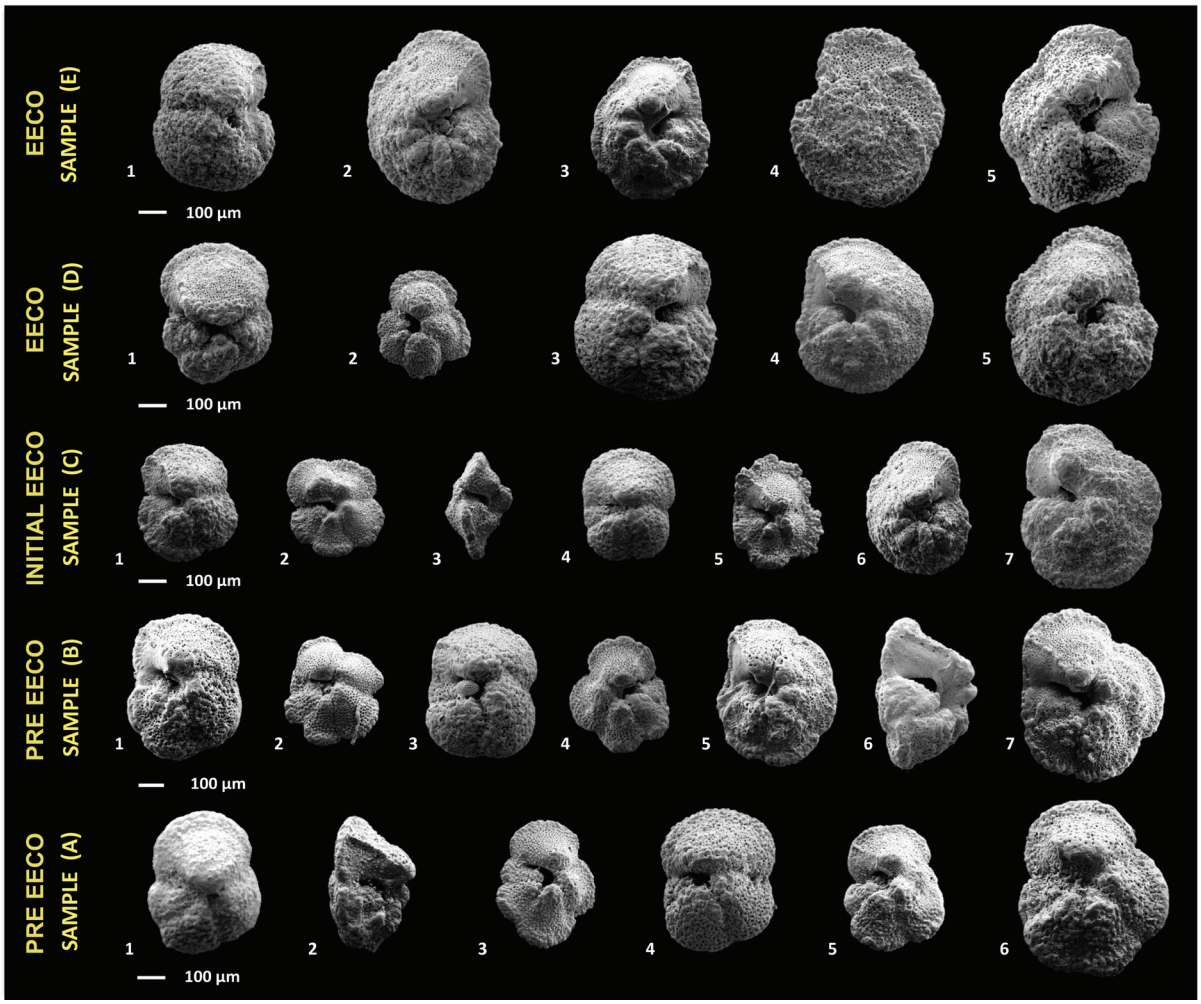

Figure 5. SEM images showing variations in size of some *Morozovella* species through the five analyzed samples at Site 1051 fro the bleaching test. Sample A (*443.58 mbsf*) 1−2: *M. subbotinae*, 3: *M. gracilis*; 4: *M. aequa*; 5: *M. marginodentata*; 6: *M. crater*. Sample B (*432.98 mbsf*) 1: *M. subbotinae*; 2: *M. garcilis*; 3: *M. aequa*; 4: *M. marginodentata*; 5: *M. aragonensis*; 7: *M. crater*. Sample C (*423.98 mbsf*) 1: *M. subbotinae*; 2−3: *M. gracilis*; 4: *M. aequa*; 5: *M. marginodentata*; 6: *M. aragonensis*; 7: *M. crater*. Sample D (*410,30 mbsf*) 1: *M. subbotinae*; 2: *M. gracilis*; 3: *M. aequa*; 4: *M. arogonensis*; 5: *M. crater*. Sample E (*395,10 mbsf*) 1: *M. aequa*; 2−3: *M. aragonensis*; 3−4: *M. crater*. Note that the almost whole *Morozovella* population displays a transitory reduction in size sample C (initial EECO).

and even enhanced test size-$\delta^{13}C$ gradients in the samples D. It is not possible to verify whether the reduction in the test size-$\delta^{13}C$ gradient is transient for *M. marginodentata* as this species is extremely rare above the sample C phase thus not allowing the collection of a sufficient number of specimens for the isotope analysis and it disappears within the main-EECO phase. The genus *Acarinina* records as well a significant, though transient, decline in test size–$\delta^{13}C$ gradient of ~0.5‰ at the samples B and C (Fig. 6). Interestingly, *M. aragonensis* and *M. crater* record an increased test size-$\delta^{13}C$ gradient (~0.5‰) in samples D and E, during the main-EECO phase.

In terms of absolute mean values, subbotinids are characterised by a lighter $\delta^{13}C$ composition (from ~0.5 to ~1.0‰) with respect to *Acarinina* and morozovellids that show $\delta^{13}C$ values comprised between ~1.0‰ and ~3.0‰ (Fig. 6). A general trend towards lighter values is clearly evident within the EECO phase in both *Acarinina* and *Morozovella* which moved from ~2‰-3‰ at sample A to 0.75‰-2.20‰ at sample E. These lighter values result therefore closer to those of *Subbotina* in sample E. The $\delta^{18}O$ record shows general lighter compositions for the surface-dweller *Morozovella* and *Acarinina* with respect to the thermocline-dweller subbotinids, as expected (e.g., Shackleton et al., 1985) (Table S5, Fig. S3).

5. Discussion

5.1 Early Eocene Carbon Cycle Perturbation at Site 1051

The bulk $\delta^{13}C$ signal from pelagic sediments with low organic carbon and substantial carbonate content should reflect past global changes in paleoceanographic conditions (i.e. composition of surface water dissolved inorganic carbon (DIC), Scholle and Arthur, 1980; Frank et al., 1999). For such sediments, almost all carbon in small volumes exists indeed as carbonate thus ensuring that, even when transformation to indurated limestone occurs, $\delta^{13}C$ values remain similar to those originally deposited on the seafloor. For such reason, the $\delta^{13}C$ record at Site 1051 (Fig. 2) can be compared to records generated elsewhere (Fig. S1).

Bulk carbonate $\delta^{13}C$ record exists across the EECO at ODP Site 1258 (Demerara Rise, western equatorial Atantic, Kirtland Turner et al., 2014), ODP Site 1262 (Walvis Ridge, southeast Atlantic, Zachos et al. 2010), DSDP Site 577 (Shatsky Rise, northwest Pacific, Dickens & Backman 2013; Luciani et al., 2016), Mead Stream and Branch Stream sections (New Zealand, Hancock et al. 2003; Nicolo et al. 2007; Slotnick et al. 2012, 2015), Possagno section (north-eastern Italy, Luciani et al., 2016) and Contessa Road section (central Italy, Coccioni et al., 2012). A detailed $\delta^{13}C$ record of benthic foraminifera (*N. truempyi*) is provided for the ODP Site 1263 (Walvis Ridge, Lauretano et al., 2016). Our overall $\delta^{13}C$ bulk record is indeed similar in shape and trends to other records being particularly consistent, also in the mean absolute values, with that from the equatorial Atlantic Site 1258 (Kirtland Turner et al., 2014). Nonetheless, mean bulk $\delta^{13}C$ values from the New Zealand sections of the Clarence Valley (Slotnick et al. 2012, 2015), from the southern Atlantic Site 1262 (Zachos et

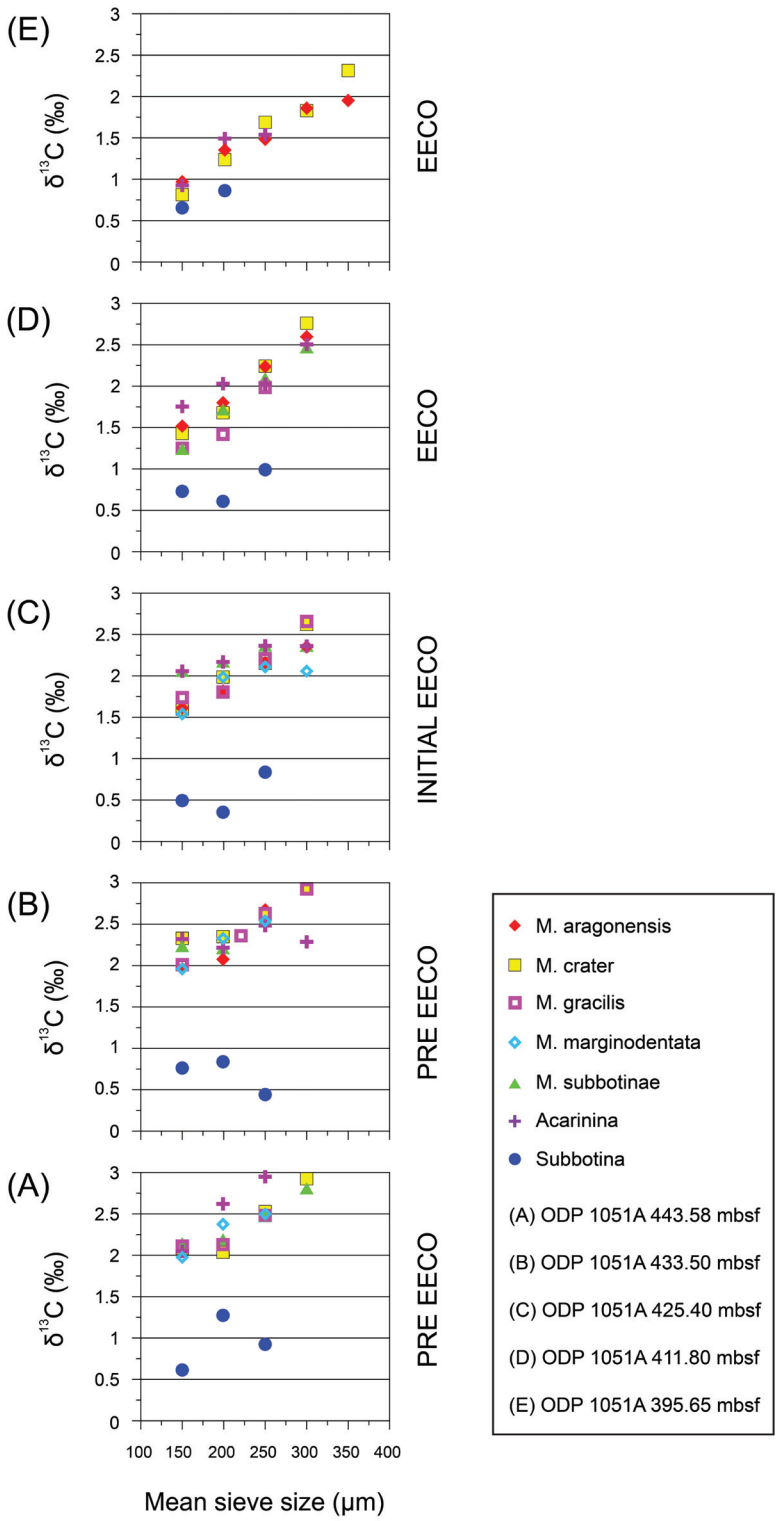

Figure 6. Planktic foraminiferal δ^{13}C-test size trends from five selected samples (A−E) located below and across the EECO at the ODP Sites 1051. Position of the analysed samples is shown in figures 2, 3. The δ^{13}C data were generated using monospecific specimens of the known photosymbiont-bearing species *Morozovella aragonensis* (red solid-diamonds), *M. crater* (yellow solid-squares), *M. gracilis* (pink open-squares), *M. marginodentata* (light-blue open-diamonds) and *M. subbotinae* (green solid-triangles), the *Acarinina* spp. (purple solid-crosses) and of the asymbiotic genus *Subbotina* (blue solid-circles). Note the reduction in test size–δ^{13}C gradient for *M. marginodentata* and *M. subbotinae* at the initial EECO (sample C). This reduction is coincident with a decrease in maximum test size (see figures 4, 5 and discussion in the text) and can be therefore related with an episode of bleaching.

al., 2010), and the equatorial Pacific Site 577 (Luciani et al. 2016) exceed those at Site 1051 by a nominally 0.4‰, 0.5‰ and 0.6‰ respectively whereas values from the Tethyan sections of Possagno (Luciani et al. 2016) and Contessa Road (Coccioni et al., 2012) are ~0.2‰ lower across the EECO. Interestingly, bulk $\delta^{13}C$ records from Site 1051 and the Possagno section, both reaching the early middle Eocene, are characterized by similar absolute values across the C21n. A significant offsets of ~0.8‰ is observed with the *N. truempyi*-based $\delta^{13}C$ curve from southern Atlantic Site 1263 (Lauretano et al., 2016). This is partially due to the fact that this latter curve is based on a benthic foraminiferal record thus reflecting variations of deep water DIC composition. In general, the offsets existing among bulk carbonate $\delta^{13}C$ values from different locations reveal recrystallization or lithification because similar offsets appear across numerous records independent of post depositional history but dependent on location (Schmitz et al., 1996; Cramer et al., 2003; Slotnick et al., 2012, 2015; Agnini et al., 2016; Luciani et al., 2016). Moreover, a clear increase in the $\delta^{13}C$ record is evident from the North Atlantic and western Tethys (low-values), through the South Atlantic and the Indian Ocean, to the Pacific (high-values), although this signature is partially related to a latitudinal component.

Superimposed on long-term trends a series of negative CIEs also can be found in the aforementioned early Paleogene stable isotope records (Figs. 2 and S1). Some correlation problems are mainly related to the diverse resolution of $\delta^{13}C$ records or to different sedimentation rates. Following Cramer et al. (2003), the CIE1–CIE5 present in the lower portion of our $\delta^{13}C$ bulk record are here correlated with the events H1, H2, I1, I2 and J. The prominent CIE6b at Site 1051 marks the worldwide documented K/X event (e.g., Cramer et al., 2003; Röhl et al., 2005; Thomas et al., 2006; Agnini et al., 2009; Westerhold and Röhl, 2009; Galeotti et al., 2010; Leon-Rodriguez and Dickens, 2010; Coccioni et al., 2012, Slotnick et al., 2012, 2015; Frontalini et al., 2016; Lauretano et al., 2016; Luciani et al., 2016), also referred as ETM3 (Zachos et al., 2010) or C24n.1n-H1 event (Kirtland-Turner et al., 2014). The minor $\delta^{13}C$ negative shifts CIE6a and CIE6c, respectively recorded closely below and above the K/X event at the C24n.1n base are more difficult to be widely correlated. However, similar shapes in the $\delta^{13}C$ curve can be detected at the equatorial Atlantic Demerara Rise (Site 1258, Kirtland-Turner et al., 2014), at the Walvis Ridge of southern Atlantic (Site 1263, Lauretano et al., 2016) and at the New Zealand Mead Stream (Slotnick et al., 2012) and Branch Stream sections (BS-CIE-6 and BS-CIE-8, being BS-CIE-7 the K/X event, Slotnick et al., 2015). The CIE7a, that is placed at the C23r/C24n.1n boundary, can be correlated with the L event that was firstly identified by Cramer et al., 2003 and successively documented in

several other locations (Contessa Road, Coccioni et al., 2012; Mead and Branch Stream, Slotnick et al., 2012, 2015a; ODP Site 1258, labelled as C23r-H1 in Kirtland-Turner et al., 2014; ODP Site 1263, Lauretano et al., 2016; DSDP Site 577, Luciani et al., 2016). The CIE7b is recorded closely above the L event and can be as well correlated with other records (Contessa Road, Coccioni et al., 2012; Mead Stream, Slotnick et al., 2012; ODP Site 1258, Kirtland-Turner et al., 2014; ODP Site 1263, Lauretano et al., 2016; DSDP Site 577, Luciani et al., 2016). Such excursions are closely spaced, similarly to the paired events that characterize the interval preceding the EECO (e.g., H1-H2 and I1-I1). We interpret therefore the CIE7b as the second shift of the paired L events. The magneto-stratigraphic position of CIE8 at Site 1051 suggests a correlation with the event named as M in Coccioni et al. (2012) and Lauretano et al. (2016), the same labelled as C23r-H2 in Kirtland-Turner et al. (2014) and possibly with the event 2 in Luciani et al. (2016). The CIE9, here named as C21n-H1 following the labelling used in Kirtland-Turner et al. (2014) is recorded at Site 1051 at the base of C21n, in a comparable stratigraphic position with a negative shift present at the Possagno $\delta^{13}C$ curve (Figs. 2, S1). From the early Eocene $\delta^{13}C$ records it appears that a major shift in frequency and amplitude of carbon isotope excursions happened during the EECO.

5.2. Oxygen-Isotopes and TEX_{86} Paleotemperature Record

The bulk oxygen stable-isotopes from Site 1051 traces the general global trend recorded by the stacked benthic foraminferal curves (Zachos et al., 2001, 2008) and the bulk oxygen profile from DSDP Site 577 (Shatsky Rise, Luciani et al., 2016) that record the lowest $\delta^{18}O$ values within the EECO. Mean values of $\delta^{18}O$ at Site 1051 for the earlier middle Eocene are significantly ”heavier” (~0.5‰) with respect to those of the early Eocene as also observed in the ^{18}O stacked benthic foraminifera curves.

Carbonate oozes that constitute the Eocene Site 1051 sediments derive from calcareous nannofossils and planktic foraminifera with a marginal contribute of benthic foraminifera that are very rare throughout (Norris et al. 1998). Since Site 1051 sediments are still “ooze” (Shipboard Scientific Party, 1998), one might expect that ^{18}O values record past mixed-layer to subsurface paleotemperatures depending on the contribution of the various components involved. Bulk carbonate ^{18}O values for Holocene oozes reveal indeed the average temperatures in the mixed layer (Shackleton and Hall, 1995; Reghellin et al., 2015). However, vital effects due to the dominant nannoplankton may increase the ^{18}O by nominally 1‰ (e.g., Bemis et al., 1998; Reghellin et al., 2015). According to Mita (2001) the stratigraphic interval of the Site 1051 here studied comprises calcareous chalk, implying that nannosfossils were

not dominant. Nevertheless, calcareous plankton preservation may also alter the original signal. Nannofossil preservation is poor to moderate with specimens marked by overgrowth (Mita, 2001). Planktic foraminifera at Site 1051, though well recognizable, present a "frosty" preservation (Sexton et al., 2006) (Fig. S2) that is known to be somewhat influenced by diagenesis. Resulting $\delta^{18}O$ values reflect therefore the partial recrystallization that occurred at seafloor temperatures (e.g., Pearson et al. 2001; Sexton et al. 2006; Pearson, 2012) that are much lower than those in the surface waters where the foraminifera calcified (e.g., Schrag et al., 1995; Pearson et al., 2001; Stap et al., 2010; Kozdon et al., 2011). The "frosty" preservation is commonly observed from oceanic sites and compromises the reliability of oxygen isotopes as paleotermometer (e.g., Pearson et al., 2001; Sexton et al., 2006). Following the consideration above, we avoid to derive temperatures from our bulk oxygen-derived.

The obtained TEX_{86}^{H} value of 0.915 at the J event CIE-peak was converted to a SST of ~36°C according to the calibration of Kim et al. (2010). A lower SST of 32.6°C was obtained using the Liu et al. (2009) non-linear equation. Our TEX_{86}-derived temperature is comparable to the SSTs reported for the PETM CIE-peak from the North Atlantic shallow-marine records of Bass River (33.5°C, Sluijs et al 2007) and from the Wilson Lake (35.7° C, Zachos et al., 2006). It must be highlighted however that the TEX_{86} proxy has the limitation related to the possible scarce preservation of GDGTs. Furthermore, the most extended range of calibration is from –3°C to 30°C (Kim et al., 2010) and has insufficient resolution to evaluate the Eocene temperatures that are estimated to be as much higher than 30°C (e.g., Pearson et al., 2007; Hollis et al., 2012; Dunkley-Jones et al., 2013). This restriction does not allow a completely reliable interpretation of TEX_{86}-derived paleotemperatures across the studied interval. Furthermore, recent studies emphasise that TEX_{86} has been calibrated on recent sea-surfaces, where latitudinal gradient is steeper, and it is commonly employed as a proxy for sea-surface temperatures, despite evidence that *Thaumarchaeota* are often most common in subsurface ocean (Ho and Laepple, 2016; Ingalls, 2016). This inappropriate calibration would have induced overestimated warming at the poles during the early Eocene (Ho and Laepple, 2016). In addition, Ingalls (2016) advises that *Thaumarchaeota* add or remove cyclopentane and cyclohexane rings in response to several environmental stressors beside temperature as it emerges from both marine water column and culture observations. As an example, when *Thaumarchaeota* live in optimal conditions display cooler temperatures than when they are stressed (Ingalls, 2016). These studies suggest therefore that TEX_{86} index unlikely will remain a proxy for temperature alone.

The terrestrial influx is minimal at Site 1051 since the BIT-value obtained for our sample at the J event CIE-peak is very low (0.126) thus implying that and the TEX_{86} derived SST is genuine. This record can be expected from Site 1051 that was drilled at the most distal location from land with respect to the other sites from the Leg 171 B transect (Shipboard Scientific Party, 1998).

5.3. Variability in Planktic Foraminiferal Population at the Early Eocene Hyperthermals and EECO

Early Eocene planktic foraminifera display at Site 1051 both striking long-term and transitory changes, the latter largely coincident with the main carbon and oxygen isotope excursions (Figs. 2, 3). Our high-resolution record clearly shows the permanent switch between *Morozvella* and *Acarinina* abundances (Luciani et al., 2016), but also highlights that this "turnover" precisely coincides with the J event.

Our data confirm that the significantly increased in abundance of *Acarinina* at the CIEs is a genuine response of the low-latitudes planktic foraminferal populations to the early Eocene hyperthermals and EECO. Similar record derives from the Tethyan Possagno section even though differential dissolution at that location may have partly amplified primary changes of the fossil assemblages (Luciani et al., 2016). Petrizzo et al. (2008) and Nguyen et al. (2009, 2011) suggest indeed that the genus *Acarinina* was more dissolution resistant than *Morozovella* and that subbotinids were the most dissolution prone group on the basis of studies on latest Paleocene-initial Eocene age sediments and laboratory experiments. Interestingly, the *Acarinina* peaks in abundances at Site 1051 are close in the absolute values to those observed in the Tethyan Possagno section across the same interval and, similarly, they mainly correspond to the CIEs (Luciani et al., 2016). D'Onofrio et al. (2014, 2016) record as well pronounced spikes in *Acarinina* abundance at the ETM2, H1 and I2 events in the Tethyan Terche section of northeastern Italy where calcareous plankton record is not biased by dissolution. The changes in abundance recorded at Site 1051 substantiate a clear susceptibility of planktic foraminifera to the Eocene climate, carbon-cycle changes and plaeoceanographic modifications.

5.4. Paleoecology of Early Eocene Planktic Foraminifera at Site 1051

The distinct increase of the test size–$\delta^{13}C$ gradients in all the analysed *Morozovella* species and *Acarinina* spp. (Fig. 6) clearly confirms that both these genera were

photosymbiont-bearing (e.g., Shacketon et al. 1985; D'Hondt et al., 1994; Norris, 1996) during the pre-EECO interval and the main EECO phase. By contrast, the absence of test size–$\delta^{13}C$ gradients in *Subbotina* specimens is coherent with asymbiotic ecology (e.g., Pearson et al., 1993; Norris, 1996; Sexton et al., 2006). In addition, the difference in the mean $\delta^{13}C$ values of the genera *Morozovella* and *Acarinina* with respect to *Subbotina* gives evidence of a diverse depth-habitat. Our data confirm that the habitat was the mixed-layer for the former and the thermocline for the latter (e.g., Shackleton et al., 1985; Boersma et al., 1987;Pearson et al., 2006 and references therein). However, isotope data on early Eocene species are scattered to date. Specifically, stable isotope records on early Eocene *Morozovella* are limited to *M. aragonensis* (Boersma et al., 1987; Pearson et al., 1993, 2001), *M. aequa* (Lu and Keller, 1996; Berggren and Norris, 1997), *M. gracilis* and *M. marginodentata* (Boersma et al., 1987). The paleobiology knowledge of *M. subbotinae* based on stable isotopes is restricted to Late Paleocene record (Shackleton et al., 1985; D'Hondt et al., 1994). All the papers above document oxygen and carbon-isotope record consistent with a mixed-layer habitat and a photosymbiotic relationship. No isotope data were so far available for *M. caucasica, M. crater* and *M. formosa.* Our record therefore provides new insights on paleobiology of the morozovellid species and on their relationships with *Acarinina* in the early Eocene mixed-layer habitat from the sub-tropical Atlantic Site 1051. According to our isotope data, *M. marginodentata* appear to have lived at a slight deeper depth with respect to the other morozovellid species (Fig. 6). Pearson et al. (2006, pp. 369-370) properly state that the morphological differences between M. *marginodentata* and *M. gracilis* are sometime subtle since "intergradation of the typical morphologies" of the two species can be found "in most early Eocene (sub)tropical fossil assemblages". Blow (1979) even suggested that M. *marginodentata* could have been an "extreme phenotype" of *M. gracilis.* Our stable carbon-isotope record shows that M. *marginodentata* and *M. gracilis* maintain some differences that suggest a constant slightly superficial habitat for the latter (Fig. 6). Oxygen isotope data confirm this evidence recording constantly higher temperatures of ~0.7°C for *M. gracilis* with respect to *M. marginodenta* (Table S5, Fig. S3). These differences might support the evidence that they were two separate species. On the other hand, in modern planktic foraminiferal fauna slightly different morphotypes often mask considerable genetic diversity that is indicative of different species (e.g., Darling et al., 2006; Darling and Wade, 2008). Interestingly, *Acarinina* spp. show in most of the studied samples slightly heavier values with respect to a number of *Morozovella* species (Fig. 6), a feature recorded as well from other Late Paleocene and early Eocene sites (e.g., Shackleton et al., 1985; Boersma et al., 1987).

These evidences may suggest for the former a slightly shallower position in the mixed-layer habitat.

The minor differences in the stable-isotope record, together with the fluctuations in abundance out of phase of the two genera at Site 1051, observed as well in other sites during the early Eocene (e.g., D'Onofrio et al., 2016; Luciani et al., 2016) imply slight differences in the ecological behaviour that possibly induced competition within the mixed-layer habitat shared by the two genera.

A reduction of ~0.5 ‰ in the $\delta^{13}C$ gradient between the thermocline (subbotinids) and mixed-layer dwellers (*Acarinina* and *Morozovella*) is evident from the pre EECO interval to the main EECO phase (Fig. 6). We interpret the offset reduction between isotopic values of shallower and thermocline dwellers as indicating a decline in the $\delta^{13}C$ gradient occurred during the EECO interval related to increased vertical mixing of carbon dioxide (e.g., Hilting et al., 2008).

5.5. Bleaching Event at the EECO Onset

We have undertaken the present study with the purpose of answering the question whether the bleaching was the main cause for the relatively rapid and permanent decline in the photosymbiont-bearing *Morozovella* at the EECO onset (Luciani et al., 2016). We are aware that many of the stressors inducing loss of the photosymbiosis (e.g., Douglas al., 2003 and references therein) may have occurred indeed during the long-lasting environmental perturbation related to the EECO, i.e. extreme warmth, possible huge pCO_2, and decrease of the surface-water pH (e.g., Zachos et al., 2008; Bijl et al., 2009; Huber and Caballero, 2011; Hollis et al., 2012; Pross et al., 2012; Inglis et al., 2015).

Our data record a reduction of the test size–$\delta^{13}C$ gradients in morozovellids at the initial EECO, just above the J event, that can prove the occurrence of a bleaching event. Interestingly, the reduction of the test-size $\delta^{13}C$ gradients involves the *Acarinina* spp. as well (Fig. 6). The reduction of the test-size $\delta^{13}C$ gradients may have however resulted also from a change in the type of hosted algal-symbionts. Living planktic foraminifera bearing chrysophyte symbionts have actually a $\delta^{13}C$ test-size gradient that is much lower than planktic foraminifera hosting dinoflagellates (e.g., Hemleben et al., 1989). We could therefore hypothesize a scenario where the marked environmental changes at the EECO onset might have temporarily favoured chrysophytes rather than dinoflagellates. Actually, some laboratory experiments on modern foraminifera indicate that planktic foraminifera can be flexible on their algal-symbiont preferences, but data refer just to genetic subgroups of dinoflgellates

(e.g., Shaked and de Vargas, 2006). Moreover, there is no indication that planktic foraminifera change their symbiont type during their life cycle or between succeeding generations (e.g., Hemleben et al., 1989; Gast and Caron, 1996). In addition, whether *Morozovella* would have maintained the photo-symbiotic relationship, even though with chrysophytes, we should expect no changes in species test-size. Considering that the reduction of the normally positive test size–$\delta^{13}C$ trend in *Morozovella* is accompanied at Site 1051 at the initial EECO by a significant decrease in maximum test-size (Figs. 4, 5) we can assume that morozovellids indeed reduced their photosymbiont relationship at the initial EECO.

The algal-symbionts may have been lost due to the morozovellid migration to deeper waters where light radiation becomes insufficient for algal photosynthesis. Inhabiting temporarily a deeper habitat would have ensured to morozovellids more favourable environmental conditions with respect to the mixed-layer, probably became hostile due to the EECO perturbation. However, both our $\delta^{13}C$ and $\delta^{18}O$ data suggest that morozovellids did not inhabit thermocline habitat at the initial EECO (Figs. 6, S3, Table S5). An alternative factor to explain the temporary bleaching in morozovellids and acarininids could be a competition with other groups of symbiont-bearing zooplankton, such as the radiolarians that could have hosted during the time interval analysed the same type of symbionts. However, detailed studies on evolutionary or widespread abundance changes within the radiolarian, chrysophyte, dinoflagellate or other microplankton groups across the EECO are so far lacking. Data from Site 1051 give evidence for a significant radiolarian increase within the main phase of the EECO and of a marked peak in abundance in coincidence with the morozovellid collapse (Fig. 3). The strengthening of warmth at the EECO onset was probably a crucial factor leading to the inhibition of photosymbiosis, even though the probable huge pCO_2 and pH reduction (e.g., Zachos et al., 2008) may have contributed to the environmental stress. Increased nutrient availability may have caused further stress for the symbiotic relationship of the oligotrophic morozovellids. Surface waters at Site 1051 may have experienced increased nutrient availability during the early part of the EECO, given the aforementioned high concentration of radiolarians, which may reflect eutrophication (e.g., Hallock, 1987). Surface-water eutrophy during the EECO at the studied site seems also supported by the early Eocene calcareous nannofossil assemblages that were described by Mita (2001) as dominated by *Coccolithus pelagicus* which is considered as a taxon with warm and eutrophic affinities (e.g., Perch-Nielsen, 1981; Agnini et al., 2006, 2007a, 2009; Fornaciari et al., 2007; Dedert et al., 2012; Tremolada and Bralower, 2004).

In summary, we record here a bleaching episode through a reduction of test-size and size-

constrained $\delta^{13}C$ gradients at the initial EECO from the sub-tropical Atlantic Site 1051 involving the morozovellids. This bleaching event occurred at the time of the permanent low-latitude morozovellid collapse in abundance, but it affected also the acarininids that proliferated concomitantly (Luciani et al., 2016). This bleaching episode was however transitory and the photo-symbiotic activity recovered for *Morozovella* and *Acarinina* within the main phase of the EECO. We cannot therefore assign the loss of photosymbiont to as the main cause for morozovellid decline at the EECO onset that still remains elusive. What we observe is that acarininids succeeded in the competition with morozovellids within the early Eocene surface-water habitat.

5.6. Reduction in Morozovellid Maximum Text-Size: not Exclusively a Consequence of Bleaching

An evident test-size reduction involves the morozovellids during the initial EECO at Site 1051 (Figs. 4, 5). As discussed above, we attribute this decrease to the bleaching episode as proved by the $\delta^{13}C$ size-constrained analysis. However, the species *M. gracilis* and *M. marginodentata* unexpectedly never recover their maximum diameter even after having restored the photo-symbiotic relationship and significantly decrease their abundance before disappearing within the main phase of the EECO (Figs. **4, 5**). This evidence is of particular interest because these species significantly contributed to the permanent morozovellid collapse in abundance. The species *Morozovella lensiformis* never recuperates at Site 1051 its maximum size as well but we cannot establish whether it was affected by a permanent loss of photo-symbionts since we were not able to obtain reliable isotope data from this species at the studied site. Decrease in test-size and abundance has been documented for the genus *Morozovelloides* just before its evolutionary disappearance in the late middle Eocene (Wade and Olsson, 2008). In that case, however, the reduced test-size was clearly related to a permanent loss of the algal photosymbiosis.

The evidence that some species at Site 1051 reduced their test-size also after the transient bleaching episode recorded at the EECO onset requires an explanation. Decrease in planktic foraminiferal test-size can be related to crossing the ecological optimum threshold due to different types of environmental stressors, in addition to the bleaching. Organisms are equipped with a certain adaptive plasticity to face environmental challenges and different phenotypes may develop in response to the imposed conditions (e.g., Mayr, 1970; Schmidt et al. 2006). There is evidence that environments may have markedly changed through the EECO thus the species *M. gracilis*, *M. marginodentata* and *M. lensiformis* may have reacted

with morphological changes through ecophenotypic plasticity within their adaptive range, resulting in the observed reduced test-size. Furthermore, planktic foraminifera may have adopted test-size reduction as a strategy to face the marked increased of surface-water temperature at the EECO. Protists require indeed more life resources, such as more oxygen or nutrients, when temperature increases since their metabolism accelerates under such conditions (e.g., O'Connor et al., 2009). In contrast, concentration of dissolved oxygen decreases in warm waters thus a strategy to optimize the resource uptake is to enlarge the ratio of surface area by reducing the cell mass and therefore the test-size (e.g., Atkinson et al., 2003). Changes in ocean chemistry may have also contributed to affect the morozovellid calcification and explain to some extent the observed test-size reduction. Recent culturing and open ocean observations suggest that acidification may affect different sized foraminifera differently, leading to reduced calcification in larger planktic foraminifera (Henehan et al., 2016). On the basis of the Henehan et al. (2016) results, we cannot exclude that morozovellids may have reduced their maximum size as a response to surface-water acidification possibly occurred at the EECO and related to the probable huge pCO_2 (e.g. Zachos et al., 2001, 2008).

The evidence that only a limited number of *Morozovella* species at Site 1051 contracted permanently their test-size within the main phase of the EECO implies different levels of tolerance to the environmental and climatic changes for the diverse species of *Morozovella*. Whatever was the cause/s of the morozovellid ecological adaptation, it came at a cost for the species involved that reduced their size and abundance.

6. Summary and Conclusions

In searching for the possible causes to explain the striking *Morozovella* decline in abundance recorded at the EECO onset from low-latitude sites (Luciani et al., 2016; Frontalini et al., 2016) we investigated different features of the morozovellid population across the EECO at the northwest Atlantic ODP Site 1051. Main results are summarized as follow.

(1) The stable carbon curve here provided allows us to relate the planktic foraminiferal changes with the CIEs recorded during the early Eocene. Such correlation proves that the marked *Morozovella* decline precisely coincide at Site 1051 with the J event. Our quantitative analysis on morozovellid species demonstrates that *M. marginodentata*, *M. gracilis, M. subbotinae* and *M. aequa,* disappearing within the main EECO phase, were the main contributors for the collapse in morozovellid abundance. This drop in abundance was not balanced by the *Morozovella* species that survived up to the middle Eocene.

(2) Short-term fluctuations in foraminiferal abundance are superimposed at Site 1051 to the long-term variations and are closely related to the shifts in the carbon cycle curve. Our data evidence that *Acarinina* records the most prominent, though transient, peaks in abundance in coincidence to the early Eocene hyperthermals and EECO, similarly to what observed in several Tethyan successions (e.g., Luciani et al., 2007; 2016; Agnini et al., 2009; D'Onofrio et al., 2016; Frontalini et al., 2016). The planktic foraminiferal record at Site 1051, which is largely unaffected by the taphonomic bias of carbonate dissolution, allows us to substantiate that *Acarinina* was a genus extraordinarily sensitive to the early Eocene climate variability. The fluctuations in abundance of *Acarinina* and *Morozovella* are out of phase at the examined site as also observed in other locations during the early Eocene (e.g., Luciani et al., 2007, 2016; D'Onofrio et al., 2016). These evidences, together with minor differences in the stable-isotope record, imply some dissimilarity in the ecological behaviour that induced competition within the mixed-layer habitat shared by the two genera.

(3) We verified here the possibility of photosymbionts loss in morozovellids, the bleaching, through the established relationship between test-size and $\delta^{13}C$ signature, as the bleaching could have been the main cause for the rapid and permanent *Morozovella* decline at the EECO onset. Algal photo-symbiosis is known to be crucial for life and calcification processes in planktic foraminifera (e.g., Be´ 1982; Be´ et al. 1982; Hemleben et al., 1989). We can therefore expect negative consequences for the foraminifera when the bleaching is forced by hostile environmental changes. Our results demonstrate that there was indeed a reduction of algal-symbiont relationships in morozovellids at the beginning of the EECO following the J event as proved by the $\delta^{13}C$ size-constrained analysis. This is also consistent with a coincident reduction of the morozovellid test-size. The strengthening of warmth at the EECO onset was probably a crucial factor leading to the inhibition of photosymbiosis, even though nutrient and pH changes may have contributed to the environmental stress. The postulated bleaching recorded at the EECO onset from the Site 1051 was however a transitory episode as photo-symbiotic activity recovered for remaining *Morozovella* species within the main phase of the EECO. We cannot therefore assign the loss of photosymbionts to the main cause for morozovellid decline at the EECO onset that remains yet elusive. A possible competition for life resources between *Morozovella* and *Acarinina* in the mixed-layer may have induced a reduced population for the former. Persistent changes in ocean chemistry or interaction with other microplankton groups may have also contributed to induce favourable habitat for continued the *Acarinina* diversification and proliferation at the EECO whereas environmental conditions surpassed a critical threshold for morozovellids.

(4) The reduction in morozovellid text-size is not limited to the bleaching episode as proved by *M. lensiformis, M. gracilis* and *M. marginodentata* that never recover their maximum test-size, even after having restored the photo-symbiotic relationship. In addition to the bleaching, the decrease in planktic foraminiferal test-size can be related to crossing the ecological optimum threshold due to the occurrence of different types of environmental stressors. Reducing the cell mass and hence the text-size is an option to optimize the resource uptake in warm water where protist metabolism accelerates thus requiring more oxygen that, on the contrary, decreases in such conditions (e.g., O'Connor et al., 2009; Atkinson et al., 2003). Furthermore, we cannot exclude that morozovellids may have reduced their maximum size as a response to possible surface-water acidification occurred at the EECO and related to the probable huge pCO_2 (e.g. Zachos et al., 2001, 2008). Recent culturing and open ocean observations suggest indeed that acidification may affect calcification preferentially in larger planktic foraminifera (Henehan et al., 2016). The evidence that only a limited number of *Morozovella* species at the Atlantic sub-tropical Site 1051 reduced permanently their test-size within the main phase of the EECO implies a different degree of tolerance to the environmental and climatic changes for the diverse species of early Eocene *Morozovella.*

Appendix A: Taxonomic List of Planktic Foraminiferal Species Cited in Text and Figures

Acarinina cuneicamerata (Blow, 1979)

Acarinina esnaensis (LeRoy, 1953)

Acarinina interposita Subbotina, 1953

Acarinina quetra (Bolli, 1957)

Astrorotalia palmerae (Cushman and Bermúdez, 1937)

Morozovella aequa **(**Cushman and Renz, 1942)

Morozovella aragonensis (Nuttal, 1930)

Morozovella caucasica (Glaessner, 1937)

Morozovella crater (Hornibrook, 1958)

Morozovella formosa (Bolli, 1957*)*

Morozovella gracilis (Bolli, 1957)

Morozovella lensiformis (Subbotina, 1953),

Morozovella marginodentata (Subbotina, 1953)

Morozovella subbotinae (Morozova, 1939)

Subbotina roesnaensis Olsson and Berggren, 2006

Subbotina patagonica (Todd and Kniker, 1952)

References

Addessi, L. (2001), Giant clam bleaching in the lagoon of Takaopto Atoll (French Polynesia), Coral Reefs, 19 (3), 220-220, doi:10.1007/PL00006957.

Agnini, C., G. Muttoni, D. V. Kent, and D. Rio (2006), Eocene biostratigraphy and magnetic stratigraphy from Possagno, Italy: The calcareous nannofossil response to climate variability, Earth Planet. Sci. Lett., 241, 815–830, doi:10.1016/j.epsl.2005.11.005.

Agnini, C., E. Fornaciari, D. Rio, F. Tateo, J. Backman, and L. Giusberti (2007), Responses of calcareous nannofossil assemblages, mineralogy and geochemistry to the environmental perturbations across the Paleocene/Eocene boundary in the Venetian pre-Alps, Mar. Micropaleontol., 63, 19–38, doi:10.1016/j.marmicro.2006.10.002.

Agnini, C., J. Backman, H. Brinkhuis, E. Fornaciari, L. Giusberti, V. Luciani, D. Rio, and A. Sluijs (2009), An early Eocene carbon cycle perturbation at similar to 52.5 Ma in the Southern Alps: Chronology and biotic response, Paleoceanography, 24, PA2209, doi:10.1029/2008PA001649.

Agnini, C., E. Fornaciari, I. Raffi, R. Catanzariti, H. Pälike, J. Backman, and D. Rio (2014), Biozonation and biochronology of Paleogene calcareous nannofossils from low and middle latitudes, Newslett. Stratigr., 47(2), 131–181, doi:10.1127/0078-0421/2014/0042.

Agnini, C., D. J. A. Spofforth, G. R. Dickens, D. Rio, H. Pälike, J. Backman, G. Muttoni, and E. Dallanave (2016), Stable isotope and calcareous nannofossil assemblage records for the Cicogna section: Toward a detailed template of late Paleocene and early Eocene global carbon cycle and nannoplankton evolution, Clim. Past, 12, 883–909, doi:10.5194/cp-12-883-2016.

Atkinson, D., B. J. Ciotti, and D. J. S. Montagnes (2003), Protists decrease in size linearly with temperature: Ca. 2.5%°C^{-1}, Proc. R. Soc. Lond. B., 270, 2605–2611, doi:10.1098/rspb.2003.2538.

Aze, T., T. H. G. Ezard, A. Purvis, H. K. Coxall, D. R. M Stewart, B. S. Wade, and P. N Pearson (2011), A phylogeny of Cenozoic macro perforate planktonic foraminifera from fossil data, Biol. Rev., 86, 900–927, doi:10.1111/j.1469-185X.2011.00178.x.

Bé, A. W. H. (1982), Biology of planktonic foraminifera, in Foraminifera: notes for a short course (Stud. Geol., 6), edited by T. W. Broadhead, 51–92, Univ. Knoxville, Tenn, USA.

Bé, A. W. H., H. J. Spero, and O. R. Anderson (1982), Effect of symbiont elimination and reinfection on the life processes of the planktonic foraminifera Globigerinoides sacculifer, Marine Biology, 70, 73–86, doi:10.1007/BF00397298.

Bemis, B. E., H. J. Spero, J. Bijma, and D. W. Lea (1998), Reevaluation of the oxygen isotopic composition of planktonic foraminifera: Experimental results and revised paleotemperature equations, Paleoceanography, 13, 150–160.

Berggren, W. A. and R. D. Norris (1997), Biostratigraphy, phylogeny and systematics of Paleocene trochospiral planktic foraminifera, Micropaleontology, 43 (Suppl. 1), 1–116.

Berggren, W. A. and P. N. Pearson (2005), A revised tropical to subtropical Paleogene planktic foraminiferal zonation, J. Foramin. Res., 35, 279–298.

Berggren, W. A., M. C. Mckenna, J. Hardenbol, and J. D. Obradovich (1978), Revised Paleogene polarity time scale, J. Geol., 86 (1), 67–81.

Bijl, P. K., S. Schouten, A. Sluijs, G.-J. Reichart, J. C. Zachos, and H. Brinkhuis (2009), Early Paleogene temperature evolution of the southwest Pacific Ocean, Nature, 461, 776–779, doi:10.1038/nature08399.

Bijl, P. K., J. A. Bendle, S. M. Bohaty, J. Pross, S. Schouten, L. Tauxe, C. E. Stickleyh, R. M. McKayi, U. Röhl, M. Olneyk, A. Sluijs, C. Escutial, H. Brinkhuisa, and Expedition 318 Scientists (2013), Eocene cooling linked to early flow across the Tasmanian Gateway, Proceedings of the National Academy of Sciences, 110 (24), 9645-9650.

Birch, H. S., H. K. Coxall, and P. N. Pearson (2012), Evolutionary ecology of Early Paleocene planktonic foraminifera: size, depth habitat and symbiosis, Paleobiology, 38, 374–390, doi:https://doi.org/10.1666/11027.1.

Blow, W. H. (1979), The Cainozoic Globigerinida: a study of the morphology, taxonomy, evolutionary relationships and the stratigraphical distribution of some Globigerinida (Mainly Globigerinacea), E.J. Brill, Leiden, 1413 pp.

Boersma, A., I. Premoli Silva, and N. Shackleton (1987), Atlantic Eocene planktonic foraminiferal biogeography and stable isotopic paleoceanography, Paleoceanography, 2, 287–331.

Bohaty, S. M., J. C. Zachos, F. Florindo, and M. L. Delaney (2009), Coupled greenhouse warming and deep-sea acidification in the middle Eocene, Paleoceanography, 24 (2), doi:10/1029/2008PA001676.

Bornemann, A., and R. D. Norris (2007), Size-related stable isotope changes in Late Cretaceous planktic foraminifera: Implications for paleoecology and photosymbiosis, Marine Micropaleontology, 65, 32–42, doi:10.1016/j .marmicro.2007.05.005.

Boyd, E. S., A. Pearson, Y. Pi, W.-J. Li, Y. G. Zhang, L. He, C. L. Zhang, and G. G. Geesey (2011), Temperature and pH controls on glycerol dibiphytanyl glycerol tetraether lipid composition in the hyperthermophilic crenarchaeon Acidilobus sulfurireducens, Extremophiles 15, 59–65. doi:10.1007/s00792-010-0339-y.

Caron, D. A., A. W. H. Bé, and O. R. Anderson (1982), Effects of variations in light intensity on life processes of the planktonic foraminifer Globigerinoides sacculifer in laboratory culture: Journal of the Marine Biological Association of the United Kingdom, 62, 435–451, doi:10.1017/S0025315400057374.

Coccioni, R., G. Bancalà, R. Catanzariti, E. Fornaciari, F. Frontalini, L. Giusberti, L. Jovane, V. Luciani, J. Savian, and M. Sprovieri (2012), An integrated stratigraphic record of the Palaeocene-lower Eocene at Gubbio (Italy), New insights into the early Palaeogene hyperthermals and carbon isotope excursions, Terra Nova, 24, 380–386, doi:10.1111/j.1365-3121.2012.01076.x.

Cramer, B. S., D. V. Kent, and M.-P. Aubry (2003), Orbital climate forcing of excursions in the late Paleocene–early Eocene (chrons C24n–C25n), Paleoceanography, 18 (4), 1097, doi:10.1029/2003PA000909.

Darling, K. F., and C. M. Wade (2008), The genetic diversity of planktic foraminifera and the global distribution of ribosomal RNA genotypes, Mar. Micropaleontol., 67 (3–4), 216–238, doi:10.1016/j.marmicro.2008.01.009.

Darling, K. F., M. Kucera, D. Kroon, and C. M. Wade (2006), A resolution for the coiling direction paradox in *Neogloboquadrina pachyderma*, Paleoceanography, 21, PA2011, doi:10.1029/2005PA001189.

Dedert, M., H. M. Stoll, D. Kroon, N. Shimizu, K. Kanamaru, and P. Ziveri (2012), Productivity response of calcareous nannoplankton to Eocene Thermal Maximum 2 (ETM2), Clim. Past, 8 (3), 977–993, doi:10.5194/cp-8-977-2012.

D'Hondt, S., J. C. Zachos, and G. Schultz (1994), Stable isotopic signals and photosymbiosis in Late Paleocene planktic foraminifera, Paleobiology, 20, 391–406.

Dickens, G. R., and J. Backman (2013), Core alignment and composite depth scale for the lower Paleogene through uppermost Cretaceous interval at Deep Sea Drilling Project Site 577. Newsletters on Stratigraphy, 46, 47–68, doi:10.1594/PANGAEA.809257.

D'Onofrio R., V. Luciani, L. Giusberti, E. Fornaciari, and M. Sprovieri (2014), Tethyan planktic foraminiferal record of the early Eocene hyperthermal events ETM2, H2 and I1 (Terche section, northeastern Italy), Rendiconti Online della Società Geologica Italiana, 31, 66-67, doi: 10.3301/ROL.2014.48.

D'Onofrio, R., V. Luciani, E. Fornaciari, L. Giusberti, F. B. Galazzo, E. Dallanave, T. Westerhold, M. Sprovieri, and S. Telch, (2016), Environmental perturbations at the early Eocene ETM2, H2, and I1 events as inferred by Tethyan calcareous plankton (Terche section, northeastern Italy), Paleoceanography, 31 (9), 1225–1247, doi: 10.1002/2016PA002940.

Douglas, A. E. (2003), Coral bleaching – how and why?, Marine Pollut Bull, 46, 385–392.

Dunkley Jones, T., P. R. Bown, P. N. Pearson, B. S. Wade, H. K. Coxall, and C. H. Lear (2008), Major shifts in calcareous phytoplankton assemblages through the Eocene-Oligocene transition of Tanzania and their implications for low-latitude primary production, Paleoceanography, 23, PA4204, doi:10.1029/2008PA001640.

Edgar K. M., S. M. Bohaty, S. J. Gibbs, P. F. Sexton, R. D. Norris, and P. A.Wilson (2012) Symbiont 'bleaching' in planktic foraminifera during the Middle Eocene Climatic Optimum, Geology 41, 15–18.

Elderfield, H., M. Vautravers, and M. Cooper (2002), The relationship between Mg/Ca, Sr/Ca, $\delta^{18}O$, and $\delta^{13}C$ of species of planktonic foraminifera, Geochemistry Geophysics Geosystems, 3, 1052, doi:10.1029/2001GC000194.

Fornaciari, E., L. Giusberti, V. Luciani, F. Tateo, C. Agnini, J. Backman, M. Oddone, and D. Rio (2007), An expanded Cretaceous Tertiary transition in a pelagic setting of the Southern Alps (central-western Tethys), Palaeogeor. Palaeoclimatol. Palaeoecol., 255, 98–131, doi:10.1016/j.palaeo.2007.02.044.

Frontalini, F., R. Coccioni, R. Catanzariti, L. Jovane, J. F. Savian, and M. Sprovieri (2016), The Eocene Thermal Maximum 3: Reading the environmental perturbations at Gubbio (Italy), Geological Society of America Special Papers, 524, SPE524-11.

Frank, T. D., M. A. Arthur, and W. E. Dean (1999), Diagenesis of Lower Cretaceous pelagic carbonates, North Atlantic: Paleoceanographic signals obscured, J. Foraminiferal Res., 29, 340–351.

Galeotti, S., S. Krishnan, M. Pagani, L. Lanci, A. Gaudio, J. C. Zachos, S. Monechi, G. Morelli, and L. J. Lourens (2010), Orbital chronology of Early Eocene hyperthermals from the Contessa Road section, central Italy, Earth Planet. Sci. Lett., 290(1–2), 192–200, doi:10.1016/j.epsl.2009.12.021.

Gast, R. J., and D. A. Caron (1996), Molecular phylogeny of symbiotic dinoflagellates from planktonic foraminifera and radiolarian, Molecular Biology and Evolution, 13, 1192–1197, doi:10.1093/oxfordjournals.molbev.a025684.

Gingerich, P. D. (2003), Mammalian response to climate change at the Paleocene–Eocene boundary, Polecat Bench record in the northern Bighorn Basin, Wyoming, Geol. Soc. Am. Spec. Pap., 369, 463–478.

Glynn, P. W. (1996), Coral reef bleaching: facts, hypotheses and implications. Glob. Change Biol., 2, 495–509.

Grottoli, A. G., L. J. Rodrigues, and C. Juarez (2004), Lipids and stable carbon isotopes in two species of Hawaiian corals, Porites compressa and Montipora verrucosa, following a bleaching event, Marine Biology, 145, 621–631.

Hallock, P. (1987), Fluctuations in the trophic resource continuum: A factor in global diversity cycles?, Paleoceanography, 2, 457–471, doi:10.1029/PA002i005p00457.

Hallock, P. (2000), Symbiont-bearing foraminifera: harbingers of global change?, Micropaleontology, 46(supplno. 1), 95–104.

Hallock, P., and M. W. Peebles (1993), Foraminifera with chlorophyte endosymbionts: habitats of six species in the Florida Keys, Marine Micropaleontology, 20(3-4), 277-292.

Hallock, P., H. K. Talge, E. M. Cockney, and R. G. Muller (1995), A new disease in a reef- dwelling foraminifera: implications for coastal sedimentation, J. Foraminiferal Res., 25, 280–286.

Hancock, H., J. L., G. R. Dickens, C. Percy Strong, C. J. Hollis, and B. D. Field (2003), Foraminiferal and carbon isotope stratigraphy through the Paleocene-Eocene transition at Dee Stream, Marlborough, New Zealand, New Zealand Journal of Geology and Geophysics, 46, 1–19.

Hemleben, C., M. Spindler, O. R. Anderson (1989), Modern planktonic foraminifera. Springer-Verlag, New York, ISBN-13: 9780387968155, 1–363.

Henehan, M. J., P. M. Hull, D. E. Penman, J. W. Rae, and D. N. Schmidt (2016), Biogeochemical significance of pelagic ecosystem function: an end-Cretaceous case study, Phil. Trans. R. Soc. B, 371(1694), 20150510, doi: 10.1098/rstb.2015.0510.

Hilting, A. K., L. R. Kump, and T. J. Bralower (2008), Variations in the oceanic vertical carbon isotope gradient and their implications for the Paleocene-Eocene biological pump, Paleoceanography, 23(3), doi: 10.1029/2007PA001458.

Ho, S. L. and Laepple T. (2016), Flat meridional temperature gradient in the early Eocene in the subsurface rather than surface ocean, Nature Geoscience, 9, 606-610, doi:10.1038/NGEO2763.

Hollis, C. J., K. W. R. Taylor, L. Handley, R. D. Pancost, M. Huber, J. B. Creech, B. R. Hines, E. M. Crouch, Morgans, H. E. G., J. S. Crampton, S. Gibbs, P. N. Pearson, and J. C. Zachos (2012), Early Paleogene temperature history of the Southwest Pacific Ocean: Reconciling proxies and models, Earth Planet. Sc. Lett., 349–350, 53–66, doi:10.1016/j.epsl.2012.06.024.

Hönisch, B., et al. (2012), The geological record of ocean acidification, Science, 335, 1058–1063, doi:10.1126/science.1208277.

Hopmans, E. C., J. W. H. Weijers, E. Schefuß, L. Herfort, J. S. Sinninghe Damsté, S. Schouten (2004), A novel proxy for terrestrial organic matter in sediments based on branched and isoprenoid tetraether lipids, Earth Planet. Sci. Lett., 224, 107–116, doi:10.1016/j.epsl.2004.05.012.

Huber, M. and R. Caballero (2011), The early Eocene equable climate problem revisited, Clim. Past, 7, 603–633, doi:10.5194/cp-7-603-2011.

Ingalls, A. E. (2016), Signal from the subsurface, Nature Geoscience, 9, 572-573, doi:10.1038/ngeo2765.

Inglis, G. N., A. Farnsworth, D. Lunt, G. L. Foster, C. J. Hollis, M. Pagani, P. E. Jardine, P. N. Pearson, P. Markwick, A. M. J. Galsworthy, L. Raynham, K. W. R. Taylor, and R. D. Pancost (2015), Descent toward the icehouse: Eocene sea surface cooling inferred from GDGT distributions, Paleoceanography, 30, 100–1020, doi:10.1002/2014PA002723, 2015.

Keating-Bitonti, C. R., L. C. Ivany, H. P. Affek, P. Douglas, and S. D. Samson (2011), Warm, not super-hot, temperatures in the early Eocene subtropics. Geology, 39 (8), 771-774.

Kennett, J. P., and L. D. Stott (1991), Abrupt deep-sea warming, palaeoceanographic changes and benthic extinctions at the end of the Palaeocene, Nature, 353, 225–229.

Kim, J.-H., J. van der Meer, S. Schouten, P. Helmke, V. Willmott, F. Sangiorgi, N. Koç, E. C. Hopmans, J. S. S. Damsté (2010), New indices and calibrations derived from the distribution of crenarchaeal isoprenoid tetraether lipids: Implications for past sea surface temperature reconstructions, Geochim. Cosmochim. Acta, 74, 4639–4654, doi:10.1016/j.gca.2010.05.027.

Kirtland-Turner, S., P. F. Sexton, C. D. Charled, and R. D. Norris (2014), Persistence of carbon release events through the peak of early Eocene global warmth, Nat. Geosci., 7, 748–751, doi:10.1038/NGEO2240, 2014.

Kozdon, R., D. C. Kelly, N. T. Kita, J. H. Fournelle, and J. W. Valley (2011), Planktonic foraminiferal oxygen isotope analysis by ion microprobe technique suggests warm tropical sea surface temperatures during the Early Paleogene, Paleoceanography, 26, PA3206, doi:10.1029/2010PA002056.

Lauretano, V., K. Littler, M. Polling, J. C. Zachos, and L. J. Lourens (2015), Frequency, magnitude and character of hyperthermal events at the onset of the Early Eocene Climatic Optimum, Clim. Past, 11, 1313–1324, doi:10.5194/cp-11-1313-2015.

Lauretano, V., F. J. Hilgen, J. C. Zachos and L. J. Lourens (2016), Astronomically tuned age model for the early Eocene carbon isotope events: A new high-resolution δ13C benthic record of ODP Site 1263 between~ 49 and~ 54 Ma, Newsletters on Stratigraphy, 49(2), 383-400.

Leon-Rodriguez, L., and G. R. Dickens (2010), Constraints on ocean acidification associated with rapid and massive carbon injections: The early Paleogene record at ocean drilling program site 1215, equatorial Pacific Ocean, Palaeogeogr. Palaeoclimatol. Palaeoecol., 298(3–4), 409–420, doi:10.1016/j.palaeo.2010.10.029.

Littler, K., U. Röhl, T. Westerhold, and J. C. Zachos (2014), A high-resolution benthic stable isotope record for the South Atlantic: Implications for orbital-scale changes in late Paleocene–early Eocene climate and carbon cycling, Earth Planet. Sc. Lett., 401, 18–30, doi:10.1016/j.epsl.2014.05.054.

Liu, Z., M. Pagani, D. Zinniker, R. DeConto, M. Huber, H. Brinkhuis, R. S. Sunita, R. M. Leckie, and A. Pearson (2009), Global cooling during the Eocene-Oligocene climate transition, Science, 323 (5918), 1187-1190.

Lourens, L. J., A. Sluijs, D. Kroon, J. C. Zachos, E. Thomas, U. Röhl, J. Bowles, and I. Raffi (2005), Astronomical pacing of late Palaeocene to early Eocene global warming events, Nature, 435, 1083–1087.

Lu, G. and G. Keller (1995), Planktic foraminiferal faunal turnovers in the subtropical Pacific during the late Paleocene to early Eocene, J. Foramin. Res., 25, 97–116.

Luciani, V. and L. Giusberti (2014), Reassessment of the early–middle Eocene planktic foraminiferal biomagnetochronology: new evidence from the Tethyan Possagno section (NE Italy) and Western North Atlantic Ocean ODP Site 1051, J. Foramin. Res., 44, 187–201.

Luciani, V., G. R. Dickens, J. Backman, E. Fornaciari, L. Giusberti, C. Agnini, and R. D'Onofrio (2016), Major perturbations in the global carbon cycle and photosymbiont-bearing planktic foraminifera during the early Eocene, Clim. Past, 12, 981–1007, doi:10.5194/cp-12-981-2016.

Mayr, E. (1970), Population, Species and Evolution, Harvard University Press, Boston.

Mita, I. (2001), Data Report: Early to late Eocene calcareous nannofossil assemblages of Sites 1051 and 1052, Blake Nose, Northwestern Atlantic Ocean, Proc. Ocean Drill. Progr., Sci. Results, 171B, 1–28.

Nguyen, T. M. P., M.-R. Petrizzo, and R. P. Speijer (2009), Experimental dissolution of a fossil foraminiferal assemblage (Paleocene–Eocene Thermal Maximum, Dababiya, Egypt): Implications for paleoenvironmental reconstructions, Mar. Micropaleontol., 73 (3–4), 241–258, doi:10.1016/j.marmicro.2009.10.005.

Nguyen, T. M. P., M.-R. Petrizzo, P. Stassen, and R. P. Speijer (2011), Dissolution susceptibility of Paleocene–Eocene planktic foraminifera: Implications for palaeoceanographic reconstructions, Mar. Micropaleontol., 81 (1–2), 1–21.

Nicolo, M. J., G. R. Dickens, C. J. Hollis, and J. C. Zachos (2007), Multiple early Eocene hyperthermals: Their sedimentary expression on the New Zealand continental margin and in the deep sea, Geology, 35 (8), 699–702.

Norris, R. D. (1996), Symbiosis as an evolutionary innovation in the radiation of Paleocene planktic foraminifera. Paleobiology 22:461–480.

Norris, R. D., D. Kroon, and A. Klaus (1998), Proceedings of the Ocean Drilling Program, Initial Reports, Proc. Ocean Drill. Progr., Sci. Results, 171B, 1–749.

O'Connor, M., M. F. Piehler, D. M. Leech, A. Anton, and J. F. Bruno (2009), Warming and resource availability shift food web structure and metabolism, Plos Biol., 7 (8), 1–6, doi:10.1371/journal.pbio.1000178.

Ogg, J. G. and L. Bardot (2001), Aptian through Eocene magnetostratigraphic correlation of the Blake Nose Transect (Leg 171B), Florida continental margin, Proc. Ocean Drill. Progr., Sci. Results, 171B, 1–58, doi:10.2973/odp.proc.sr.171B.104.2001.

Olsson, R. K., C. Hemleben, W. A. Berggren, and B. T. Huber (1999), Atlas of Paleocene Planktonic Foraminifera, Smithsonian Contribution to Paleobiology, vol. 85, pp. 225, Smithsonian Institution Press, Washington D. C.

Pearson, P. N. (2012), Oxygen isotopes in foraminifera: Overview and historical review, Paleontol. Soc. Pap., 18, 1–38.

Pearson, P. N., N. J. Shackleton, and M. A. Hall (1993), Stable isotope paleoecology of middle Eocene planktonic foraminifera and multispecies isotope stratigraphy, DSDP Site 523, South Atlantic, J. Foraminiferal Res., 23, 123-140, doi:10.2113/gsjfr.23.2.123.

Pearson, P. N., P. W Ditchfield, J. Singano, K. G. Harcourt-Brown, C. J. Nicholas, R. K. Olsson, N. J. Shackleton, and M. A. Hall (2001), Warm tropical sea surface temperatures in the Late Cretaceous and Eocene epochs, Nature, 413, 481–487, doi:10.1038/35097000.

Pearson, P. N., R. K. Olsson, C. Hemblen, B. T. Huber, and W. A. Berggren (Eds.) (2006), Atlas of Eocene Planktonic Foraminifera, Cushman Special Publication, vol. 41, pp. 513, Department of Geology East Carolina Univ., Greenville.

Pearson, P. N., B. E. van Dongen, C. J. Nicholas, R. D. Pancost, S. Schouten, J. M. Singano, and B. S. Wade (2007), Stable warm tropical climate through the Eocene Epoch, Geology, 35 (3), 211-214.

Perch-Nielsen, K. (1981), Nouvelles observations sur les nannofossiles calcaires a la limite Cretace-Tertiaire pres de El Kef, Tunisie, Cahiers de Micropaléontol., 3, 25–36.

Peters, E. C. (1993), Disease of other invertebrate phyla: porifera, cnidaria, ctenophora, annelida, Echinodermata, in Pathology of marine and estuarine organisms, edited by Couch, J. A., and J. W. Fournie, CRC Press, Boca Raton, pp 393–449.

Petrizzo, M.-R., G. Leoni, R. P. Speijer, B. De Bernardi, and F. Felletti (2008), Dissolution susceptibility of some Paleogene planktonic foraminifera from ODP Site 1209 (Shatsky Rise, Pacific Ocean), J. Foraminiferal Res., 38(4), 357–371.

Premoli Silva, I., and A. Boersma (1988), Atlantic Eocene planktonic foraminiferal historical biogeography and paleohydrographic indices, Palaeogeogr. Palaeoclimatol. Palaeoecol., 67(3-4), 315–356, doi:10.1016/0031-0182(88)90159-9.

Pross, J., L. Contreras, P. K. Bijl, D. R. Greenwood, S. M. Bohaty, S. Schouten, J. A. Bendle U. Röhl, L. Tauxe, J. I. Raine, E. Claire, C. E. Huck, T. van de Flierdt, S. R. Stewart, S. S. R. Jamieson, C. E. Stickley, B. van de Schootbrugge, C. Escutia, and H. Brinkhuis (2012), Persistent near-tropical warmth on the Antarctic continent during the early Eocene Epoch, Nature, 488, 73–77, doi:10.1038 /nature11300.

Quillévéré, F., R. D. Norris, I. Moussa, and W. A. Berggren (2001), Role of photosymbiosis and biogeography in the diversification of early Paleogene acarininids (planktonic foraminifera), Paleobiology, 27(2), 311–326, doi:10.1666/0094-8373(2001)027<0311:ROPABI>2.0.CO;2.

Raffi, I., and B. De Bernardi (2008), Response of calcareous nannofossils to the Paleocene–Eocene Thermal Maximum: Observations on composition, preservation and calcification in sediments from ODP Site 1263 (Walvis Ridge—SW Atlantic), Marine Micropaleontology, 69(2), 119-138.

Reghellin, D., H. K. Coxall, G. R. Dickens, and J. Backman, (2015), Carbon and oxygen isotopes of bulk carbonate in sediment deposited beneath the eastern equatorial Pacific over the last 8 million years, Paleoceanography, 30(10), 1261-1286.

Röhl, U., T. Westerhold, S. Monechi, E. Thomas, J. C. Zachos, and B. Donner (2005), The third and final early Eocene Thermal Maximum: Characteristics, timing, and mechanisms of the "X" event, Geol. Soc. Am. Abstr. Program, 37 (7), 264.

Scheibner, C., and R. P. Speijer (2008), Late Paleocene–early Eocene Tethyan carbonate platform evolution—a response to long-and short-term paleoclimatic change, Earth-Science Reviews, 90 (3), 71-102.

Scholle, P. A., and M. A. Arthur (1980), Carbon isotope fluctuations in Cretaceous pelagic limestones: potential stratigraphic and petroleum exploration tool, American Association of Petroleum Geologists Bulletin, 64, 67–87.

Schouten, S., E. C. Hopmans, E. Schefuss, and J. S. Sinninghe Damsté (2002), Distributional variations in marine crenarchaeotal membrane lipids: A new tool for reconstructing ancient sea water temperatures? Earth Planet. Sci. Lett., 204, 265–274, doi:10.1016/S0012-821X(02)00979-2.

Schouten, S., E. C. Hopmans, J. S. Sinninghe Damsté (2013), The organic geochemistry of glycerol dialkyl glycerol tetraether lipids: A review, Org. Geochem. 54, 19–61, doi:10.1016/j.orggeochem.2012.09.006.

Schmitz, B., R. P. Speijer, and M. P. Aubry (1996), Latest Paleocene benthic extinction event on the southern Tethyan shelf (Egypt): Foraminiferal stable isotopic ($\delta^{13}C$, $\delta^{18}O$) records, Geology, 24 (4), 347-350.

Schmidt, D. N., D. Lazarus, J. R. Young, and M. Kucera (2006), Biogeography and evolution of body size in marine plankton, Earth Sci. Rev., 78, 239–266, doi:10.1016/j.earscirev.2006.05.004.

Schrag, D. P., D. J. Depaolo, and F. M. Richter (1995), Reconstructing past sea surface temperatures: Correcting for diagenesis of bulk marine carbonate, Geochim. Cosmochim. Acta, 59, 2265–2278, doi:10.1016/0016-7037(95)00105-9.

Sexton, P. F., P. A. Wilson, and P. N. Pearson (2006), Microstructural and geochemical perspectives on planktic foraminiferal preservation: 'Glassy' versus 'Frosty', Geochemistry Geophysics Geosystems, v. 7, Q12P19, doi:10.1029/2006GC001291.

Sexton, P. F., R. D. Norris, P. A. Wilson, H. Pälike, T. Westerhold, U. Röhl, C. T. Bolton, and S. Gibbs (2011), Eocene global warming events driven by ventilation of oceanic dissolved organic carbon, Nature, 471, 349–353, doi:10.1038/nature09826.

Shackleton, N. J. and M. A. Hall (1995), Stable isotope records in bulk sediments (Leg 138), Proc. Ocean Drill. Progr., Sci. Results, 138, 797–805, doi:10.2973/odp.proc.sr.171B.104.2001.

Shackleton, N. J., R. M. Corfield, and M. A. Hall (1985), Stable isotope data and the ontogeny of Paleocene planktonic foraminifera, The Journal of Foraminiferal Research, 15(4), 321-336.

Shaked, Y., and C. de Vargas (2006), Pelagic photosymbiosis: rDNA assessment of diversity and evolution of dinoflagellate symbionts and planktonic foraminiferal hosts: Marine Ecology Progress Series, 325, 59–71, doi:10.3354/meps325059.

Shipboard Scientific Party, (1998), Site 1051, in Proceeding Ocean Drilling Program, Initial Reports, 171B, edited by Norris, R. D., D. Kroon, A. Klaus, I. T. Alexander, L. P. Bardot, C. E. Barker, J.-P. Bellier, C. D. Blome, L. J. Clarke, J. Erbacher, K. L. Faul, B. T. Holmes, M. Huber, M. E. Katz, K. G. MacLeod, S. Marca, F. C. Martinez-Ruiz, I. Mita, M. Nakai, J. G. Ogg, D. K. Pak, T. K. Pletsch, J. M. Self-Trail, N. J. Shackleton, J. Smit, W. Ussler III, D. K. Watkins, J. Widmark, P. A. Wilson, L. A. Baez, and E. Kapitan-White, Ocean Drilling Program, College Station,TX, 171–239, doi:10.2973/odp.proc.ir.171b.105.1998.

Slotnick, B. S., G. R. Dickens, M. J. Nicolo, C. J. Hollis, J. S. Crampton, and J. C. Zachos (2012), Large-amplitude variations in carbon cycling and terrestrial weathering during the latest Paleocene and earliest Eocene: The record at Mead Stream, New Zealand, J. Geol., 120(5), 487–505, doi:10.1086/666743.

Slotnick, B. S., G. R. Dickens, C. J. Hollis, J. S. Crampton, P. S. Strong, and A. Phillips (2015), The onset of the Early Eocene Climatic Optimum at Branch Stream, Clarence River valley, New Zealand, New Zeal. J. Geol. Geop., 58, 1–19, doi:10.1080/00288306.2015.1063514.

Sluijs, A., G. J. Bowen, H. Brinkhuis, L. J. Lourens, and E. Thomas (2007), The Paleocene–Eocene thermal maximum super greenhouse:biotic and geochemical signatures, age models and mechanismsof global change, in Deep-Time Perspectives on ClimateChange, edited by Williams, M., A. M. Haywood, F. J. Gregory, and D. N. Schmidt, Micropalaeont. Soc. Spec. Publ., GeologicalSociety, London, 323–350.

Spero, H. J. (1992), Do planktic foraminifera accurately record shifts in the carbon isotopic composition of seawater pCO2?, Marine Micropaleontol, 19, 275–285.

Spero, H. J., and M. J. DeNiro (1987), The influence of photosynthesis on the $\delta^{18}O$ and $\delta^{13}C$ values of planktonic foraminiferal shell calcite, Symbiosis, 4, 213–228.

Spero, H. J., and D. F. Williams (1988), Extracting environmental information from planktonic foraminiferal $\delta^{13}C$ data, Nature, 335, 717–719.

Spero, H. J., and D. W. Lea (1993), Intraspecific stable isotope variability in the planktic foraminifera Globigerinoides sacculifer: Results from laboratory experiments, Marine Micropaleontology, v. 22, p. 221–234, doi:10.1016/0377 -8398(93)90045-Y.

Spero, H. J., I. Lerche, and D. F. Williams (1991), Opening the carbon isotope ‘‘vital effect’’ black box, 2, quantitative model for interpreting foraminiferal carbon isotope data, Paleoceanography, 6, 639–655.

Stap, L., L. Lourens, A. van Dijk, S. Schouten, and E. Thomas (2010), Coherent pattern and timing of the carbon isotope excursion and warming during Eocene Thermal Maximum 2 as recorded in planktic and benthic foraminifera, Geochem. Geophys. Geosyst., 11, Q11011, doi:10.1029/2010GC003097.

Suzuki, A., M. K. Gagan, K. Fabricius, P. J. Isdale, I. Yukino, and H. Kawahata (2003), Skeletal isotope microprofiles of growth and perturbations in Porites corals during the 1997–1998 mass bleaching event, Coral Reefs, 22 (4), 357–369.

Takagi, H., K. Moriya, T. Ishimura, A. Suzuki, H. Kawahata, and H. Hirano (2015), Exploring photosymbiotic ecology of planktic foraminifers from chamber-by-chamber isotopic history of individual foraminifers, Paleobiology, 41 (1), 108-121, http://dx.doi.org/10.1017/pab.2014.7.

Talge, H. K., and P. Hallock (1995), Cytological examination of symbiont loss in a benthic foraminifera, Amphistegina gibbosa, Marine Micropaleontol, 26, 107–113.

Talge, H. K., and P. Hallock (2003), Ultrastructural responses in field-bleached and experimentally stressed Amphistegina gibbosa (Class Foraminifera), J. Eukaryot. Microbiol., 50, 324–333.

Taylor, K. W. R., M. Huber, C. J. Hollis, M. T. Hernandez-Sanchez, and R. D. Pancost (2013), Re-evaluating modern and Palaeogene GDGT distributions: Implications for SST reconstructions, Glob. Planet. Change, 108, 158–174, doi:10.1016/j.gloplacha.2013.06.011.

Thomas, E. (1998), Biogeography of the late Paleocene benthic foraminiferal extinction, in Late Paleocene-early Eocene climaticand biotic events in the marine and terrestrial Records,edited by Aubry, M.-P., S. Lucas, and W. A. Berggren, Columbia University Press, New York, 214–243.

Thomas, E., H. Brinkhuis, M. Huber, and U. Röhl (2006), An ocean view of the early Cenozoic Greenhouse world, Oceanography, 19, 94–103.

Tremolada, F., and T. J. Bralower (2004), Nannofossil assemblage fluctuations during the Paleocene-Eocene thermal maximum at Sites 213 (Indian Ocean) and 401 (North Atlantic Ocean): Palaeoceanographic implications, Mar. Micropaleontol., 52 (1), 107–116, doi:10.1016/j.marmicro.2004.04.002.

Uda, I., A. Sugai, Y. H. Itoh, and T. Itoh (2001), Variation in molecular species of polar lipids from Thermoplasma acidophilum depends on growth temperature, Lipids, 36, 103–105, doi:10.1007/s11745-001-0914-2

Van Hinsbergen, D. J. J., L. V. de Groot, S. J. van Schaik, W. Spakman, P. K. Bijl, A. Sluijs, C. G. Langereis, and H. Brinkhuis (2015), A Paleolatitude Calculator for Paleoclimate Studies, PLoS ONE, 10, e0126946, doi:10.1371/journal.pone.0126946.

Wade, B. S., and R. K. Olsson (2009), Investigation of pre-extinction dwarfing in Cenozoic planktonic foraminifera, Palaeogeogr. Palaeoclimatol. Palaeoecol., 284, 39–46.

Wade, B. S., N. Al-Sabouni, C. Hemleben, and D. Kroon (2008), Symbiont bleaching in fossil planktonic foraminifera, Evolutionary Ecology, 22, 253–265, doi:10.1007/s10682-007-9176-6.

Wade, B. S., P. N. Pearson, W. A. Berggren, and H. Pälike (2011), Review and revision of Cenozoic tropical planktonic foraminiferal biostratigraphy and calibration to the geomagnetic polarity and astronomical time scale, Earth Sci. Rev., 104(1-3), 111–142, doi:10.1016/j.earscirev.2010.09.003.

Wendler, I., B. T. Huber, K. G. MacLeod, and J. E. Wendler (2013), Stable oxygen and carbon isotope systematics of exquisitely preserved Turonian foraminifera from Tanzania—understanding isotopic signatures in fossils, Marine Micropaleontology, 102, 1-33, http://dx.doi.org/10.1016/j.marmicro.2013.04.003.

Westerhold, T., and U. Röhl (2009), High resolution cyclostratigraphy of the early Eocene—New insights into the origin of the Cenozoic cooling trend, Clim. Past, 5(3), 309–327, doi:10.5194/cp-5-309-2009.

Westerhold, T., U. Röhl, T. Frederichs, S. M. Bohaty, and J. C. Zachos (2015), Astronomical calibration of the geological timescale: Closing the middle Eocene gap, Clim. Past, 11 (9), 1181–1195, doi:10.5194/cp-11-1181-2015.

Williams, D. E., and P. Hallock (2004), Bleaching in Amphistegina gibbosa d'Orbigny (Class Foraminifera): Observations from laboratory experiments using visible and ultraviolet light, Marine Biology, 145 (4), 641-649.

Yamaguchi, T., and R. D. Norris (2012), Deep-sea ostracode turnovers through the Paleocene-Eocene thermal maximum in DSDP Site 401, Bay of Biscay, North Atlantic, Mar. Micropaleontol., 86–87, 32–44.

Zachos, J. C., Pagani, M., Sloan, L., Thomas, E., and K. Billups (2001), Trends, rhythms, and aberrations in global climate 65Ma to Present, Science, 292, 686–693.

Zachos, J. C., U. Röhl, S. A. Schellenberg, A. Sluijs, D. A. Hodell, D. C. Kelly, et al. (2005), Rapid acidification of the ocean during the Paleocene-Eocene thermal maximum, Science, 308, 1611–1615, doi:10.1126/science.1109004.

Zachos, J. C., S. Schouten, S. Bohaty, Sluijs A, Brinkhuis H, Gibbs S, Bralower T, and Quattlebaum T. (2006), Extreme warming of mid-latitude coastal ocean during the Paleocene-Eocene Thermal Maximum: inferences from TEX_{86} and isotope data, Geology, 34, 737–740, doi:10.1130/G22522.1.

Zachos, J. C., G. R. Dickens, and R. E. Zeebe (2008), An early Cenozoic perspective on greenhouse warming and carbon-cycle dynamics, Nature, 451(7176), 279-283, doi:10.1038/nature06588.

Zachos, J. C., H. K. McCarren, B. Murphy, U. Röhl, and T. Westerhold (2010), Tempo and scale of late Paleocene and early Eocene carbon isotope cycles: Implications for the origin of hyperthermals, Earth Planet. Sci. Lett., 299, 242–249, doi:10.1016/j.epsl.2010.09.004.

CHAPTER V

Planktic foraminiferal response to early Eocene carbon cycle perturbations in the Southeast Atlantic Ocean (ODP Site 1263)

To be submitted

Abstract

We present here quantified counts of early Eocene planktic foraminiferal assemblages from Ocean Drilling Program (ODP) Site 1263 at Walvis Ridge (southeast Atlantic) to explore their possible relationship with climate variability and carbon cycle perturbations. The early Eocene was an intriguing interval characterized by long-term climate and carbon cycle changes and short-term events referred to as "hyperthermals". The Cenozoic peak of Earth surface temperatures and probably atmospheric pCO_2 were reached at the Early Eocene Climatic Optimum (EECO; ~49–53 Ma). A striking switch between two important calcifiers of the tropical-subtropical early Paleogene oceans, the genera *Morozovella* and *Acarinina*, occurred at low-latitudes of the northern hemisphere, close to the carbon isotope excursion (CIE) referred to as the J event (~53 Ma), which marks the beginning of the EECO. Specifically, the relative abundance of *Morozovella* permanently decreased by at least two thirds across the J event, along with a progressive decrease in the number of species. Concomitantly, the genus *Acarinina* almost doubled its abundance and subsequently diversified within the EECO. Site 1263 was located at a latitude of ~40° south during the early Eocene therefore affording a temperate southern hemisphere setting to examine early Eocene changes in planktic foraminiferal assemblages. The site was chosen because of geochemical and cyclostratigraphic data that provide a detailed stratigraphic framework.

Our results show transient fluctuations in planktic foraminferal abundance consisting of acarininid peaks and accompanying morozovellid and subbotinid decreases that generally coincide with major CIEs. We also record the rapid permanent change in foraminiferal assemblages. Specifically, we document the permanent decrease in *Morozovella* abundance at the beginning of the EECO, although this decline is delayed by ~165 kyr with respect to the low-latitudes in the northern hemisphere. We speculate that this delay can be explained with a temporary migration of the warm water morozovellids southwards at the initiation of EECO warmth, but suffering consequently of the unfavourable environmental conditions triggered by the persistent EECO perturbation. Our data confirm therefore that the *Acarinina* over *Morozovella* turnover was global and related to the EECO rather than local factors, even though the triggering mechanisms for this striking change still remain elusive. We hypothesize that a competition in the mixed-layer played a significant role in the switch in abundance that favoured *Acarinina* over *Morozovella* at the beginning of the EECO. A competition between the two genera is deducible by their anti-phase variations in abundances recorded at the early Paleogene hyperthermals in different settings and confirmed for Site 1263. The prolonged EECO perturbation may have exceeded the optimal conditions to allow

morozovellids to proliferate thus permitting acarininids to dominate the surface-water habitat. In addition, we document at Site 1263 the virtual disappearance within the EECO of the biserial chiloguembelinids, commonly considered as inhabiting the Oxygen Minimum Zone, and a certain reduction in abundance of the thermocline-dweller subbotinids as a result of ecological niches contraction. The significant and permanent modifications recorded by the foraminiferal assemblages at Site 1263 emphasize the prominent effect of the long-lasted EECO perturbation that superimposed and prevailed on the ephemeral changes linked to the early Eocene hyperthermals.

1. Introduction

From a paleoclimate perspective, the early Paleogene represents an exceptionally interesting and dynamic time of Earth's history. About 59 million years ago (Ma), temperatures across Earth's surface began rising so as to reach an extended interval of peak Cenozoic global warmth commonly called the Early Eocene Climatic Optimum (EECO, e.g. Zachos et al., 2001, 2008; Huber and Caballero, 2011; Hollis et al., 2012; Pross et al., 2012). Average high-latitude and deep ocean temperatures within the EECO likely exceeded those at present day by at least 10°C (Zachos et al., 2008; Bijl et al., 2009; Huber and Caballero, 2011; Hollis et al., 2012; Pross et al., 2012; Inglis et al., 2015). However, during the long-term early Paleogene warming and also within the EECO, our planet experienced several short-term (~40-200 kyr) global warming episodes, now referred to as hyperthermals (e.g., Kennett and Stott 1991; Cramer et al., 2003; Lourens et al., 2005; Nicolo et al., 2007; Zachos et al., 2010; Coccioni et al., 2012; Kirtland-Turner et al., 2014; Littler et al., 2014; Lauretano et al., 2016).

Considerable scientific interest has been focused on understanding the early Paleogene hyperthermals, especially the most prominent example, the Paleocene-Eocene thermal maximum (PETM, ~56 Ma). This is because several of the hyperthermals were clearly associated with massive input of carbon to the ocean and atmosphere, as well as profound turnovers in various biotic ecosystems. Indeed, for these reasons, the PETM is often suggested as the best past analogue for current and future climate change (e.g., Pagani et al., 2006; O'Connor et al., 2010; McInerny and Wing, 2011; Zeebe and Zachos, 2013). Interestingly, though, less attention has been dedicated to the EECO and the long-lasting impacts of extraordinary global warmth, especially in terms of biotic response. In fact, even a formal definition of EECO, first widely introduced by Zachos et al. (2001), remains problematic. Recent work (Slotnick et al., 2015; Lauretano et al., 2015; Luciani et al., 2016) has tried to resolve the terminology and stratigraphic issues by defining the EECO as the

interval comprised between a significant carbon cycle perturbation known as the "J event" (Cramer et al., 2003) and the appearance of *Discoaster sublodoensis*, a well-calibrated and easily recognizable calcareous nannofossil biohorizon. The EECO thus spans from approximately 53 to 49 Ma, and its beginning occurred near the boundary of polarity chrons C24n.2r and C24n.3n.

Significant plant and mammal turnovers occurred indeed on land during the EECO (Wing et al., 1991; Zonneveld et al., 2000; Wilf et al., 2003; Falkowski et al., 2005; Woodburne et al., 2009; Figueirido et al., 2012). In the marine realm, evolutionary turnover happened as well, in particular the origin of modern calcareous nannofossil community structure (Agnini et al., 2006, 2014; Schneider et al., 2011; Shamrock et al., 2012) and possibly of diatoms (Sims et al., 2006; Oreshkina, 2012). These observations, both from continents and the oceans, support a hypothesis that long-term climate change during the EECO may have forced biotic evolution (Ezard et al., 2011).

Planktic foraminifera represent a fantastic class of organisms in which to examine links between past climate and evolution (e.g., Corfield, 1987; Kelly et al., 1996, 1998; Quillévéré and Norris, 2003, Ezard et al., 2011; Fraass et al., 2015; Luciani et al., 2016). This is because they include numerous species, they precipitate carbonate tests, and they are abundant in many marine sediment records, which, at least on geological time scales, can be deemed continuous (e.g., Schmidt et al., 2004; Ezard et al., 2011; Fraass et al., 2015). A major turnover in planktic foraminifera occurred near the onset of the EECO (Luciani et al., 2016). This turnover involved two genera, *Morozovella* and *Acarinina,* which were important calcifiers of the tropical and subtropical early Paleogene oceans. More specifically, the abundance and diversity of *Morozovella* decreased significantly while the abundance and diversity of *Acarinina* increased significantly (e.g., Norris, 1991; Schmidt et al., 2004; Pearson et al., 2006; Aze et al., 2011; Ezard et al., 2011; Fraass et al., 2015; Luciani et al., 2016). At multiple and widespread low-latitude locations in the northern hemisphere (Fig. 1), this "switch" in *Morozovella* and *Acarinina* genera happened rapidly and very close to the J event (Frontalini et al, 2016; Luciani et al., 2016). While tempting to suggest that the evolution of planktic foraminifera was crucially affected by the crossing of some critical threshold in surface water conditions (e.g., increased temperature or decreased pH) at the start of the EECO, detailed records of planktic foraminifera assemblages across this interval remain scarce (Fig. 1).

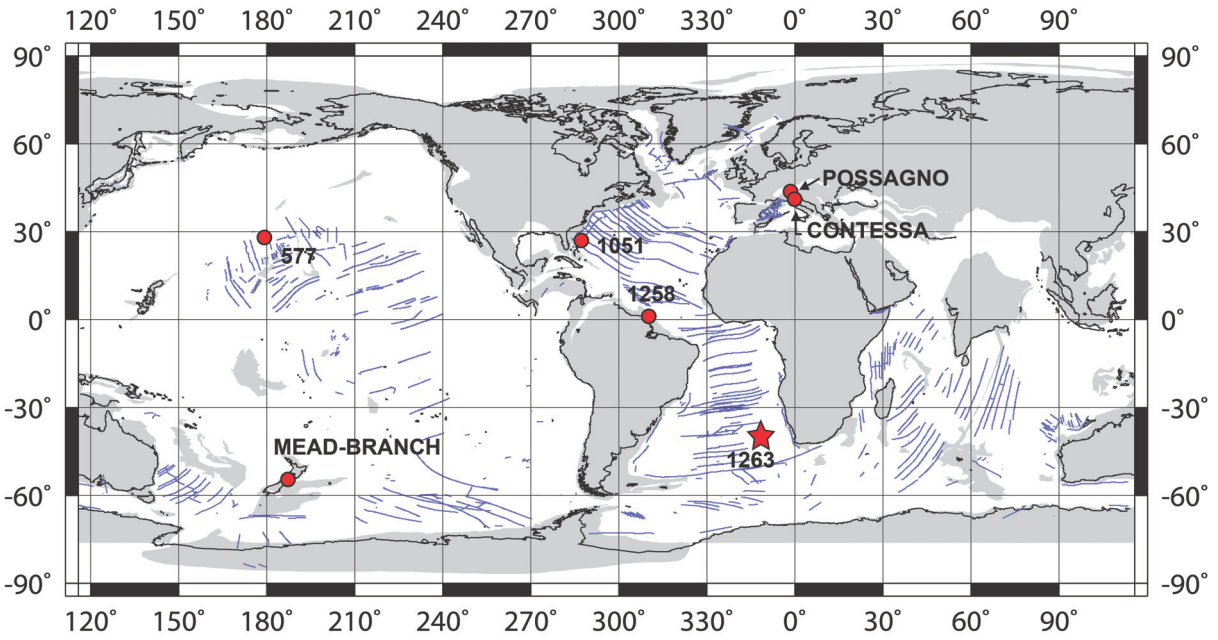

Figure 1. Approximate location of the studied site (star) during the early Eocene. at ~50 Ma. Also shown are the other successions with planktic foraminiferal changes or $\delta^{13}C$ record across the EECO. Base map is from http://www.odsn/de/services/paleomap.html with paleolatitudes modified for Sites 577, 1051, 1258 and 1263, Branch and Mead Stream sections according to www.paleolatitude.org model version 1.2 (Van Hinsbergen et al., 2015). Possagno and Contessa paleolatitudes are based on the http://www.odsn.de/odsn/services/paleomap/adv_map.html model since are not yet available at www.paleolatitude.org.

In this study, we examine planktic foraminiferal assemblages in lower Eocene sediment at Ocean Drilling Program (ODP) Site 1263 on Walvis Ridge in the southeast Atlantic Ocean (Fig. 1). Previous work on the lower Eocene interval at this site provides a solid and fairly detailed stratigraphic framework (e.g., Lourens et al., 2005; Westerhold et al., 2007, Stap et al. 2009, 2010a, 2010b; Lauretano et al., 2015, 2016), and shows that the carbonate-rich interval contains abundant, rather well-preserved planktic foraminifera (Shipboard Scientific Party, 2004). However, the planktic foraminfera assemblages have not been studied at high-resolution. Site 1263 was probably located at ~40° S latitude during the early Eocene (Van Hinsbergen et al., 2015). Consequently, the site presents an opportunity to view early Eocene planktic foraminiferal assemblage changes, especially the possible switch between morozovellids and acarininids at a southern temperate latitude location.

2. Materials and Methods

2.1. ODP Site 1263: Location and Lithology

Site 1263 is located in the southeast Atlantic (28°31.98′ S, 2°46.77′ E) and, at 2717 m below sea level (mbsl), a few hundred meters below the crest of Walvis Ridge (Zachos et al., 2004). Both the latitude and water depth of this site likely have changed over the Cenozoic. During the early Eocene, the location was probably positioned southward by ~10° (Van Hinsbergen et al., 2015) (Fig. 1) and at a shallower depth of ~1500 m (Zachos et al. 2004).

The upper Paleocene and lower Eocene succession at Site 1263 is especially known because it is relatively thick with minimal burial (Zachos et al. 2004). It was also cored in four adjacent holes (1263A–1263D), so that core gaps and core overlaps can be ascertained (Shipboard Scientific Party, 2004; Westerhold et al., 2007, 2015). The location preserves an apparently complete and relatively expanded record of the early Eocene (Lauretano et al., 2016).

Crucially, and consistent with a lower-bathyal depositional environment, lower Paleogene sediment at Site 1263 generally has a high carbonate content ($CaCO_3$ ~90–95% by weight) (Fig. 2), Late Paleocene and early Eocene sedimentation mainly consists of foraminiferal-bearing nannofossil ooze and chalky ooze deposited with sedimentation rates between 10 and 30 m/Myr (Zachos et al., 2004). However, these sediments also show pronounced variability at the dm- to m-scale, as clearly expressed in the magnetic susceptibility (MS), colour reflectance and other high-resolution core logging data. These variations in physical properties principally relate to changes in carbonate content, with highs in MS reflecting lows in carbonate content (e.g., Cramer et al., 2003; Zachos et al., 2005, 2010; Lourens et al., 2005; Westerhold et al., 2007, 2008; Westerhold and Röhl, 2009; Galeotti et al., 2010; Coccioni et al., 2012). The intervals with very high MS/low carbonate also represent established hyperthermal events (e.g., Zachos et al., 2005, 2010; Lourens et al., 2005; Westerhold et al., 2007; Stap et al., 2009, 2010a; Lauretano et al., 2015, 2016), which furthermore have been related to extremes in eccentricity and precession (Zachos et al. 2004, 2005, 2010; Westerhold et al., 2007; Lauretano et al., 2015, 2016).

We adopt the revised composite depth (rmcd) scale provided by Westerhold et al. (2007, 2015) that combines the depth records from cores at different holes. We thus sampled the interval between 297.16 and 240.21 rmcd from Hole 1263B. Given previous work at Site 1263, including alignment of physical property and stable isotope data (e.g. Lourens et al.,

2005; Westerhold et al., 2007, Stap et al. 2009, 2010a, 2010b; Lauretano et al., 2015, 2016) and calcareous nannofossil and benthic foraminifera information across various hyperthermals (e.g. Dedert et al., 2012, 2014; Gibbs et al., 2012; D'Haenens et al., 2014), our sampling should therefore span several million years of the early Paleogene, especially including the J event and the start of the ECCO.

2.2. Bulk Sediment Stable Isotopes

A set of 140 samples, with a sampling resolution varying from ~30 cm to ~50 cm, were used to generate bulk sediment stable isotope records at Site 1263 (Table S1). Samples were firstly freeze-dried and then pulverized manually in a mortar. Amounts of ~0.5g of powdered samples were acidified at 50°C to be analysed. Bulk isotope analyses were performed at the UCL Bloomsbury Environmental Isotope Facility using the Gas Bench II and Cardiff University (UK) using a Thermo Finnigan MAT 252 mass spectrometer coupled with a Kiel III carbonate preparation device. Results are reported in conventional delta notation ($\delta^{13}C$ and $\delta^{18}O$) with reference to the Vienna Pee Dee Belemnite (VPDB) standard. An internal standard (with $\delta^{18}O$=–2.43‰ and $\delta^{13}C$=2.43‰ versus VPDB) was measured between every sixth sample ensuring an analytical precision within 0.04 and 0.08‰ for $\delta^{13}C$ and $\delta^{18}O$ respectively. Additional duplicate analyses were conducted on 9 selected samples giving reproducibility better than 0.1 for carbon and 0.2‰ for oxygen isotopes.

2.3. Planktic Foraminiferal Proxies for Carbonate Dissolution and Productivity

The extreme global warming episodes that characterized the early Eocene are marked by dissolution of carbonate in deep-sea settings (e.g., Zachos et al., 2005; Stap et al., 2009; Leon-Rodriguez and Dickens, 2010). This correspondence, which is particularly obvious in MS records from Walvis Ridge sections (Fig. 2), presumably occurs because massive input of carbon to the ocean and atmosphere during the hyperthermals shoals the CCD and lysocline (Dickens et al., 1997; Zeebe et al., 2009). This is important to realize when examining early Paleogene planktic foraminifera assemblages, because their tests are differentially prone to dissolution and more so than both benthic foraminifera tests and most calcareous nannosfossils (e.g., Berger, 1970; Bé et al., 1975; Thunell and Honjo, 1981; Hancock and Dickens, 2005; Petrizzo et al., 2008; Nguyen et al., 2009, 2011; Leon-Rodriguez and Dickens, 2010; Nguyen and Speijer, 2014). Dissolution can therefore modify the composition of planktic foraminiferal assemblages significantly.

To evaluate possible dissolution effects across the studied section at Site 1263, we chose three different proxies. These proxy measurements were determined on 75 samples. The sample spacing varied between 30 and 40 cm across several major carbon cycle perturbations, and from 40 cm to 1 m through remaining intervals (Table S1). The proxies are the following:

(1) The fragmentation index (*F index*). Planktonic foraminifera tend to break into fragments when they begin to dissolve (e.g., Berger, 1970, 1973; Bé et al., 1975; Leon-Rodriguez and Dickens, 2010; Nguyen and Speijer, 2014). Consequently, fragmentation is a commonly adopted proxy for planktic foraminiferal dissolution. The *F index* (expressed as a percentage) was calculated here according to Berger (1970): the ratio between fragments or partially dissolved planktic foraminiferal tests versus entire tests on ~300 individuals. Amongst the fragmented tests, we included all planktic foraminiferal specimens showing missing or deteriorated chambers and substantial breakage.

(2) The planktic over benthic (*P/B*) ratio. Most planktic foraminifera preferentially dissolve relative to benthic foraminifera (e.g., Nguyen et al., 2009, 2011; Nguyen and Speijer, 2014). The P/B ratio, usually adopted, with some cautions, for paleobathymetric estimates (e.g., Murray, 1976; Van der Zwaan et al., 1990), therefore also can be applied as a dissolution index (e.g., Nguyen et al., 2009; Nguyen and Speijer, 2014). The P/B index was here calculated on ~ 300 entire specimens and is expressed as 100 * P/(P + B).

(3) The weight percent coarse fraction (*WPCF*). Planktic foraminifera, including "juvenile" specimens, generally exceed 38 μm. Dissolution of planktic foraminifera, such as observed with seafloor sediment within the lysocline, thus modifies bulk sediment grain size (e.g., Berger et al., 1982). The *WPCF* was calculated as the ratio between the weights of the coarse dry fraction (≥38 μm) and the bulk dry sediment (Hancock and Dickens, 2005). All three parameters come with caveats (Hancock and Dickens, 2005). For example, calcareous nannofossil productivity will affect the *WPCF*. Nevertheless, in pelagic sediments not affected by dissolution, the *WPCF* can be used as an indicator of planktic foraminiferal productivity (Hancock and Dickens, 2005).

2.4. Planktic Foraminiferal Distribution and Abundances

We collected data on planktic foraminifera on the same 75 samples used for dissolution proxies (Table S1). Planktic foraminifera were studied on washed residues using a stereomicroscope with an incident light beam. The residues were prepared by immersing previously freeze-dried bulk samples in deionized water. Disaggregation occurred in a time

varying from few hours to 3 days, depending on the compactness of the sediments. When disaggregated, samples were washed over piled >63 and >38μm sieves. After each washing, sieves were immerged in a methylene blue bath in order to colour planktic foraminifera potentially trapped in the sieve mesh. This is an easy method to exclude possible contaminations amongst different samples. The separated fractions of each washed residues were dried at <50 °C.

The taxonomic criteria adopted to identify planktic foraminiferal genera and species follow Pearson et al. (2006, and references therein). Relative abundances of planktic foraminiferal genera were generated at Site 1263 by counting at least 300 complete specimens in random splits from the ≥ 63μm size fractions and are expressed in percentages. Some foraminiferal genera were grouped according to their paleoecological affinities as reported by Pearson et al. (2006). Accordingly, the *Subbotina* group includes the genera *Subbotina* and *Parasubbotina*, and the chiloguembelinids comprise the genera *Chiloguembelina* and *Zeauvigerina*. We keep separated the species *Subbotina senni*, since this taxon occupied a different habitat with respect to other subbotinids. Specifically, this species is considered a mixed-layer form that sank to middle mixed-layer or deeper depths during gametogenesis (Pearson et al., 1993; Pearson et al., 2006 and references therein).

2.5. Chronology

Using high-resolution variations in sediment composition, including benthic foraminifera stable isotopes, Lauretano et al. (2016) presented a detailed astronomically tuned age model for the lower Eocene interval at Site 1263. We use this age model, which places the J event (280.85 rmcd) at 53.273 Ma.

3. Results

3.1. Bulk Carbon Isotope Records

The bulk sediment $\delta^{13}C$ record (Fig. 2, Table S1) exhibits both trends and excursions. In the basal part of the studied interval (297.16 to 281.87 rmcd), $\delta^{13}C$ values average ~1.2‰ with no clear trend. Bulk sediment carbon isotope values generally decrease by ~0.25‰ between 280.77 and 274.25 rmcd. The $\delta^{13}C$ values gradually increase above this interval, reaching a maximum of ~1.9‰ in the uppermost part of the investigated interval. High-

frequency $\delta^{13}C$ variations are superimposed on these basic trends, most obviously several negative carbon isotope excursions (CIEs) with magnitudes ranging from 0.4‰ to 0.7‰ (Fig. 2, Table S1).

Although the absolute values of $\delta^{13}C$ vary, both the trends and CIEs have been observed in other carbon isotope records spanning all or part of the EECO. This includes bulk sediment $\delta^{13}C$ records at the neighbouring ODP Site 1262 (Walvis Ridge, Zachos et al. 2010), ODP Site 1258 (Demerara Rise, west equatorial Atlantic, Kirtland-Turner et al., 2014), ODP Site 1051 (Blake Nose, northwest Atlantic, see Chapter IV), DSDP Site 577 (Shatsky Rise, northwest Pacific, Luciani et al., 2016), and the Branch and Mead Stream sections in New Zealand (Slotnick et al. 2012, 2015). Importantly, the correspondence also can be observed in the benthic foraminiferal (*Nuttalides truempyi*) $\delta^{13}C$ record at Site 1263 (Lauretano et al., 2016) (Figs. 2, 3). The variations in $\delta^{13}C$ through the Early Eocene are truly global and signify changes in the composition of dissolved inorganic carbon (DIC) pools of the ocean. We note the ~1‰ offset in absolute $\delta^{13}C$ values between the bulk and benthic foraminifera records, which principally reflects differences between surface and deep ocean DIC composition as well as differences between the carbon isotope fractionation by calcareous nannofossils and benthic foraminifera.

We interpret and label the primary CIEs following Coccioni et al. (2012) and Lauretano et al. (2016), who extended the alphabetic ordering scheme initiated by Cramer et al. (2003) to the benthic foraminiferal $\delta^{13}C$ record Site 1263 (Fig. 2). The minimum value of ~0.6‰ at 275.22 rmcd corresponds to the K/X (or ETM3) event. We recognize below this horizon the Eocene Thermal Maximum 2 (ETM2 or H1), H2, I1, I2, and J events, and above this horizon the L to U events. This correlation allows us to accurately identify the stratigraphic position of biotic events, even where potential core gaps exist in our hole, such as proximal to the ETM2, I2, M, R and the U events.

Most of the documented CIEs at Site 1263 correspond to peaks in MS (Shipboard Scientific Party, 2004), although the magnitudes of peaks in MS are not proportionally even to the magnitudes of CIEs (Fig. 2). The O and T events, for example, have relatively small CIEs, but marked peaks in MS (> 60), whereas the J, M and L1 events display low values in MS (<30), despite relatively large CIEs.

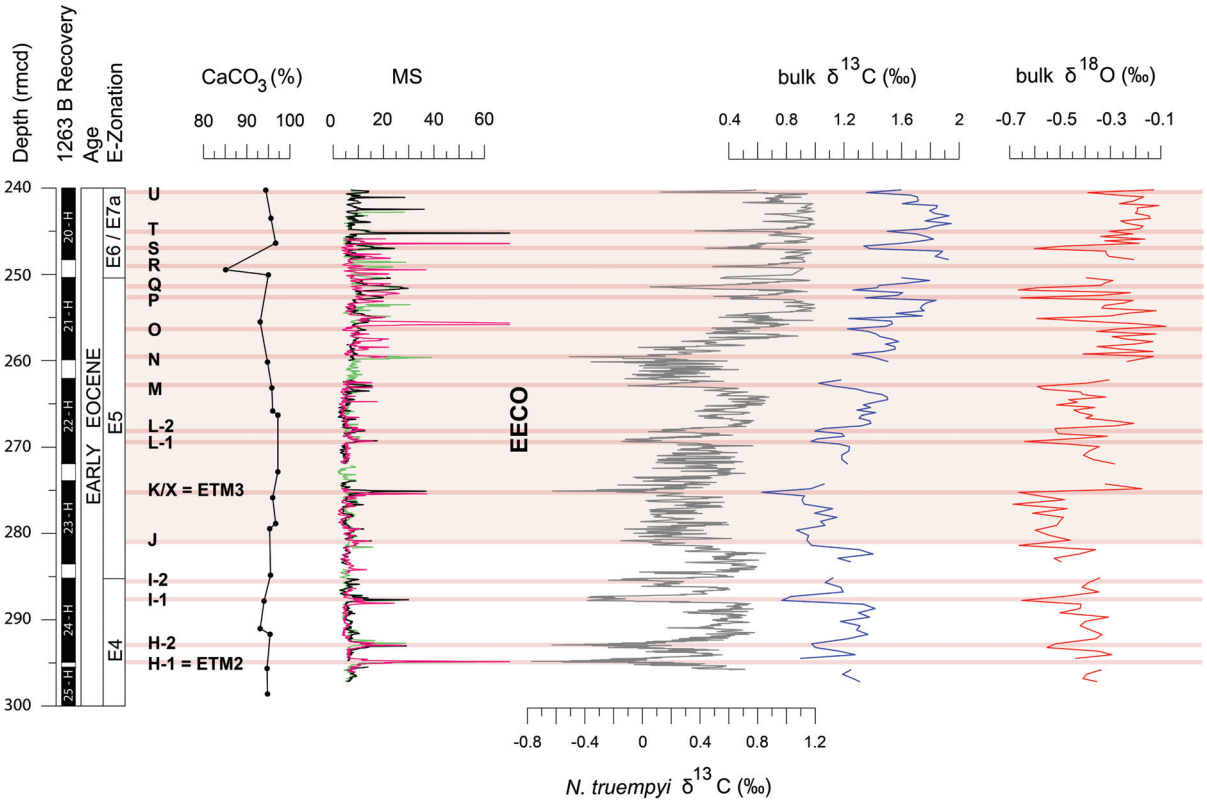

Figure 2. Early Eocene $\delta^{13}C$ records ODP Site 1263, with the bulk sediment record coming from this study (blue) and benthic foraminiferal *N. truempyi* record coming from Lauretano et al. (2016) (grey). The magnetic susceptibility (MS) and the $CaCO_3$ content records derive from the Shipboard Scientific Party (2004). The green, black and pink colours in the MS profile are for Hole A, B and C, respectively. Planktic foraminfieral E-zonation follows Wade et al. (2011) as partly modified by Luciani and Giusberti (2014). Main carbon isotope excursions are labelled according to Lauretano et al. (2016). The pink shaded band defines the Early Eocene Climatic Optimum (EECO) interval.

3.2. Bulk Oxygen Isotope Records

The bulk sediment oxygen isotopes at Site 1263 (Fig. 2, Table S1) vary between –0.1‰ and ~–0.7‰, with an average value of –0.36‰. At a basic level, and more specifically, this curve shows a slight and gradual decrease in values from the base to the K/X event. In this interval the average value is of –0.46‰. Immediately above the K/X event, bulk sediment $\delta^{18}O$ values increase by about 0.4‰. The $\delta^{18}O$ values then oscillate around a mean value of ~–0.3‰ through the top of the investigated interval. Superimposed to these general trends are a series of negative $\delta^{18}O$ excursions that reach values of ~–0.7‰. These appear to strictly correlate with the identified CIEs (Fig. 2). Similar trends of increase in overall $\delta^{18}O$ values have been observed in other bulk $\delta^{18}O$ profiles (Possagno section, Luciani et al., 2016; Site 1258, Kirtland-Turner et al., 2014; Site 577, Luciani et al., 2016; Site 1051, Chapter IV), although they are not consistently overlapping having different absolute values. As noted below, planktic foraminifera at Site 1263 exhibit a "frosty" texture (*sensu* Sexton et al., 2006). Moreover, discoasterids in the studied section commonly have calcite overgrowths

(Shipboard Scientific Party, 2004). These observations imply some degree of recrystallization in bulk sediment, which presumably occurred at or beneath the seafloor (e.g., Pearson et al. 2001; Sexton et al. 2006; Pearson, 2012). Bulk sediment $\delta^{18}O$ records are complicated as a proxy for temperature because they represent mixtures of different components that fractionate ^{18}O differently (e.g., Reghellin et al., 2013). Diagenetic alteration impacts the complex original ^{18}O signal further, because temperatures on the seafloor and over the upper few hundred meters of seafloor are generally colder than near surface waters where most tests were precipitated (e.g., Schrag et al., 1995; Pearson et al., 2001; Stap et al., 2010; Kozdon et al., 2011). Absolute temperature estimates made from the bulk $\delta^{18}O$ record at Site 1263 would be almost assuredly incorrect. Nevertheless, the CIEs manifest in our $\delta^{18}O$ data. This can be explained by a twofold mechanism. First, the CIEs represent hyperthermals, when surface water temperatures were significantly warmer, or biological constituents with lower $\delta^{18}O$ were significantly more abundant. Second, diagenesis involving carbonate dissolution and recrystallization occurred at a very local scale (<1 m) (Schlanger and Douglas, 1974; Matter et al., 1975; Arthur et al., 1984; Kroenke et al., 1991; Borre and Fabricus, 1998; Frank et al., 1999), so that the short-term $\delta^{18}O$ anomalies remain.

3.3. Variations in Dissolution and Productivity Proxies

The curve of *F index* at Site 1263 is characterized by minimum values of ~10% and oscillates around a mean value of ~32% (Fig. 4, Table S2). Importantly, the major peaks in *F index* coincide with the prominent CIEs. In our record, the ETM2, I1, J, K/X, L, M, P and S events have, respectively, *F index* values of 54%, 52%, 63%, 45%, 44%, 90%, 51% and 58%. However, the magnitudes of the CIEs are not proportional with the amplitudes of the *F index* peaks.

The *P/B* profile shows relatively constant values throughout the early Eocene, averaging ~97%. Minor reductions to 92% and 88% coincide with the J and the M events, respectively (Fig. 4, Table S2).

The *WPCF* fluctuates between ~0.02% and ~2.6%, oscillating around a mean value of ~1.4% (Fig. 4, Table S2). However, a modest decrease in mean *WPCF* occurs from the base to the top of the investigated interval, so that values move from ~1.6% in the interval below the paired L events to ~1.2% within the main phase of the EECO. High-frequency variations in the *WPCF* curve do not strictly correlate with the CIEs, except for a ~1% decrease recorded across the M event, which coincides with the highest *F index.*

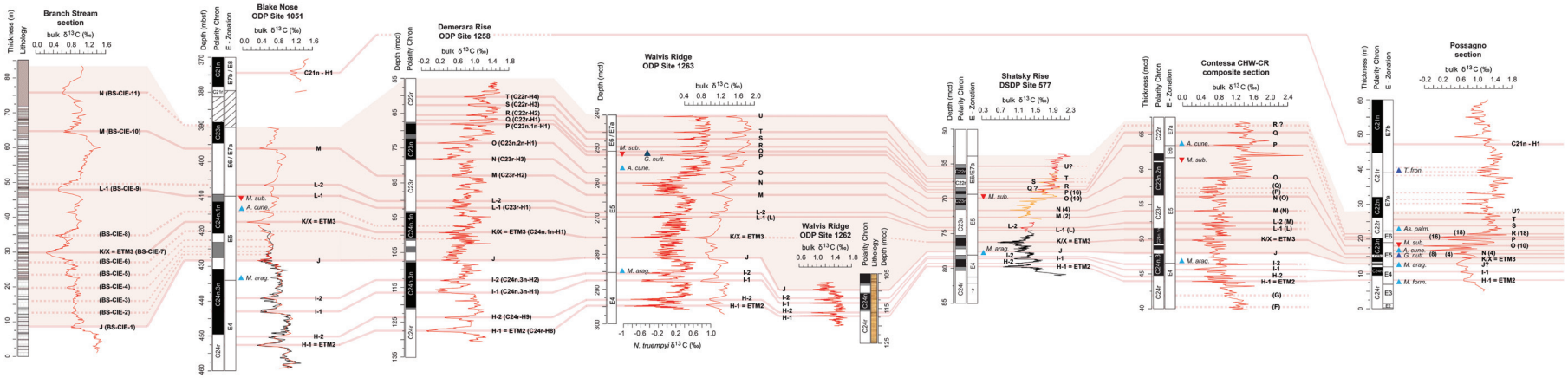

Figure 3. Correlation of carbon isotope records spanning the early Eocene from several sites worldwide distributed. These are: the Branch Stream (New Zealand, Slotnick et al., 2015), the ODP Site 1051 (Blake Nose, Luciani et al., 2016; chapter IV), Site 1258 (Demerara Rise, Kirtland-Turner et al., 2014), Site 1263 (Walvis Ridge, Lauretano et al., 2016, this study), Site 1262 (Walvis Ridge, Zachos et al., 2010), the DSDP Site 577 (Shatsky Rise, Cramer et al., 2003; Luciani et al., 2016), the Contessa Road section (central Italy, Coccioni et al., 2012) and the Possagno (north-eastern Italy, Luciani et al., 2016). Where possible, magnetostratigraphy, lithology and planktic foraminiferal zonation are given. Records from Cramer et al. (2003) at Sites 577 and 1051 are in black colour. At Site 577 $\delta^{13}C$ data are aligned following Dickens and Backman (2013); orange colour refers to hole 577A and red colour to Hole 577A. Carbon isotope excursions (CIEs) are highlighted with pink bands and labelled following the alphabetical order of Cramer et al. (2003) and of Kirtland-Turner et al. (2014) for the C21n-H1 event. Original labels used by different authors are shown in brackets. Dashed bands indicate events not consistently correlated. Correlation problems are mainly related to different resolution of $\delta^{13}C$ records and sedimentation rates. The pink shaded band defines the Early Eocene Climatic Optimum (EECO) interval. Main planktic foraminferal events are shown as light- blue triangles (bases), dark-blue triangles (bases rare) and red triangles (tops). M. form.= *Morozovella formosa*; M. arag.= *Morozovella aragonensis*; A. cune.= *Acarinina cuneicamerata; M. sub.= Morozovella subbotinae; As. pal. = Astrorotalia palmerae; G. nutt.= Guembelitroides nuttalli; T. fron.= Turborotlia frontosa.*

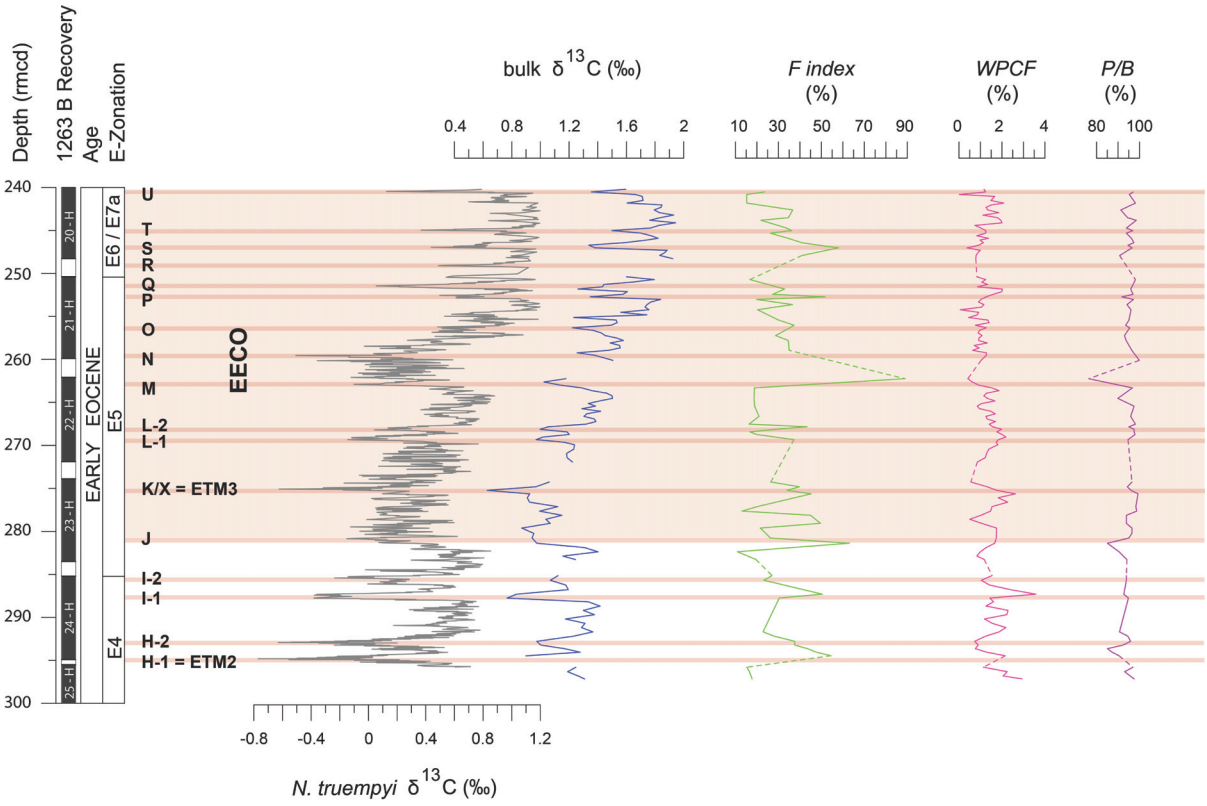

Figure 4. Early Eocene bulk sediment carbon stable-isotope composition from this study (blue) and from Lauretano et al. (2016), based on benthic foraminiferal *N. truempyi* (grey) at the Oceanic Drilling Project (ODP) Site 1263 plotted against the dissolution proxies: fragmentation index (*F index*), weight percent coarse fraction (*WPCF*), and plankton benthos ratio (*P/B*). Planktic foraminfieral E-zonation follows Wade et al. (2011) as partly modified by Luciani and Giusberti (2014). Main carbon isotope excursions are labelled according to Lauretano et al. (2016).

3.4. Planktic Foraminiferal Biostratigraphy

Planktic foraminifera at Site 1263 are abundant and diverse in all samples investigated. Although the tests show classic "frosty" preservation, *sensu* Sexton et al. (2006), they are well preserved, allowing unambiguous identification at the species level. The main early Eocene planktic foraminiferal biohorizons, as defined by bases (B) or tops (T) of species in the Wade et al. (2011) zonal scheme, can be identified at Site 1263. However, there are some subtle differences, as noted by Luciani and Giusberti (2014) and described below. Site 1263 does not have a reliable magnetostratigraphy, so we tentatively refer our planktic foraminiferal events to correlation with the magnetostratigraphy of the equatorial ODP Site 1258 (Demerara Rise) (see Fig. 3 and Fig. 5 in Lauretano et al. (2016). We emphasize the position of the bioevents here recognized also with respect to the main CIEs, considering that the correlation between these two sites is based on exceptional correspondence of the $\delta^{13}C$ curves and identified CIEs globally recognized.

Base of *Morozovella aragonensis.* This event, that identifies the E4/E5 boundary (Wade et al., 2011), occurs at Site 1263 at 285.69 rmcd, in the middle-upper part of Subchron C24n.3n, according to the correlation with Site 1258. A comparable magnetostratigraphic position for this event has been found in the Tethyan Contessa sections (Coccioni et al., 2012) and in the north-western Atlantic ODP Site 1051 (Luciani et al., 2016) (see Fig. 3). The B of *M. aragonensis* is at Site 1263 almost coincident (slightly above) with the I2 event showing a precise correspondence with the Contessa section record (Coccioni et al., 2012). At Site 1051 and possibly at Site 577 and Tethyan Possagno section the B of *M. aragonensis* has been recorded in a similar position, but apparently somewhat higher with respect to the I2 event (Lu and Keller, 1995; Luciani et al., 2016; chapter IV). The B of *M. aragonensis* may present some uncertainty in the identification of true *M. aragonensis* from its ancestor *M. lensiformis*, that could explain a certain diachronism (Pearson et al., 2006). We recognize here *M. aragonensis* from *M. lensiformis* by its truly plano-convex test, truncated-cone shape, and rounded peripheral outline.

Base of *Acarinina cuneicamerata.* This event occurs at 256.32 rmcd in the upper part of Subchron C23n.2n, according to the correlation with Site 1258, and just above the O CIE (Fig. 3). The B of *A. cuneicamerata* is recorded in a reversal order with the T of *M. subbotinae* differently from what stated in the Wade et al. (2011) zonal scheme and from what recorded at the Contessa section (Coccioni et al., 2012). Our data from Site 1263 confirms therefore the record from the Possagno section and Atlantic Site 1051 (Luciani and Giusberti, 2014). However, at Site 1051 the B of *A. cuneicamerata* occurs earlier with respect to Site 1263 as it is recorded between the K/X and L events, at the CIE labelled as CIE6b (Fig. 3). Luciani and Giusberti (2014) tentatively proposed the B of *Astrorotalia* (*Planorotalites) palmerae* as an alternative event to mark the boundary between the Zones E6 and E7a. However, the absence of *A. palmerae* at Site 1263, that is known to have a patchy distribution (Toumarkine & Luterbacher, 1985; Hancock et al., 2002), does not permit to define this boundary. We therefore combine together Zones E6 and E7a. The first specimens of *A. cuneicamerata* at Site 1263 are rare but typical and evenly distributed.

Base rare (Br) of *Guembelitroides nuttalli*. This event occurs at 251.55 rmcd in the lower part of the Zone E6/E7a, at the base of C22r according to the magnetostratigraphic correlation with Site 1258. This event is recorded slightly above the Q event, close to the T of *M. subbotinae* (see below). Our datum from site 1263 confirms the earlier first appearance of this species as documented by Luciani and Giusberti (2014) at the Tethyan Possagno section with respect to the Wade et al. (2011) zonal scheme where this event is considered as detecting the

base of the middle Eocene Zone E8. Luciani and Giusberti (2014) noticed that the base of Zone E8 could be alternatively identified through the common presence of *Guembelitroides nuttalli*. The Br of *G. nuttalli* at Site 1263 however is observed at a significantly higher position with respect to the rare first occurrence of this species as recorded at Possagno (Fig. 3) (Luciani and Giusberti, 2014). *Guembelitroides nuttalli* at Site 1263 is typical but small sized and very rare up to the top of the studied succession.

Top of *Morozovella subbotinae.* This event, that marks the top of Zone E5, occurs at 251 rmcd, at the base of C22r according to the magnetostratigraphic correlation with Site 1258, differently from Wade et al. (2011) that consider the T of *M. subbotinae* as occurring within the Subchron C23n.1n. With reference to the $\delta^{13}C$ curve, the T of *M. subbotinae* is recorded at Site 1263 slightly above the Q CIE. At the Contessa section of central Italy (Coccioni et al., 2012) this bioevent occurs at the C23n.1n, between the O and P events (following to our interpretation of CIEs in Fig. 3), similarly to the Possagno section and Site 577. At Site 1051 the T of *M. subbotinae* was recorded in a significantly lower position as coincident with the L2 event, at the base of C23r (Luciani et al., 2016 and chapter IV) (Fig. 3). Luciani et al. (2016) already underlined the significant diachronism of this event. However, in absence of a revision of the Wade et al. (2011) zonal scheme, the T of *M. subbotinae* is still the present marker for the top of Zone E5. At Site 1263 the specimens of this taxon are relatively small in the final interval of their occurrence.

3.5. Variations in Planktic Foraminiferal Abundances

The early Eocene planktic foraminiferal assemblages display both long-term and transient changes across the investigated interval at Site 1263 (Fig. 5, Table S3). Major changes mainly involve the mixed-layer dwelling warm-index acarininids and morozovellids (e.g., Boersma et al., 1987; Pearson et al., 1993, 2006), which collectively represent the most abundant planktic foraminiferal taxa throughout. The most prominent change, which occurs between the J and K/X events, involves a strong and permanent reduction in morozovellid abundances from a mean value of ~23% in samples below ~278 rmcd to a mean value of ~9% in samples above. Moreover, qualitative observation regarding the *Morozovella* species distribution reveals that, in the pre-EECO interval, *M. aequa* and *M. subbotinae* are the dominant taxa, *M. lensiformis* and *M. crater* are relatively common, *M. formosa, M. gracilis and M. marginodentata* are

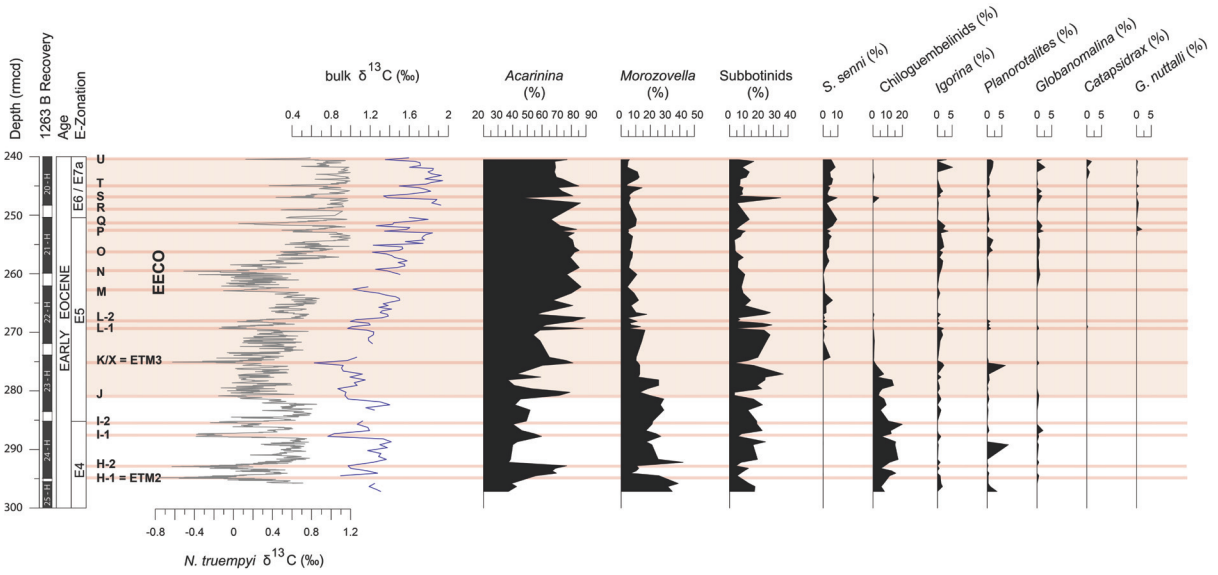

Figure 5. Relative abundances of planktic foraminiferal genera across the early Eocene interval at the ODP Site 1263. Blue bulk carbon stable-isotope curve is from this study; black curve is from Lauretano et al. (2016). Main carbon isotope excursions are labelled according to Lauretano et al. (2016).

quite rare. Within the EECO, *M. aragonensis* and *M. crater* become the most common taxa along with moderate occurrences of *M. aequa*, *M. formosa*, and *M. lensiformis*. The species *M. gracilis, M. marginodentata* and *M. subbotinae* progressively decrease in abundance and disappear within the EECO.

In contrast to the morozovellid trend, the abundance and diversity of acarininids increases upward. Tests of the genus *Acarinina* comprise ~53% of assemblages in the pre-EECO interval below the K/X event, but comprise ~75% above this event. The species *A. coaligensis* and *A. soldadoensis* are the dominant taxa throughout. However, *A. interposita*, *A. esnaensis* and *A. wilcoxensis* are relatively common in the pre-EECO interval, whereas *A. cuneicamerata, A. primitiva* and *A. quetra* become more common in the upper part of the investigated interval.

In the studied interval at Site 1263, a long-term reduction in subbotinid abundance happens across the EECO, whereby the mean value of their abundance in assemblages drops from ~16% to ~9%. Much of this change occurs above the paired L events, specifically around 266.63 rmcd (Fig. 5, Table S3).

The three dominant taxa also display high-frequency variations in abundance superimposed on long-term trends. At a basic level, short-term fluctuations in the abundance of *Acarinina* coincide with anti-phase changes in the abundances of *Morozovella* and *Subbotina.* This relationship is particularly evident across the CIEs, where acarininids generally increase and reach peaks in abundances >70% of the total assemblage. Most

prominent is the peak of ~90 % in acarininids across the paired L events. Interestingly, abundances of morozovellids and subbotinids often recover suddenly above the CIEs (Fig. 5). Here, of course, it should be recognized that such changes in abundances reflect a closed-sum effect, where the drop in one genus necessarily forces a rise in another genus.

A major and permanent drop in the chiloguembelinid group also occurs at the start of the EECO (Fig. 5, Table S3). Mean abundances of this group are ~10 % in the pre-EECO interval but approach zero above the K/X event *Igorina*, *Planorotalites*, *Globanomalina*, *Catapsidrax* and *Globigerinoides nuttalli* are very rare in the assemblages throughout the early Eocene, and never exceed 5% in terms of total planktonic foraminifera abundance. These forms do not display significant variations within the investigated interval.

4. Discussion

4.1. Low Carbonate Dissolution and Decrease in Planktic Foraminiferal Productivity at Site 1263 during the EECO

The minor long-term variations displayed by the three dissolutions proxies adopted at Site 1263 indicate that the genuine biotic signal is mostly preserved and only marginally affected by the selective dissolution. Actually, the *F index*, *WPCF* and *P/B* curves remain almost unchanged within the EECO (Fig. 4). The *F index* shows a certain increase in coincidence of some CIEs related to major hyperthermals, even though the increase is not proportional to the CIE intensity. Actually, the highest value corresponds with the event labelled as M (Fig. 4). A certain decrease of *WPCF* and *P/B* at the same event denotes that the lysocline may have intercepted to some extent the depositional environment at Site 1263, causing some dissolution in planktic foraminferal assemblages during the M event. The variation in the abundance of planktic foraminferal genera however is in line with the other intervals related to CIEs thus suggesting that the dissolution did not affect selectively the planktic foraminferal assemblages.

Given the low impact of dissolution inferred by the dissolution proxies, the long-term decease in the *WPCF* (Fig. 4) can be interpreted as signal of decrease in planktic foraminiferal productivity during the EECO. This long-term reduction is probably linked to the drop in *Morozovella* abundance since decline in subbotinids was somewhat balanced by the abundance displayed by *Subbotina senni* (Fig. 5). A similar decrease in planktic foraminiferal

productivity has been recorded in the Tethyan Possagno section during the EECO and referred as well to the decrease in morozovellid abundance (Luciani et al., 2016).

4.2. Planktic Foraminiferal Response at Site 1263: the Permanent *Morozovella* and *Acarinina* Switch in Abundances at the EECO Onset

Our record provides new insight on the impact of the EECO on planktic foraminiferal genera that characterized the assemblages of the temperate setting from the southern hemisphere as represented by Site 1263. The integrated biotic and carbon stable-isotope stratigraphy here provided allows us to relate the planktic foraminiferal fluctuations with the main C-cycle perturbations occurred in the southeastern Atlantic across the early Eocene interval. Such correlation reveals indeed that the remarkable planktic foraminiferal changes observed at Site 1263 appear strongly related with the EECO and, at higher frequency, with the CIEs that preceded and continued to occur within the EECO (Fig. 5). The comparison with the early Eocene planktic foraminiferal variations so far documented at the EECO (Frontalini et al., 2016; Luciani et al., 2016) highlights that the response of planktic foraminifera at Sites 1263 shows similarities and some differences. Specifically, we record a permanent drop in *Morozovella* abundance, consisting in a reduction of more than a half of relative abundance, slightly above the J event. We confirm therefore that the morozovellid decline recorded at low-latitude (Frontalini et al., 2016; Luciani et al., 2016) occurred as well at the temperate latitude of southern hemisphere in the Atlantic ocean. The switch between the two dominant surface-dwellers *Acarinina* and *Morozovella* appears however more gradual at Site 1263 and slightly delayed with respect to the Atlantic Site 1051 where it occurs precisely at the J event (Luciani et al., 2016, Chapter IV). On the basis of the age model provided by Lauretano et al. (2016) for the Site 1263 we estimate the time of the decline beginning at ~53.05 Ma, ~165 kyr after the J event. The pre-EECO mean percentage of the warm-index *Morozovella* at Site 1263 is lower (~23%, Fig. 5) than the abundance recorded at the tropical Atlantic Site 1051 (~40%) and Pacific Site 577 (~30%) (Luciani et al., 2016). The lower morozovellid abundance at Site 1263 is probably related to its temperate rather than tropical paleolatitude. We speculate that the slightly delayed drop in morozovellid abundance at Site 1263 can be explained with a temporary migration of morozovellids southwards as firstly benefitting of the EECO warmth, but in turn suffering of the unfavourable environmental conditions triggered by the persistence of the EECO perturbation.

4.3. Chiloguembelinid and Subbotinid Changes at Site 1263 across the EECO: Signal of Ecological Niches Reduction in the Upper Water-Column

The diversified planktic forminiferal assemblages at Site 1263, that include relatively common occurrence of chiloguembelinids in the lower portion of the interval investigated, supports the existence of a stratified water column with a moderately expanded oxygen minimum zone (OMZ) (Fig. 5). Chiloguembelinids have been actually traditionally interpreted as taxa well adapted to low-oxygen environments and therefore occupying the OMZ habitat (e.g., Boersma et al., 1987; Boersma and Premoli Silva, 1989). Chiloguembelinids moved from ~10% of mean abundance to virtual absence above the K/X event. This striking change results permanent at Site 1263 for the remaining part of the interval investigated. A possible explanation for this chiloguembelinid disappearance may support the hypothesis of significant warming in sub-surface waters and consequent destratification of the water-column at this mid-latitude location. A certain reduction in the thermocline-dweller cold-index subbotinids (e.g., Boersma et al., 1987; Pearson et al., 1993, 2006), that occurs above the paired L events, appears in line as well with the signal of warming in subsurface water within the EECO, consequent destratification of the water-column and contraction of the ecological niches. It seems unlikely that the relative abundance of *Subbotina senni,* that appears in correspondence to the K/X event, may have balanced the subbotinid decrease since this taxon occupied a different habitat, such as the mixed-layer then sinking during gametogenesis to middle-mixed layer or deeper depths (Pearson et al., 1993; Pearson et al., 2006 and references therein). A gradual reduction in the $\delta^{13}C$ isotopic offset between the shallower and thermocline dwellers was recently documented at Site 1051 during the main phase of the EECO (Chapter IV). This change is also accompanied with a decrease of ~0.5 ‰ in the $\delta^{18}O$ gradient between mixed-layer dwellers *Acarinina* and *Morozovella* and thermocline dweller subbotinids. These decreases are interpretable as indication of possible thermal destratification occurred during the EECO. The long lasting warming of deep waters and consequent increasing in vertical mixing of carbon dioxide should have resulted in the concomitant decline in the $\delta^{13}C$ gradient during the EECO interval (e.g., Hilting et al., 2008).

4.4. High-Frequency Planktic Foraminiferal Variations in Abundance at the main Carbon Isotope Excursions

Short-term fluctuations in abundance of the most abundant genera *Acarinina Morozovella* and *Subbotina* occur in correspondence to the main CIEs (Fig. 5) and clearly display anti-

phase trends. Specifically, acarininids generally increase across the CIEs whereas morozovellids and subbotinids usually decrease to suddenly recover above the events (Fig. 5). Although a different behaviour between the surface-dweller warm-indices acarininids and the thermocline-dweller, cold-indices subbotinids is expected, it can appear atypical the opposite behavior of the two genera, *Morozovella* and *Acarinina* that are known to share similar ecological affinities (e.g., Boersma et al., 1987; Pearson et al., 1993, 2006 and references therein). The striking dominance of *Acarinina* over *Morozovella* has been largely documented during early Eocene hyperthermals such as PETM, ETM2–I1 and K/X events in several low-latitude successions from the Tethyan domain (Arenillas et al., 1999; Molina et al., 1999; Ernst et al., 2006; Guasti and Speijer, 2007; Luciani et al., 2007; Agnini et al., 2009; D'Onofrio et al., 2016; Luciani et al., 2016). This signal has been related to the transient increase in surface-water of nutrient availability coupled with intense warming (Arenillas et al., 1999; Molina et al., 1999; Ernst et al., 2006; Guasti and Speijer, 2007; Luciani et al., 2007; Agnini et al., 2009, D'Onofrio et al., 2016). The surface-water eutrophication has been in turn interpreted as due to accelerated hydrological cycle and enhanced riverine discharge occurred during these events for regions located in proximity of the continental margins (e.g. Schmitz and Pujalte, 2007; Giusberti et al., 2007; Schulte et al., 2011; Slotnick et al., 2012, 2015; Pujalte et al., 2015). At Site 1263 we do not have evidence of terrigenous input either of increased eutrophy; the sporadic occurrence throughout of radiolarians, considered as eutrophy indicators (e.g., Hallock, 1987), confirms oligo-mesotrophic conditions at the surface waters. Our data highlight therefore that the anti-phase variation in abundance between *Acarinina* over *Morozovella* is not restricted to the Tethyan domain. It probably derives from a competition within the same habitat rather than to increased surface-water eutrophy supposed to be better tolerated by acarininids (e.g., Luciani et al., 2007; Agnini et al., 2009; D'Onofrio et al., 2016; Luciani et al., 2016).

4.5. Causes of the Permanent *Morozovella* Decline at the EECO Onset: Bleaching, Change in Ocean Chemistry or Competition in the Mixed-Layer?

The triggering causes of the permanent and widespread *Morozovella* decline at the EECO onset are still unknown. We briefly summarize some hypotheses shown below.

The loss of algal photosymbionts has been thought to represent a potential mechanism to explain the rapid morozovellid decline at the start of the EECO (Luciani et al., 2016) since endosymbionts play an important role in foraminiferal calcification, longevity and growth, allowing the host to succeed in oligotrophic environment (e.g., Be´ 1982; Be´ et al. 1982;

Hemleben et al., 1989). A number of stressors causing the bleaching, such as the prolonged and extreme warmth (Zachos et al., 2008; Bijl et al., 2009; Huber and Caballero, 2011; Hollis et al., 2012; Hönisch, B., et al., 2012; Pross et al., 2012; Inglis et al., 2015) or the huge pCO_2 and possible decrease in surface-water pH (Pearson and Palmer, 2000; Fletcher et al., 2008; Lowenstein and Demicco, 2006; Smith et al., 2010; Hyland and Sheldon, 2013) are actually believed to be occurred during the long-lasted EECO perturbation. The bleaching test performed at Site 1051 (Chapter IV) demonstrates that morozovellids reduced indeed their algal-symbiont relationships at the beginning of the EECO after the J event but the recorded bleaching was a transitory effect. Moreover, bleaching involves as well the acarininids that increased their abundance concomitantly. The bleaching test at Site 1051 described in Chapter IV excludes therefore the permanent lost of photosymbiosis as the cause of the definitive morozovellid decline.

Persistent changes in ocean chemistry may have also contributed to reach unfavourable habitat for morozovellid calcification. However, little consensus still exists as to whether, or to what extent, chemical and physical factors could affect foraminiferal calcification. Henehan et al. (2016) approach the question of environmental control on changing foraminiferal calcification intensity (i.e., mass increase per unit size increase) from multiple perspectives, including observations from culturing and the open ocean with models of ontogenetic growth. Results from both culture experiments and core-top measurements on the recent *Globigerinoides ruber* suggest that neither temperature, nor seawater Mg/Ca ratios affect the calcification intensity, but that acidification significantly reduces calcification in adult-stage foraminifera, supporting previous open-ocean observations (e.g. Barker and Elderfield, 2002; Marshall et al., 2013). Henehan et al. (2016) therefore tentatively suggest that "carbonate chemistry affects different sized foraminifera differently, with acidification leading to reduced calcification in larger foraminifera, but conversely exerting little control (or even favouring calcification) in small individuals". Measures on maximum size of morozovellid shells were performed at Site 1051 combined with size-restricted $\delta^{13}C$ analysis to test possible bleaching at the EECO, thought as a possible cause of their permanent decline, as aforementioned (Chapter IV). Results highlight a reduction in the maximum test-size diameter in the whole *Morozovella* population at EECO even when the algal-photosymbiont relationship was restored (Chapter IV). On the basis of the Henehan et al. (2016) results, we cannot exclude that morozovellids may have reduced their maximum size as a response to surface-water acidification possibly occurred at the EECO and related to the probable huge pCO_2 (e.g. Zachos et al., 2001, 2008).

The morozovellid test-size reduction recorded at Site 1051 (Chapter IV) may have been also a strategy adopted by planktic foraminifera as a response to the marked increased surface-water temperature at the EECO. Protist metabolism accelerates when temperature increases and more life resources are required such as more oxygen or nutrients (e.g., O'Connor et al., 2009). In contrast, concentration of dissolved oxygen decreases in warm waters, so a strategy to optimize the resource uptake is to enlarge the ratio of surface area by reducing the cell mass and consequently the size-test (e.g., Atkinson et al., 2003). The reduced dimension of morozovellid tests, either whether initially adopted as life-strategy or forced by surface-water acidification, may have became detrimental for morozovellids hampering to recover in abundance and diversity during the long-lasted EECO event. This consideration seems particularly reasonable for the *Morozovella* species that reduced their maximum sizes and gradually disappeared within the EECO at Site 1051 such as *M. aequa*, *M. gracilis*, *M. marginodentata* and *M. subbotinae* (Chapter IV). Nevertheless, the reasons why, under the extreme and prolonged EECO conditions, a possible response to accelerated metabolism and/or surface-water acidification selectively affected morozovellids remain unknown.

An alternative explanation for the morozovellid decline includes a strengthened competition between *Morozovella* and *Acarinina*. The anti-phase variations in abundances between *Acarinina* over *Morozovella* recorded in different settings at the Eocene hyperthermal events and confirmed by our data from Site 1263, strongly suggest indeed a clear competition between these two genera in the mixed-layer habitat during conditions of extreme warmth. We can expect therefore that the prolonged EECO perturbation may have definitively exceeded the optimal conditions to allow morozovellid proliferation thus permitting acarininids to dominate the mixed-layer habitat.

5. Summary and Conclusions

Our record provides new insight on the impact of the EECO on planktic foraminiferal genera that characterized the assemblages of the temperate setting from the southern hemisphere, as represented by Site 1263. The integrated planktic foraminfieral quantitative analysis and carbon stable-isotope stratigraphy here provided allow us to relate the long-term and short-term planktic foraminiferal fluctuations with the main C-cycle perturbations occurred in the south-eastern Atlantic during the early Eocene.

We document a distinct decline in abundance of *Morozovella* and increase of *Acarinina* at the beginning of the EECO, similarly to the record from low-latitude where this switch in

abundance occurred at the J event (Chapter IV). The comparison with the early Eocene planktic foraminiferal variations so far documented at the EECO highlights that the response of the planktic foraminifera at Sites 1263 shows similarities but also some differences. The pre-EECO mean percentage of the warm-index *Morozovella* at Site 1263 is lower than the abundance recorded at the tropical Atlantic Site 1051 and Pacific Site 577 (Luciani et al., 2016; Chapter IV). The lower morozovellid abundance at Site 1263 is probably related to its temperate rather than tropical paleolatitude. Moreover, the morozovellid decline at Site 1263 is delayed of ~165 kyr with respect to the low-latitude. We speculate that that this delay can be explained with a temporary migration of the warm water morozovellids southwards at the initiation of EECO warmth, but suffering consequently of the unfavourable environmental conditions triggered by the persistent EECO perturbation.

Our data confirm therefore that the *Acarinina* over *Morozovella* turnover was global and related to the EECO rather than local factors, even though the triggering mechanisms for this striking change still remain elusive. Besides potential changes in ocean chemistry such as surface waters acidification, we hypothesize that a competition in the mixed-layer played a significant role in the switch in abundance that favoured *Acarinina* over *Morozovella* at the beginning of the EECO. A competition between the two genera is deducible by their anti-phase variations in abundances recorded at the early Paleogene hyperthermals in different settings and confirmed for Site 1263. The prolonged EECO perturbation may have definitively exceeded the optimal conditions to allow morozovellids proliferating thus permitting acarininids to dominate the surface-water habitat.

In addition, we document at Site 1263 the virtual disappearance within the EECO of the biserial chiloguembelinids, commonly considered as inhabiting the OMZ, and a certain reduction in abundance of the thermocline-dweller subbotinids. We interpret these critical changes as signal of upper water-column destratification and associated contraction of ecological niches, possibly related to subsurface water warming.

The three dissolutions proxies investigated at Site 1263 indicate that the genuine biotic signal is mostly preserved and only marginally affected by the selective dissolution. On the basis of these evidences we interpret the long-term decrease in the WPCF values as signal of reduction in planktic foraminiferal productivity during the EECO, likely related to the morozovellid decline in abundance.

The significant and permanent modifications recorded by the foraminiferal assemblages at Site 1263 emphasize the prominent effect of the long-lasted EECO perturbation that superimposed and prevailed on the ephemeral changes linked to the early Eocene

hyperthermals.

Appendix A: Taxonomic List of Planktic Foraminiferal Species Cited in Text and Figures

Acarinina coaligensis (Cushman and Hanna, 1927)

Acarinina cuneicamerata (Blow, 1979)

Acarinina esnaensis (LeRoy, 1953)

Acarinina interposita Subbotina, 1953

Acarinina primitiva (Finlay, 1947).

Acarinina quetra (Bolli, 1957).

Acarinina soldadoensis (Brönnimann, 1952)

Acarinina wilcoxensis (Cushman and Ponton, 1932)

Astrorotalia palmerae (Cushman and Bermúdez, 1937)

Guembelitrioides nuttalli (Hamilton, 1953)

Morozovella aequa (Cushman and Renz, 1942)

Morozovella aragonensis (Nuttal, 1930)

Morozovella crater (Hornibrook, 1958)

Morozovella formosa (Bolli, 1957*)*

Morozovella gracilis (Bolli, 1957)

Morozovella lensiformis (Subbotina, 1953)

Morozovella marginodentata (Subbotina, 1953)

Morozovella subbotinae (Morozova, 1939)

Subbotina senni (Beckmann, 1953)

Appendix B: Taxonomic List of Calcareous Nannofossil Taxa Cited in Text and Figures

Discoaster sublodoensis Bramlette and Sullivan, 1961

References

Agnini, C., J. Backman, H. Brinkhuis, E. Fornaciari, L. Giusberti, V. Luciani, D. Rio, and A. Sluijs (2009), An early Eocene carbon cycle perturbation at similar to 52.5 Ma in the Southern Alps: Chronology and biotic response, Paleoceanography, 24, PA2209, doi:10.1029/2008PA001649.

Agnini, C., E. Fornaciari, I. Raffi, R. Catanzariti, H. Pälike, J. Backman, and D. Rio (2014), Biozonation and biochronology of Paleogene calcareous nannofossils from low and middle latitudes, Newslett. Stratigr., 47(2), 131–181, doi:10.1127/0078-0421/2014/0042.

Agnini, C., G. Muttoni, D. V. Kent, and D. Rio (2006), Eocene biostratigraphy and magnetic stratigraphy from Possagno, Italy: The calcareous nannofossil response to climate variability, Earth Planet. Sci. Lett., 241, 815–830, doi:10.1016/j.epsl.2005.11.005.

Arenillas, I., E. Molina, and B. Schmitz (1999), Planktic foraminiferal and $\delta^{13}C$ isotopic changes across the Paleocene/Eocene boundary at Possagno (Italy), Int. J. Earth Sci., 88, 352–364.

Atkinson, D., B. J. Ciotti, and D. J. S. Montagnes (2003), Protists decrease in size linearly with temperature: Ca. 2.5%°C^{-1}, Proc. R. Soc. Lond. B., 270, 2605–2611, doi:10.1098/rspb.2003.2538.

Aze, T., T. H. G. Ezard, A. Purvis, H. K. Coxall, D. R. M Stewart, B. S. Wade, and P. N. Pearson (2011), A phylogeny of Cenozoic macroperforate planktonic foraminifera from fossil data, Biol. Rev., 86, 900–927, doi:10.1111/j.1469-185X.2011.00178.x.

Barker, S., & Elderfield, H. (2002). Foraminiferal calcification response to glacial-interglacial changes in atmospheric CO2. *Science*, *297*(5582), 833-836.

Bé, A. W. H. (1982), Biology of planktonic foraminifera, in Foraminifera: notes for a short course (Stud. Geol., 6), edited by T. W. Broadhead, pp 51–92, Univ. Knoxville, Tenn, USA.

Bé, A. W. H., W. M. John, and M. H. Stanley (1975), Progressive dissolution and ultrastructural breakdown of planktic foraminifera, Cushman Foundation for Foraminiferal Research Special Publication, 13, 27–55.

Bé, A. W. H., H. J. Spero, and O. R. Anderson (1982), Effect of symbiont elimination and reinfection on the life processes of the planktonic foraminifera Globigerinoides sacculifer, Marine Biology, 70, 73–86, doi:10.1007/BF00397298.

Berger, W. H. (1970), Planktonic foraminifera – selective solution and lysocline, Mar. Geol., 8, 111–138.

Berger, W. H., and E. L. Winterer (1974), Plate stratigraphy and the fluctuating carbonate line, Spec. Publ. Int. Assoc. Sedimentol., 1, 11– 48.

Berggren,W. A. and P. N. Pearson (2005), A revised tropical to subtropical Paleogene planktic foraminiferal zonation, J. Foramin. Res., 35, 279–298.

Berggren, W. A., D. V. Kent, C. C. Swisher, and M.-P. Aubry (1995), A revised Cenozoic geochronology and chronostratigraphy, in Geochronology, Time Scales and Global Stratigraphic Correlation: a unified temporal framework for an historical geology, edited by Berggren, W. A., et al., SEPM Special Publication 54, p. 129–212.

Berner, R. A., & Raiswell, R. (1983), Burial of organic carbon and pyrite sulfur in sediments over Phanerozoic time: a new theory. Geochimica et Cosmochimica Acta, 47(5), 855-862.

Bijl, P. K., S. Schouten, A. Sluijs, G.-J. Reichart, J. C. Zachos, and H. Brinkhuis (2009), Early Paleogene temperature evolution of the southwest Pacific Ocean, Nature, 461, 776–779, doi:10.1038/nature08399.

Bijl, P. K., J. A. Bendle, S. M. Bohaty, J. Pross, S. Schouten, L. Tauxe, C. E. Stickley, R. M. McKay, U. Röhl, M. Olney, A. Sluijs, Escutia C. Dotti, H. Brinkhuis, and Expedition 318 Scientists (2013), Eocene cooling linked to early flow across the Tasmanian Gateway, P. Natl. Acad. Sci. USA, 110, 9645–9650, doi:10.1073/pnas.1220872110.

Boersma, A., and I. Premoli Silva (1989), Atlantic paleogene biserial heterohelicid foraminifera and oxygen minima, Paleoceanography, 4(3), 271–286, doi:10.1029/PA004i003p00271.

Boersma, A., I. Premoli Silva, and N. Shackleton (1987), Atlantic Eocene planktonic foraminiferal biogeography and stable isotopic paleoceanography, Paleoceanography, 2, 287–331.

Cande, S. C., and D. V. Kent (1995), Revised calibration of the geomagnetic polarity timescale for the Late Cretaceous and Cenozoic, J . Geophys. Res., 100, 6093 – 6095, doi:10.1029/94JB03098.

Clementz, M., S. Bajpai, V. Ravikant, J. G. M. Thewissen, N. Saravanan, I. B. Singh, and V. Prasad (2011), Early Eocene warming events and the timing of terrestrial faunal exchange between India and Asia, Geology, 39(1), 15–18, doi:10.1130/G31585.1.

Coccioni, R., M. Sideri, F. Frontalini, and A. Montanari (2016), The *Rotalipora cushmani* extinction at Gubbio (Italy): Planktonic foraminiferal testimonial of the onset of the Caribbean large igneous province emplacement?, Geological Society of America Special Papers, 524, 81–96.

Corfield, R. M. (1987), Patterns of evolution in Palaeocene and Eocene planktonic foraminifera. *Micropalaeontology of carbonate environments. Ellis Horwood, Chichester, England*, 93-110.

Cramer, B. S., D. V. Kent, and M.-P. Aubry (2003), Orbital climate forcing of excursions in the late Paleocene–early Eocene (chrons C24n–C25n), Paleoceanography, 18(4), 1097, doi:10.1029/2003PA000909.

Dallanave, E., Agnini, C., Bachtadse, V., Muttoni, G., Crampton J. S., Strong, C. P., Hines, B. H., Hollis, C. J., and Slotnick, B. S.: Early to middle Eocene magneto-biochronology of the southwest Pacific Ocean and climate influence on sedimentation: Insights from the Mead Stream section, New Zealand, Geol. Soc. Am. Bull., 127, 643–660, 2015.

Dedert, M., H. M. Stoll, D. Kroon, N. Shimizu, K. Kanamaru, and P. Ziveri (2012), Productivity response of calcareous nannoplankton to Eocene Thermal Maximum 2 (ETM2), Clim. Past, 8(3), 977–993, doi:10.5194/cp-8-977-2012.

Dedert, M., H. Stoll, S. Kars, J. R. Young, N. Shimizu, D. Kroon, L. Lourens, and P. Ziveri (2014), Temporally variable diagenetic overgrowth on deep-sea nannofossil carbonates across Palaeogene hyperthermals and implications for isotopic analyses, Mar. Micropaleontol., 107, 18–31.

D'haenens, S., A. Bornemann, P. Stassen, and R. P. Speijer (2012), Multiple early Eocene benthic foraminiferal assemblage and $\delta^{13}C$ fluctuations at DSDP Site 401 (Bay of Biscay-NE Atlantic), Mar. Micropaleontol., 88–89, 15–35, doi:10.1016/j.marmicro.2012.02.006.

D'haenens, S., A. Bornemann, P. Claeys, U. Röhl, E. Steurbaut, and R. P. Speijer (2014), A transient deep-sea circulation switch during Eocene Thermal Maximum 2, Paleoceanography, 29, 370–388, doi:10.1002/2013PA002567.

Dingle, R. V., & Lavelle, M. (1998). Late Cretaceous–Cenozoic climatic variations of the northern Antarctic Peninsula: new geochemical evidence and review. *Palaeogeography, Palaeoclimatology, Palaeoecology*, *141*(3), 215-232.

D'Onofrio, R., V. Luciani, L. Giusberti, E. Fornaciari, and M. Sprovieri (2014), Tethyan planktic foraminiferal record of the early Eocene hyperthermal events ETM2, H2 and I1 (Terche section, northeastern Italy), Rendiconti Online della Società Geologica Italiana, 31, 66–67, doi:10.3301/ROL.2014.48.

Dunkley Jones, T., D. J. Lunt, D. N. Schmidt, A. Ridgwell, A. Sluijs, P. J. Valdez, and M. A. Maslin (2013), Climate model and proxy data constraints on ocean warming across the Paleocene–Eocene Thermal Maximum, Earth Sci. Rev., 125, 123–145.

Ernst, S. R., E. Guasti, C. Dupuis, and R. P. Speijer (2006), Environmental perturbation in the southern Tethys across the Paleocene/Eocene boundary (Dababiya, Egypt): foraminiferal and clay mineral records, Mar. Micropaleontol., 60, 89–111.

Ezard, T. H. G., T. Aze, P. N. Pearson, and A. Purvis (2011), Interplay between changing climate and species' ecology drives macroevolutionary dynamics, Science, 332, 349–351.

Falkowski, P. G., M. E. Katz, A. J. Milligan, K. Fennel, B. S. Cramer, M. P. Aubry, R. A. Berner, M. J. Novacek, and W. M. Zapol (2005), Mammals evolved, radiated, and grew in size as the concentration of oxygen in Earth's atmosphere increased during the past 100 million years, Science, 309, 2202–2204.

Figueirido, B., C. M. Janis, J. A. Pérez-Claros, M. De Renzi, and P. Palmqvist (2012), Cenozoic climate change influences mammalian evolutionary dynamics, P. Natl. Acad. Sci. USA, 109, 722–727.

Fletcher, B. J., S. J. Brentnall, C. W. Anderson, R. A. Berner, and D. J. Beerling (2008), Atmospheric carbon dioxide linked with Mesozoic and early Cenozoic climate change, Nat. Geosci., 1, 43–48.

Fraass, A. J., D. K. Kelly, and S. E. Peters (2015), Macroevolutionary history of the planktic foraminifera, Annu. Rev. Earth Pl. Sc., 43, 139–66, doi:10.1146/annurev-earth-060614-105059.

Frontalini, F., R. Coccioni, R. Catanzariti, L. Jovane, J. F. Savian, & M. Sprovieri (2016), The Eocene Thermal Maximum 3: Reading the environmental perturbations at Gubbio (Italy), Geological Society of America Special Papers, 524.

Galeotti, S., S. Krishnan, M. Pagani, L. Lanci, A. Gaudio, J. C. Zachos, S. Monechi, G. Morelli, and L. J. Lourens (2010), Orbital chronology of Early Eocene hyperthermals from the Contessa Road section, central Italy, Earth Planet. Sci. Lett., 290(1–2), 192–200, doi:10.1016/j.epsl.2009.12.021.

Gibbs, S. J., P. R. Bown, B. H. Murphy, A. Sluijs, K. M. Edgar, H. Pälike, C. T. Bolton, and J. C. Zachos (2012), Scaled biotic disruption during early Eocene global warming events, Biogeosciences, 9(11), 4679–4688, doi:10.5194/bg-9-4679-2012.

Giusberti, L., D. Rio, C. Agnini, J. Backman, E. Fornaciari, F. Tateo, and M. Oddone (2007), Mode and tempo of the Paleocene–Eocene thermal maximum in an expanded section from the Venetian pre-Alps, Geol. Soc. Am. Bull., 119, 391–412, doi:10.1130/B25994.1.

Gradstein, F. M., Ogg, J. G., Schmitz, M., & Ogg, G. (Eds.). (2012). *The geologic time scale 2012 2-volume set*. elsevier.

Guasti, E., and Speijer R. P. (2007), The Paleocene–Eocene thermal maximum in Egypt and Jordan: an overview of the planktic foraminiferal record, Geol. Soc. Spec. Pap., 424, 53–67.

Hancock, H. J. L., and G. R. Dickens (2005), Carbonate dissolution episodes in Paleocene and Eocene sediment, Shatsky Rise, west-central Pacific, in Proceedings of the Ocean Drilling Program, Scientific Results, vol. 198, edited by T. J. Bralower, I. Premoli Silva, and M. J. Malone, 1-24, Texas A&M Univ., College Station. [Available at World Wide Web http://www-odp.tamu.edu/publications/198_SR/116/116.htm.].

Hancock, H. J., Chaproniere, G. C., Dickens, G. R., & Henderson, R. A. (2002), Early Palaeogene planktic foraminiferal and carbon isotope stratigraphy, Hole 762C, Exmouth Plateau, northwest Australian margin. *Journal of Micropalaeontology*, *21*(1), 29-42.

Henehan, M. J., Hull, P. M., Penman, D. E., Rae, J. W., & Schmidt, D. N. (2016), Biogeochemical significance of pelagic ecosystem function: an end-Cretaceous case study. *Phil. Trans. R. Soc. B*, *371*(1694), 20150510.

Hemleben, C., Spindler, M., and Anderson, O. R. (Eds.) (1989), Modern planktonic foraminifera, Springer-Verlag, New York, ISBN-13: 9780387968155, 1–363.

Hilgen, F. J., Kuiper, K. F., & Lourens, L. J. (2010), Evaluation of the astronomical time scale for the Paleocene and earliest Eocene. *Earth and Planetary Science Letters*, *300*(1), 139-151.

Hilting, A. K., Kump, L. R., & Bralower, T. J. (2008), Variations in the oceanic vertical carbon isotope gradient and their implications for the Paleocene-Eocene biological pump. *Paleoceanography*, *23*(3).

Ho, S. L.,and T. Laepple (2012), Flat meridional temperature gradient in the early Eocene in the subsurface rather than surface ocean, Nature Geosci., 9, 606–613, doi: 10.1038/NGEO2763.

Hollis, C. J., K. W. R. Taylor, L. Handley, R. D. Pancost, M. Huber, J. B. Creech, B. R. Hines, E. M. Crouch, H. E. G. Morgans, J. S. Crampton, S. Gibbs, P. N. Pearson, and J. C. Zachos (2012), Early Paleogene temperature history of the Southwest Pacific Ocean: Reconciling proxies and models, Earth Planet. Sc. Lett., 349–350, 53–66, doi:10.1016/j.epsl.2012.06.024.

Hönisch, B., et al. (2012), The geological record of ocean acidification, Science, 335, 1058–1063, doi:10.1126/science.1208277.

Huber, M. and R. Caballero (2011), The early Eocene equable climate problem revisited, Clim. Past, 7, 603–633, doi:10.5194/cp-7-603-2011.

Hyland, E. G., N. D. Sheldon, and M. Fan (2013), Terrestrial paleoenvironmental reconstructions indicate transient peak warming during the early Eocene climatic optimum, Geol. Soc. Am. Bull., 125, 1338–1348.

Inglis, G. N., A. Farnsworth, D. Lunt, G. L. Foster, C. J. Hollis, M. Pagani, P. E. Jardine, P. N. Pearson, P. Markwick, A. M. J. Galsworthy, L. Raynham, K. W. R. Taylor, and R. D. Pancost (2015), Descent toward the icehouse: Eocene sea surface cooling inferred from GDGT distributions, Paleoceanography, 30, 100–1020, doi:10.1002/2014PA002723.

Kennett, J. P., and L. D. Stott (1991), Abrupt deep-sea warming, palaeoceanographic changes and benthic extinctions at the end of the Palaeocene, Nature, 353, 225–229.

Kirtland-Turner, S., P. F. Sexton, C. D. Charled, and R. D. Norris (2014), Persistence of carbon release events through the peak of early Eocene global warmth, Nat. Geosci., 7, 748–751, doi:10.1038/NGEO2240, 2014.

Lauretano, V., K. Littler, M. Polling, J. C. Zachos, and L. J. Lourens (2015), Frequency, magnitude and character of hyperthermal events at the onset of the Early Eocene Climatic Optimum, Clim. Past, 11, 1313–1324, doi:10.5194/cp-11-1313-2015.

Lauretano, V., F. J. Hilgen, J. C. Zachos and L. J. Lourens (2016), Astronomically tuned age model for the early Eocene carbon isotope events: A new high-resolution $\delta^{13}C$ benthic record of ODP Site 1263 between~ 49 and~ 54 Ma, Newsletters on Stratigraphy, 49(2), 383-400.

Leon-Rodriguez, L., and G. R. Dickens (2010), Constraints on ocean acidification associated with rapid and massive carbon injections: The early Paleogene record at ocean drilling program site 1215, equatorial Pacific Ocean, Palaeogeogr. Palaeoclimatol. Palaeoecol., 298(3–4), 409–420, doi:10.1016/j.palaeo.2010.10.029.

Littler, K., U. Röhl, T. Westerhold, and J. C. Zachos (2014), A high-resolution benthic stable isotope record for the South Atlantic: Implications for orbital-scale changes in late Paleocene–early Eocene climate and carbon cycling, Earth Planet. Sc. Lett., 401, 18–30, doi:10.1016/j.epsl.2014.05.054.

Lourens, L. J., A. Sluijs, D. Kroon, J. C. Zachos, E. Thomas, U. Röhl, J. Bowles, and I. Raffi (2005), Astronomical pacing of late Palaeocene to early Eocene global warming events, Nature, 435, 1083–1087.

Lowenstein, T. K., and R. V. Demicco (2006), Elevated Eocene atmospheric CO_2 and its subsequent decline, Science, 313, 1928, doi:10.1126/science.1129555.

Luciani, V. and L. Giusberti (2014), Reassessment of the early–middle Eocene planktic foraminiferal biomagnetochronology: new evidence from the Tethyan Possagno section (NE Italy) and Western North Atlantic Ocean ODP Site 1051, J. Foramin. Res., 44, 187–201.

Lu, G. (1995), Paleocene-Eocene transitional events in the ocean: Faunal and isotopic analyses of planktic foraminifera, PhD Thesis, Princeton University, Princeton, 1–284.

Lu, G. and G. Keller (1995), Planktic foraminiferal faunal turnovers in the subtropical Pacific during the late Paleocene to early Eocene, J. Foramin. Res., 25, 97–116.

Luciani, V. and L. Giusberti (2014), Reassessment of the early–middle Eocene planktic foraminiferal biomagnetochronology: new evidence from the Tethyan Possagno section (NE Italy) and Western North Atlantic Ocean ODP Site 1051, J. Foramin. Res., 44, 187–201.

Luciani, V., L. Giusberti, C. Agnini, J. Backman, E. Fornaciari, and D. Rio (2007), The Paleocene–Eocene Thermal Maximum as recorded by Tethyan planktonic foraminifera in the Forada section (northern Italy), Mar. Micropaleontol., 64(3), 189–214, doi:10.1016/j. marmicro.2007.05.001.

Luciani, V., G. R. Dickens, J. Backman, E. Fornaciari, L. Giusberti, C. Agnini, and R. D'Onofrio (2016), Major perturbations in the global carbon cycle and photosymbiont-bearing planktic foraminifera during the early Eocene, Clim. Past, 12, 981–1007, doi:10.5194/cp-12-981-2016.

Marshall, J. D. (1992), Climatic and oceanographic isotopic signals from the carbonate rock record and their preservation, Geol. Mag., 129(02), 143–160.

Molina, E., I. Arenillas, and A. Pardo (1999), High resolution planktic foraminiferal biostratigraphy and correlation across the Palaeocene/Eocene boundary in the Tethys, B. Soc. Géol. Fr., 170, 521–530.

Murray, J. W. (1976), A method of determining proximity of marginal seas to an ocean, Mar. Geol., 22, 103–119.

Nguyen, T. M. P., and R. P. Speijer (2014), A new procedure to assess dissolution based on experiments on Pliocene–Quaternary foraminifera (ODP Leg 160, Eratosthenes Seamount, Eastern Mediterranean), Mar. Micropaleontol., 106, 22–39, doi:10.1016/j.marmicro.2013.11.004.

Nguyen, T. M. P., M.-R. Petrizzo, and R. P. Speijer (2009), Experimental dissolution of a fossil foraminiferal assemblage (Paleocene–Eocene Thermal Maximum, Dababiya, Egypt): Implications for paleoenvironmental reconstructions, Mar. Micropaleontol., 73(3–4), 241–258, doi:10.1016/j.marmicro.2009.10.005.

Nicolo, M. J., G. R. Dickens, C. J. Hollis, and J. C. Zachos (2007), Multiple early Eocene hyperthermals: Their sedimentary expression on the New Zealand continental margin and in the deep sea, Geology, 35(8), 699–702.

Norris, R. D. (1991), Biased extinction and evolutionary trends, Paleobiology,17, 388–399.

O'Connor, M., M. F. Piehler, D. M. Leech, A. Anton, and J. F. Bruno (2009), Warming and resource availability shift food web structure and metabolism, Plos Biol., 7(8), 1–6, doi:10.1371/journal.pbio.1000178.

Olsson, R. K., C. Hemleben, W. A. Berggren, and B. T. Huber (1999), Atlas of Paleocene Planktonic Foraminifera, Smithsonian Contribution to Paleobiology, vol. 85, pp. 225, Smithsonian Institution Press, Washington D. C.

Oreshkina, T. V. (2012), Evidence of late Paleocene–early Eocene hyperthermalevents in biosiliceous sediments of Western Siberia andadjacent areas, Aust. J. Earth Sci., 105, 145–153.

Pross, J., L. Contreras, P. K. Bijl, D. R. Greenwood, S. M. Bohaty, S. Schouten, J. A. Bendle U. Röhl, L. Tauxe, J. I. Raine, E. Claire, C. E. Huck, T. van de Flierdt, S. R. Stewart, S. S. R. Jamieson, C. E. Stickley, B. van de Schootbrugge, C. Escutia, and H. Brinkhuis (2012), Persistent near-tropical warmth on the Antarctic continent during the early Eocene Epoch, Nature, 488, 73–77, doi:10.1038 /nature11300.

Pujalte, V., Baceta, J. I., & Schmitz, B. (2015). A massive input of coarse-grained siliciclastics in the Pyrenean Basin during the PETM: the missing ingredient in a coeval abrupt change in hydrological regime. Climate of the Past, 11(12), 1653-1672.

Pearson, P. N., & Palmer, M. R. (2000). Atmospheric carbon dioxide concentrations over the past 60 million years. *Nature*, *406*(6797), 695-699.

Pearson, P. N., N. J. Shackleton, and M. A. Hall (1993), Stable isotope paleoecology of middle Eocene planktonic foraminifera and multispecies isotope stratigraphy, DSDP Site 523, South Atlantic, J. Foraminiferal Res., 23, 123-140, doi:10.2113/gsjfr.23.2.123.

Pearson, P. N., R. K. Olsson, C. Hemblen, B. T. Huber, and W. A. Berggren (Eds.) (2006), Atlas of Eocene Planktonic Foraminifera, Cushman Special Publication, vol. 41, pp. 513, Department of Geology East Carolina Univ., Greenville.

Petrizzo, M. R. (2007), The onset of the Paleocene–Eocene Thermal Maximum(PETM) at Sites 1209 and 1210 (Shatsky Rise, PacificOcean) as recorded by planktonic foraminifera, Mar. Micropaleontol.,63, 187–200.

Petrizzo, M.-R., G. Leoni, R. P. Speijer, B. De Bernardi, and F. Felletti (2008), Dissolution susceptibility of some Paleogene planktonic foraminifera from ODP Site 1209 (Shatsky Rise, Pacific Ocean), J. Foraminiferal Res., 38(4), 357–371.

Pross, J., L. Contreras, P. K. Bijl, D. R. Greenwood, S. M. Bohaty, S. Schouten, J. A. Bendle, U. Röhl, L. Tauxe, J. I. Raine, E. Claire, C. E. Huck, T. van de Flierdt, S. R. Stewart, S. S. R. Jamieson, C. E. Stickley, B. van de Schootbrugge, C. Escutia, and H. Brinkhuis (2012), Persistent near-tropical warmth on the Antarcticcontinent during the early Eocene Epoch, Nature, 488, 73–77, doi:10.1038 /nature11300.

Ridgwell, A., and Zeebe, R. E. (2005), The role of the global carbonate cycle in the regulation and evolution of the Earth system, Earth and Planetary Science Letters, 234(3), 299-315.

Röhl, U., T. Westerhold, S. Monechi, E. Thomas, J. C. Zachos, and B. Donner (2005), The third and final early Eocene Thermal Maximum: Characteristics, timing, and mechanisms of the “X” event, Geol. Soc. Am. Abstr. Program, 37 (7), 264.

Schmidt, D. N., S. Renaud, J. Bollmann, R. Schiebel, and H. R. Thierstein (2004), Size distribution of Holocene planktic foraminifer assemblages: Biogeography, ecology and adaptation, Mar. Micropaleont., 50(3–4), 319–338, doi:10.1016/S0377-8398(03)00098-7.

Schmitz, B., and V. Pujalte (2007), Abrupt increase in seasonal extreme precipitation at the Paleocene-Eocene boundary, Geology, 35, 215–218.

Schneider, L. J., T. J. Bralower, and L. J. Kump (2011), Response ofnannoplankton to early Eocene ocean destratification, Palaeogeogr.Palaeocl., 310, 152–162.

Schulte, P., C. Scheibner, and R. C. Speijer (2011), Fluvial discharge and sea-level changes controlling black shale deposition during the Paleocene–Eocene Thermal Maximum in the Dababiya Quarry section, Egypt, Chem. Geol., 285, 167–183, doi:10.1016/j.chemgeo.2011.04.004.

Sexton, P. F., P. A. Wilson, and P. N. Pearson (2006), Microstructural and geochemical perspectives on planktic foraminiferal preservation: 'Glassy' versus 'Frosty', Geochemistry Geophysics Geosystems, v. 7, Q12P19, doi:10.1029/2006GC001291.

Sexton, P. F., R. D. Norris, P. A. Wilson, H. Pälike, T. Westerhold, U. Röhl, C. T. Bolton, and S. Gibbs (2011), Eocene global warming events driven by ventilation of oceanic dissolved organic carbon, Nature, 471, 349–353, doi:10.1038/nature09826.

Shamrock, J. L., Watkins, D. K., & Johnston, K. W. (2012), Eocene biogeochronology and magnetostratigraphic revision of ODPHole 762C, Exmouth Plateau (northwest Australian Shelf). *Stratigraphy*, *9*(1), 55.

Shipboard Scientific Party (2004), Site 1263, in Zachos, J. C., D. Kroon, P. Blum, et al., Proc. ODP, Init. Repts., 208, College Station, TX (Ocean Drilling Program), 1–87, doi:10.2973/odp.proc.ir.208.104.2004

Sigman, D. M., Hain, M. P., & Haug, G. H. (2010), The polar ocean and glacial cycles in atmospheric CO2 concentration. *Nature*, *466*(7302), 47-55.

Sims, P. A., Mann, D. G., & Medlin, L. K. (2006), Evolution of the diatoms: insights from fossil, biological and molecular data. *Phycologia*, *45*(4), 361-402.

Slotnick, B. S., G. R. Dickens, M. J. Nicolo, C. J. Hollis, J. S. Crampton, and J. C. Zachos (2012), Large-amplitude variations in carbon cycling and terrestrial weathering during the latest Paleocene and earliest Eocene: The record at Mead Stream, New Zealand, J. Geol., 120(5), 487–505, doi:10.1086/666743.

Slotnick, B. S., G. R. Dickens, C. J. Hollis, J.S. Crampton, P. S. Strong, and A. Phillips (2015), The onset of the EarlyEocene Climatic Optimum at Branch Stream, Clarence Rivervalley, New Zealand, New Zeal. J. Geol. Geop., 58, 1–19, doi:10.1080/00288306.2015.1063514.

Sluijs, A., S. Schouten, M. Pagani, M. Woltering, H. Brinkhuis, J. S. Sinninghe Damsté, G. R. Dickens, M. Huber, G. Reichart, R. Stein, J. Matthiessen, L. J. Lourens, N. Pedentchouk, J. Backman, K. Moran, and the Expedition 302 Scientists (2006), Subtropical Arctic Ocean temperatures during the Palaeocene/Eocene thermal maximum, Nature, 441, 610–613,doi:10.1038/nature04668.

Sluijs, A., G. J. Bowen, H. Brinkhuis, L. J. Lourens, and E. Thomas (2007), The Paleocene–Eocene thermal maximum super greenhouse: biotic and geochemical signatures, age models and mechanisms of global change, in Deep-Time Perspectives on Climate Change, edited by Williams, M., A. M. Haywood, F. J. Gregory, and D. N. Schmidt, Micropalaeont. Soc. Spec. Publ., Geological Society, London, 323–350.

Sluijs, A., S. Schouten, T. H. Donders, P. L. Schoon, U. Röhl, G.-J. Reichart, F. Sangiorgi, J. H. Kim, J. S. Sinninghe Damsté, and H. Brinkhuis (2009), Warm and wet conditions in the Arctic region during Eocene Thermal Maximum 2, Nat. Geosci., 2(11), 1–4, doi:10.1038/ngeo668.

Smith, R. Y., D. R. Greenwood, and J. F. Basinger (2010), Estimating paleoatmospheric pCO2 during the Early Eocene Climatic Optimum from stomatal frequency of Ginkgo, Okanagan Highlands, British Columbia, Canada, Palaeogeogr. Palaeocl., 293, 120–131.

Stap, L., A. Sluijs, E. Thomas, and L. J. Lourens (2009), Patterns and magnitude of deep sea carbonate dissolution during Eocene Thermal Maximum 2 and H2, Walvis Ridge, Southeastern Atlantic Ocean, Paleoceanography, 24, PA1211, doi:10.1029/2008PA001655.

Stap, L., L. J. Lourens, E. Thomas, A. Sluijs, S. Bohaty, and J. C. Zachos (2010a), High-resolution deep-sea carbon and oxygen isotope records of Eocene Thermal Maximum 2 and H2, Geology, 38, 607–610, doi:10.1130/G30777.1.

Stap, L., L. J. Lourens, A. van Dijk, S. Schouten, and E. Thomas (2010b), Coherent pattern and timing of the carbon isotope excursion and warming during Eocene Thermal Maximum 2 as recorded in planktic and benthic foraminifera, Geochem. Geophys. Geosyst., 11, Q11011, doi:10.1029/2010GC003097.Thomas, 1998;

Thomas, E., J. C. Zachos, and T. J. Bralower (2000), Deep-sea environments on a warm earth: latest Paleocene-early Eocene, in Warm Climates in Earth History, edited by Huber, B., K. MacLeod, and S. Wing, Cambridge University Press, Cambridge, UK.

Thunell, R. C., & Honjo, S. (1981). Calcite dissolution and the modification of planktonic foraminiferal assemblages, Marine Micropaleontology, 6(2), 169-182.

Toumarkine, M., and H. Luterbacher (1985), Paleocene and Eocene planktic foraminifera, in Plankton Stratigraphy, edited by H. M. Bolli, J. B. Saunders, and K. Perch-Nielsen, pp. 87–154, Cambridge Univ. Press, Cambridge, U. K.

Vandenberghe, N., F. J. Hilgen, R. P. Speijer, J. G. Ogg, F. M. Gradstein, O. Hammer, C. J. Hollis, and J. J. Hooker (2012) The Paleogene Period, in The Geologic Time Scale 2012, edited by Gradstein, F., J. G. Ogg, M. D. Schmitz, and G. M. Ogg, 855–921, Elsevier, Amsterdam.

Van der Zwaan, G. J., Jorissen, F. J., & De Stigter, H. C. (1990). The depth dependency of planktonic/benthic foraminiferal ratios: constraints and applications. Marine Geology, 95(1), 1-16.

Van Hinsbergen, D. J. J., L. V. de Groot, S. J., van Schaik, W. Spakman, P. K. Bijl, A. Sluijs, C. G. Langereis, and H. Brinkhuis (2015), A Paleolatitude Calculator for Paleoclimate Studies, PLoS ONE, 10, e0126946, doi:10.1371/journal.pone.0126946.

Wade, B. S., P. N. Pearson, W. A. Berggren, and H. Pälike (2011), Review and revision of Cenozoic tropical planktonic foraminiferal biostratigraphy and calibration to the geomagnetic polarity and astronomical time scale, Earth Sci. Rev., 104(1–3), 111–142, doi:10.1016/j.earscirev.2010.09.003.

West, R. M., and M. R. Dawson (1978), Vertebrate paleontology and the Cenozoic history of the North Atlantic region, Polarforschung, 48(1/2), 103-119.

Westerhold, T., U. Röhl, H. K. McCarren, and J. C. Zachos (2009), Latest on the absolute age of the Paleocene–Eocene Thermal Maximum (PETM): new insights from exact stratigraphic position of key ash layers+ 19 and− 17, Earth and Planetary Science Letters, 287(3), 412-419.

Westerhold, T., U. Röhl, J. Laskar, I. Raffi, J. Bowles, L. J. Lourens, and J. C. Zachos (2007), On the duration of magnetochrons C24r and C25n and the timing of early Eocene global warming events: Implications

from the Ocean Drilling Program Leg 208 Walvis Ridge depth transect, Paleoceanography, 22, PA2201, doi:10.1029/2006PA001322.

Westerhold, T., U. Röhl, T. Frederichs, S. M. Bohaty, and J. C. Zachos (2015), Astronomical calibration of the geological timescale: Closing the middle Eocene gap, Clim. Past, 11(9), 1181–1195, doi:10.5194/cp-11-1181-2015.

Wilf, P., R. N. Cúneo, K. R. Johnson, J. F. Hicks, S. L. Wing, and J. D. Obradovich (2003), High plant diversity in Eocene South America:evidence from Patagonia, Science, 300, 122–125.

Wing, S. L., T. M. Bown, and J. D. Obradovich (1991), Early Eocene biotic and climatic change in interior western North America, Geology, 19, 1189–1192.

Woodburne, M. O., G. F. Gunnell, and R. K. Stucky (2009), Climate directly influences Eocene mammal faunal dynamics in North America, P. Natl. Acad. Sci. USA, 106, 13399–13403.

Yapp, C. J. (2004), Fe (CO 3) OH in goethite from a mid-latitude North American Oxisol: estimate of atmospheric CO 2 concentration in the Early Eocene “climatic optimum”, Geochimica et Cosmochimica Acta, 68(5), 935-947.

Zachos, J. C., M. Pagani, L. Sloan, E. Thomas, and K. Billups (2001), Trends, rhythms, and aberrations in global climate 65 Ma to present, Science, 292, 686–693, doi:10.1126/science.1059412.

Zachos, J. C., D. Kroon, P. Blum, et al. (2004), Proc. ODP, Init. Repts., 208, College Station, TX (Ocean Drilling Program), doi:10.2973/odp.proc.ir.208.2004.

Zachos, J. C., et al. (2005), Rapid acidification of the ocean during the Paleocene-Eocene thermal maximum, Science, 308, 1611–1615, doi:10.1126/science.1109004.

Zachos, J. C., G. R. Dickens, and R. E. Zeebe (2008), An early Cenozoic perspective on greenhouse warming and carbon-cycle dynamics, Nature, 451(7176), 279-283, doi:10.1038/nature06588.

Zachos, J. C., H. K. McCarren, B. Murphy, U. Röhl, and T. Westerhold (2010), Tempo and scale of late Paleocene and early Eocene carbon isotope cycles: Implications for the origin of hyperthermals, Earth Planet. Sci. Lett., 299, 242–249, doi:10.1016/j.epsl.2010.09.004.

Zonneveld, K. A., and G. A. Brummer (2000), (Palaeo-) ecological significance, transport and preservation of organic-walled dinoflagellate cysts in the Somali Basin, NW Arabian Sea. Deep Sea Research Part II: Topical Studies in Oceanography, 47(9), 2229-2256.

CHAPTER VI

Change from dominant dextral to sinistral coiling in planktic foraminifera *Morozovella* during the Early Eocene Climatic Optimum

To be submitted

Abstract

The coiling direction of trochospiral planktic foraminifera is a widely investigated morphological feature in living species and in upper Quaternary sediment. However, this morphological trait remains scarcely documented in older marine sediment. Here we investigate the coiling direction within *Morozovella* populations from sections at two ocean drilling sites in the Atlantic that span the Early Eocene Climatic Optimum (EECO; ~49-53 Ma). The symbiont-bearing surface-dweller planktic foraminiferal genus *Morozovella* is of particular interest because of its dominance in tropical-subtropical early Paleogene assemblages, and the time interval is of interest of an abrupt and permanent decline in abundance and taxonomic diversity of *Morozovella* at the J event, near the beginning of the EECO. Our results demonstrate that morozovellids display a dominant dextral preference during the interval preceding the EECO at both the studied sites. However, all species show a first, prominent flip to sinistral coiling mode starting slightly above the J event. This switch from dextral to sinistral coiling became permanent for most of the *Morozovella* species slightly after the K/X event. Temporary but significant switches towards sinistral coiled morphotypes also occurred at both sites during several pre-EECO hyperthermal events. We record therefore a remarkable variation in the coiling mode of *Morozovella* during extreme warming intervals of the early Paleogene. Our record sheds new light on the coiling direction preferences of Paleogene planktic foraminifera. Previous interpretations favour genetic explanations for coiling flips rather than ecological responses. Our present data cannot validate or disprove the former idea, but should stimulate renewed thought on the latter idea.

1. Introduction

Evolutionary trends of planktic foraminifera and major modifications in their abundance often appear to correlate with significant changes in climate, although the relationship remains insufficiently resolved (e.g., Schmidt et al., 2004; Ezard et al., 2011; Fraass et al., 2015). Early Paleogene represents an especially important interval for which to understand such linkages between foraminifera and climate (Fraass et al., 2015; Luciani et al., 2016). Earth surface generally warmed from the Late Paleocene through the Early Eocene Climatic Optimum (EECO, ~49-53 Ma), a loosely defined interval of peak Cenozoic warmth (Zachos et al., 2001, Luciani et al., 2016) when temperatures exceeded those of present day by at least 10 °C (Zachos et al., 2008; Bijl et al., 2009; Huber and Caballero, 2011; Hollis et al., 2012;

Pross et al., 2012; Inglis et al., 2015). Superimposed on this long-term thermal trend were several short-lived (~40-200 kyr) warming events, referred to as hyperthermals (e.g., Lourens et al., 2005; Nicolo et al., 2007; Laurentano et al., 2016). Although they have different magnitudes, hyperthermals share several key characteristics beyond evidence for excess warmth, most notably negative carbon isotope ($\delta^{13}C$) excursions (CIEs) and evidence for dissolution of deep-sea carbonate (e. g., Zachos et al., 2005; Leon-Rodriguez and Dickens, 2010). The most extreme hyperthermal was the Paleocene/Eocene Thermal Maximum (PETM; e.g., Kennett and Stott, 1991; Zachos et al., 2010; McInerney and Wing, 2011) at ~56 Ma (e.g., Westerhold et al., 2008), when global temperatures increased 5-8°C (e.g., McInerney and Wing, 2011; Dunkley-Jones et al., 2013), and marine carbonate typically records a >–3‰ negative $\delta^{13}C$ excursion (above references). However, other notable hyperthermal events include the H-1, I-1, J and K/X events (e.g. Cramer et al., 2003; Lourens et al., 2005; Nicolo et al., 2007; Agnini et al., 2009; Stap et al., 2009, 2010; Zachos et al., 2010; Coccioni et al. 2012; Kirtland Turner et al., 2014; Littler et al., 2014; Lauretano et al., 2015) with the J event initiating the EECO (Slotnick et al., 2012, 2015; Lauretano et al., 2016; Luciani et al. 2016).

Major turnovers within planktic foraminferal assemblages occurred during the early Paleogene, consisting in diversification for some taxa and species reductions for other groups (e.g., Norris, 1991; Schmidt et al., 2004; Pearson et al., 2006; Aze et al., 2011; Ezard et al., 2011; Fraass et al., 2015). The symbiont-bearing surface-dweller planktic foraminiferal genus *Morozovella* is of particular interest because of its dominance in tropical-subtropical assemblages of early Paleogene oceans (e.g., Boersma and Premoli Silva, 1983; Premoli Silva and Boersma, 1988). However, within foraminiferal assemblage records at multiple sites (Fig. 1), this genus shows a sharp and permanent decline in relative abundance, as well as a reduction in taxonomic diversity, at the beginning of the EECO. In fact, this striking change in morozovellids closely corresponds to the CIE marking the J event (Luciani et al., 2016), which occurred at ~53 Ma and near the boundary between polarity chrons C24n.2r and C24n.3n (Slotnick et al., 2015; Laurentano et al., 2015). The morozovellid decline has been documented clearly at DSDP Site 577 (northwest Pacific), ODP Site 1051 (northwest Atlantic) and the Possagno section (northern Italy) (Luciani et al., 2016; Chapter IV). At these three locations, the relative abundance of *Morozovella* in planktic foraminiferal assemblages drops by more than two thirds across the J event (Luciani et al, 2016). A marked drop in *Morozovella* abundance also has been recorded at the Contessa section (central Italy), although at the top of C24n.2n and slightly after the J event (Frontalini et al., 2016). At ODP

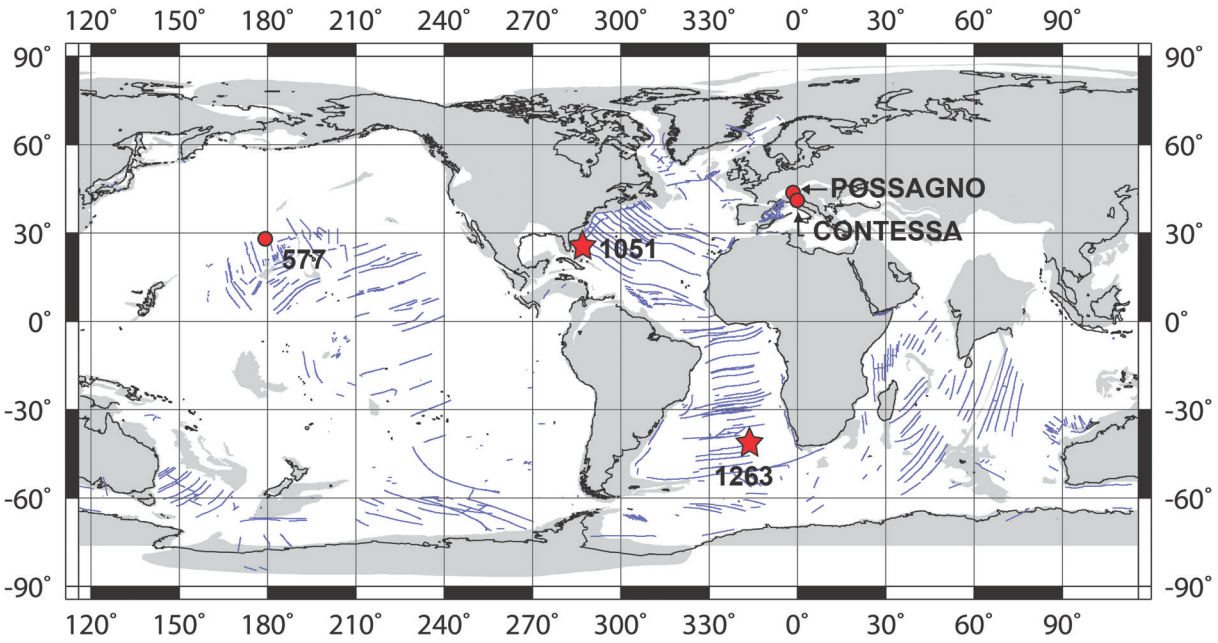

Figure 1. Approximate locations of the studied sites (stars) during the early Eocene. Also shown are the other successions recording planktic foraminiferal changes across the EECO. Base map is from http://www.odsn/de/services/paleomap.html with paleolatitudes modified for Sites 577, 1051 and 1263 according to www.paleolatitude.org model version 1.2 (Van Hinsbergen et al., 2015). Possagno and Contessa paleolatitudes are based on the http://www.odsn.de/odsn/services/paleomap/adv_map.html model since are not yet available at www.paleolatitude.org.

Site 1263 (southwest Atlantic), *Morozovella* abundance decreases by more than half slightly after the J event (Chapter V). At all five of these locations (Fig. 1), the pronounced drop in morozovellid abundance is accompanied by an increase in the relative abundance and diversification of the genus *Acarinina* (e.g., Pearson et al., 2006; Aze et al., 2011; Fraas et al., 2015; Luciani et al., 2016).

Environmental stress due to anthropogenic burning of fossil fuels and concomitant warming pose outstanding questions regarding environmental change and biotic responses. A more complete comprehension of the dramatic morozovellid decline at the start of the EECO therefore presents a fascinating focal point for study. Planktic foraminifera with a trochospiral arrangement of chambers, such as *Morozovella*, can grow their shells by adding chambers in a clockwise (dextral) or counter-clockwise (sinistral) direction, as observed in spiral-side view. This is interesting because, as discussed below, coiling switches can relate to ecophenotypic adaption (e.g., a morphological response to variation in temperature or other environmental parameters) or genetic variance (i.e., morphologically similar species with different environmental preference). So do various morozovellids display major changes in coiling direction, and if so, how do these relate to the major change in abundance and diversity across

the J event?

We explore here changes in the coiling direction of *Morozovella* shells for multiple species at two of the aforementioned locations where the major change in morozovellid abundance has been documented: ODP Site 1051 and ODP Site 1263 (Fig. 1). We demonstrate significant changes in coiling direction occur near the start of the EECO.

2. Background

2.1. Coiling Direction in Planktic Foraminifera and its Significance

Coiling direction is a characteristic morphological feature of certain planktic foraminifer. Morphologically defined species with trochospiral tests can have populations with subequal proportions of right- and left-coiled tests, but can also have populations dominated by a strong preference for either spiral direction. In the geological record, distinct shifts in the ratio of coiling direction for a "species" (hereafter the "coiling ratio") have been observed in space and time.

For the present-day ocean and late Neogene sediment, the relationship between the coiling ratio of a species and environmental parameters has been quantitatively described and extensively utilized, often to reconstruct paleoceanographic conditions (e.g., Ericson et al., 1955, Bandy, 1959, 1972; Saito, 1976; Bond et al., 1993; Xu et l., 1995; Renaud and Schmidt, 2003; Martinez et al., 2007). The best-known example is *Neogloboquadrina pachyderma*, where sinistrally coiled forms have a modern polar distribution and dextrally coiled forms have a sub-polar distribution (e.g., Kucera and Kennett, 2002; Bauch et al., 2003). Traditionally, changes in the coiling ratio have been assumed to reflect ecophenotypic adaptation (e.g., Ericson, 1959; Ericson et al., 1954; Bandy, 1960; Boltovskoy, 1973). However, for *N. pachyderma*, genetic signatures demonstrate that the sinistral and dextral morphotypes actually represent separate species (Darling et al., 2004) with the latter renamed *Neogloboquadrina incompta* (Darling et al., 2006), as originally described by Cifelli (1961). The coiling direction in *N. pachyderma* is, therefore, a genetic trait, heritable through time, rather than a morphological feature reflecting ecophenotypic variation (Darling et al., 2006). On the other hand, Darling et al. (2003) found that left- and right-coiled individuals within morphotypes of *Globorotalia truncatulinoides* and *Globigerina bulloides* have the same genetic signatures. The co-occurrence of species that exhibit different coiling directions might suggest environmental controls on morphology. This supposition is confirmed by Ujiié and

Asami (2014), who show (a) both sinistral and dextral coiling morphotypes in genetically similar Type II *Globorotalia truncatulinoides*, and (b) the two inversely coiled forms within Type II differ in ecology as both left- and right-coiled populations have a proper niche partitioning in different water masses (Ujiié and Asami, 2014).

Most of the recent planktic foraminferal cryptic species clearly display ecological preferences for different water-masses (e.g., Ujiié et al., 2010; Morard et al., 2016). Adaptation to environmental change, therefore, may enable speciation of planktic foraminfera. For example, the niche partitioning between dextral and sinistral *G. truncatulinoides* Type II may suggest that these forms have the potential to genetically diverge from each other, similar to *Globigerinoides ruber*, which contains two sister genetic types in the Mediterranean Sea (Aurahs et al., 2009). It appears that chemical-physical parameters and water-mass boundary have the potential to provide separation for speciation also in absence of geographic barriers.

An original attempt to understand whether the planktic foraminiferal coiling direction might be controlled by reproductive modes has been made on *Neogloboquadrina pachyderma,* population by Khare et al. (2012). Even though dimorphism due to sexual/asexual reproduction modes in planktonic foraminifera has yet to be demonstrated, in laboratory culture the right coiling forms of the species *Neogloboquadrina pachyderma* have showed a possible asexual reproduction (Kimoto and Tsuchiya, 2006). Specifically, in spite of right coiling morphotypes of the parental test all gamonts produced left coiling morphotypes. These results suggest that two alternative reproductive phases in the life cycle of *N. pachyderma* are possible and that the coiling direction might be controlled by the reproductive generations in one genotype. Following this assumption, Khare et al. (2012) compared the coiling direction and mean proloculus size, assumed as potentially reflecting sexual and asexual reproduction modes, within planktic foraminiferal assemblages from the southwestern Indian Ocean. Results revealed that these parameters were not related and authors deduced therefore the absence of any relationship between the coiling direction and reproductive modes (as expressed in terms of mean proloculus size). Khare et al. (2012) therefore pointed out that the coiling direction in the studied planktic foraminifera is influenced more by the properties of the water masses rather than by the reproductive modes. On the other hand, further studies are needed to substantiate the occurrence of asexual reproduction in *N. pachyderma* life cycle as well as in other planktic foraminifera. Consequently the relationship between coiling direction change and reproductive modes still remains a hypothesis.

From the considerations above it appears evident that the true meaning and mechanisms

of planktic forminferal switch in coiling direction still represent an open question. Even considering of primary importance the ecophenotypic response to explain the coiling reverse, numerous controversies exist about which are the environmental parameters that primarily influence the coiling directions changes (e.g., Boltovoskoy and Wright, 1976; Malmgren, 1984; Collins, 1990, Khare et al., 2012 and reference therein). A plethora of alternative explanations has been proposed such as seasonal effect, water depth, test size, differential predation, modification in salinity and/or other water-masses properties, such as temperature, water density and even paleomagnetism, (Scott, 1974; see review in Khare et al., 2012, and reference therein). However, at present, available evidences were not straightforward enough to confidently agree or disagree with one or more of the suggested factors as the potential cause inducing change in planktic foraminiferal coiling directions.

2.2. Planktic Foraminiferal Coiling Direction Change during the Cretaceous and Paleogene

Sinistral and dextral coiling preferences in a number of morphologically defined species have been recorded in Upper Cretaceous and lower Paleogene successions (e.g., Bolli, 1950; Pearson, 1993; Norris and Nishi, 2001; Hancock, 2005; Coccioni et al., 2016). We briefly overview these cases, along with suggested causes for the morphological changes.

The pattern of coiling direction of the latest Cenomanian planktic foraminiferal *Rotalipora cushmani* population has been recently investigated in the interval preceding its disappearance in the central-western Tethys from the classical Tethyan Bottaccione section (Gubbio, Italy) (Coccioni et al., 2016). This section is the type locality of the C_{org}-rich Bonarelli Level that is the sedimentary expression of the worldwide latest Cenomanian oceanic anoxic event 2 (OAE 2, e.g., Schlanger and Jenkyns, 1976). Coccioni et al. (2016) distinguish a *R. cushmani* morphotype with right-coiling preferences in the ~55 kyr preceding the deposition of organic matter. The *Rotalipora. cushmani* right-coiling preference has been also observed from the uppermost Cenomanian of the Western Interior Seaway (USA), the Vocontian Basin (southeast France), and the Wadi Bahloul Formation (central Tunisia) (Desmares et al., 2008). Coccioni et al. (2016) do not exclude that these morphotypes could represent cryptic species, even though the morphological variability within *Rotalipora cushmani* has generally been referred as intraspecific flexibility or ecophenotypy (e.g., Hecht, 1976; Kennett, 1976; Healy-Williams and Williams, 1981; Healy-Williams et al., 1985). Essentially, the analysis of Coccioni et al. (2016) favours an extreme environmental change as triggering the morphological variations observed within the terminal *R. cushmani.*

Specifically, marked variations in the physicochemical properties of seawater were related to volcanic discharge that characterized the ~55 kyr preceding the onset of OAE2 and linked to the major phase of the Caribbean large igneous province emplacement (Du Vivier et al., 2014; Loewen et al., 2013). The pulse of volcanic activity was associated to increased eutrophy both by emission of biolimiting metal and because causing rapid rise of pCO_2 that turned the climate in a strengthened greenhouse mode thus accelerating the continental weathering (e.g., Pegram and Turekian, 1999; Mort et al., 2007; Turgeon and Creaser, 2008, Barclay et al., 2010; Jenkyns, 2010). However, it is not possible to establish to date the primary environmental disruption causing the right coiling preference in the terminal *R. cushmani*.

Hancock (2005) demonstrated a prominent coiling switch from dextral to sinistral in the late Paleocene surface-dwelling planktic foraminifera *Igorina albeari* at three low latitude sites from the central Pacific Ocean at ~59 Ma. The morphological change coincides with widespread dissolution throughout the central Pacific Ocean and with a positive $\delta^{13}C$ excursion that occurred near the base of the Paleocene Carbon Isotope Maximum (PCIM, Zachos, 2001). At one of the sites examined (Hole 865B), apparent cooling of the deep thermocline coincides with the switch to a sinistrally dominated population. However, the coiling shift may not reflect a change in temperature *per se* (Hancock, 2005). This is because stable isotopes from *I. albeari* specimens suggest that both sinistral and dextral coiled morphotypes occupied similar surface-water masses whatever genetically or ecologically generated the differences between the two morphotypes. Therefore, the reversal to sinistral coiling mode did not involve significant change in depth ecology that implies a temperature change. The coiling reversal is ascribed to change in other ecological parameters such as feeding strategy for nutrient availability that may have caused the observed decline of dextral morphotypes at the Pacific tropic localities (Hancock, 2005). Whatever were the triggering reasons, the recorded coiling shift at the Pacific Ocean provides an important biomarker that coincides with the PCIM and occurred between the lowest occurrences of *Heliolithus kleinpelli* and *Globanomalina pseudomenardii* (Hancock, 2005).

Pearson (1993), in his proposal for a lineage phylogeny of Paleogene planktic foraminifera, noted an interesting observation concerning the coiling preferences of members of the *M. velascoensis* group, which became extinct in the earliest Eocene. This group was characterized by dominantly sinistral coiling. By contrast, members of the *Morozovella aequa* group, which include *M. subbotinae*, *M. gracilis*, *M. lensiformis* were characterized by dominantly dextral coiling. However, according to Bolli (1950) and Luterbacher (1964), the *M. lensiformis* group, reversed its preferred direction of coiling from dextral to sinistral at the

extinction level of the *M. subbotinae.* The aforementioned changes in coiling direction have been related to evidence of genetic divergence (Pearson, 1993). However, the observed switches were not directly related by the aforementioned authors with stable-isotope stratigraphy.

Norris and Nishi (2001) examined the relationships between planktic foraminifera and preferences in coiling direction from an exquisite evolutionary perspective. The authors draw attention to the evidence that at least four major radiations of planktic foraminifera in Late Cretaceous, Paleocene, middle Eocene, and Neogene were initiated from ancestors with proportionate coiling (about 50% of dextral and sinistral) but subsequently species acquired a dominance of sinistral or dextral morphotypes (Norris and Nishi, 2001 and references therein). In particular, Norris and Nishi (2001) analysed the coiling of the Paleogene planktic foraminifera from the mid-Pacific equatorial Site 856 and found a recurrent pattern of coiling in foraminiferal evolution. This pattern consists in the maintenance in each radiation of a preferential coiling until the extinction of the clade. In addition, species with proportionate coiling consistently appear to be the founders of successive diversifications. The authors conclude therefore that the coiling patterns are heritable and not environmentally controlled. Norris and Nishi (2001) observe also that, on evolutionary timescales, species with proportionate coiling seem less susceptible to extinction than species dominated by sinistral or dextral forms probably because they keep greater genetic variability than species with biased coiling. As an example, Upper Maastrichtian foraminifera were predominantly dextral and are not known to revert to proportionate coiling (Bolli 1971; Malmgren 1989), but only the few species with proportionate coiling actually survived the Cretaceous/Paleogene mass extinction. However, Norris and Nishi (2001) recognize that the occurrence of opposite-coiled individuals in virtually every planktic foraminiferal population suggests that all species may retain the genetic key that allow them to coil either way and therefore a flip to a particular coiling mode may be difficult but not impossible.

Brummer and Kroon (1988) exploring the causal mechanisms controlling the coiling direction in modern planktic foraminifera, conclude that the coiling shifts observed in the fossil record were most likely not driven by environmental factors but genetically determined.

Our purpose of research focus on a restricted interval of time with respect to Pearson (1993) and Norris and Nishi (2001) but refers to a higher resolution analysis specifically dedicated to the *Morozovella* genus that suffered a striking decline in abundance and in taxonomic diversity at the EECO interval. In addition, possible switches in coiling direction of the *Morozovella* species are for the first time displayed alongside the long-term and

transient prominent changes in the carbon cycle, as expressed by the $\delta^{13}C$ stable isotope record.

3. Selected Locations: ODP Sites 1051 and 1263

The two sections selected for this study come from ODP Site 1051 on Blake Nose (NW Atlantic) and ODP Site 1263 on Walvis Ridge (SE Atlantic). At both sites, the lower Eocene interval has very good stratigraphy (Figs. 2, 3), determined through key calcareous nannofossil and planktic foraminifera datums, polarity chron boundaries, and detailed carbon isotope records (Site 1051: Norris et al., 1998; Mita, 2001; Cramer et al., 2003; Luciani and Giusberti, 2014; Luciani et al., 2016; Chapter IV; Site 1263: Lourens et al., 2005; Westerhold et al., 2007, Stap et al. 2009, 2010a, 2010b; Lauretano et al. 2015, 2016).

Site 1051 is located at 30° 03.2' N, 76° 21.5' W, but was positioned slightly to the south during the early Eocene (Ogg and Bardot, 2001; Van Hinsbergen et al., 2015). The present water depth is 1992 m, and may have been similar or slightly shallower during the Paleocene and early Eocene as determined through benthic foraminiferal assemblages (1000-2000 m; Norris et al., 1998) or subsidence and sedimentation rate calculations (2200 m ~50 Ma; Bohaty et al. (2009). The interval studied here is from 452.24 to 353.10 mbsf at Hole 1051A (the same as investigated by Luciani et al., 2016 and in chapter IV). This succession has high sedimentation rate and good sediment recovery, except between ~382 and ~390 mbsf, which contains significant chert (Shipboard Scientific Party, 1998).

Site 1263 is located at 28°31.98′ S, 2°46.77′ E, and a few hundred meters below the crest of the Walvis Ridge at 2717 m water depth (Zachos et al., 2004). During the early Eocene, the position was ~40° S and farther from the Equator (Van Hinsbergen et al., 2015), and water depth was ~1500 m and significantly shallower (Zachos et al. 2004). Early Eocene sediments exhibit decimeter- to meter-scale bedding cycles, as expressed in the magnetic susceptibility (MS), colour reflectance and other records (Zachos et al. 2004; Lauretano et al al. 2015; 2016). These cycles are related to eccentricity and precession cycles and, because multiple holes were drilled at Site 1263, can be used to make a spliced sediment record with depths in "revised m composite depth" (rmcd) (Westerhold et al., 2007, 2015). The site has good sedimentary recovery and an apparently complete lower Eocene succession that mainly consists of nannofossil ooze, chalk and marls. Considerable work has been conducted at Site 1263, including calcareous nannofossil and benthic foraminifera information across several of

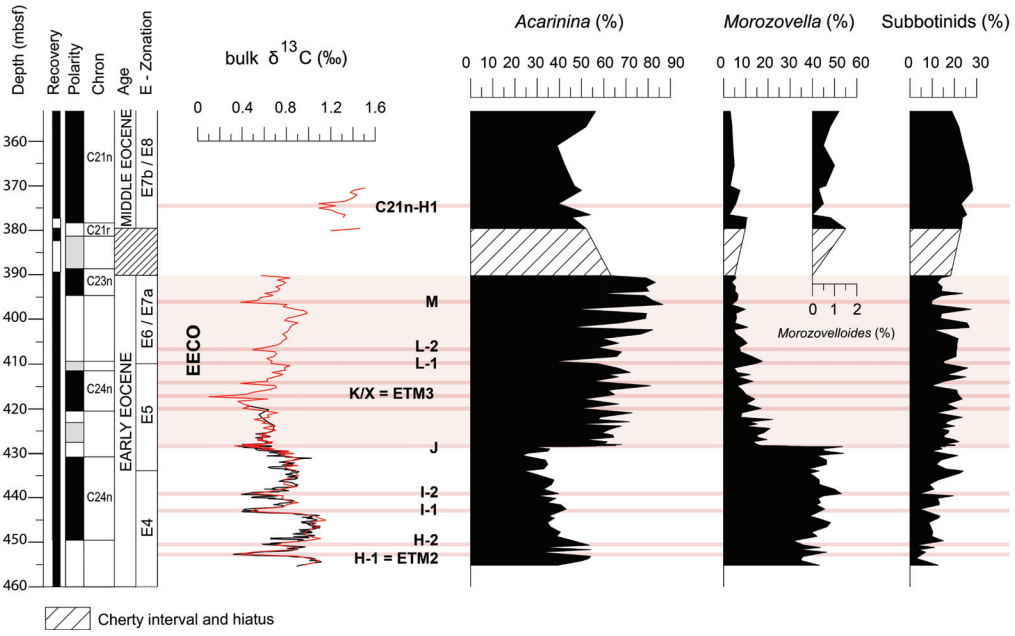

Figure 2. Stratigraphy, bulk sediment $\delta^{13}C$ composition, relative abundances of *Acarinina*, *Morozovella, Morozovelloides* and subbotinids (≥63 μm size fraction) from the Ocean Drilling Program (ODP) Site 1051, Blake Nose Plateau, subtropical North Atlantic Ocean (from Chapter IV, modified). Black $\delta^{13}C$ curve is from Cramer et al. (2003). Subbotinids include the genera *Subbotina* and *Parasubbotina* that had paleoecological affinities (Pearson et al., 2006, and references therein). Planktic foraminiferal biostratigraphy is from Luciani et al. (2016), who applied the zonal scheme of Wade et al. (2011) and included the modifications provided by Luciani and Giusberti (2014). Magnetostratigraphy comes from Ogg and Bardot (2001) but with an important modification to polarity chron labeling provided by Luciani et al. (2016). The thin light-red bands highlight the main carbon isotope excursions (CIEs). We consider the onset of the EECO as coinciding with the J event, in agreement to Luciani et al. (2016). Note the marked and permanent decline of *Morozovella* at the J event.

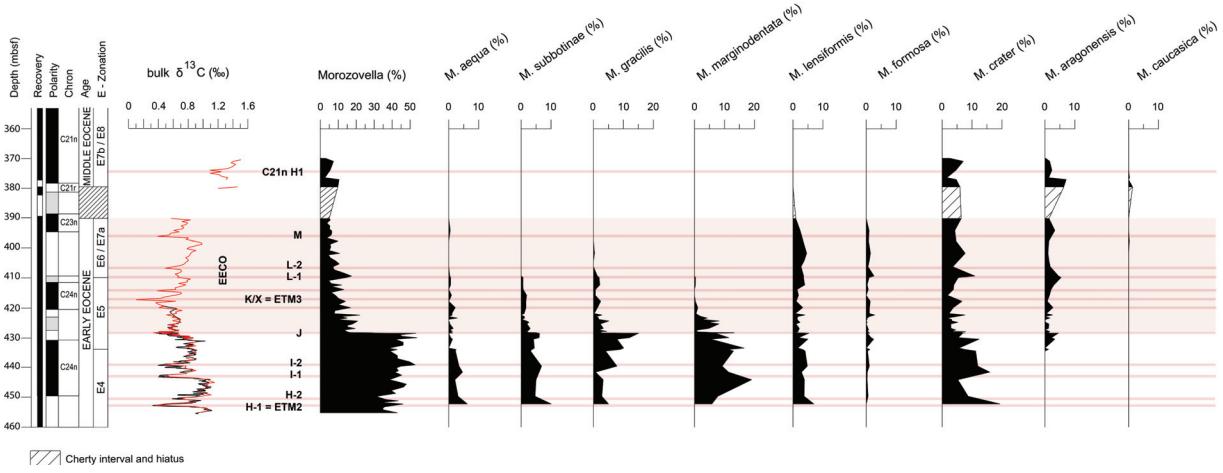

Figure 3. Variation in abundance across the EECO of all the *Morozovella* species (≥63 μm size fraction) and bulk carbonate $\delta^{13}C$ for the early and early middle Eocene at the ODP Site 1051. From Chapter IV, modified. Note that *M. gracilis* and *M. marginodentata* record the most important reduction in abundance at the beginning of the EECO. The adopted taxonomic criteria follow Pearson et al. (2006).

the hyperthermals ETM2, H2, I1 and I2 (e.g., Dedert et al., 2012, 2014; Gibbs et al., 2012; D'Haenens et al., 2014). New data on planktic foraminiferal assemblages also now exist (Chapter V). In summary, there is a very solid stratigraphic framework for the early Eocene at Site 1263.

4. Methods and Biostratigraphy

Planktic foraminifera were analysed on 50 selected samples from the early to early middle Eocene at Site 1051, ranging from 452.24 to 369.9 mbsf. The sample spacing varies from 5 cm to 10 cm across the J event, from 40 cm to 2 m within the EECO and from 40 cm to 3 m below and above. Analyses on planktic foraminifera at Site 1263 were performed on 68 samples spanning the early Eocene interval comprised between 297.16 rmcd and 240.21 rmcd. The residues were prepared by immersing previously freeze-dried samples in deionized water. Disaggregation occurred in a time varying from few hours to 3 days, depending on the compactness of the sediments. When disaggregated, samples were washed over a >63 micron sieve. Sieves were immerged in a methylene blue bath after each washing in order to colour planktic foraminifera potentially trapped in the sieve mesh. This is an easy method to exclude possible contaminations amongst different samples. Washed residues were dried at <50 °C. The taxonomic criteria adopted in this study follow Olsson et al. (1999) and Pearson et al. (2006). The washed residues were examined under an incident light stereomicroscope for their planktic foraminiferal content. Evaluation on changes in coiling direction was performed by counting the right-coiled, i.e. the dextral specimens and the left-coiled, i.e. the sinistral individuals within each *Morozovella* species on a statistical sample comprised between 50 and 150 specimens, depending on the availability. The counts are expressed in percentages with respect to the total *Morozovella* population. Error in coiling direction counts is expressed as standard deviation and shown in Figure S1 and S2 with bars coinciding with $\pm 1\sigma$. The adopted taxonomic criteria follow Olsson et al. (1999) and Pearson et al. (2006).

Site 1051 planktic foraminiferal biostratigraphy comes from Luciani et al. (2016), who applied the zonal scheme of Wade et al. (2011) and included the modification provided by Luciani and Giusberti (2014). Specifically, Zone E6 is invalid as defined by Wade et al. (2011) due to diachronous first appearance of the marker *Acarinina cuneicamerata* thus *Astrorotalia palmerae* has been tentatively proposed as the new marker for Zone E6 (Luciani and Giusberti, 2014). Actually *A. palmerae* is absent at Site 1051 therefore Zones E6/E7a have been combined.

At Site 1263 the main early Eocene planktic foraminiferal biohorizons, e.g., bases (B) and tops (T) of the Wade et al. (2011) zonal scheme were identified (see chapter V). Specifically, the B of *Morozovella aragonensis* (285.69 rmcd) identifies the E4/E5 boundary. Zones E6/E7a have been merged also at Site 1263 due to the absence of *A. palmerae* and because the B of *Acarinina cuneicamerata* (256.32) rmcd is confirmed to have occurred below the T of *Morozovella subbotinae* as well at Site 1263, as noticed for Site 1051 and the Tethyan Possagno section (Luciani and Giusberti, 2014).

5. Results

5.1. *Morozovella* Coiling-Direction Changes at the EECO from Site 1051

Changes in morozovellid coiling direction are here compared with the main carbon cycle perturbations, as expressed by the $\delta^{13}C$ curve. The negative carbon isotope excursions (CIE) are correlated with the events widely recognized on the basis of their bio-magnetostratigraphic position (Fig. 4) and labelled according to Cramer et al. (2003), Coccioni et al. (2012) Lauretano et al. (2016) and Kirtland-Turner et al. (2014) (see chapter IV).

The *Morozovella* population shows a general trend characterized by a remarkable shift from dominant dextral to dominant sinistral from the base of the succession up to the earlier middle Eocene interval (Fig. 4). Such change involves all the *Morozovella* species and occurred in two main steps. A first sharp but transient peak of sinistral-coiling taxa (81%) is recorded at Site 1051 slightly after the J event (423.42 mbsf) and abruptly interrupt the prevailing dextral-coiling that characterises the interval preceding the EECO (94% of dextral specimens in average, Fig. 4). A second shift of 74% sinistral is documented at 413.8 mbsf, ~3.5 m above the CIE corresponding to the K/X event where the sinistral-coiling becomes dominant for most of the *Morozovella* species. Above this shift, only the species *M. crater* and *M. lensiformis* returned to a rather proportionally coiled morphotypes in the upper part of C23r. All the other species retain a dominant sinistral coiling. Specifically, *Morozovella aragonensis*, *M. caucasica* and *M. crater* maintain in the middle Eocene an almost total sinistral coiling (98%, 100%, 88% respectively). The dextral to sinistral long-lasting switch occurs close to the base of Zone E6/E7a. Moderate but significant increases of sinistral morphotypes are recorded by most of the *Morozovella* species in coincidence with the pre-EECO C-cycle perturbations such as ETM2, I1, I2 and J event, but also in correspondence with the CIEs recorded within the EECO, labelled as L1 and L2 and M (Fig. 4). Precisely,

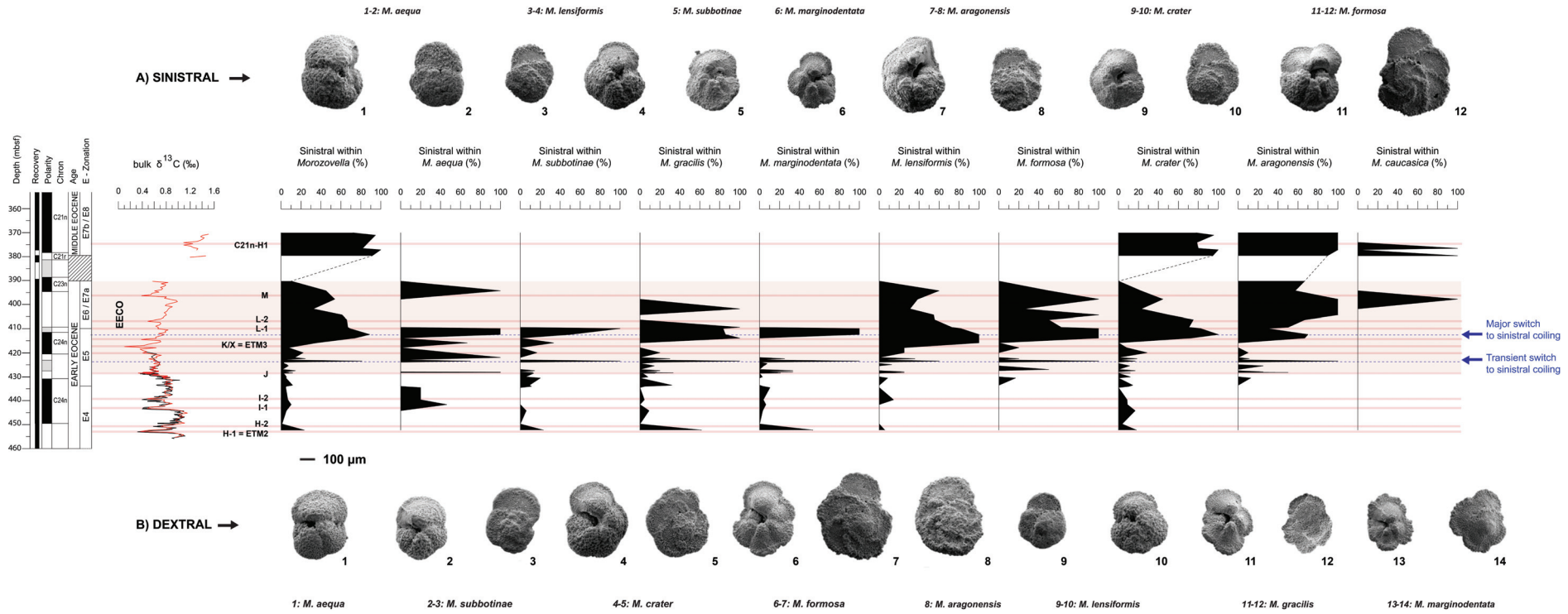

Figure 4. Changes in coiling direction within the *Morozovella* species (≥63 µm size fraction) at Atlantic Site 1051 across the EECO interval and the earlier middle Eocene. Stable isotope data is from Chapter IV. Bio-magnetostratigraphy is from Luciani et al. (2016). Note the marked but transitory flip from dominant dextral to dominant sinistral coiling of all the *Morozovella* species slightly above the J event and the major long-lasted switch slightly above the K/X event. Below the EECO interval the dextral coiling is prevailing in morozovellids with moderate increases of sinistral morphotypes during some of the pre-EECO hyperthermals. Examples of sinistral (upper part of the figure), dominating in the upper part of the studied succession, and dextral (upper part of the figure) *Morozovella* at Site 1051A are also shown. (A, sinistral morphotypes) 1, 7, 9, 11: sample 395.1 mbsf; 2: sample 407.17 mbsf; 3, 4, 8: sample 405.22 mbsf; 5:sample 410.3 mbsf; 6, 10, 12: sample 423.42 mbsf. (B, dextral morphotypes) 1, 3, 11: sample 443.58 mbsf; 2: sample 432.42; 4, 9, 12: sample 428.4 mbsf; 5, 8, 10: 427.99 mbsf; 6, 7, 13, 14: 428.34 mbsf.

M. gracilis and *M. marginodentata* reached peaks of 61% and 53% in sinistral individuals across the ETM2 whereas *M. crater* and *M. subbotinae* recorded a minor increase (18% and 23% respectively). The sinistral morphotypes of *M. aequa* and *M. crater* rise up to the 46% and 17% at the I1. The sinistral *M. aragonensis* and *M. lensiformis* increase up to 25% at 427.91 mbsf, in correspondence to the J event whereas *M. crater*, *M. gracilis*, *M. marginodentata* and *M. subbotinae* reaching peaks of 17%, 33%, 20% and 14% respectively at 427.4 mbsf level.

5.2. *Morozovella* coiling-direction changes at the EECO from Site 1263

The *Morozovella* genus displays trends in the coiling direction preference similar to that record from Site 1051 as compared with the $\delta^{13}C$ curve. At Site 1263 main CIEs are interpreted according to Lauretano et al. (2016) (Fig. 5). A remarkable and persistent switch from dominant dextral (~68%) to dominant sinistral (~80%) is evident above the CIE corresponding to the K/X event (Fig. 5). However, we cannot precisely locate the change due to a 2.5 m core gap in this tract. Significant increases of sinistral morphotypes are recorded by the *Morozovella* genus in coincidence with the ETM2 and H2 CIEs. Precisely, sinistrally coiled *Morozovella* increase of ~52% at the ETM2 and of ~35% at the H2 CIE. A ~20% in percentage of sinistral forms is retained up to the I1 event (Fig. 5). Slightly above the J event a pronounced peak of sinistral forms is evident since morozovellids move from ~90% of dextral coiled morphotypes to ~53% of sinistral forms (Fig. 5). A temporary return to an almost equal ratio between the dextral and sinistral morphotypes occurred between the M and O CIEs within the main phase of the EECO.

6. Discussion

6.1. Carbon Cycle Perturbations and Eocene Coiling Flips at Sites 1051 and 1263

A relationship between flips in the coiling character and main carbon cycle perturbations, as expressed by the $\delta^{13}C$ records, appears evident at sites 1051 and 1263 from our results (Figs. 4, 5). The correspondence between the sinistral coiling direction switches and hyperthermal events evokes a sort of causal effect and needs some reflections. Moreover, the fact that the coiling variation is somewhat proportional to the strength of carbon cycle perturbation, with major changes recorded at the ETM2 and close to the K/X event, reinforce the idea of an interaction between environmental changes occurred at the events and the

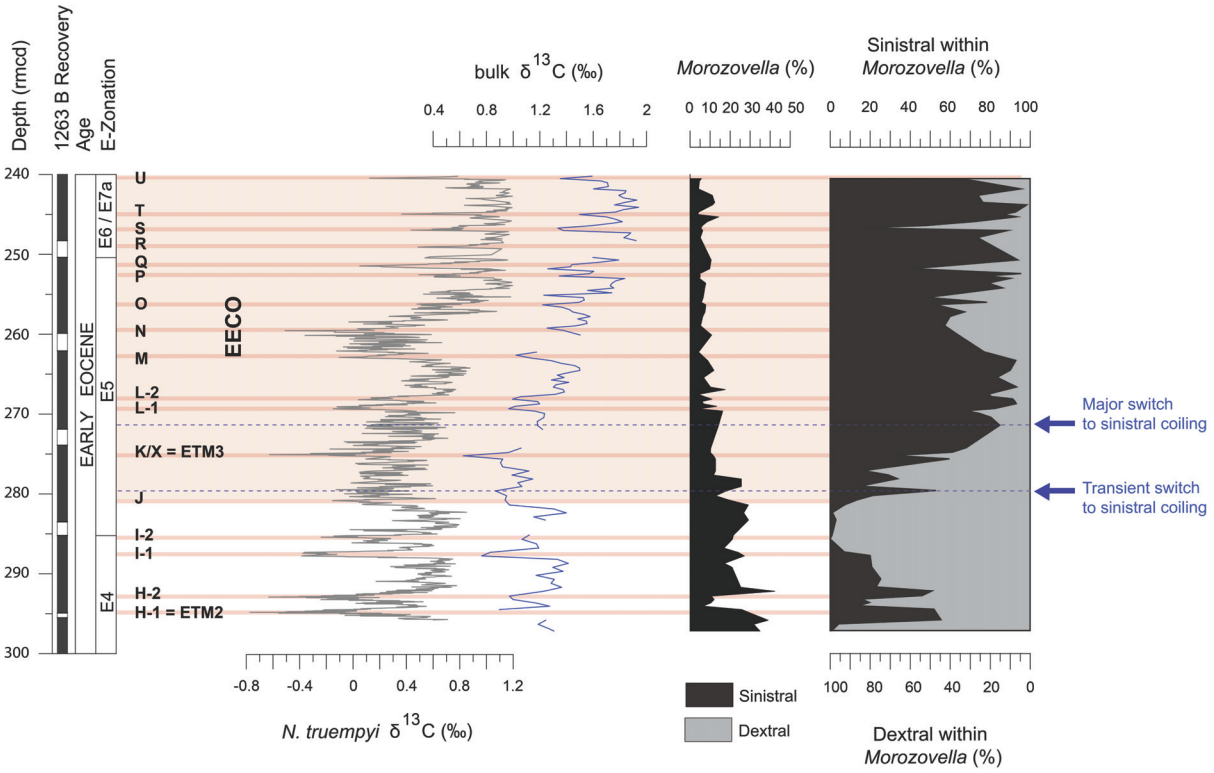

Figure 5. Early Eocene changes in coiling direction within the *Morozovella* genus (≥63 µm size fraction) at the ODP Site 1263 plotted against the benthic foraminifera *Nuttallides truempyi* (Lauretano et al., 2016) and bulk $\delta^{13}C$ (Chapter V) records. The missing data in the bulk $\delta^{13}C$ curve correspond to unrecovered intervals. The thin light-red bands highlight the main carbon isotope excursions (CIEs) interpreted and labelled according to Lauretano et al. (2016). We consider the onset of the EECO as coinciding with the J event, in agreement to Luciani et al. (2016). The relative *Morozovella* abundance is also shown (data from Chapter V). Note the consistent drop in abundance of morozovellids occurring in the interval between the J and K/X events. Note also the marked but transitory flip from dominant dextral to dominant sinistral coiling of the *Morozovella* genus slightly above the J event and the remarkable change from dominant dextral to dominant sinistral coiling above the K/X event. Below the EECO interval the dextral coiling is prevailing in morozovellids with moderate increases of sinistral morphotypes during some of the pre-EECO hyperthermals. This record is in good agreement with data from Site 1051 (see Fig. 4).

coiling flips. A certain delay is however recorded at Site 1051 between the J event, when occurred the morozovellid decline, and the prominent short-lived shift to the sinistral-coiled morozovellids recorded at both sites. This post-J prominent shift to sinistral coiled is recorded slightly above (~1.5 m) the level where morozovellids suffered a bleaching episode (see Chapter IV). Even though the closely spaced occurrence of these events may suggest possible link we cannot demonstrate a cause-and-effect relationship between the bleaching episode and the coiling change. Nevertheless, it looks like that after the J event the predisposition to the sinistral coiling mode became progressively more persistent reaching the apex slightly above the K/X event. On the basis of the age model provided by Lauretano et al. (2016) for the Site 1263 we estimate the time of this switch at ~52.55 Ma, ~281 kyr after the K/X event. It does not seem a coincidence that these changes occurred within the initial phase of the EECO that

may have generated effects that overlaid those of the single hyperthermal events.

The dextral coiling dominance within all the early Eocene *Morozovella* species in the lower part of the successions studied is in agreement with previous works (e.g., Norris and Nishi, 2001) that consider this character inherited by the ancestor lineage. However, at the equatorial Pacific ODP Site 865 studied by Norris and Nishi (2001), no shifts are recorded in the upper E5 (their P7) or E6/E7a (their P8/lower P9) zones differently from our data. It is possible that this apparently different record derives from a lower resolution at the ODP Site 865. This is expected from the great amount of data collected by the aforementioned authors that includes in their work the coiling mode of all tropical Paleogene planktic foraminiferal genera. The only exception is the switch from dominant dextral to sinistral morphotypes in the *M. aragonensis* specimens that occurred at the Atlantic Site 1051 sites as well in the Pacific location in the upper part of the early Eocene Zone E5.

6.2. Morozovellid Coiling and Reproductive Mode

The asexual reproduction for the recent planktic foraminifera has been proposed as one of the possible driving factors controlling the coiling mode (e.g., Kimoto and Tsuchiya, 2006; Khare et al., 2012) thus we discuss below about this possibility with regard to our case.

It is well known that benthic foraminifera can adopt alternatively sexual or asexual reproductive mode resulting in dimorphic shells that show differences in size and proloculus. Specifically, smaller shells with larger proluculi derive from asexual reproduction whereas larger shells bearing small proloculi are originated by gamic reproduction. A general reduction in maximum test-size was recorded in all the morozovellid species within the EECO (see Chapter IV), with the exception of *M. aragonensis* and *M. crater*. However, the supposition that early Eocene switches in coiling direction was controlled by asexual reproduction seem improbable, either because it is not fully demonstrated for planktic foraminifera and also because the decrease in maximum test size occurred for some species below the EECO onset where dextral coiling consistently dominated.

6.3. Coiling Changes within the different *Morozovella* Species at Site 1051

As regards the coiling change within the different *Morozovella* species at Site 1051, we note that *M. gracilis* and *M. marginodentata* appears to be the more prone to change the coiling direction (Fig. 4). It is difficult to understand whether a link existed with this evidence and the fact that these species show the main collapse in abundance at the EECO onset (Fig.

4). Other considerations concern the behaviour of the species *M. lensiformis, M. crater* and *M. aragonensis*. The first two species, after the prominent and protracted dominance of sinistral mode after the K/X event, display an almost equivalent occurrence of dextral and sinistral forms in the remaining early Eocene interval (Fig. 4). On the contrary, the latter species preserves the sinistral coiling mode also in the earlier middle Eocene. Our data reveal therefore that the early Eocene *Morozovella* species were able to change their coiling direction even after the maintenance of a preferred coil for a prolonged time interval. This evidence partly conflicts with the Norris and Nishi (2001) observation that Paleogene planktic foraminifera preserve in each species radiation a preferential coiling until the extinction and that the proportionate coiling consistently originated successive diversifications. Moreover, the consideration that species with proportionate coiling are less susceptible to extinction since they are more genetically flexible (Norris and Nishi, 2001) seems not effective as regards our record of *M. lensiformis* that disappeared not too long after the change to proportionate coiling (early Eocene Zone E6/E7a, e.g., Pearson et al., 2006; Aze et al., 2011). On the contrary, the species *M. aragonensis*, that retains an exclusive sinistral coiling up to the middle Eocene and should be more susceptible to extinction according to Norris and Nishi (2001), is the most long-lived species (top of Zone E9, e.g., Wade et al., 2011). Our record proves that return to a rather equal coiling mode is less infrequent that previously thought but it not ensures longevity for the species either the appearance of new clades, as testified by our data on *M. lensiformis* and *M. aragonensis*, also when compared with the known distribution and evolutionary significance of the species (e.g., Pearson et al., 2006; Aze et al., 2011; Norris and Nishi, 2001).

6.4. Change in Coiling Direction: Genetically or Environmentally Driven?

Our results definitely demonstrate that early Eocene planktic foraminferal species were able to change from a particular coiling mode to the opposite. Norris and Nishi (2001) deduce that coiling patterns in Paleogene tropical planktonic foraminifers was not environmentally controlled but likely heritable through time. According to these authors changes in coiling direction are possible because species retain the genetic key that allows them to coil one way or the reverse. We cannot validate or disprove a genetic origin of the observed morphotypes at the examined sites or demonstrate that morphotypes might have further diverged genetically in different species through adaptation to diverse environmental conditions. In the scenario where sinistral and dextral forms are characters genetically heritable we should conclude that the early Eocene carbon cycle and climate variability influenced cryptic speciation. According

to the evidence from recent planktic foraminifera, the cryptic speciation is probably induced by a clear separation within the water masses of the ecological niches (e.g., Ujiié et al., 2010; Ujiié and Asami, 2014; Morard et al., 2016). However, the $\delta^{13}C$ analysis on single *Morozovella* species (see Chapter IV) at Site 1051 demonstrates that morozovellids were not subject to significant water-depth changes and retained a mixed-layer habitat through the early Eocene. Our analysis was evidently performed on prevailing dextral specimens before the EECO onset and on sinistral morphotypes within the EECO. It is intriguing in any case that the recorded remarkable change occurred within the extended EECO warmth, after the marked drop in abundance of the genus *Morozovella* (Fig. 2) and heralded by temporary switches coinciding with the early Eocene hyperthermal events at both the Atlantic sites investigated. We need more effort to understand the meaning of these modifications, including a more comprehensive knowledge of the EECO. To date, geochemical data are not detailed enough to provide evidence for water-masses changes such as sea-surface temperature variability at the coiling switches. We know that during the EECO temperatures may have exceeded those of present day by at least 10 °C (Zachos et al., 2008; Bijl et al., 2009; Huber and Caballero, 2011; Hollis et al., 2012; Pross et al., 2012; Inglis et al., 2015) but direct and detailed data from Site 1051 and Site 1263 are so far lacking. Oxygen stable isotopes from both the studied sites are indeed affected by a certain degree of planktic foraminiferal recrystallization (Chapter IV and V) and calcareous nannofossil overgrowth (Mita, 2001) therefore the bulk carbonate $\delta^{18}O$ temperatures would represent a combination of a primary surface water signal and a secondary signal. Other temperature proxies, such as TEX_{86} or Mg/Ca are restricted to one level for the former at Site 1051 (see Chapter IV) or totally lacking for the latter.

Increased surface water eutrophy has been invoked as a possible feature that influenced the coiling change (e.g., Khare et al., 2012 and reference therein), as for the latest Cenomanian *Rotalipra cushmani* dextral coiling preference (Coccioni et al., 2016). Surface waters at Site 1051 may have experienced increased nutrient availability during the EECO, given the high abundance of radiolarians (see figure 3 of Chapter IV), which may reflect eutrophication (e.g., Hallock, 1987). Surface-water eutrophy at Site 1051 during the EECO seems also supported by the early Eocene calcareous nannofossil assemblages dominated by the eutrophic *Coccolithus pelagicus* (e.g, Perch-Nielsen, 1981; Agnini et al., 2006, 2007a, 2009; Fornaciari et al., 2007; Dedert et al., 2012; Tremolada and Bralower, 2004). Nevertheless, no indication of increased surface water eutrophy exists for Site 1263 (Chapter V).

6.5. Coiling Change as Powerful Biostratigrahic Tool

The links reported in the literature between coiling and environmental factors are useful for stratigraphic correlation and palaeoenvironmental interpretations either whether the forms were genetically distinct or ecophenotypic types (e.g., Berggren et al., 1995; Wade et al., 2011). One example is the *Pulleniatina* coiling-direction pattern occurred during the Pliocene from ~6 to ~3.5 Ma (Saito, 1976; Keigwin, 1978). This genus displays systematic changes with time in the coiling direction providing useful tools for Atlantic and Indo-Pacific correlations of marine sediments. The Atlantic coiling of *Pulleniatina* were no longer correlative with the Indo-Pacific pattern after ~3.5 Ma due to the emergence of the Panama Isthmus that interrupted marine connection of the two oceanic provinces (Saito, 1976; Keigwin, 1978). Another case is the switch from sinistral to dextral coiling in *Neogloboquadrina acostaensis* recorded concomitantly in several sites of the North Atlantic in the middle of Chron C3An(1r) (Hooper and Weaver, 1987; Hodell et al., 1994). This flip to prevailing dextral morphotypes in *N. acostaensis* was associated with an increase in $\delta^{18}O$ values that have been interpreted as reflecting cooling of the surface water (Dudley and Goodney, 1979) or variation in nannofossil assemblage composition (Paull and Thierstein, 1987). The *N. acostaensis* switch in coiling direction represents as a powerful biostratigraphic event occurred about 100 kyr below the onset of the Latest Miocene Glaciation (e.g. Hodell et al., 2001).

Our record from the early to earlier middle Eocene Sites 1051 and 1263 highlights that the recorded morozovellid coiling variations, independently from the triggering mechanisms, have the potentiality to be a powerful biostratigraphic tool for correlation. The two selected Sites 1051 and 1263 represent two rather separate settings in the Atlantic ocean, a subtropical latitude location of the northern hemisphere for the former, and a temperate southern hemisphere setting for the latter (Ogg and Bardot, 2001; Van Hinsbergen et al., 2015). Remarkably, both (1) the transitory but marked flip to sinistral coiling slightly after the J event and (2) the long-lasting sinistral preferences of morozovellids above the K/X event show a substantial correspondence in the two analysed sites, located at different latitude of the Atlantic Ocean. This correspondence stimulates further high-resolution studies to verify whether the changes observed in the Atlantic Ocean can be detected elsewhere. Analyses of early Eocene coiling direction are in progress on the *Morozovella* population from other settings, such as the equatorial Atlantic Demerara Rise Site 1258 and the Tethyan Possagno section (NE Italy).

7. Summary and Conclusions

Our record provides new insight on the relationship between the early Eocene carbon-cycle changes and the coiling direction of trochospiral planktic foraminiferal genus *Morozovella*. We investigated the coiling direction within *Morozovella* populations from sections at the two widely separated ODP Atlantic sites 1051and 1263 that span the EECO (~49-53 Ma), the interval when Earth surface temperatures and atmospheric pCO_2 reached their Cenozoic maximum (e.g., Zachos et al., 2001; 2008). The symbiont-bearing surface-dweller planktic foraminiferal genus *Morozovella* is of particular interest because of its dominance in tropical-subtropical early Paleogene assemblages, and the time interval is of interest because of an abrupt and permanent decline in the abundance and taxonomic diversity of *Morozovella* at the carbon isotope excursion known as the J event (e.g., Cramer et sl., 2003), which marks the beginning of the EECO (Luciani et al., 2016).

The coiling direction of trochospiral planktic foraminifera is a widely investigated morphological feature in living species and Plio-Pleistocene sediments. In recent and Quaternary oceans, sinistral and dextral forms generally dominate colder and warmer waters, respectively (e.g., Kucera and Kennett, 2002; Bauch et al., 2003). However, the true causes of coiling direction remain an intriguing problem. Several studies indicate that other factors besides temperature might influence foraminiferal coiling directions (e.g., salinity, seasonal effects, water density, reproductive strategy, Khare et al., 2012, and reference therein). Moreover, it has been proved that most of the recent sinistral and dextral morphotypes are actually genetically separated and adapted to different water-masses (e.g., Darling et al., 2006).

Our results demonstrate that morozovellids display a dominant dextral preference during the interval preceding the EECO at both sites. However, all species show a first, prominent flip to sinistral coiling mode starting slightly after the J event. This switch from dextral to sinistral coiling became permanent for most of the *Morozovella* species slightly after the K/X event. Temporary but significant switches towards sinistral coiled morphotypes also occurred at both sites during several pre-EECO hyperthermal events. The correspondence between the sinistral coiling direction switches and hyperthermal events suggests a sort of causal effect.

We record therefore a remarkable variation in the coiling mode of *Morozovella* during extreme warming intervals of the early Paleogene. Our record sheds new light on the coiling direction preferences of Paleogene planktic foraminifera and demonstrates that early Eocene planktic foraminiferal species were able to change from a particular coiling mode to the opposite, differently from what previously thought (Norris and Nishi, 2001). We need more

effort to understand the meaning of these modifications, including a comprehensive knowledge of the EECO. Present geochemical data are not reliable enough to provide evidence of variability in sea surface temperature or in other parameters behind the coiling changes. Previous interpretations favour genetic explanations for coiling flips rather than ecological responses (e.g., Norris and Nishi, 2001). Our present data cannot validate or disprove these ideas, but should stimulate renewed thought on the matter.

Our record further highlights that the recorded coiling variations might be a powerful biostratigraphic tool for correlation and stimulates further high-resolution studies to verify whether the changes observed in the Atlantic Ocean can be detected elsewhere.

Appendix A: Taxonomic List of Planktic Foraminiferal Species Cited in Text and Figures

Acarinina cuneicamerata (Blow, 1979)
Astrorotalia palmerae (Cushman and Bermúdez, 1937)
Globanomalina pseudomenardii (Bolli, 1957)
Globigerina bulloides d'Orbigny, 1826
Globigerinoides ruber (d'Orbigny, 1839)
Globorotalia truncatulinoides (d'Orbigny, 1839)
Igorina albeari Cushman and Bermudez, 1949
Morozovella aequa (Cushman and Renz, 1942)
Morozovella aragonensis (Nuttall, 1930)
Morozovella caucasica (Glaessner, 1937)
Morozovella crater (Hornibrook, 1958)
Morozovella gracilis (Bolli, 1957)
Morozovella lensiformis (Subbotina, 1953)
Morozovella marginodentata (Subbotina, 1953)
Morozovella subbotinae (Morozova, 1939)
Morozovella velascoensis (Cushman, 1925)
Neogloboquadrina acostaensis (Blow, 1959)
Neogloboquadrina pachyderma (Ehrenberg, 1861)
Neogloboquadrina incompta (Cifelli, 1961)
Pulleniatina Cushman, 1927
Rotalipora cushmani Brotzen, 1942

Appendix B: Taxonomic List of Calcareous Nannofossil Taxa Cited in Text and Figures

Coccolithus pelagicus (Wallich) J.Schiller 1930
Heliolithus kleinpelli Sullivan, 1964

References

Agnini, C., G. Muttoni, D. V. Kent, and D. Rio (2006), Eocene biostratigraphy and magnetic stratigraphy from Possagno, Italy: The calcareous nannofossil response to climate variability, Earth Planet. Sci. Lett., 241, 815–830, doi:10.1016/j.epsl.2005.11.005.

Agnini, C., E. Fornaciari, D. Rio, F. Tateo, J. Backman, and L. Giusberti (2007), Responses of calcareous nannofossil assemblages, mineralogy and geochemistry to the environmental perturbations across the Paleocene/Eocene boundary in the Venetian pre-Alps, Mar. Micropaleontol., 63, 19–38, doi:10.1016/j.marmicro.2006.10.002.

Agnini, C., J. Backman, H. Brinkhuis, E. Fornaciari, L. Giusberti, V. Luciani, D. Rio, and A. Sluijs (2009), An early Eocene carbon cycle perturbation at similar to 52.5 Ma in the Southern Alps: Chronology and biotic response, Paleoceanography, 24, PA2209, doi:10.1029/2008PA001649.

Aurahs, R., G. W. Grimm, V. Hemleben, C. Hemleben, and M. Kucera (2009), Geographical distribution of cryptic genetic types in the planktonic foraminifer *Globigerinoides ruber*, Molecular Ecology, 18(8), 1692-1706.

Aze, T., T. H. G. Ezard, A. Purvis, H. K. Coxall, D. R. M Stewart, B. S. Wade, and P. N. Pearson (2011), A phylogeny of Cenozoic macroperforate planktonic foraminifera from fossil data, Biol. Rev., 86, 900–927, doi:10.1111/j.1469-185X.2011.00178.x.

Bandy, O. L. (1960), The geologic significance of coiling ratios in the foraminifer Globigerina pachyderma (Ehrenberg), J. Paleontol., 34, 671–681.

Bandy, O. L. (1972), Origin and development of *Globorotalia* (*Turborotalia*) *pachyderma* (Ehrenberg), Micropaleontology, 18, 294–318.

Barclay, R. S., J.C. McElwain, and B. B. Sageman (2010), Carbon sequestration activated by a volcanic CO_2 pulse during Ocean Anoxic Event 2, Nature Geoscience, v. 3, p. 205–208, doi:10.1038/ngeo757.

Bauch, D., K. Darling, J. Simstich, H. A. Bauch, H. Erlenkeuser, and D. Kroon (2003), Palaeoceanographic implications of genetic variation in living North Atlantic N. pachyderma, Nature, 424, 299–302.

Berggren, W. A., D. V. Kent, C. C. Swisher III, and M.-P. Aubry (1995), A revised Cenozoic geochronology and chronostratigraphy, in Geochronology, time scales and global stratigraphic correlation, edited by Berggren, W. A, D. V. Kent, M.-P. Aubry, and J. Hardenbol, SEPM Special Publication, 54, 129–212.

Bijl, P. K., S. Schouten, A. Sluijs, G.-J. Reichart, J. C. Zachos, and H. Brinkhuis (2009), Early Paleogene temperature evolution of the southwest Pacific Ocean, Nature, 461, 776–779, doi:10.1038/nature08399.

Boersma, A., and I. Premoli Silva (1983), Paleocene planktonic foraminiferal biogeography and the paleoceanography of the Atlantic-Ocean, Micropaleontology, 29, 355–381.

Bohaty, S. M., J. C. Zachos, F. Florindo, and M. L. Delaney (2009), Coupled greenhouse warming and deep-sea acidification in the middle Eocene, Paleoceanography, v. 24 (2), doi:10/1029/2008PA001676.

Bolli, H. M. (1950), The direction of coiling in the evolution of some Globorotaliidae, Contributions from the Cushman Foundation for Foraminiferal Research, 1, 82-89.

Bolli, H. M. (1971), The direction of coiling in planktonic foraminifera, in The micropaleontology of oceans edited by Funnell, B. M., and W. R. Riedel, pp. 639–648, Cambridge University Press, Cambridge.

Boltovskoy, E. (1973), Note on the determination of absolute surface water temperature by means of the foraminifer *Globigerina bulloides* d'Orbigny, Palaeontol. Z., 47, 152–155.

Boltovoskoy, E., and R. Wright (1976), Recent Foraminifera, edited by Dr. W. Junke, publication The Hague.

Bond, G., W. Broecker, S. Johnsen, J. McManus, L. Labeyrie, J. Jouzel, and G. Bonani (1993), Correlations between climate records from North Atlantic sediments and Greenland ice, *Nature*, *365*(6442), 143-147.

Brummer, G.-J. A., and D. Kroon (1988), Genetically controlled planktonic foraminiferal coiling ratios as tracers of past ocean dynamics, in Planktonic foraminifers as tracers of ocean-climate history, edited by Brummer, G. J. A., and D. Kroon, pp. 293–298, Free University Press, Amsterdam.

Cifelli, R. (1961), Globigerina incompta, a new species of pelagic foraminifera from the North Atlantic, Contrib. Cushman Found. Foramin. Res. 12, 83–86.

Coccioni, R., G. Bancalà, R. Catanzariti, E. Fornaciari, F. Frontalini, L. Giusberti, L. Jovane, V. Luciani, J. Savian, and M. Sprovieri (2012), An integrated stratigraphic record of the Palaeocene-lower Eocene at Gubbio (Italy), New insights into the early Palaeogene hyperthermals and carbon isotope excursions, Terra Nova, 24, 380–386, doi:10.1111/j.1365-3121.2012.01076.x.

Coccioni, R., M. Sideri, F. Frontalini, and A. Montanari (2016), The *Rotalipora cushmani* extinction at Gubbio (Italy): Planktonic foraminiferal testimonial of the onset of the Caribbean large igneous province emplacement?, Geological Society of America Special Papers, 524, 81–96.

Collins, L. S. (1990), The correspondence between water temperature and coiling direction in *Bulimina*: Paleoceanography, 5, 289–294, doi:10.1029/PA005i003p00289.

Cramer, B. S., D. V. Kent, and M.-P. Aubry (2003), Orbital climate forcing of excursions in the late Paleocene–early Eocene (chrons C24n–C25n), Paleoceanography, 18(4), 1097, doi:10.1029/2003PA000909.

Darling, K. F., M. Kucera, C. M. Wade, P. von Langen, and D. Pak (2003), Seasonal distribution of genetic types of planktonic foraminifer morphospecies in the Santa Barbara Channel and its paleoceanographic implications, Paleoceanography, 18(2), 1032, doi:10.1029/2001PA000723.

Darling, K. F., M. Kucera, C. J. Pudsey, and C. M. Wade (2004), Molecular evidence links cryptic diversification in polar plankton to Quaternary climate dynamics, Proc. Natl. Acad. Sci. U.S.A., 101, 7657–7662.

Darling, K. F., M. Kucera, D. Kroon, and C. M. Wade (2006), A resolution for the coiling direction paradox in *Neogloboquadrina pachyderma*, Paleoceanography, 21.

Dedert, M., H. M. Stoll, D. Kroon, N. Shimizu, K. Kanamaru, and P. Ziveri (2012), Productivity response of calcareous nannoplankton to Eocene Thermal Maximum 2 (ETM2), Clim. Past, 8(3), 977–993, doi:10.5194/cp-8-977-2012.

Dedert, M., H. Stoll, S. Kars, J. R. Young, N. Shimizu, D. Kroon, L. Lourens, and P. Ziveri (2014), Temporally variable diagenetic overgrowth on deep-sea nannofossil carbonates across Palaeogene hyperthermals and implications for isotopic analyses, Mar. Micropaleontol., 107, 18–31.

Desmares, D., D. Grosheny, and B. Beaudoin (2008), Ontogeny and phylogeny of upper Cenomanian rotaliporids (Foraminifera), Marine Micropaleontology, 69, 91–105, doi:10.1016/j.marmicro.2008.07.003.

D'haenens, S., A. Bornemann, P. Claeys, U. Röhl, E. Steurbaut, and R. P. Speijer (2014), A transient deep-sea circulation switch during Eocene Thermal Maximum 2, Paleoceanography, 29, 370–388, doi:10.1002/2013PA002567.

Dudley, W. C., and D. E. Goodney (1979), Oxygen isotope content of coccoliths grown in culture, Deep Sea Research Part A, Oceanographic Research Papers, 26(5), 495-503.

Dunkley Jones, T., P. R. Bown, P. N. Pearson, B. S. Wade, H. K. Coxall, and C. H. Lear (2008), Major shifts in calcareous phytoplankton assemblages through the Eocene-Oligocene transition of Tanzania and their implications for low-latitude primary production, Paleoceanography, 23, PA4204, doi:10.1029/2008PA001640.

Du Vivier, A. D. C., D. Selby, B. B. Sageman, I. Jarvis, D. R. Gröcke, and S. Voigt (2014), Marine $^{187}Os/^{188}Os$ isotope stratigraphy reveals the interaction of volcanism and ocean circulation during Oceanic Anoxic Event 2, Earth and Planetary Science Letters, 389, 23–33, doi:10.1016/j.epsl.2013.12.024.

Ericson, D. B. (1959), Coiling direction of *Globigerina pachyderma* as a climatic index, Science, 130, 219–220.

Ericson, D. B., G. Wollin, and J. Wollin (1955), Coiling direction of *Globorotalia truncatulinoides* in deep-sea cores, Deep Sea Research (1953), 2(2), 152–158.

Ezard, T. H. G., T. Aze, P. N. Pearson, and A Purvis (2011), Interplay between changing climate and species' ecology drives macroevolutionary dynamics, Science, 332, 349–351.

Fornaciari, E., L. Giusberti, V. Luciani, F. Tateo, C. Agnini, J. Backman, M. Oddone, and D. Rio (2007), An expanded Cretaceous Tertiary transition in a pelagic setting of the Southern Alps (central-western Tethys), Palaeogeor. Palaeoclimatol. Palaeoecol., 255, 98–131, doi:10.1016/j.palaeo.2007.02.044.

Fraass, A. J., D. K. Kelly, and S. E. Peters (2015), Macroevolutionary history of the planktic foraminifera, Annu. Rev. Earth Pl. Sc., 43, 139–66, doi:10.1146/annurev-earth-060614-105059.

Frontalini, F., R. Coccioni, R. Catanzariti, L. Jovane, J. F. Savian, & M. Sprovieri (2016), The Eocene Thermal Maximum 3: Reading the environmental perturbations at Gubbio (Italy), Geological Society of America Special Papers, 524.

Gibbs, S. J., P. R. Bown, B. H. Murphy, A. Sluijs, K. M. Edgar, H. Pälike, C. T. Bolton, and J. C. Zachos (2012), Scaled biotic disruption during early Eocene global warming events, Biogeosciences, 9(11), 4679–4688, doi:10.5194/bg-9-4679-2012.

Hallock, P. (1987), Fluctuations in the trophic resource continuum: A factor in global diversity cycles?, Paleoceanography, 2, 457–471, doi:10.1029/PA002i005p00457.

Hancock, H. J. L. (2005), Chapter III, Coiling shifts and stable isotope changes in the late Paleocene planktic foraminifera *Igorina albeari*: expression and significance, in Early Paleogene planktic foraminiferal assemblages in Australasian sequences: link to past changes in climate and carbon cycling, PhD thesis, James Cook University, North Queensland, Australia.

Healy-Williams, N., and D. F. Williams (1981), Fourier analysis of test shape of planktonic foraminifera, Nature, 289, 485–487, doi:10.1038/289485a0.

Healy-Williams, N., R. Ehrlich, and D. F. Williams (1985), Morphometric and stable isotopic evidence for subpopulations of *Globorotalia truncatulinoides*, Journal of Foraminiferal Research, 15, 242–253, doi:10.2113/gsjfr.15.4.242.

Hecht, A. D. (1976), An ecologic model for test size variation in recent planktonic foraminifera: applications to the fossil record, Journal of Foraminiferal Research, 6, 295–311, doi:10.2113/gsjfr.6.4.295.

Hodell, D. A., R. H. Benson, D. V. Kent, A. Boersma, and R. E Bied. (1994), Magnetostratigraphic, biostratigraphic, and stable isotope stratigraphy of an Upper Miocene drill core from the Salé Briqueterie (northwestern Morocco): A high-resolution chronology for the Messinian stage, Paleoceanography, 9(6), 835-855.

Hodell, D. A., J. H. Curtis, F. J. Sierro, and M. E. Raymo (2001), Correlation of late Miocene to early Pliocene sequences between the Mediterranean and North Atlantic, Paleoceanography, 16(2), 164-178.

Hollis, C. J., K. W. R. Taylor, L. Handley, R. D. Pancost, M. Huber, J. B. Creech, B. R. Hines, E. M. Crouch, H. E. G. Morgans, J. S. Crampton, S. Gibbs, P. N. Pearson, and J. C. Zachos (2012), Early Paleogene temperature history of the Southwest Pacific Ocean: Reconciling proxies and models, Earth Planet. Sc. Lett., 349–350, 53–66, doi:10.1016/j.epsl.2012.06.024.

Hooper, P. W. P., and P. P. E. Weaver (1987), Late Neogene species of the genus *Neogloboquadrina Bandy* in the North Atlantic: a biostratigraphic, paleoceanographic and phylogenetic review, Micropaleontology of carbonate environments, 21-43.

Huber, M. and R. Caballero (2011), The early Eocene equable climate problem revisited, Clim. Past, 7, 603–633, doi:10.5194/cp-7-603-2011.

Jenkyns, H. C. (2010), Geochemistry of oceanic anoxic events, Geochemistry, Geophysics, Geosystems, 11, 3004, doi:10.1029/2009GC002788.

Keigwin, L. D. (1978), Pliocene closing of the Isthmus of Panama, based on biostratigraphic evidence from nearby Pacific Ocean and Caribbean Sea cores, Geology, 6(10), 630-634.

Kennett, J. P. (1976), Phenotypic variation in some Recent and late Cenozoic planktonic foraminifera, in Foraminifera, edited by Hedley, R. H., and C. G. Adams, Vol. 2, p. 111–170, New York, Academy Press.

Kennett, J. P., and L. D. Stott (1991), Abrupt deep-sea warming, palaeoceanographic changes and benthic extinctions at the end of the Palaeocene, Nature, 353, 225–229.

Khare, N., A. Mazumder, and P. Govil (2012), Do changes in coiling directions in planktonic foraminifera correspond to dimorphic reproduction?, Oceanology, 52, 364–371, doi:10.1134/S0001437012030058.

Kimoto, K., and M. Tsuchiya (2006), The “unusual” reproduction of planktic foraminifera: an asexual reproductive phase of *Neogloboquadrina pachyderma* (Ehrenberg), Anuário do Instituto de Geociências, UFRJ **29**, 461.

Kirtland-Turner, S., P. F. Sexton, C. D. Charles, and R. D. Norris (2014), Persistence of carbon release events through the peak of early Eocene global warmth, Nat. Geosci., 12, 1–17, doi:10.1038/ngeo2240.

Kucera, M., and J. P. Kennett (2002), Causes and consequences of a middle Pleistocene origin of the modern planktonic foraminifer *Neogloboquadrina pachyderma* sinistral, *Geology*, *30*(6), 539–542.

Inglis, G. N., A. Farnsworth, D. Lunt, G. L. Foster, C. J. Hollis, M. Pagani, P. E. Jardine, P. N. Pearson, P. Markwick, A. M. J. Galsworthy, L. Raynham, K. W. R. Taylor, and R.D. Pancost (2015), Descent toward the icehouse: Eocene sea surface coolinginferred from GDGT distributions, Paleoceanography, 30, 100–1020, doi:10.1002/2014PA002723.

Leon-Rodriguez, L., and G. R. Dickens (2010), Constraints on ocean acidification associated with rapid and massive carbon injections: The early Paleogene record at ocean drilling program site 1215, equatorial Pacific Ocean, Palaeogeogr. Palaeoclimatol. Palaeoecol., 298(3–4), 409–420, doi:10.1016/j.palaeo.2010.10.029.

Lauretano, V., K. Littler, M. Polling, J. C. Zachos, and L. J. Lourens (2015), Frequency, magnitude and character of hyperthermal events at the onset of the Early Eocene Climatic Optimum, Clim. Past, 11, 1313–1324, doi:10.5194/cp-11-1313-2015.

Lauretano, V., F. J. Hilgen, J. C. Zachos and L. J. Lourens (2016), Astronomically tuned age model for the early Eocene carbon isotope events: A new high-resolution $\delta^{13}C$ benthic record of ODP Site 1263 between~ 49 and~ 54 Ma, Newsletters on Stratigraphy, 49(2), 383-400.

Littler, K., U. Röhl, T. Westerhold, and J. C. Zachos (2014), A high-resolution benthic stable isotope record for the South Atlantic: Implications for orbital-scale changes in late Paleocene–early Eocene climate and carbon cycling, Earth Planet. Sc. Lett., 401, 18–30, doi:10.1016/j.epsl.2014.05.054.

Loewen, M. W., R. A. Duncan, A. J. R. Kent, and K. Krawl (2013), Prolonged plume volcanism in the Caribbean Large Igneous Province: new insights from Curaçao and Haiti, Geochemistry, Geophysics, Geosystems, 14, 4241–4259, doi:10.1002/ggge.20273.

Lourens, L. J., A. Sluijs, D. Kroon, J. C. Zachos, E. Thomas, U. Röhl, J. Bowles, and I. Raffi (2005), Astronomical pacing of late Palaeocene to early Eocene global warming events, Nature, 435, 1083–1087.

Luciani, V. and L. Giusberti (2014), Reassessment of the early–middle Eocene planktic foraminiferal biomagnetochronology: new evidence from the Tethyan Possagno section (NE Italy) and Western North Atlantic Ocean ODP Site 1051, J. Foramin. Res., 44, 187–201.

Luciani, V., G. R. Dickens, J. Backman, E. Fornaciari, L. Giusberti, C. Agnini, and R. D'Onofrio (2016), Major perturbations in the global carbon cycle and photosymbiont-bearing planktic foraminifera during the early Eocene, Clim. Past, 12, 981–1007, doi:10.5194/cp-12-981-2016.

Luterbacher, H. (1964), Studies in some *Globorotalia* from the Paleocene and lower Eocene of the Central Apennines, Inaugural-dissertation, Buchdruckerei Birkhäuser,

Malmgren, B.A. (1984), Analysis of the environmental influence of the morphology of *Ammonia beccarii* (Linné) in southern European salinas, Geobios, 17, 737–746, doi:10.1016/S0016-6995(84)80118-7.

Malmgren, B. A. (1989), Coiling patterns in terminal Cretaceous planktonic foraminifera, Journal of Foraminiferal Research, 19, 311–323.

Martinez, J. I., G. Mora, and T. T. Barrows (2007), Paleoceanographic conditions in the Western Caribbean Sea for the last 560 Kyr as inferred from planktonic foraminifera, Marine Micropaleontology, 64, 177–188, doi:10.1016/j.marmicro.2007.04.004.

McInerney, F. A., and S. L. Wing (2011), The Paleocene-Eocene Thermal Maximum: A perturbation of carbon cycle, climate, and biosphere with implications for the future, Annu. Rev. Earth Planet. Sci., 39(1), 489–516, doi:10.1146/annurev-earth-040610-133431.Mita, 2001

Mita, I. (2001), Data Report: Early to late Eocene calcareous nannofossil assemblages of Sites 1051 and 1052, Blake Nose, Northwestern Atlantic Ocean, in Proc. Ocean Drill. Progr., Sci. Results, 171B, edited by Kroon, D., R. D. Norris, and A. Klaus, 1–28, Available from World Wide Web: <http://www-odp.tamu.edu/publications/171B_SR/chap_07/chap_07.htm>.

Morard, R., M. Reinelt, C. M. Chiessi, J. Groeneveld, and M. Kucera (2016), Tracing shifts of oceanic fronts using the cryptic diversity of the planktonic foraminifera *Globorotalia inflate*, Paleoceanography, 31(9), 1193–1205.

Mort, H. P., T. Adatte, K. B. Follmi, G. Keller, P. Steinmann, V. Matera, Z. Berner, and D. Stuben (2007), Phosphorus and the roles of productivity and nutrient recycling during oceanic anoxic event 2, Geology, 35, 483–486, doi:10.1130/G23475A.1.

Nicolo, M. J., G. R. Dickens, C. J. Hollis, and J. C. Zachos (2007), Multiple early Eocene hyperthermals: Their sedimentary expression on the New Zealand continental margin and in the deep sea, Geology, 35(8), 699–702.

Norris, R. D. (1991), Biased extinction and evolutionary trends, Paleobiology,17, 388–399.

Norris, R. D., and H. Nishi (2001), Evolutionary trends in coiling of tropical Paleogene planktic foraminifera, Paleobiology, 27, 327– 347.

Norris, R. D., D. Kroon, and A. Klaus (1998), Proceedings of the Ocean Drilling Program, Initial Reports, Proc. Ocean Drill. Progr., Sci. Results, 171B, 1–749.

Ogg, J. G., and L. Bardot (2001), Aptian through Eocene magnetostratigraphic correlation of the Blake Nose Transect (Leg 171B), Florida continental margin, Proc. Ocean Drill. Progr., Sci. Results, 171B, 1–58, doi:10.2973/odp.proc.sr.171B.104.2001.

Olsson, R. K., C. Hemleben, W. A. Berggren, and B. T. Huber (1999), Atlas of Paleocene Planktonic Foraminifera, Smithsonian Contribution to Paleobiology, vol. 85, pp. 225, Smithsonian Institution Press, Washington D. C.

Paull, C. K., and H. R. Thierstein (1987), Stable isotopic fractionation among particles in Quaternary coccolith-sized deep-sea sediments, Paleoceanography, 2(4), 423-429.

Pearson, P. N., N. J. Shackleton, and M. A. Hall (1993), Stable isotope paleoecology of middle Eocene planktonic foraminifera and multispecies isotope stratigraphy, DSDP Site 523, South Atlantic, J. Foraminiferal Res., 23, 123-140, doi:10.2113/gsjfr.23.2.123.

Pearson, P. N., R. K. Olsson, C. Hemblen, B. T. Huber, and W. A. Berggren (Eds.) (2006), Atlas of Eocene Planktonic Foraminifera, Cushman Special Publication, vol. 41, pp. 513, Department of Geology East Carolina Univ., Greenville.

Pegram, W. J., and K. K. Turekian (1999), The osmium isotopic composition change of Cenozoic sea water as inferred from a deep-sea core corrected for meteoritic contributions, Geochimica et Cosmochimica Acta, 63, 4053–4058, doi:10.1016/S0016-7037(99)00308-7.

Perch-Nielsen, K. (1981), Nouvelles observations sur les nannofossiles calcaires a la limite Cretace-Tertiaire pres de El Kef, Tunisie, Cahiers de Micropaléontol., 3, 25–36.

Premoli Silva, I., and A. Boersma (1988), Atlantic Eocene planktonic foraminiferal historical biogeography and paleohydrographic indices, Palaeogeogr. Palaeoclimatol. Palaeoecol., 67(3-4), 315–356, doi:10.1016/0031-0182(88)90159-9.

Pross, J., L. Contreras, P. K. Bijl, D. R. Greenwood, S. M. Bohaty, S. Schouten, J. A. Bendle, U. Röhl, L. Tauxe, J. I. Raine, E. Claire, C. E. Huck, T. van de Flierdt, S. R. Stewart, S. S. R. Jamieson, C. E. Stickley, B. van de Schootbrugge, C. Escutia, and H. Brinkhuis (2012), Persistent near-tropical warmth on the Antarcticcontinent during the early Eocene Epoch, Nature, 488, 73–77, doi:10.1038 /nature11300.

Renaud, S. and D. N. Schmidt (2003), Habitat tracking as a response of the planktic foraminifer *Globorotalia truncatulinoides* to environmental fluctuations during the last 140 kyr, Marine Micropaleontology, 49, 97–122, doi:10.1016/S0377-8398(03)00031-8.

Saito, T. (1976), Geologic significance of coiling direction in the planktonic foraminifera *Pulleniatina*, Geology, 4, 305–309.

Schlanger, S. O., and H. C. Jenkyns (1976), Cretaceous oceanic anoxic events: causes and consequences, Geologie en Mijnbouw, 55, 179–184.

Schmidt, D. N., S. Renaud, J. Bollmann, R. Schiebel, and H. R. Thierstein (2004), Size distribution of Holocene planktic foraminifer assemblages: Biogeography, ecology and adaptation, Mar. Micropaleont., 50(3–4), 319–338, doi:10.1016/S0377-8398(03)00098-7.

Scott, G. H. (1974), Biometry of the Foraminiferal Shell, in Foraminifera, edited by Hedley R. H., and C. G. Adams, 55–152, Academic Press, London.

Shipboard Scientific Party, (1998), Site 1051, in Proceeding Ocean Drilling Program, Initial Reports, 171B, edited by Norris, R. D., D. Kroon, A. Klaus, I. T. Alexander, L. P. Bardot, C. E. Barker, J.-P. Bellier, C. D. Blome, L. J. Clarke, J. Erbacher, K. L. Faul, B. T. Holmes, M. Huber, M. E. Katz, K. G. MacLeod, S. Marca, F. C. Martinez-Ruiz, I. Mita, M. Nakai, J. G. Ogg, D. K. Pak, T. K. Pletsch, J. M. Self-Trail, N. J. Shackleton, J. Smit, W. Ussler III, D. K. Watkins, J. Widmark, P. A. Wilson, L. A. Baez, and E. Kapitan-White, Ocean Drilling Program, College Station,TX, 171–239, doi:10.2973/odp.proc.ir.171b.105.1998, 1998.Slotnick, B. S., G. R. Dickens, M. J. Nicolo, C. J. Hollis, J. S. Crampton, and J. C. Zachos (2012), Large-amplitude variations in carbon cycling and terrestrial weathering during the latest Paleocene and earliest Eocene: The record at Mead Stream, New Zealand, J. Geol., 120(5), 487–505, doi:10.1086/666743.

Slotnick, B. S., G. R. Dickens, C. J. Hollis, J.S. Crampton, P. S. Strong, and A. Phillips (2015), The onset of the EarlyEocene Climatic Optimum at Branch Stream, Clarence Rivervalley, New Zealand, New Zeal. J. Geol. Geop., 58, 1–19, doi:10.1080/00288306.2015.1063514.

Stap, L., A. Sluijs, E. Thomas, and L. J. Lourens (2009), Patterns and magnitude of deep sea carbonate dissolution during Eocene Thermal Maximum 2 and H2, Walvis Ridge, Southeastern Atlantic Ocean, Paleoceanography, 24, PA1211, doi:10.1029/2008PA001655.

Stap, L., L. J. Lourens, E. Thomas, A. Sluijs, S. Bohaty, and J. C. Zachos (2010a), High-resolution deep-sea carbon and oxygen isotope records of Eocene Thermal Maximum 2 and H2, Geology, 38, 607–610, doi:10.1130/G30777.1.

Stap, L., L. J. Lourens, A. van Dijk, S. Schouten, and E. Thomas (2010b), Coherent pattern and timing of the carbon isotope excursion and warming during Eocene Thermal Maximum 2 as recorded in planktic and benthic foraminifera, Geochem. Geophys. Geosyst., 11, Q11011, doi:10.1029/2010GC003097.

Tremolada, F., and T. J. Bralower (2004), Nannofossil assemblage fluctuations during the Paleocene-Eocene thermal maximum at Sites 213 (Indian Ocean) and 401 (North Atlantic Ocean): Palaeoceanographic implications, Mar. Micropaleontol., 52(1), 107–116, doi:10.1016/j.marmicro.2004.04.002.

Turgeon, S. C., and R. A. Creaser (2008), Cretaceous oceanic anoxic event 2 triggered by a massive magmatic episode, Nature, 454, 323–326, doi:10.1038/nature07076.

Ujiié, Y., and T. Asami (2014), Temperature is not responsible for left-right reversal in pelagic unicellular zooplanktons, Journal of Zoology, 293(1), 16–24.

Ujiié, Y., T. de Garidel-Thoron, S. Watanabe, P. Wiebe, and C. de Vargas (2010), Coiling dimorphism within a genetic type of the planktonic foraminifer *Globorotalia truncatulinoides*, Marine Micropaleontology, 77(3), 145–153.

Van Hinsbergen, D. J. J., L. V. de Groot, S. J., van Schaik, W. Spakman, P. K. Bijl, A. Sluijs, C. G. Langereis, and H. Brinkhuis (2015), A Paleolatitude Calculator for Paleoclimate Studies, PLoS ONE, 10, e0126946, doi:10.1371/journal.pone.0126946.

Wade, B. S., P. N. Pearson, W. A. Berggren, and H. Pälike (2011), Review and revision of Cenozoic tropical planktonic foraminiferal biostratigraphy and calibration to the geomagnetic polarity and astronomical time scale, Earth Sci. Rev., 104(1–3), 111–142, doi:10.1016/j.earscirev.2010.09.003.

Westerhold, T., U. Röhl, J. Laskar, I. Raffi, J. Bowles, L. J. Lourens, and J. C. Zachos (2007), On the duration of magnetochrons C24r and C25n and the timing of early Eocene global warming events: Implications from the Ocean Drilling Program Leg 208 Walvis Ridge depth transect, Paleoceanography, 22, PA2201, doi:10.1029/2006PA001322.

Westerhold, T., U. Röhl, I. Raffi, E. Fornaciari, S. Monechi, V. Reale, J. Bowles, and H. F. Evans (2008), Astronomical calibration of the Paleocene time, Palaeogeogr. Palaeoclimatol. Palaeoecol., 257, 377–403, doi:10.1016/j.palaeo.2007.09.016.

Westerhold, T., U. Röhl, T. Frederichs, S. M. Bohaty, and J. C. Zachos (2015), Astronomical calibration of the geological timescale: Closing the middle Eocene gap, Clim. Past, 11(9), 1181–1195, doi:10.5194/cp-11-1181-2015.

Xu, X., K. Kimoto, and M. Oda (1995), Predominance of left-coiling *Globorotalia truncatulinoides* (d'Orbigny) between 115.000 and 50.000 yrs, The Quaternary Research, 34(1), 39–47.

Zachos, J. C., M. Pagani, L. Sloan, E. Thomas, and K. Billups (2001), Trends, rhythms, and aberrations in global climate 65 Ma to present, Science, 292, 686–693, doi:10.1126/science.1059412.

Zachos, J. C., D. Kroon, P. Blum, et al. (2004), Proc. ODP, Init. Repts., 208, College Station, TX (Ocean Drilling Program), doi:10.2973/odp.proc.ir.208.2004.

Zachos, J. C., et al. (2005), Rapid acidification of the ocean during the Paleocene-Eocene thermal maximum, Science, 308, 1611–1615, doi:10.1126/science.1109004.

Zachos, J. C., G. R. Dickens, and R. E. Zeebe (2008), An early Cenozoic perspective on greenhouse warming and carbon-cycle dynamics, Nature, 451(7176), 279-283, doi:10.1038/nature06588.

Zachos, J. C., H. K. McCarren, B. Murphy, U. Röhl, and T. Westerhold (2010), Tempo and scale of late Paleocene and early Eocene carbon isotope cycles: Implications for the origin of hyperthermals, Earth Planet. Sci. Lett., 299, 242–249, doi:10.1016/j.epsl.2010.09.004.

Supplementary materials and dataset

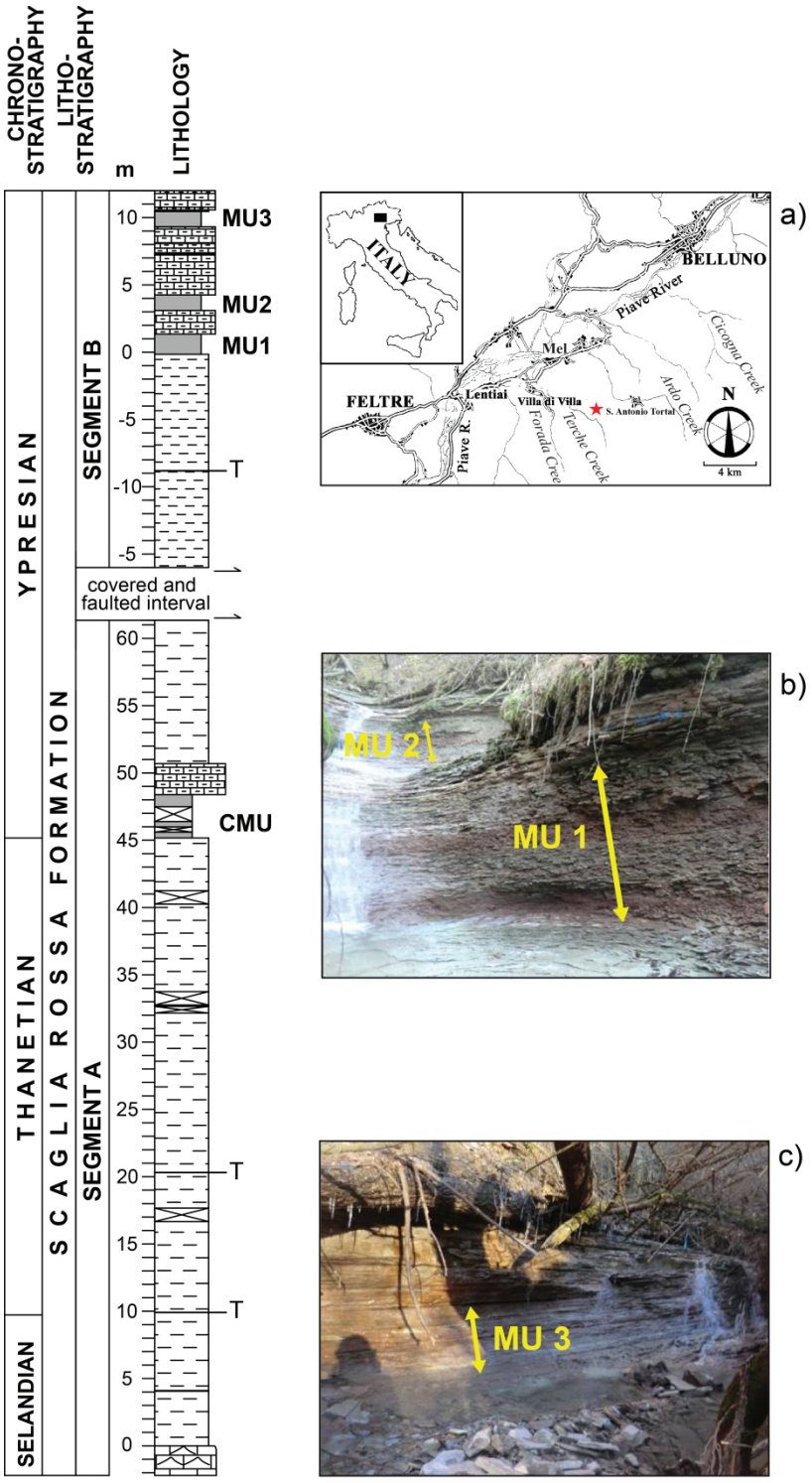

Figure S1. The complete lithological log of the Terche section, plotted against lithostratigraphy and chronostratigraphy (on the left). Location and photographs of the Terche section in northeastern Italy (on the right): (a) geographic map with location of the studied section (red star) in the Piave river valley (Belluno Province); (b) The marly-units MU1 and MU2 and (c) MU3 clearly recognizable in the segment B, the main object of this study. MU1, MU2 and MU3 correspond to the negative carbon excursions of ETM2, H2 and I1, respectively. The CMU is the lithological expression of the Paleocene-Eocene Thermal Maximum. For lithological symbols see figure 2.

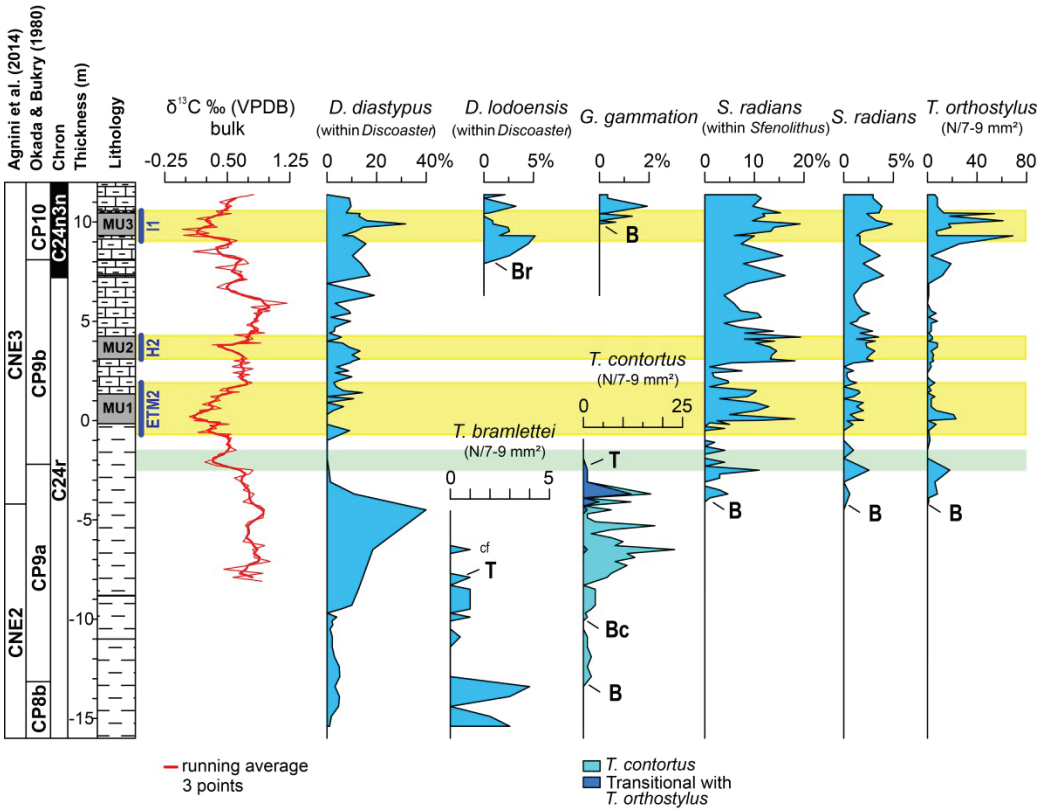

Figure S2. Relative abundances of calcareous nannofossil zonal markers from the segment B of the Terche section. For lithological symbols see figure 2.

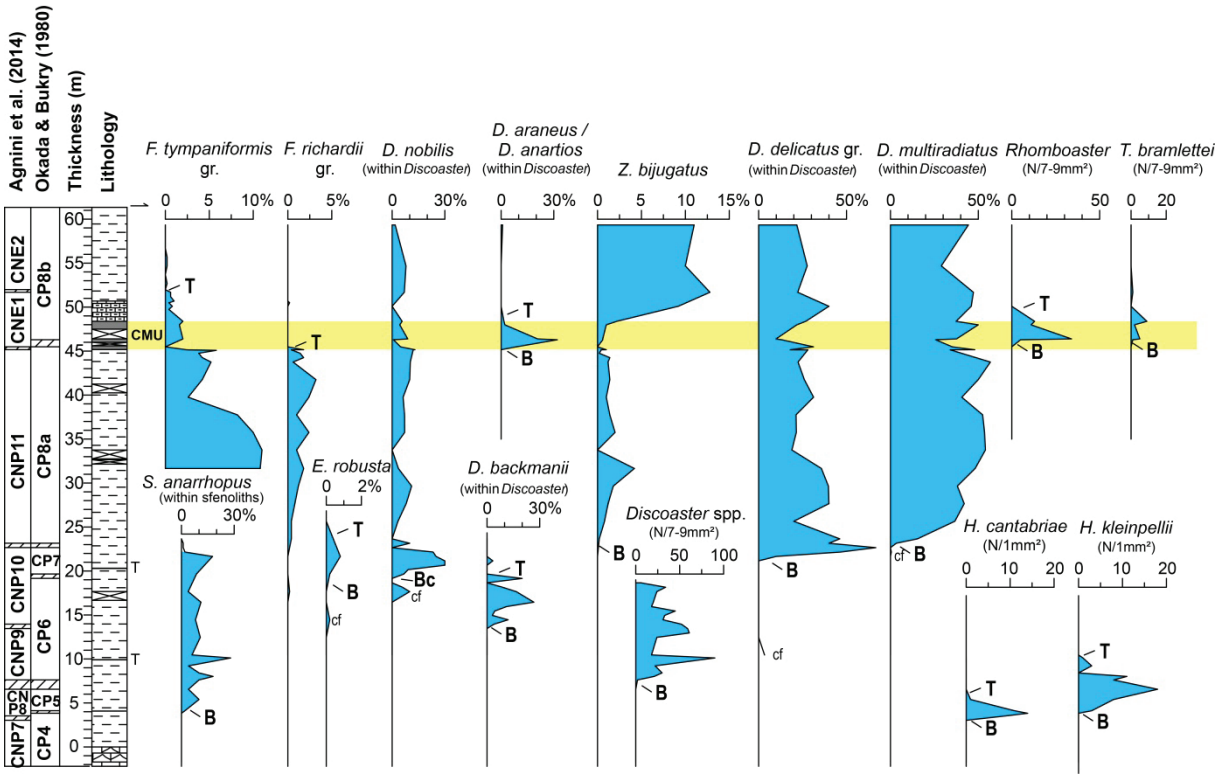

Figure S3. Relative abundances of calcareous nannofossil zonal markers from the segment A of the Terche section. The striped bands in the zonal scheme columns represent the uncertainty derived from the sample spacing. The zonal boundaries are placed at the middle level between two successive samples. For lithological symbols see figure 2.

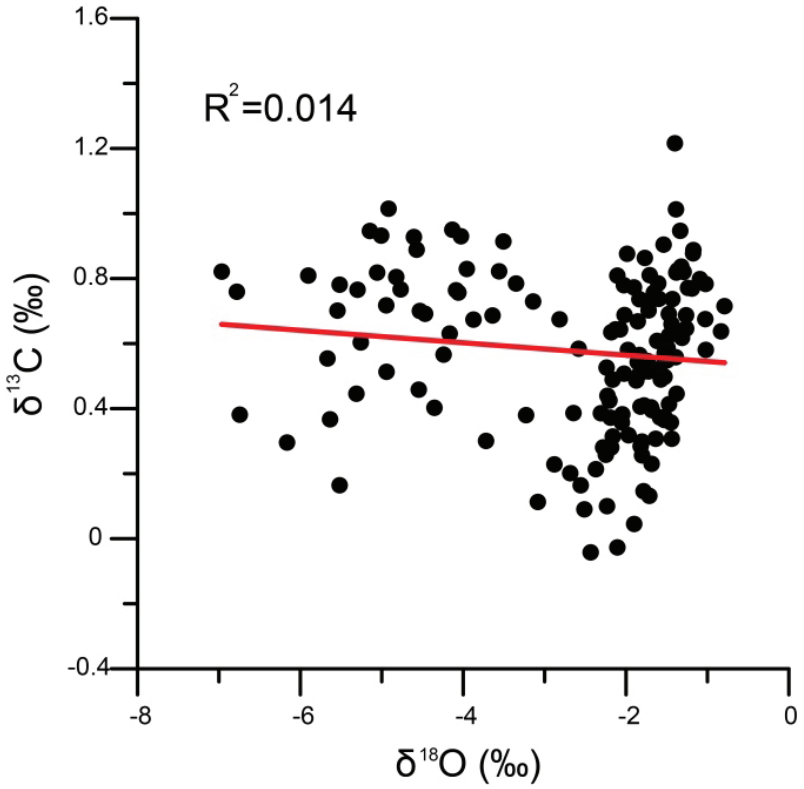

Figure S4. Cross plot of the Terche stable isotope record ($\delta^{13}C$ vs $\delta^{18}O$) from the investigated interval (segment B).

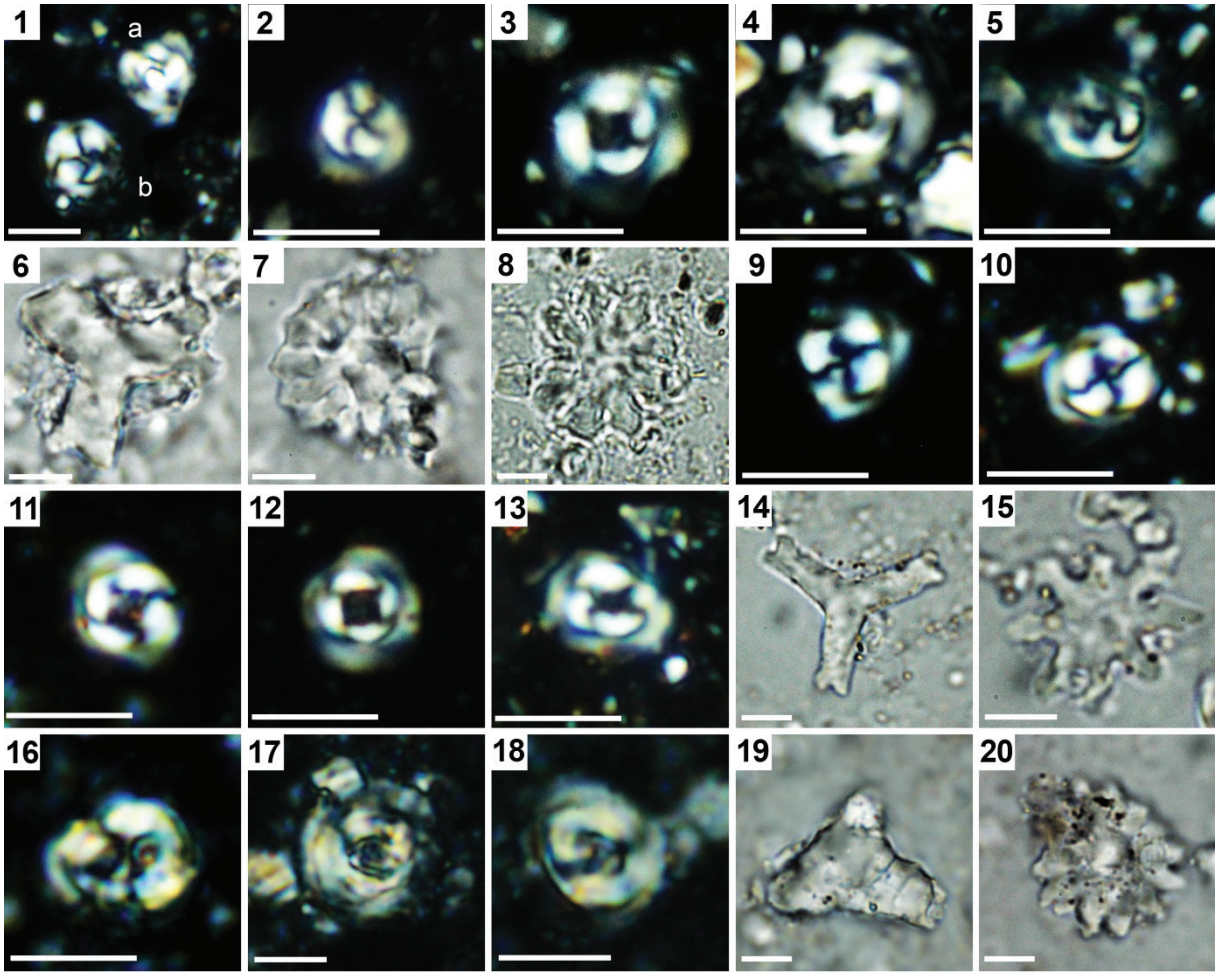

Plate S1. Photomicrographs of selected calcareous nannofossil taxa from three interval showing different stages of overgrowth and etching at the Terche section. Scale bar 5 µm. 1–8: sample TRE/13 –370 within the pre-ETM2 interval (etching E3/E2, overgrowth O3). 1,2–Toweius pertusus [Sullivan, 1965] Romein, 1979; crossed nicols;1a– specimen with central area overgrown; 1b,2–specimens with a well preserved central area. 3,4–Toweius callosus Perch-Nielsen, 1971; crossed nicols; 3–specimen with a well preserved central area; 4–specimen with a central area partly overgrown. 5–Toweius sp.; crossed nicols; specimen with central area heavily overgrown. 6–Tribrachiatus orthostylus (Bramlette and Riedel, 1954) Shamrai, 1963; parallel light; specimen moderately overgrown. 7–Discoaster diastypus Bramlette and Sullivan, 1961; parallel light; specimen moderately overgrown. 8–Discoaster binodosus Martini, 1958; parallel light; specimen moderately overgrown. 9–13: sample TRE/13 +19/+20 at ETM2 CIE peak (etching E4, overgrowth O1/O2). 9–11–Toweius pertusus [Sullivan, 1965] Romein, 1979; crossed nicols; 9,10– specimen with a well preserved central area; 11–specimen with a central area partly dissolved. 12–Toweius callosus Perch-Nielsen, 1971; crossed nicols; specimen with a well preserved central area. 13–Toweius sp.; crossed nicols; specimen with central area heavily dissolved. 14–15: sample TRE/13 +6/+10 within the ETM2 onset (etching E3/E4, overgrowth O1/O2). 14–Tribrachiatus orthostylus (Bramlette and Riedel, 1954) Shamrai, 1963; parallel light; specimen slightly overgrown. 15–Discoaster binodosus Martini, 1958; parallel light; specimen slightly overgrown. 16–20: sample TRE/13 +990 within the I1 recovery (etching E3, overgrowth O3/O4). 16–Toweius pertusus (Sullivan, 1965) Romein, 1979; crossed nicols; specimen with central area overgrown. 17–Toweius callosus Perch-Nielsen, 1971; crossed nicols; specimen with central area overgrown. 18–Toweius cf. callosus Perch-Nielsen, 1971; crossed nicols; specimen with central area heavily overgrown. 19–Tribrachiatus orthostylus (Bramlette and Riedel, 1954) Shamrai, 1963; parallel light; specimen heavily overgrown. 20–Discoaster diastypus Bramlette and Sullivan, 1961; parallel light; specimen heavily overgrown.

Table S1.1. Calcareous nannofossil visual dissolution index: qualitative estimation of etching (Q_E) based on the modified scales from Roth and Thierstein (1972), Adelseck et al. (1973), and Roth (1983).

DEGREE OF DISSOLUTION		DESCRIPTION	Q_E SCORE
E1	No etching	Coccoliths appear pristine.	**5**
E2	Slightly etched	Serrate outlines, partial dissolution of the more delicate structures, presence of abundant small placoliths.	**4**
E3	Moderately etched	Slightly to moderately irregular outlines, partial dissolution of delicate structures, presence of common/scarce small placoliths.	**3**
E4	Heavily etched	Strongly irregular outlines, fragmented material, delicate structures and some species dissolved, presence of rare small placoliths.	**2**
E5	Fully etched	Much fragmented material, only solution-resistant species left.	**1**

Table S1.2. Calcareous nannofossil visual overgrowth index: qualitative estimation of overgrowth (Q_O) based on the modified scale from Dedert et al. (2014).

DEGREE OF OVERGROWTH		DESCRIPTION	Qo_o SCORE
O1	Minimally overgrown	Thin specimens with biogenically sculpted surfaces.	**5**
O2	Slightly overgrown	Extended coccolith elements, thickened cross-bars, etc.	**4**
O3	Moderately overgrown	Thick specimens with angular crystal faces.	**3**
O4	Heavily overgrown	Delicate central structures are thickened and partially obscured.	**2**
O5	Fully overgrown	The overgrowth heavily blurs the diagnostic characters of many taxa. The identification is difficult.	**1**

Table S2.1. Distribution of calcareous nannofossil zonal markers across the segment B of the Terche section.

Samples	Thickness (cm) (0 m level = ETM2)	*D. diastypus* (%)	*D. lodoensis* (%)	*S. radians* (%)	*Girgisia gammation* (%)	*T. contortus* (7-9 mm^2)	*T. orthostylus* (7-9 mm^2)	*T. bramlettei* (7-9 mm^2)
TRE/13 +1137	1137	0,0	2,1	10,3	0,3	0,0	6,0	0,0
TRE/13 1119/1120	1119,5	9,0	0,0	11,4	0,3	0,0	8,0	0,0
TRE/13 +1079	1079	9,7	3,2	9,7	1,9	0,0	8,0	0,0
TRE/13 +1045,5	1045,5	7,7	0,6	15,3	0,3	0,0	13,0	0,0
TRE/13 +1042	1042	13,3	0,0	11,7	0,0	0,0	54,0	0,0
TRE/13 +1029	1029	12,9	0,0	12,1	1,3	0,0	18,0	0,0
TRE/13 +1006	1006	16,1	0,9	9,6	0,0	0,0	61,0	0,0
TRE/13 +999	999	–	–	–	0,7	–	–	–
TRE/13 +990	990	31,7	0,9	19,2	0,0	0,0	17,0	0,0
TRE/13 +973	973	14,5	2,4	14,0	0,0	0,0	19,0	0,0
TRE/13 +953	953	11,7	2,6	13,3	0,0	0,0	7,0	0,0
TRE/13 +931,75	931,75	6,3	1,6	6,0	0,0	0,0	8,0	0,0
TRE/13 +930	930	10,3	5,2	10,0	0,0	0,0	69,0	0,0
TRE/13 +890	890	15,7	4,5	7,4	0,0	0,0	26,0	0,0
TRE/13 +830	830	10,3	2,6	15,7	0,0	0,0	3,0	0,0
TRE/13 +790	790	13,8	0,0	7,8	0,0	0,0	19,0	0,0
TRE/13 +730	730	17,3	0,0	16,2	0,0	0,0	12,0	0,0
TRE/13 +690	690	0,0	0,0	8,6	0,0	0,0	1,0	0,0
TRE/13 +630	630	19,0	0,0	3,9	0,0	0,0	1,0	0,0
TRE/11 +590	590	3,3	0,0	5,9	0,0	0,0	0,0	0,0
TRE/11 +552	552	8,8	0,0	7,2	0,0	0,0	3,0	0,0
TRE/11 +540	540	9,5	0,0	10,7	0,0	0,0	7,0	0,0
TRE/11 +520	520	1,6	0,0	11,4	0,0	0,0	1,0	0,0
TRE/11 +500	500	9,5	0,0	6,3	0,0	0,0	8,0	0,0
TRE/11 +490	490	7,1	0,0	3,9	0,0	0,0	3,0	0,0
TRE/11 +470	470	3,2	0,0	6,8	0,0	0,0	3,0	0,0
TRE/11 +450	450	2,9	0,0	13,8	0,0	0,0	3,0	0,0
TRE/11 +440	440	1,0	0,0	8,1	0,0	0,0	1,0	0,0
TRE/11 +420	420	5,8	0,0	19,3	0,0	0,0	4,0	0,0
TRE/11 +410	410	3,8	0,0	8,0	0,0	0,0	4,0	0,0
TRE/11 +400	400	0,0	0,0	14,1	0,0	0,0	1,0	0,0
TRE/11 +390	390	6,3	0,0	10,3	0,0	0,0	8,0	0,0
TRE/11 +370	370	8,8	0,0	13,2	0,0	0,0	8,0	0,0
TRE/11 +350	350	13,3	0,0	14,5	0,0	0,0	3,0	0,0
TRE/11 +330	330	10,1	0,0	13,6	0,0	0,0	5,0	0,0

TRE/11 +310	310	13,2	0,0	13,2	0,0	0,0	4,0	0,0
TRE/11 +300	300	10,6	0,0	18,2	0,0	0,0	5,0	0,0
TRE/11 +290	290	9,3	0,0	5,3	0,0	0,0	2,0	0,0
TRE/11 +270	270	3,9	0,0	1,0	0,0	0,0	3,0	0,0
TRE/11 +250	250	8,7	0,0	7,5	0,0	0,0	1,0	0,0
TRE/11 +240	240	3,3	0,0	1,5	0,0	0,0	0,0	0,0
TRE/11 +220	220	10,0	0,0	1,9	0,0	0,0	0,0	0,0
TRE/11 +200	200	4,5	0,0	4,7	0,0	0,0	3,0	0,0
TRE/11 +190	190	2,7	0,0	4,8	0,0	0,0	6,0	0,0
TRE/11 +170	170	3,8	0,0	1,0	0,0	0,0	1,0	0,0
TRE/11 +150	150	6,7	0,0	10,4	0,0	0,0	3,0	0,0
TRE/11 +140	140	14,3	0,0	10,0	0,0	0,0	0,0	0,0
TRE/11 +120	120	0,0	0,0	8,6	0,0	0,0	6,0	0,0
TRE/11 +110	110	10,7	0,0	3,0	0,0	0,0	3,0	0,0
TRE/11 +90	90	0,0	0,0	10,2	0,0	0,0	3,0	0,0
TRE/11 +70	70	6,7	0,0	12,9	0,0	0,0	3,0	0,0
TRE/11 +50	50	2,5	0,0	10,5	0,0	0,0	7,0	0,0
TRE/11 +30	30	0,0	0,0	5,0	0,0	0,0	21,0	0,0
TRE/11 +6/+10	8	0,0	0,0	18,2	0,0	0,0	23,0	0,0
TRE/11 0/+2	1	0,0	0,0	10,5	0,0	0,0	4,0	0,0
TRE/11 0/-3	-1,5	0,0	0,0	2,5	0,0	0,0	1,0	0,0
TRE/11 -19/-20	-19,5	0,0	0,0	5,0	0,0	0,0	7,0	0,0
TRE/11 -12	-12	–	–	1,0	–	–	–	–
TRE/11 -30	-30	–	–	0,0	–	–	–	–
TRE/11 -40	-40	–	–	4,0	–	–	–	–
TRE/11 -50/-52	-51	9,1	0,0	0,0	0,0	0,0	1,0	0,0
TRE/11 -60	-60	–	–	0,0	–	–	–	–
TRE/11 -80	-80	–	–	0,0	–	–	–	–
TRE/11 -100	-100	0,0	0,0	0,0	0,0	0,0	2,0	0,0
TRE/11 -110	-110	–	–	2,0	–	–	–	–
TRE/11 -120	-120	–	–	1,0	–	–	–	–
TRE/11 -130	-130	–	–	0,0	–	–	–	–
TRE/11 -150	-150	-9,1	0,0	4,1	0,0	0,0	0,0	0,0
TRE/13 -170	-170			0,0				
TRE/11 -190	-190	0,0	0,0	0,0	0,3	0,0	0,0	0,0
TRE/13 -210	-210	–	–	4,0	–	–	–	–
TRE/13 -230	-230	–	–	0,0	–	–	–	–
TRE/11 -250	-250	0,8	0,0	11,0	0,0	0,0	18,0	0,0
TRE/13 -270	-270	–	–	3,0	–	–	–	–
TRE/13 -290	-290	–	–	3,0	–	–	–	–
TRE/13 -310	-310	1,4	0,0	0,0	0,0	0,0	6,0	0,0
TRE/13 -330	-330	–	–	0,0	–	–	–	–
TRE/13 -350	-350	–	–	3,0	–	–	–	–
TRE/13 -370	-370	11,0	0,0	4,7	0,0	5,0	8,0	0,0
TRE/13 -390	-390	–	–	1,0	–	0,0	1,0	0,0

TRE/13 -410	-410	–	–	0,0	–	8,0	1,0	0,0
TRE/13 -430	-430	–	–	0,0	–	0,0	0,0	0,0
TRE/13 -450	-450	39,9	0,0	0,0	0,0	6,0	0,0	0,0
TRE/13 -470	-470	–	–	0,0	–	1,0	0,0	0,0
TRE/13 -490	-490	–	–	0,0	–	1,0	0,0	0,0
TRE/13 -510	-510	–	–	0,0	–	3,0	0,0	0,0
TRE/13 -530	-530	–	–	0,0	–	18,0	0,0	0,0
TRE/13 -550	-550	–	–	0,0	–	7,0	0,0	0,0
TRE/13 -570	-570	–	–	0,0	–	2,0	0,0	0,0
TRE/13 -590	-590	–	–	0,0	–	7,0	0,0	0,0
TRE/13 -610	-610	–	–	0,0	–	10,0	0,0	0,0
TRE/13 -630	-630	–	–	0,0	–	8,0	0,0	0,0
TRE/13 -650	-650	18,5	0,0	0,0	0,0	22,0	0,0	cf
TRE/13 -670	-670	–	–	0,0	–	11,0	0,0	0,0
TRE/13 -690	-690	–	–	0,0	–	13,0	0,0	0,0
TRE/13 -710	-710	–	–	0,0	–	8,0	0,0	0,0
TRE/13 -730	-730	–	–	0,0	–	11,0	0,0	0,0
TRE/13 -770	-770	–	–	–	–	7,0	0,0	0,0
TRE/13 -790	-790	–	–	–	–	6,0	0,0	1,0
TRE/13 -830	-830	–	–	–	–	0,0	0,0	0,0
TRE/13 -850	-850	12,7	0,0	0,0	0,0	3,0	0,0	1,0
TRE13-930	-930	10,0	0,0	–	0,0	3,0	0,0	1,0
TRE13-950	-950	5,6	0,0	–	–	2,0	0,0	1,0
TRE13-970	-970	0,0	0,0	–	–	0,5	0,0	0,0
TRE13-990	-990	3,9	0,0	–	–	1,0	0,0	1,0
TRE13-1010	-1010	2,0	0,0	–	–	0,0	0,0	0,0
TRE13-1030	-1030	2,3	0,0	–	–	0,0	0,0	0,0
TRE13-1050	-1050	1,2	0,0	–	–	0,0	0,0	0,0
TRE13-1090	-1090	2,1	0,0	–	0,0	1,0	0,0	0,5
TRE15-1140	-1140	2,1	–	–	–	1,0	0,0	0,0
TRE15-1190	-1190	3,0	–	–	–	2,0	0,0	0,0
TRE15-1240	-1240	4,9	–	–	–	1,0	0,0	0,0
TRE15-1290	-1290	5,1	–	–	–	2,0	0,0	0,0
TRE15-1340	-1340	3,2	–	–	–	0,0	0,0	4,0
TRE15-1390	-1390	5,0	–	–	–	0,0	0,0	3,0
TRE15-1440	-1440	4,7	–	–	–	0,0	0,0	0,0
TRE15-1490	-1490	1,8	–	–	–	0,0	0,0	2,0
TRE15-1540	-1540	1,0	–	–	–	0,0	0,0	3,0

Table S2.2. Distribution of calcareous nannofossil zonal markers across the segment A of the Terche section.

Samples	Thickness (cm)	*Discoaster araneus/anartios* (% within Discoaster)	*Discoaster backmanii (% within Discoaster)*	*Discoaster delicatus* gr *(% within Discoaster)*	*Discoaster multiradiatus* (% within Discoaster)	*Discoaster nobilis* gr. (% within Discoaster)	*Discoaster mohleri* (% within Discoaster)	*Sphenolithus anarrhopus* (% within Sphenolithus)	*Ericosonia robusta* (≥ 9µm)	*Fasciculithus tympaniformis* gr (%)	*Fasciculithus richardii* gr. (%)	*Zygrhablithus bijugatus* (%)	*Rhomboaster* spp. (7-9 mm^2)	*Tribrachiatus bramlettei* (7-9 mm^2)
TRC14-88	5934	1	0	22	44	2	8	0	0	0	0	11	0	0
TRC14-84	5469	0	0	28	29	8	8	2	0	0	0	10	0	0
TRC14-80	5169	0	0	22	47	7	3	0	0	1	0	13	0	1
TRC14-79	5119	–	–	–	–	–	–	–	–	1	0	–	–	–
TRC14-78	5069	–	–	–	–	–	–	–	–	1	0	–	–	–
TRC14-77	5050	–	–	–	–	–	–	–	–	0	0	–	–	–
TRC14-76	5010	0	0	40	46	0	4	0	0	1	0	9	0	0
TRC14-72	4839	2	0	27	37	6	5	0	0	2	0	2	13	9
TRC14-71	4799	2	0	22	50	4	2	0	0	2	0	1	11	2
TRC14-70	4639	21	0	10	38	9	4	0	0	2	0	1	34	5
TRC14-69	4629	32	0	13	26	1	5	0	0	2	0	1	5	1
TRC14-68	4549	9	0	31	35	5	2	0	0	0	0	0	0	0
TRC14-67	4516	0	0	18	48	13	4	0	0	2	2	1	0	0
TRC14-66b	4515	0	0	28	34	12	4	0	0	3	0	0	0	0
TRC14-66	4509	–	–	–	–	–	–	0	0	6		0	0	0
TRC14-65	4476	–	–	–	–	–	–	–	–	4	1	0	–	–
TRC14-64	4426	–	–	–	–	–	–	–	–	4	2	1	–	–
TRC14-63	4376	0	0	22	57	10	3	0	0	5	1	1	0	0
TRC14-59	4176	0	0	26	50	10	7	0	0	4	3	1	0	0
TRC14-57	3976	0	0	31	41	6	13	0	0	3	2	1	0	0
TRC14-53	3776	0	0	21	52	7	9	0	0	8	1	1	0	0
TRC14-49	3576	0	0	21	54	7	7	0	0	10	2	2	0	0
TRC14-45	3376	0	0	19	54	0	11	0	0	11	1	0	0	0
TRC14-42	3166	0	0	36	48	4	4	0	0	11	2	4	0	0
TRC14-38	2966	0	0	40	38	11	8	0	0	6	1	2	0	0
TRC14-34	2766	0	0	40	42	8	6	0	0	8	1	1	0	0
TRC14-30	2566	0	0	20	37	3	23	0	0	7	0	1	0	0
TRC14-26	2366	0	0	46	15	0	38	0	0	6	0	0	0	0
TRC14-25	2316	0	0	40	3	10	37	1	–	–	–	–	–	–
TRC14-24	2266	0	0	67	0	0	20	1	–	–	–	–	–	–
TRC14-23	2216	0	0	47	1	23	10	2	–	–	–	–	–	–
TRC14-22	2166	0	0	10	0	25	40	18	1	2	0	0	0	0
TRC14-21	2116	0	3	0	0	30	37	–	–	–	–	–	–	–
TRC14-20	2066	0	0	0	0	30	30	–	–	–	–	–	–	–
TRC14-19	2016	0	0	0	0	9	77	–	–	–	–	–	–	–
TRC14-18	1966	0	0	0	0	7	87	9	0	5	0	0	0	0

TRC14-17	1916	0	20	0	0	0	63	–	–	–	–	–	–	–
TRC14-16	1866	0	0	0	0	0	83	–	–	–	–	–	–	–
TRC14-15	1816	0	9	0	0	6	74	–	–	–	–	–	–	–
TRC14-14	1766	0	17	0	0	10	70	4	0	6	0	0	0	0
TRC14-13	1646	0	27	0	0	0	70	11	0	4	0	0	0	0
TRC14-12	1596	0	11	0	0	0	67	–	–	–	–	–	–	–
TRC14-11	1546	0	4	0	0	0	84	–	–	–	–	–	–	–
TRC14-10	1496	0	3	0	0	0	91	–	–	–	–	–	–	–
TRC14-9	1446	0	12	0	0	0	82	8	0	2	0	0	0	0
TRC14-5	1246	0	0	0	0	0	90	11	0	6	0	0	0	0
TRC14-1	1046	0	0	3	0	0	93	6	0	2	0	0	0	0

Table S2.3 Distribution of calcareous nannofossil zonal markers across the lower part of segment A at the Terche section

Samples	Thickness (cm)	*Heliolithus cantabriae* (1 mm^2)	*Heliolithus kleinpellii* (1 mm^2)	*Sphenolithus anarrhopus* (% within Sphenolithus)
TRH/10 1009-1014	1012	0	1	28
TRH/10 922	922	0	3	4
TRH/10 842	842	0	0	10
TRH/10 802	802	0	11	18
TRH/10 762	762	0	8	10
TRH/10 656	656	0	18	4
TRH/10 540	540	1	8	10
TRH/10 411-413	412	11	3	2
TRH/10 383	383	14	0	0
TRH/10 353	353	9	0	0
TRH/10 303	303	0	0	0
TRH/10 223	223	0	0	0
TRH/10 23	23	0	0	0
TRH/10 -65	-65	0	0	0
TRH/10 -175	-175	0	0	0

Table S3. Carbonate content ($CaCO_3$ %), carbon and oxygen stable isotopes at the Terche section.

Samples	Thickness (0 cm level= ETM2)	$CaCO_3$%	$\delta^{13}C$ (‰)	$\delta^{18}O$ (‰)
TRE/13 -810	-810	56,69	0,91	-3,51
TRE/13 -790	-790	55,22	0,57	-4,24
TRE/13 -770	-770	59,49	0,93	-4,61
TRE/13 -750	-750	53,18	0,46	-4,55
TRE/13 -728	-728	57,88	0,78	-3,35
TRE/13 -710	-710	63,11	1,01	-4,92
TRE/13 -690	-690	55,82	0,82	-6,97
TRE/13 -670	-670	56,75	0,83	-3,96
TRE/13 -650	-650	54,46	0,80	-4,82
TRE/13 -630	-630	57,36	0,95	-4,13
TRE/13 -610	-610	50,89	0,69	-3,64
TRE/13 -590	-590	59,78	0,73	-3,14
TRE/13 -570	-570	55,02	0,77	-5,30
TRE/13 -550	-550	53,08	0,77	-4,77
TRE/13 -530	-530	53,92	0,72	-4,95
TRE/13 -510	-510	57,04	0,76	-6,78
TRE/13 -490	-490	59,74	0,93	-4,03
TRE/13 -470	-470	53,89	0,93	-5,01
TRE/13 -450	-450	52,53	0,95	-5,15
TRE/13 -430	-430	57,96	0,89	-4,57
TRE/13 -410	-410	53,56	0,69	-2,02
TRE/13 -390	-390	63,12	0,78	-5,52
TRE/13 -370	-370	53,74	0,82	-3,56
TRE/13 -350	-350	54,48	0,69	-4,47
TRE/13 -330	-330	56,41	0,76	-4,06
TRE/13 -310	-310	57,31	0,67	-3,87
TRE/13 -290	-290	59,29	0,76	-4,09
TRE/13 -270	-270	49,76	0,58	-2,58
TRE/13 -250	-250	55,38	0,81	-5,90
TRE/11 -230	-230	55	0,38	-2,05
TRE/11 -210	-210	59	0,23	-1,69
TRE/11 -190	-190	54	0,37	-1,53
TRE/11 -170	-170	61	0,40	-1,68
TRE/11 -150	-150	55	0,61	-1,62
TRE/11 -130	-130	60	0,51	-1,72
TRE/11 -120	-120	57	0,49	-1,87
TRE/11 -110	-110	51	0,53	-2,24
TRE/11 -100	-100	56	0,52	-1,62
TRE/11 -90	-90	62	0,55	-1,53
TRE/11 -80	-80	63	0,44	-2,23
TRE/11 -70	-70	56	0,55	-1,74
TRE/11 -60	-60	58	0,15	-1,78

TRE/11 -50/-52	-51	55	0,26	-2,25
TRE/11 -40	-40	47	0,37	-1,58
TRE/11 -30	-30	55	0,31	-1,64
TRE/11 -25	-25	52	0,28	-1,82
TRE/11 -19/-20	-19,5	50	0,52	-1,72
TRE/11 -12	-12	38	0,31	-2,16
TRE/11 -8	-8	38	0,40	-1,69
TRE/11 -3/0	-1,5	36	0,10	-2,23
TRE/11 0/+2	1	40	0,26	-1,80
TRE/11 +2/+6	4	27	0,23	-2,88
TRE/11 +6/+10	8	21	0,11	-3,08
TRE/11 +19/+20	19,5	24	0,05	-1,90
TRE/11 +30	30	25	0,63	-2,18
TRE/11 +40	40	41	0,21	-2,37
TRE/11 +50	50	39	0,16	-2,56
TRE/11 +60	60	32	0,42	-2,20
TRE/11 +70	70	31	0,36	-2,05
TRE/11 +80	80	32	0,20	-2,69
TRE/11 +90	90	39	0,28	-2,28
TRE/11 +100	100	49	0,41	-1,47
TRE/11 +110	110	52	0,39	-2,65
TRE/11 +120	120	47	0,30	-1,80
TRE/11 +130	130	43	0,50	-1,53
TRE/11 +140	140	57	0,51	-2,02
TRE/11 +143	143	54	0,64	-1,41
TRE/11 +150	150	53	0,41	-1,78
TRE/11 +160	160	58	0,45	-1,38
TRE/11 +170	170	64	0,64	-0,83
TRE/11 +180	180	46	0,74	-1,84
TRE/11 +190	190	56	0,80	-1,09
TRE/11 +200	200	63	0,69	-1,26
TRE/11 +210	210	60	0,67	-2,82
TRE/11 +220	220	60	0,62	-1,47
TRE/11 +230	230	57	0,77	-1,19
TRE/11 +240	240	60	0,57	-1,53
TRE/11 +250	250	67	0,72	-0,79
TRE/11 +260	260	69	0,81	-1,71
TRE/11 +270	270	58	0,56	-1,39
TRE/11 +280	280	49	0,64	-2,13
TRE/11 +290	290	65	0,77	-1,24
TRE/11 +300	300	57	0,58	-1,98
TRE/11 +310	310	51	0,74	-1,43
TRE/11 +320	320	50	0,70	-1,72
TRE/11 +330	330	47	0,65	-1,26
TRE/11 +340	340	46	0,64	-2,07
TRE/11 +350	350	42	0,54	-1,86
TRE/11 +351,5	351,5	40	–	–
TRE/11 +360	360	41	0,50	-1,55

TRE/11 +370	370	40	0,39	-2,31
TRE/11 +380	380	46	0,32	-1,97
TRE/11 +390	390	55	0,90	-1,54
TRE/11 +396	396	54	0,66	-1,44
TRE/11 +400	400	45	0,69	-1,47
TRE/11 +410	410	48	0,81	-2,11
TRE/11 +420	420	52	0,78	-2,03
TRE/11 +430	430	60	0,59	-1,49
TRE/11 +440	440	59	0,95	-1,33
TRE/11 +450	450	65	0,77	-1,90
TRE/11 +460	460	60	0,88	-1,18
TRE/11 +470	470	64	0,84	-1,32
TRE/11 +480	480	64	0,73	-1,69
TRE/11 +490	490	63	0,78	-1,02
TRE/11 +500	500	63	0,88	-1,99
TRE/11 +511,5	511,5	62	0,82	-1,29
TRE/11 +520	520	64	0,86	-1,77
TRE/11 +530	530	67	0,89	-1,17
TRE/11 +540	540	64	0,82	-1,38
TRE/11 +552	552	64	1,01	-1,39
TRE/11 +570	570	65	0,79	-1,60
TRE/11 +590	590	61	1,22	-1,40
TRE/11 +610	610	66	0,83	-1,37
TRE/13 +630	630	66	0,67	-1,86
TRE/13 +650	650	64	0,60	-5,26
TRE/13 +670	670	59	0,37	-2,19
TRE/13 +690	690	66	0,49	-1,57
TRE/13 +710	710	69	0,74	-1,60
TRE/13 +712	712	65	0,70	-4,53
TRE/13 +730	730	61	0,63	-4,17
TRE/13 +750	750	59,58	0,68	-1,03
TRE/13 +750BIS	750	57	0,38	-3,23
TRE/13 770	770	61	0,36	-1,45
TRE/13 +790	790	66	0,76	-1,66
TRE/13 +810	810	56	0,70	-5,54
TRE/13 +830	830	66	0,56	-1,84
TRE/13 +850	850	64	0,09	-2,51
TRE/13 +870	870	61	0,51	-4,94
TRE/13 +890	890	69	–	–
TRE/11 +905	905	64	0,62	-1,31
TRE/13 +920	920	64	0,45	-5,31
TRE/13 +930	931,75	56	–	–
TRE/13 +931.75	943	37	-0,03	-2,11
TRE/13 +943	953	34	0,28	-2,18
TRE/13 +953	963	55	0,16	-5,52
TRE/13 +963	973	41	-0,04	-2,43
TRE/13 +973	983	43,26	0,38	-6,74
TRE/13 +983	990	53,01	0,31	-1,44

TRE/13 +990	999	43,77	0,30	-3,72
TRE/13 +999	1006	50,96	0,30	-6,16
TRE/13 +1006	1016	49,22	0,13	-1,71
TRE/13 +1016	1029	50,95	0,37	-5,64
TRE/13 +1029	1042	52,83	0,55	-1,50
TRE/13 +1042	1045	58,94	0,40	-4,35
TRE/13 +1045.5	1045,5	59,77	0,37	-1,53
TRE/13 +1057	1057	57,44	0,51	-1,83
TRE/13 +1072	1072	64,22	0,49	-2,16
TRE/13 +1079	1079	67,51	0,55	-5,67
TRE/13 +1099	1099	65,55	0,41	-1,82
TRE/13+1119/+1120	1119,5	73,04	0,58	-1,02
TRE/13 +1137	1137	72,73	0,82	-5,06

Table S4.1. Calcareous nannofossil dissolution and preservation proxies at the Terche section: the species richness (Diversity), the qualitative indices of etching (Q_E) and overgrowth (Q_O), the relative abundance (%) of Toweius species with a well preserved central area ($T_{species}$) and the Toweius Discoaster ratio (T/D, %).

Samples	Thickness (cm) (0 cm level= ETM2)	Diversity (n° taxa)	Etching	Q_E score	Overgrowth	Q_O score	*Toweius callosus* (%)	*Toweius eminens/tovae* (%)	*Toweius occultatus* (%)	*Toweius pertusus* (%)	*Toweius* sp.1 (%)	*Toweius* spp. (%)	Total *Toweius* (%)	*Toweius* spp. (%)	relative abundance (%) of *Toweius* species with a well preserved central area (T*species*)	*Toweius* (%)	*Discoaster* (%)	*Toweius*/*Discoaster* (%)
TRE/13 +1137	1137	22	E3	3	O2/O3	4	3,3	0,0	0,3	10,2	1,6	0,7	16,1	4,1	95,9	16,1	4,3	3,8
TRE/13 +1119/1120	1120	19	E3	3	O3/O4	3	5,6	0,0	0,0	12,8	0,3	6,6	25,2	26,0	74,0	25,2	3,0	8,6
TRE/13 +1079	1079	25	E3/E2	3,5	O3/O4	3	1,9	0,0	0,0	10,9	2,3	3,2	18,3	17,5	82,5	18,3	1,9	9,5
TRE/13 +1045,5	1046	22	E3	3	O3	3	4,2	0,0	0,0	7,4	1,9	2,6	16,2	16,0	84,0	16,2	2,6	6,3
TRE/13 +1042	1042	28	E3	3	O3/O4	3	6,3	0,0	0,0	4,7	1,7	4,0	16,7	24,0	76,0	16,7	5,3	3,1
TRE/13 +1029	1029	28	E3	3	O3	3	4,6	0,0	0,0	8,6	0,3	5,0	18,5	26,8	73,2	18,5	8,6	2,2
TRE/13 +1006	1006	24	E3	3	O3/O4	3	2,7	0,0	0,0	10,3	0,3	3,3	16,6	20,0	80,0	16,6	1,3	12,5
TRE/13 +990	990	26	E3	3	O3/O4	3	2,0	0,7	0,0	10,5	0,0	4,6	17,6	25,9	74,1	17,6	2,3	7,7
TRE/13 +973	973	25	E3/E4	2,5	O2	4	4,5	1,3	0,0	7,4	1,9	3,9	19,0	20,3	79,7	19,0	3,2	5,9
TRE/13 +953	953	21	E3/E4	2,5	O2	4	3,2	0,0	0,0	12,3	0,3	2,9	18,8	15,5	84,5	18,8	0,6	29,0
TRE/13 +931,75	931,8	23	E3	3	O2/O3	4	4,2	0,0	0,0	8,4	1,9	1,6	16,2	10,0	90,0	16,2	1,0	16,7
TRE/13 +930	930	26	E2/E3	3,5	O3	3	3,9	0,0	0,0	9,8	2,6	1,3	17,7	7,4	92,6	17,7	3,0	6,0
TRE/13 +890	890	20	E2/E3	3,5	O3	3	1,3	0,3	0,0	14,7	1,6	3,6	21,6	16,7	83,3	21,6	1,3	16,5
TRE/13 +830	830	24	E3	3	O2/O3	4	4,7	0,3	0,0	8,7	4,7	1,0	19,3	5,2	94,8	19,3	1,7	11,6
TRE/13 +790	790	23	E2/E3	3,5	O3	3	2,0	0,7	0,0	12,1	1,0	2,9	18,6	15,8	84,2	18,6	3,3	5,7
TRE/13 +730	730	30	E3	3	O3	3	5,4	0,3	0,0	7,4	3,0	2,7	18,7	14,3	85,7	18,7	2,7	7,0
TRE/13 +690	690	18	E4	2	O2	4	0,3	1,0	0,0	15,1	1,3	3,8	21,5	17,9	82,1	21,5	1,9	11,2
TRE/13 +630	630	20	E3	3	O3	3	8,0	0,0	0,0	4,0	2,7	0,0	14,7	0,0	100,0	14,7	0,7	22,0
TRE/11 +590	590	23	E3/E4	2,5	O3/O4	3	2,9	1,3	0,0	6,1	1,3	3,9	15,5	25,0	75,0	15,5	1,6	9,6
TRE/11 +552	552	26	E3	3	O3	3	5,3	0,0	0,3	5,0	4,1	0,0	14,8	0,0	100,0	14,8	1,9	7,8
TRE/11 +540	540	20	E3/E2	3,5	O3	3	2,0	0,3	0,0	8,1	1,6	2,0	14,0	14,0	86,0	14,0	2,0	7,2
TRE/11 +520	520	22	E3/E2	3,5	O3/O4	3	1,6	1,0	0,0	9,9	1,9	3,8	18,2	21,1	78,9	18,2	1,0	19,0

Samples	Thickness (cm) (0 cm level= ETM2)	Diversity (n° taxa)	Etching	Q_E score	Overgrowth	Q_O score	*Toweius callosus* (%)	*Toweius eminens/tovae* (%)	*Toweius occultatus* (%)	*Toweius pertusus* (%)	*Toweius* sp.1 (%)	*Toweius* spp. (%)	Total *Toweius* (%)	*Toweius* spp. (%)	relative abundance (%) of *Toweius* species with a well preserved central area (T*species*)	*Toweius* (%)	*Discoaster* (%)	*Toweius/Discoaster* (%)
TRE/11 +500	500	21	E3	3	O3	3	3,9	0,0	0,0	3,9	3,6	0,0	11,4	0,0	100,0	11,4	2,3	5,0
TRE/11 +490	490	21	E3	3	O3	3	2,9	1,3	0,0	7,8	3,6	2,9	18,6	15,8	84,2	18,6	2,0	9,5
TRE/11 +470	470	25	E3/E2	3,5	O3/O4	3	2,7	0,9	0,0	7,3	1,8	3,9	16,7	23,6	76,4	16,7	3,0	5,5
TRE/11 +450	450	19	E3	3	O3	3	4,8	0,0	0,0	3,2	4,2	0,0	12,3	0,0	100,0	12,3	2,3	5,4
TRE/11 +440	440	22	E3/E4	2,5	O3	3	2,6	1,7	0,0	13,2	2,6	3,6	23,8	15,3	84,7	23,8	2,6	9,0
TRE/11 +420	420	25	E3	3	O2/O3	4	7,4	1,0	0,0	9,0	5,1	0,6	23,1	2,8	97,2	23,1	3,2	7,2
TRE/11 +410	410	27	E3	3	O3	3	8,1	0,3	0,0	3,2	2,9	0,6	15,3	4,3	95,7	15,3	7,8	2,0
TRE/11 +400	400	24	E3/E4	2,5	O2	4	5,7	1,0	0,0	5,1	2,2	0,3	14,3	2,2	97,8	14,3	2,2	6,4
TRE/11 +390	390	22	E3	3	O3/O4	3	3,5	1,0	0,0	10,2	3,2	3,2	21,1	15,2	84,8	21,1	1,6	13,2
TRE/11 +370	370	21	E3/E4	2,5	O2/O3	4	3,6	1,3	0,0	14,2	4,6	3,0	26,8	11,1	88,9	26,8	1,7	16,2
TRE/11 +350	350	24	E3	3	O2	4	6,6	0,3	0,0	4,7	4,1	0,3	16,0	2,0	98,0	16,0	1,9	8,5
TRE/11 +330	330	25	E3/E4	2,5	O2	4	1,0	0,7	0,0	10,6	3,0	3,6	18,8	19,3	80,7	18,8	4,0	4,8
TRE/11 +310	310	28	E3	3	O3	3	1,3	0,7	0,0	3,6	3,6	0,0	9,2	0,0	100,0	9,2	4,6	2,0
TRE/11 +300	300	29	E3	3	O3	3	1,2	0,3	0,0	3,9	3,9	0,0	9,2	0,0	100,0	9,2	3,0	3,1
TRE/11 +290	290	24	E3/E4	2,5	O3	3	1,6	1,6	0,0	7,8	2,9	4,9	19,0	25,9	74,1	19,0	3,3	5,8
TRE/11 +270	270	24	E3/E4	2,5	O2/O3	4	2,3	1,3	0,0	11,8	5,2	4,6	25,2	18,2	81,8	25,2	2,0	12,8
TRE/11 +250	250	22	E3	3	O3	3	1,3	2,0	0,0	3,3	5,9	0,0	12,5	0,0	100,0	12,5	1,7	7,6
TRE/11 +240	240	22	E3	3	O2/O3	4	2,6	1,0	0,0	7,5	4,2	4,2	19,5	21,7	78,3	19,5	1,3	15,0
TRE/11 +220	220	23	E3/E4	2,5	O3	3	3,9	1,0	0,0	11,3	3,2	5,8	25,2	23,1	76,9	25,2	1,3	19,5
TRE/11 +200	200	29	E3/E2	3,5	O3	3	3,8	2,2	0,6	1,9	4,7	0,9	14,2	6,7	93,3	14,2	3,1	4,5
TRE/11 +190	190	24	E3	3	O3	3	6,2	0,6	0,0	4,5	4,2	2,6	18,2	14,3	85,7	18,2	2,3	8,0
TRE/11 +170	170	22	E3	3	O3	3	6,8	1,6	0,0	8,4	5,8	2,3	25,0	9,1	90,9	25,0	2,6	9,6

Samples	Thickness (cm) (0 cm level= ETM2)	Diversity (n° taxa)	Etching	Q_E score	Overgrowth	Q_O score	*Toweius callosus* (%)	*Toweius eminens/tovae* (%)	*Toweius occultatus* (%)	*Toweius pertusus* (%)	*Toweius* sp.1 (%)	*Toweius* spp. (%)	Total *Toweius* (%)	*Toweius* spp. (%)	relative abundance (%) of *Toweius* species with a well preserved central area (T*species*)	*Toweius* (%)	*Discoaster* (%)	*Toweius*/*Discoaster* (%)
TRE/11 +150	150	31	E3	3	O3	3	4,5	2,1	0,6	2,4	3,9	1,5	15,1	10,0	90,0	15,1	4,2	3,6
TRE/11 +140	140	31	E3/E4	2,5	O2	4	3,3	4,2	0,7	2,9	3,6	1,6	16,3	10,0	90,0	16,3	5,2	3,1
TRE/11 +120	120	31	E3	3	O3	3	3,7	2,7	1,3	1,7	5,6	1,3	16,3	8,2	91,8	16,3	5,6	2,9
TRE/11 +110	110	28	E3	3	O3	3	5,4	0,6	0,0	11,2	6,7	3,5	27,6	12,8	87,2	27,6	6,4	4,3
TRE/11 +90	90	29	E3/E4	2,5	O2	4	7,6	1,6	0,0	8,9	9,9	3,6	31,6	11,5	88,5	31,6	3,6	8,7
TRE/11 +70	70	27	E3/E4	2,5	O1/O2	5	4,2	1,3	0,0	12,4	6,2	2,3	26,5	8,6	91,4	26,5	3,3	8,1
TRE/11 +60	60	–	E3/E4	2,5	O2	4	1,7	0,0	0,0	5,7	2,0	2,3	11,7	20,0	80,0	11,7	3,0	3,9
TRE/11 +50	50	25	E3	3	O3	3	3,8	2,7	0,4	3,0	11,8	0,4	22,0	1,7	98,3	22,1	3,8	5,8
TRE/11 +30	30	20	E3/E4	2,5	O2/O3	4	5,3	0,0	0,0	14,9	1,3	4,0	25,4	15,6	84,4	25,4	3,0	8,6
TRE/11 +19/20	19,5	–	E4	2	O1/O2	5	3,0	0,7	0,0	11,3	5,0	7,0	27,0	25,9	74,1	27,0	2,7	10,1
TRE/11 +6/+10	8	21	E3/E4	2,5	O1/O2	5	6,6	0,0	0,0	10,6	9,6	1,0	27,8	3,6	96,4	27,8	1,0	28,0
TRE/11 0/+2	0	20	E3	3	O2/O3	4	2,1	3,2	0,2	3,5	19,0	0,0	28,0	0,0	100,0	28,0	1,7	16,9
TRE/11 0/-3	-1,5	26	E3	3	O2/O3	4	5,6	2,0	0,0	7,9	9,5	3,0	28,0	10,6	89,4	28,0	2,6	10,6
TRE/11 -19/-20	-19,5	25	E3	3	O2/O3	4	7,8	0,6	0,0	9,4	6,6	1,6	26,0	6,0	94,0	26,0	3,4	7,5
TRE/11 -50/-52	-51	23	E3	3	O3	3	5,3	0,7	0,0	5,3	5,3	2,3	18,8	12,3	87,7	18,8	1,6	11,4
TRE/11 -100	-100	25	E3	3	O3	3	3,3	0,7	0,0	5,3	5,0	0,3	14,6	2,3	97,7	14,6	2,3	6,3
TRE/11 -150	-150	22	E3/E2	3,5	O3	3	3,3	0,3	0,0	3,9	5,9	2,3	15,7	14,6	85,4	15,7	3,9	4,0
TRE/11 -190	-190	19	E3/E2	3,5	O3	3	1,7	0,8	0,0	2,9	2,1	1,5	9,0	16,3	83,7	9,0	0,7	13,6
TRE/11 -250	-250	23	E3/E2	3,5	O3	3	3,5	1,0	0,0	9,9	4,1	2,5	21,0	12,1	87,9	21,0	1,6	13,2
TRE/13 -310	-310	26	E3/E2	3,5	O3	3	3,6	1,3	0,0	5,3	4,3	1,0	15,6	6,4	93,6	15,6	3,0	5,2
TRE/13 -370	-370	25	E3/E2	3,5	O3	3	4,3	3,4	0,0	9,5	2,4	2,4	22,0	11,1	88,9	22,0	2,7	8,0
TRE/13 -450	-450	22	E3/E2	3,5	O3	3	4,0	3,6	0,0	7,3	1,3	3,0	19,2	15,5	84,5	19,2	3,0	6,4

Table S4.2. Planktic foraminiferal dissolution and productivity proxies at the Terche section: the fragmentation index (*F-index*, %), the weight percent coarse fraction (*WPCF*, %) the plankton benthos ratio (*P/B*, %).

Samples	Thickness (0 cm level= ETM2)	*F-index* (%)	*WPCF* (%)	*P/B* (%)
TRE/13 -790	-790	5,4	4,88	95,51
TRE/13 -750	-750	–	–	94,58
TRE/13 -710	-710	5,1	5,60	97,72
TRE/13 -630	-630	5,4	6,44	96,69
TRE/13 -550	-550	7,1	4,54	96,10
TRE/13 -470	-470	7,5	4,09	92,69
TRE/13 -390	-390	11,5	4,85	93,86
TRE/13 -310	-310	10,6	4,38	96,59
TRE/11 -230	-230	14,4	5,00	96,85
TRE/11 -210	-210	15,0	5,43	95,35
TRE/11 -190	-190	14,1	4,16	96,13
TRE/11 -170	-170	9,5	5,21	95,33
TRE/11 -150	-150	11,5	4,93	97,65
TRE/11 -120	-120	15,0	4,14	96,94
TRE/11 -100	-100	–	5,47	96,41
TRE/11 -90	-90	13,4	6,02	–
TRE/11 -80	-80	–	7,93	93,97
TRE/11 -70	-70	–	6,37	–
TRE/11 -60	-60	19,7	6,74	96,04
TRE/11 -50/-52	-51	–	5,76	–
TRE/11 -40	-40	–	5,15	96,44
TRE/11 -30	-30	12,3	4,71	–
TRE/11 -25	-25	–	6,35	–
TRE/11 -19/-20	-19,5	19,3	5,89	98,51
TRE/11 -12	-12	–	6,84	–
TRH/11 -8	-8	24,8	6,87	–
TRE/11 -3/0	-1,5	18,1	5,69	97,00
TRE/11 0/+2	1	14,1	4,28	–
TRE/11 +2/+6	4	21,0	2,15	–
TRE/11 +6/+10	8	28,3	1,29	–
TRE/11 +19/+20	20	25,9	1,45	96,35
TRE/11 +30	30	24,3	4,33	–
TRE/11 +40	40	22,8	6,63	97,39
TRE/11 +50	50	24,3	5,83	–
TRE/11 +60	60	28,4	6,57	95,51
TRE/11 +70	70	25,8	3,53	–
TRE/11 +80	80	29,2	4,23	96,74
TRE/11 +90	90	21,3	3,52	–
TRE/11 +100	100	–	4,79	95,47
TRE/11 +110	110	–	4,76	–
TRE/11 +120	120	21,0	4,38	95,95
TRE/11 +130	130	18,5	5,07	–

TRE/11 +150	150	16,5	5,40	92,75
TRE/11 +180	180	15,4	4,86	94,71
TRE/11 +190	190	14,2	6,49	–
TRE/11 +197,5/200	198,75	–	4,89	–
TRE/11 +200	200	16,5	6,55	93,82
TRE/11 +220	220	–	5,63	97,05
TRE/11 +250	250	18,3	6,73	92,86
TRE/11 +280	280	–	5,04	94,24
TRE/11 +300	300	14,3	6,77	94,84
TRE/11 +310	310	20,4	5,09	–
TRE/11 +320	320	17,8	5,65	94,57
TRE/11 +340	340	24,1	6,59	93,42
TRE/11 +350	350	26,9	4,66	–
TRE/11 +360	360	29,1	5,04	94,44
TRE/11 +370	370	25,9	4,61	–
TRE/11 +380	380	27,1	3,62	92,78
TRE/11 +400	400	25,6	4,50	95,49
TRE/11 +420	420	19,6	4,85	94,96
TRE/11 +450	450	16,9	6,73	94,46
TRE/11 +500	500	13,4	6,32	94,75
TRE/11 +540	540	16,3	6,31	92,50
TRE/11 +590	590	18,8	5,31	94,22
TRE/13 +630	630	18,4	6,94	94,19
TRE/13 +710	710	9,6	7,42	94,99
TRE/13 +750	750	12,5	4,79	94,12
TRE/13 +830	830	14,1	6,17	95,37
TRE/11 +905	905	14,6	5,90	92,63
TRE/13 +931,75	931,75	7,4	6,51	95,76
TRE/13 +943	943	6,6	4,77	–
TRE/13 +953	953	9,5	4,64	95,95
TRE/13 +963	963	24,9	5,64	–
TRE/13 +973	973	24,8	4,80	92,89
TRE/13 +983	983	13,5	5,37	–
TRE/13 +990	990	13,5	5,67	96,01
TRE/13 +999	999	17,6	4,33	–
TRE/13 +1006	1006	21,0	4,93	91,76
TRE/13 +1029	1029	16,8	5,14	94,29
TRE/13 +1057	1057	18,3	5,20	94,89
TRE/13+1119/+1120	1120	19,7	6,38	95,92

Table S5. Relative abundances (%) of planktic foraminiferal genera and radiolarians at the Terche section.

Sample	Thickness (0 cm level= ETM2)	No. Total counted specimens	*Morozovella (%)*	*Acarinina (%)*	*Subbotina* gr. (%)	Chiloguembeinids (%)	*Planorotalites (%)*	*Globanomalina (%)*	*Pseudohastigerina (%)*	No. counted planktic foraminifera	No. counted radiolarians	No. Total counted specimens	Radiolarians (%)
TRE/13 -790	-790	312	28,8	14,4	41,7	12,8	0,3	1,3	0,6	312	3	315	1,0
TRE/13 -710	-710	314	31,5	16,9	39,5	9,6	1,3	0,6	0,6	374	3	377	0,8
TRE/13 -630	-630	302	34,4	22,2	33,8	7,0	2,0	0,3	0,3	317	1	318	0,3
TRE/13 -550	-550	316	36,4	23,7	27,8	10,4	1,3	0,3	0,0	312	1	313	0,3
TRE/13 -470	-470	310	42,3	27,4	16,5	12,3	1,0	0,0	0,6	308	2	310	0,6
TRE/13 -390	-390	343	39,1	37,6	17,8	4,1	1,2	0,3	0,0	305	3	308	1,0
TRE/13 -310	-310	310	41,0	35,8	17,1	4,5	0,6	0,6	0,3	310	6	316	1,9
TRE/11 -230	-230	303	41,3	36,0	16,8	4,0	1,0	1,0	0,0	305	8	313	2,6
TRE/11 -210	-210	300	37,7	35,7	18,7	4,0	2,7	1,0	0,3	288	10	298	3,4
TRE/11 -190	-190	298	40,9	34,2	16,8	5,7	1,0	1,0	0,3	298	12	310	3,9
TRE/11 -170	-170	307	38,4	34,9	19,9	4,9	1,0	0,7	0,3	316	7	323	2,2
TRE/11 -150	-150	288	38,2	33,0	19,8	6,3	1,4	0,0	1,4	300	8	308	2,6
TRE/11 -120	-120	303	38,3	36,0	19,1	4,6	0,3	1,3	0,3	300	4	304	1,3
TRE/11 -100	-100	300	35,3	41,3	18,3	2,3	1,0	1,3	0,3	–	–	–	–
TRE/11 -90	-90	310	36,8	41,6	16,1	2,6	0,6	1,3	1,0	310	9	319	2,8
TRE/11 -80	-80	297	39,1	35,4	14,8	6,1	2,4	2,0	0,3	297	6	303	2,0
TRE/11 -70	-70	299	40,5	38,8	14,0	3,3	1,0	1,3	1,0	299	5	304	1,6
TRE/11 -60	-60	300	34,3	42,7	17,7	2,0	1,7	1,0	0,7	300	6	306	2,0
TRE/11 -50/-52	-51	299	38,1	37,1	23,1	1,3	0,0	0,0	0,3	299	8	307	2,6
TRE/11 -40	-40	291	36,1	41,9	16,5	4,1	1,0	0,0	0,3	–	–	–	–
TRE/11 -30	-30	288	34,7	51,7	10,1	2,8	0,0	0,3	0,3	288	6	294	2,0
TRE/11 -19/-20	-19,5	293	31,4	51,9	13,3	2,0	0,7	0,3	0,3	293	4	297	1,3
TRE/11 -12	-12	301	34,2	58,5	5,3	1,0	0,0	0,7	0,3	301	11	312	3,5
TRH/11 -8	-8	302	39,1	45,7	10,9	3,3	0,3	0,3	0,3	302	4	306	1,3
TRE/11 -3/0	-1,5	296	36,5	56,4	3,0	3,0	0,0	1,0	0,0	296	8	304	2,6
TRE/11 0/+2	1	290	39,0	49,3	6,2	3,4	1,0	0,7	0,3	290	6	296	2,0
TRE/11 +2/+6	4	300	42,7	54,7	0,7	1,3	0,0	0,3	0,3	300	8	308	2,6
TRE/11 +6/+10	8	335	44,48	53,43	0,90	0,60	0,00	0,30	0,30	302	11	313	3,5
TRE/11 +19/+20	19,5	331	50,2	48,9	0,0	0,3	0,0	0,3	0,3	298	7	305	2,3
TRE/11 +30	30	299	38,1	56,9	1,3	1,7	0,0	1,3	0,7	299	26	325	8,0
TRE/11 +40	40	300	45,0	51,3	1,0	1,7	0,0	0,3	0,7	300	31	331	9,4
TRE/11 +50	50	301	38,2	57,8	2,0	1,0	0,3	0,0	0,7	301	51	352	14,5
TRE/11 +60	60	299	42,5	55,2	0,7	1,0	0,0	0,3	0,3	299	34	333	10,2
TRE/11 +70	70	303	42,9	56,1	0,0	0,7	0,0	0,0	0,3	302	31	333	9,3
TRE/11 +80	80	321	41,4	54,5	1,9	2,2	0,0	0,0	0,0	321	42	363	11,6
TRE/11 +90	90	311	32,8	63,0	1,3	2,6	0,0	0,3	0,0	310	25	335	7,5
TRE/11 +110	110	316	25,3	67,7	2,2	4,1	0,0	0,6	0,0	317	29	346	8,4
TRE/11 +120	120	295	31,5	65,4	1,7	0,0	0,3	0,7	0,3	296	23	319	7,2

TRE/11 +130	130	306	38,9	56,2	3,3	1,0	0,7	0,0	0,0	306	16	322	5,0
TRE/11 +150	150	310	31,0	47,7	17,4	2,6	0,3	0,3	0,6	310	4	314	1,3
TRE/11 +180	180	315	43,8	36,2	12,7	4,4	0,6	1,0	1,3	314	7	321	2,2
TRE/11 +190	190	310	41,0	35,8	16,5	5,5	0,3	0,6	0,3	310	0	310	0,0
TRE/11 +200	200	297	38,7	39,7	14,1	6,1	0,7	0,0	0,7	297	8	305	2,6
TRE/11 +220	220	288	31,9	39,2	20,1	7,3	0,0	1,0	0,3	288	7	295	2,4
TRE/11 +250	250	301	24,9	41,5	22,9	8,0	0,7	0,7	1,3	301	5	306	1,6
TRE/11 +280	280	329	26,7	43,2	14,9	14,9	0,0	0,0	0,3	299	9	308	2,9
TRE/11 +300	300	299	33,4	50,8	13,0	2,3	0,3	0,0	0,0	299	4	303	1,3
TRE/11 +310	310	299	26,8	58,9	6,0	4,0	0,0	3,0	1,3	299	11	310	3,5
TRE/11 +320	320	295	24,4	64,7	5,4	2,0	0,3	2,4	0,7	295	12	307	3,9
TRE/11 +340	340	288	32,3	59,7	4,2	1,4	0,0	1,4	1,0	288	15	303	5,0
TRE/11 +350	350	305	32,5	60,0	2,0	2,0	0,7	2,0	1,0	336	31	367	8,4
TRE/11 +360	360	288	33,0	62,5	0,7	2,4	0,0	0,7	0,7	291	25	316	7,9
TRE/11 +370	370	295	28,1	64,4	2,4	1,7	0,7	1,4	1,4	312	17	329	5,2
TRE/11 +380	380	290	33,8	60,3	2,1	2,8	0,0	0,7	0,3	317	24	341	7,0
TRE/11 +400	400	298	35,9	57,0	3,4	3,0	0,0	0,3	0,3	305	18	323	5,6
TRE/11 +420	420	304	32,6	53,3	8,2	4,9	0,3	0,0	0,7	301	10	311	3,2
TRE/11 +450	450	298	36,2	45,3	13,8	3,7	0,3	0,7	0,0	349	4	353	1,1
TRE/11 +500	500	313	32,6	40,9	18,8	5,8	0,6	0,6	0,6	352	8	360	2,2
TRE/11 +540	540	301	38,9	37,9	19,9	1,7	0,7	0,7	0,3	301	4	305	1,3
TRE/11 +590	590	302	38,4	34,8	21,5	4,0	0,7	0,3	0,3	302	12	314	3,8
TRE/13 +630	630	307	35,2	32,6	29,3	2,3	0,3	0,3	0,0	304	13	317	4,1
TRE/13 +710	710	311	35,0	24,4	37,9	2,3	0,0	0,3	0,0	311	3	314	1,0
TRE/13 +750	750	300	43,0	25,3	29,0	2,7	0,0	0,0	0,0	320	8	328	2,4
TRE/13 +830	830	317	41,0	29,3	22,4	5,7	0,0	0,9	0,6	326	4	330	1,2
TRE/11 +905	905	309	34,0	35,9	27,2	1,9	0,0	1,0	0,0	316	5	321	1,6
TRE/13 +931,75	931,75	302	28,5	51,3	18,5	1,0	0,0	0,3	0,3	296	12	308	3,9
TRE/13 +943	943	318	44,7	45,6	8,2	0,9	0,0	0,6	0,0	331	22	353	6,2
TRE/13 +953	953	306	34,0	51,0	10,5	3,9	0,0	0,7	0,0	336	20	356	5,6
TRE/13 +963	963	319	21,6	55,5	17,9	3,8	0,3	0,3	0,6	301	18	319	5,6
TRE/13 +973	973	325	27,1	56,0	14,2	1,5	0,6	0,0	0,6	303	66	369	17,9
TRE/13 +983	983	301	35,9	43,5	16,9	3,0	0,3	0,0	0,3	312	16	328	4,9
TRE/13 +990	990	324	30,6	39,5	28,1	1,2	0,0	0,6	0,0	304	7	311	2,3
TRE/13 +999	999	302	27,5	52,0	18,9	0,7	0,0	0,7	0,3	301	16	317	5,0
TRE/13 +1006	1006	306	19,6	55,6	21,9	1,0	0,7	0,7	0,7	310	10	320	3,1
TRE/13 +1029	1029	309	34,3	43,4	19,1	1,9	0,3	0,6	0,3	334	27	361	7,5
TRE/13 +1057	1057	320	31,9	35,3	24,7	6,3	0,3	1,3	0,3	300	9	309	2,9
TRE/13+1119/+1120	1120	314	36,9	37,3	20,4	5,4	0,0	0,0	0,0	304	3	307	1,0

Table S6. Relative abundances (%) of calcareous nannofossil main taxa at the Terche section.

Samples	Thickness (cm) (0 cm level= ETM2)	Total	Total *Sphenolithus* (*Sphenolithus spp.* +*S. radians*) (%)	*Discoaster (%)*	*Zygrhablithus bijugatus (%)*	*Prinsius (%)*	*Thoracosphaera* spp. (%)	*Ericsonia (%)*	*Coccolithus pelagicus (%)*	*Toweius (%)*	*Chiasmolithus (%)*	Cretaceous reworked (%)
TRE/13 +1137	1137	304	28,6	4,3	2,6	9,2	3,3	2,0	18,8	16,1	0,3	5,6
TRE/13 +1119/1120	1119,5	305	25,9	3,0	9,5	2,0	3,0	0,3	20,0	25,2	0,3	4,9
TRE/13 +1079	1079	311	39,9	1,9	6,4	5,1	2,6	1,3	11,3	18,3	1,0	3,9
TRE/13 +1045,5	1045,5	309	23,3	2,6	9,4	12,6	1,3	2,3	20,7	16,2	0,0	3,6
TRE/13 +1042	1042	300	20,0	5,3	12,7	12,0	1,0	2,0	19,7	16,7	1,0	4,0
TRE/13 +1029	1029	302	21,9	8,6	8,9	0,7	2,6	2,3	25,5	18,5	0,0	4,3
TRE/13 +1006	1006	301	34,6	1,3	6,0	2,0	2,7	3,0	25,6	16,6	0,3	1,3
TRE/13 +990	990	306	25,5	2,3	12,4	2,6	1,6	2,0	23,5	17,6	0,0	7,2
TRE/13 +973	973	310	27,7	3,2	12,6	5,2	2,6	4,8	17,7	19,0	0,3	3,9
TRE/13 +953	953	309	14,6	0,6	15,5	3,2	1,6	3,9	32,0	18,8	0,6	3,9
TRE/13 +931,75	931,75	308	21,8	1,0	8,1	10,4	1,6	3,2	24,7	16,2	0,0	3,2
TRE/13 +930	930	305	16,4	3,0	8,9	8,5	1,3	2,3	28,9	17,7	1,3	2,6
TRE/13 +890	890	306	22,2	1,3	17,6	1,6	2,0	2,0	25,5	21,6	0,3	1,3
TRE/13 +830	830	300	23,3	1,7	15,7	7,0	1,3	2,3	21,3	19,3	0,7	3,7
TRE/13 +790	790	307	25,1	3,3	16,9	3,3	0,7	1,3	21,5	18,6	0,3	3,3
TRE/13 +730	730	299	24,7	2,7	15,4	8,0	1,7	3,0	19,4	18,7	0,7	1,3
TRE/13 +690	690	312	22,4	1,9	20,2	2,2	1,0	1,3	21,2	21,5	0,0	1,9
TRE/13 +630	630	300	25,7	0,7	27,7	10,3	2,3	2,3	12,0	14,7	0,3	2,0
TRE/11 +590	590	310	21,9	1,6	17,7	3,5	1,9	1,9	28,4	15,5	0,6	1,0
TRE/11 +552	552	318	26,1	1,9	18,9	10,4	2,2	2,8	19,5	14,8	0,9	1,3
TRE/11 +540	540	307	24,4	2,0	23,8	3,9	1,3	1,3	23,5	14,0	0,7	1,6
TRE/11 +520	520	313	14,1	1,0	24,3	5,8	2,2	6,1	20,4	18,2	0,3	1,3
TRE/11 +500	500	306	20,9	2,3	25,8	14,7	1,6	3,6	15,4	11,4	0,3	1,6
TRE/11 +490	490	307	16,6	2,0	19,2	5,5	1,6	2,9	28,3	18,6	0,0	2,0
TRE/11 +470	470	330	22,1	3,0	21,2	5,5	1,8	2,4	19,1	16,7	1,2	3,0
TRE/11 +450	450	310	21,0	2,3	19,0	13,5	1,6	1,6	23,2	12,3	0,6	1,9
TRE/11 +440	440	303	20,5	2,6	19,1	5,9	2,3	1,3	18,8	23,8	0,3	2,0
TRE/11 +420	420	312	18,3	3,2	18,9	8,7	2,9	1,9	20,2	23,1	0,6	0,3
TRE/11 +410	410	308	16,2	7,8	27,3	9,4	1,9	4,2	13,6	15,3	0,6	0,6
TRE/11 +400	400	314	22,6	2,2	28,0	8,9	1,9	3,5	13,7	14,3	0,3	2,9
TRE/11 +390	390	313	21,7	1,6	13,7	7,0	2,2	3,2	23,3	21,1	0,3	2,2
TRE/11 +370	370	302	17,5	1,7	9,6	6,6	1,0	3,6	26,2	26,8	0,7	3,6
TRE/11 +350	350	319	21,6	1,9	14,4	13,5	2,2	4,4	18,5	16,0	0,6	4,1
TRE/11 +330	330	303	19,5	4,0	17,2	8,3	2,0	2,0	20,5	18,8	0,3	3,3
TRE/11 +310	310	306	17,3	4,6	23,5	13,7	1,0	5,9	17,6	9,2	0,7	2,3
TRE/11 +300	300	337	16,3	3,0	22,3	17,5	0,3	11,6	12,8	9,2	0,9	3,3
TRE/11 +290	290	306	18,6	3,3	20,3	9,2	3,9	2,6	17,6	19,0	1,0	2,3
TRE/11 +270	270	305	19,3	2,0	18,4	6,9	2,6	2,6	15,7	25,2	0,0	2,0
TRE/11 +250	250	303	13,2	1,7	33,7	14,2	1,7	5,3	11,9	12,5	0,0	2,3

TRE/11 +240	240	307	21,8	1,3	16,0	4,9	3,6	1,3	24,4	19,5	0,0	2,6
TRE/11 +220	220	310	17,4	1,3	16,8	6,5	1,3	2,9	20,0	25,2	1,0	2,3
TRE/11 +200	200	318	13,5	3,1	30,2	16,7	2,5	4,4	11,9	14,2	0,0	0,9
TRE/11 +190	190	308	26,9	2,3	21,4	7,8	1,3	1,6	13,3	18,2	0,3	0,0
TRE/11 +170	170	308	20,8	2,6	16,2	7,5	1,3	1,9	21,1	25,0	0,0	1,0
TRE/11 +150	150	332	14,5	4,2	32,2	10,5	0,9	3,0	11,7	15,1	0,9	0,3
TRE/11 +140	140	306	16,3	5,2	31,0	12,1	1,6	0,7	8,2	16,3	1,0	2,0
TRE/11 +120	120	301	11,6	5,6	30,2	5,6	1,3	2,7	18,3	16,3	0,7	2,7
TRE/11 +110	110	312	13,1	6,4	17,0	4,5	1,6	2,6	23,4	27,6	0,3	1,9
TRE/11 +90	90	304	19,4	3,6	2,3	6,9	1,6	4,3	19,3	31,6	1,0	6,6
TRE/11 +70	70	306	10,1	3,3	2,0	10,1	3,6	5,6	27,1	26,5	0,7	7,8
TRE/11 +60	60	300	14,3	3,0	12,6	10,3	3,3	6,7	17,7	11,7	1,0	4,3
TRE/11 +50	50	301	21,7	3,8	13,3	6,1	1,5	1,5	20,2	22,1	0,0	5,3
TRE/11 +30	30	303	13,2	3,0	4,3	4,6	3,6	4,6	21,5	25,4	0,0	16,8
TRE/11 +19/20	19,5	300	13,0	2,7	2,7	5,0	2,3	5,0	15,0	27,0	1,0	13,3
TRE/11 +6/+10	8	302	7,3	1,0	0,0	4,3	0,7	6,3	30,8	27,8	0,3	14,6
TRE/11 0/+2	1	301	18,9	1,7	5,3	8,0	0,7	5,0	18,3	28,0	0,0	6,0
TRE/11 0/-3	-1,5	304	13,2	2,6	2,0	11,2	1,6	4,6	24,7	28,0	0,7	7,6
TRE/11 -19/-20	-19,5	319	18,8	3,4	6,9	10,7	1,9	1,6	24,1	26,0	0,6	2,5
TRE/11 -50/-52	-51	304	24,0	1,6	8,6	7,9	1,0	2,6	25,0	18,8	0,0	4,9
TRE/11 -100	-100	302	20,9	2,3	10,3	11,3	1,0	0,7	30,8	14,6	1,0	1,0
TRE/11 -150	-150	305	24,3	3,9	12,5	14,1	1,6	1,6	21,6	15,7	0,0	2,0
TRE/11 -190	-190	300	28,3	0,7	16,7	19,3	3,3	0,7	14,5	9,0	0,3	2,7
TRE/11 -250	-250	314	23,2	1,6	8,3	17,8	0,3	1,0	18,5	21,0	0,3	2,5
TRE/13 -310	-310	302	15,2	3,0	14,9	13,9	1,3	0,7	26,8	15,6	0,3	3,6
TRE/13 -370	-370	328	13,1	2,7	9,1	14,0	0,3	1,8	29,3	22,0	1,5	0,9
TRE/13 -450	-450	302	18,2	3,0	6,6	9,3	1,0	1,7	35,4	19,2	1,3	1,0
TRE/13 -650	-650	274	19,6	2,6	9,3	14,9	1,6	2,5	25,2	17,1	1,2	0,9
TRE/13 -850	-850	255	19,3	4,7	7,2	16,7	0,7	5,6	19,3	18,6	1,3	2,3

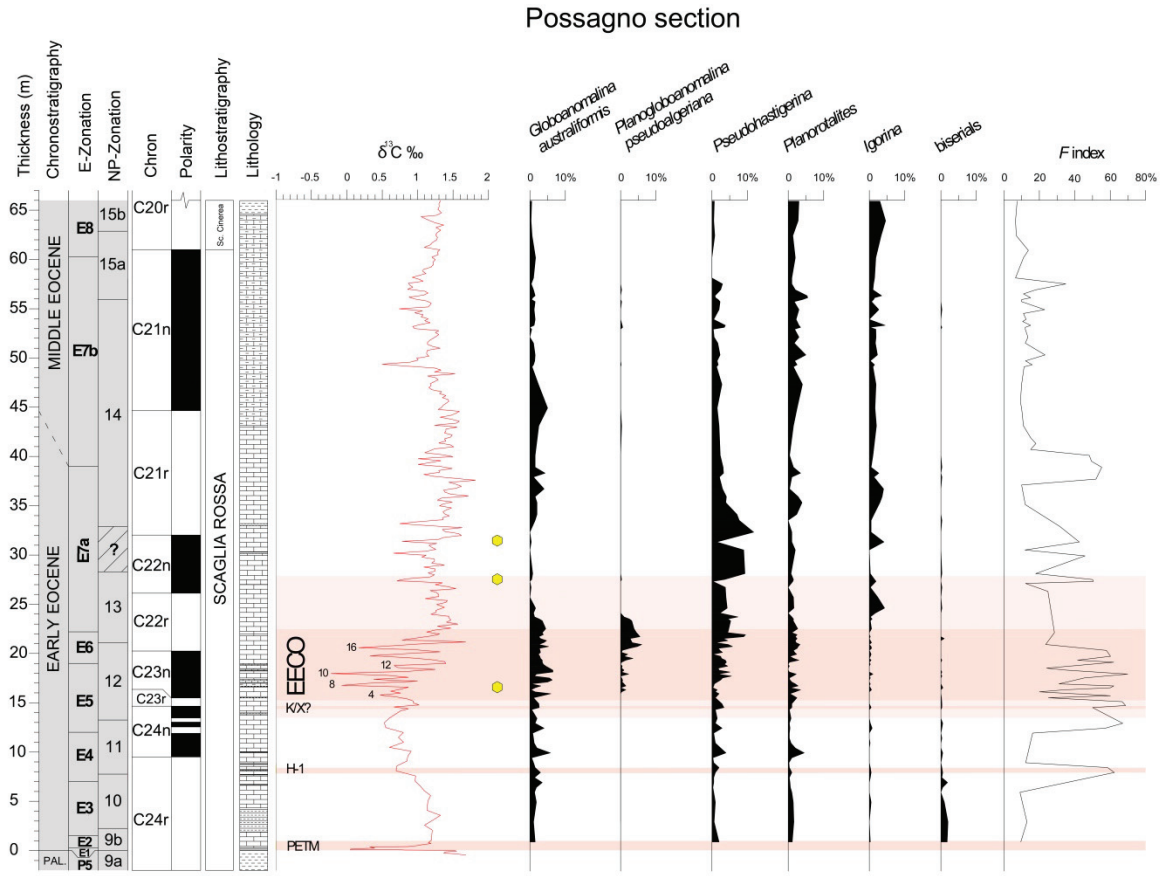

Figure S1. The Possagno section and its $\delta^{13}C$ record (Fig. 4) with measured relative abundances of minor planktic foraminiferal genera and fragmentation index (F-index). Filled yellow hexagons show occurrences of abundant radiolarians. Lithological symbols and early Eocene events are the same as those in Fig. 4.

Table S1. Stable isotopes from the Carcoselle Quarry (Possagno).

Thickness (0 m level= PETM)	$\delta^{13}C$ (‰)	$\delta^{18}O$ (‰)	Thickness (0 m level= PETM)	$\delta^{13}C$ (‰)	$\delta^{18}O$ (‰)
-0,43	1,55	-2,36	13,50	0,61	-1,79
-0,33	1,37	-2,57	14,20	0,76	-1,35
-0,23	1,39	-2,20	14,40	0,87	-1,23
-0,18	1,46	-2,55	14,60	0,67	-1,74
-0,13	1,55	-2,21	14,80	1,02	-1,42
-0,08	1,51	-2,29	15,00	0,94	-1,51
-0,03	0,83	-2,50	15,20	0,94	-1,58
0,01	0,72	-2,63	15,40	0,86	-1,79
0,03	0,05	-2,70	15,60	0,70	-1,41
0,08	0,06	-2,60	15,80	0,47	-1,97
0,13	0,26	-2,52	16,00	0,76	-1,70
0,18	0,40	-2,44	16,20	0,62	-2,16
0,23	0,36	-2,58	16,40	0,76	-2,08
0,28	0,33	-2,57	16,60	0,87	-1,79
0,33	0,86	-1,96	16,80	-0,07	-3,25
0,43	1,00	-2,19	17,00	0,31	-2,16
0,53	1,07	-1,90	17,20	1,00	-1,66
0,63	1,19	-2,07	17,40	0,38	-2,11
0,73	1,15	-2,19	17,60	0,87	-1,63
0,83	1,17	-2,13	17,80	0,57	-2,43
0,98	1,19	-2,40	18,00	-0,22	-3,64
2,00	1,21	-2,18	18,20	0,85	-1,90
2,50	1,10	-2,27	18,40	1,25	-1,59
3,00	1,21	-2,36	18,60	0,72	-2,59
3,50	1,32	-1,97	18,80	0,67	-1,73
4,00	1,13	-2,06	19,00	1,40	-1,49
4,50	1,14	-1,75	19,20	1,38	-0,81
5,00	1,15	-1,54	19,40	1,19	-1,60
5,50	1,18	-1,69	19,60	0,88	-1,89
6,00	1,09	-1,66	19,80	0,33	-2,31
6,50	1,03	-1,80	20,00	0,83	-1,64
7,00	0,96	-1,80	20,20	1,32	-1,91
7,50	0,97	-1,70	20,40	0,97	-1,69
8,00	0,70	-1,61	20,60	0,17	-2,27
8,50	0,70	-1,62	20,80	0,61	-1,79
9,00	0,85	-1,62	21,00	1,05	-1,87
9,50	0,86	-1,75	21,20	1,68	-0,78
10,00	0,91	-1,39	21,40	0,78	-2,72
10,50	0,62	//	21,60	//	//
11,00	0,80	//	21,80	1,20	-2,07
11,50	0,73	-1,87	22,00	1,31	-1,96
12,00	0,80	-1,66	22,20	1,13	-2,11
12,50	0,55	-1,95	22,40	1,25	-1,99
13,00	0,53	-1,99	22,60	1,47	-1,64

22,80	1,28	-1,72	32,60	1,35	-1,84
23,00	1,57	-1,19	32,80	1,63	-1,12
23,20	1,41	-1,76	33,00	1,15	-2,29
23,40	1,47	-1,83	33,20	0,75	-2,58
23,60	1,45	-1,69	33,40	1,00	-2,02
23,80	1,44	-1,75	33,60	1,36	-1,20
24,00	1,19	-1,91	33,80	1,35	-1,63
24,20	1,26	-1,85	34,00	1,45	-1,49
24,40	1,26	-1,94	34,20	1,38	-1,73
24,70	1,38	-1,13	34,40	1,36	-1,84
25,00	1,27	-1,81	34,60	1,41	-1,63
25,20	1,40	-1,51	34,80	1,48	-1,16
25,40	1,42	-1,50	35,00	1,31	-1,87
25,60	1,11	-1,91	35,20	1,36	-1,64
25,80	1,30	-1,92	35,40	1,49	-1,77
26,00	1,30	-1,74	35,60	1,28	-1,79
26,20	1,27	-1,38	35,80	1,34	-1,72
26,40	1,18	-1,74	36,00	1,72	-1,19
26,60	1,54	-1,11	36,20	1,47	-1,69
26,80	1,43	-1,25	36,40	1,39	-2,15
27,00	1,25	-1,66	36,60	1,37	-1,74
27,20	1,35	-1,41	36,80	1,54	-1,60
27,40	0,71	-2,45	37,00	1,62	-1,43
27,60	0,83	-2,15	37,20	1,54	-1,72
27,80	1,18	-1,62	37,40	1,44	-1,86
28,00	1,24	-1,70	37,60	1,82	-0,92
28,20	1,15	-1,74	37,80	1,52	-1,65
28,40	1,25	-1,80	38,00	1,24	-2,66
28,60	1,25	-1,62	38,20	1,09	-1,83
28,80	1,09	-2,23	38,40	1,31	-1,46
29,00	1,38	-1,92	38,60	1,30	-1,71
29,20	1,20	-2,16	38,80	1,49	-1,66
29,40	1,24	-1,79	39,00	1,32	-1,75
29,60	1,24	-1,74	39,20	1,01	-2,09
29,80	1,06	-2,23	39,40	1,18	-2,19
30,00	1,12	-1,81	39,60	1,33	-1,94
30,20	0,66	-2,40	39,80	1,01	-1,98
30,40	1,12	-1,67	40,00	1,50	-1,55
30,60	1,26	-1,66	40,20	1,36	-1,91
30,80	1,20	-1,81	40,40	1,10	-1,71
31,00	1,16	-1,94	40,60	1,18	-1,78
31,20	1,27	-1,87	40,80	1,24	-1,89
31,40	0,78	-3,10	41,00	1,51	-1,63
31,60	1,29	-1,65	41,20	1,46	-1,65
31,80	1,37	-2,18	41,40	1,30	-1,98
32,00	1,62	-1,47	41,60	1,40	-1,52
32,20	1,58	-1,70	41,80	1,38	-1,69
32,40	1,39	-1,79	42,00	1,47	-1,44

42,20	1,49	-1,43	52,20	1,26	-1,37
42,40	1,38	-1,65	52,40	1,30	-1,48
42,60	1,40	-1,66	52,60	1,25	-1,36
42,80	1,40	-1,67	52,80	1,30	-1,26
43,00	1,56	-1,42	53,00	0,96	-2,02
43,20	1,24	-2,19	53,20	0,93	-1,80
43,40	1,55	-1,41	53,40	1,03	-1,36
43,60	1,59	-1,27	53,60	1,18	-1,14
43,80	1,48	-1,73	53,80	1,10	-1,29
44,00	1,32	-1,84	54,00	1,15	-1,11
44,20	1,47	-1,61	54,20	1,05	-1,29
44,40	1,54	-1,41	54,40	1,08	-1,25
44,60	1,59	-1,27	54,60	0,96	-1,58
44,80	1,29	-2,02	54,80	1,07	-1,50
45,00	1,34	-1,66	55,00	0,74	-1,99
45,20	1,36	-1,71	55,20	1,15	-1,45
45,60	1,44	-1,46	55,40	1,18	-1,29
45,80	1,43	-1,55	55,60	1,19	-1,25
46,00	1,35	-1,59	55,80	1,13	-1,33
46,20	1,40	-1,64	56,00	0,96	-1,57
46,40	1,31	-1,43	56,20	0,88	-1,76
46,60	1,34	-1,42	56,40	1,09	-1,27
46,80	1,20	-1,89	56,60	1,15	-1,45
47,00	1,16	-1,58	56,80	1,10	-1,26
47,20	1,19	-1,67	57,00	0,86	-1,93
47,40	1,18	-1,65	57,20	0,93	-1,85
47,60	1,23	-1,73	57,40	0,89	-1,39
47,80	1,29	-1,56	57,60	0,87	-1,86
48,00	1,26	-1,70	57,80	1,08	-1,06
48,20	1,14	-1,78	58,00	1,03	-1,35
48,40	1,53	-1,03	58,20	0,92	-1,61
48,60	1,24	-1,82	58,40	1,03	-1,32
48,80	1,33	-1,13	58,60	1,12	-1,22
49,00	1,24	-1,43	58,80	1,08	-1,52
49,20	0,82	-2,21	59,00	1,08	-1,48
49,40	0,50	-2,55	59,25	1,19	-1,52
49,60	0,90	-1,57	59,50	1,23	-1,32
49,80	1,01	-1,48	59,75	1,22	-1,39
50,00	0,99	-1,59	60,00	1,25	-1,42
50,20	1,16	-1,28	60,25	1,20	-1,50
50,40	1,13	-1,44	60,50	1,29	-1,43
50,60	1,13	-1,61	60,75	1,28	-1,36
50,80	1,14	-1,63	61,00	1,31	-1,40
51,00	1,32	-1,25	61,25	1,10	-1,87
51,20	1,21	-1,71	61,50	1,18	-1,72
51,40	1,14	-1,69	61,75	1,21	-1,47
51,60	1,14	-1,69	62,00	1,27	-1,23
51,80	1,17	-1,70	62,25	1,28	-1,41

62,50	1,26	-1,76	64,35	1,05	-1,84
62,75	1,28	-1,59	64,50	1,27	-1,45
63,00	1,33	-1,38	64,75	1,34	-1,37
63,25	1,26	-1,41	65,10	1,29	-1,33
63,50	1,37	-1,35	65,40	1,31	-1,29
63,75	1,24	-1,65	65,70	1,30	-1,36
64,00	1,16	-1,66	66,00	1,32	-1,55

Table S2. Stable isotope composition of early Eocene bulk carbonate at Site 577

Hole	Core	Section	Interval		Depth (mbsf)	Offset (m)	Depth (mcd)	$\delta^{13}C$ (‰)	$\delta^{18}O$ (‰)
			top (cm)	bott. (cm)					
577*	8	3	30	32	67,10	-3,50	63,60	2,05	0,11
577*	8	3	35	37	67,15	-3,50	63,65	2,19	-0,11
577*	8	3	45	47	67,25	-3,50	63,75	2,24	-0,01
577*	8	3	50	52	67,30	-3,50	63,80	2,18	0,22
577*	8	3	55	57	67,35	-3,50	63,85	2,21	-0,03
577*	8	3	60	62	67,40	-3,50	63,90	2,33	0,61
577*	8	3	65	67	67,45	-3,50	63,95	2,14	-0,61
577*	8	3	70	72	67,50	-3,50	64,00	2,09	0,07
577*	8	3	75	77	67,55	-3,50	64,05	2,09	-0,24
577*	8	3	80	82	67,60	-3,50	64,10	2,03	0,04
577*	8	3	85	87	67,65	-3,50	64,15	2,14	-0,28
577*	8	3	90	92	67,70	-3,50	64,20	2,14	-0,03
577*	8	3	95	97	67,75	-3,50	64,25	2,08	-0,18
577*	8	3	100	102	67,80	-3,50	64,30	2,00	0,02
577*	8	3	105	107	67,85	-3,50	64,35	1,95	-0,17
577*	8	3	110	112	67,90	-3,50	64,40	1,74	-0,48
577*	8	3	115	117	67,95	-3,50	64,45	2,14	-0,03
577*	8	3	120	122	68,00	-3,50	64,50	2,07	-0,25
577*	8	3	125	127	68,05	-3,50	64,55	1,97	-0,24
577*	8	3	130	132	68,10	-3,50	64,60	1,98	-0,40
577*	8	3	135	137	68,15	-3,50	64,65	1,88	-0,23
577*	8	3	140	142	68,20	-3,50	64,70	1,87	-0,57
577*	8	3	145	147	68,25	-3,50	64,75	2,07	-0,21
577*	8	4	5	7	68,35	-3,50	64,85	1,98	-0,07
577*	8	4	10	12	68,40	-3,50	64,90	1,95	-0,58
577*	8	4	15	17	68,45	-3,50	64,95	1,90	-0,34
577*	8	4	20	22	68,50	-3,50	65,00	1,99	-0,31
577*	8	4	25	27	68,55	-3,50	65,05	2,03	-0,37
577*	8	4	30	32	68,60	-3,50	65,10	2,04	-0,36
577*	8	4	35	37	68,65	-3,50	65,15	2,02	-0,26
577*	8	4	40	42	68,70	-3,50	65,20	2,02	-0,33
577*	8	4	45	47	68,75	-3,50	65,25	1,92	-0,21
577*	8	4	50	52	68,80	-3,50	65,30	1,75	-0,49
577*	8	4	55	57	68,85	-3,50	65,35	1,94	-0,26
577*	8	4	60	62	68,90	-3,50	65,40	2,01	-0,37
577*	8	4	65	67	68,95	-3,50	65,45	2,00	-0,11

577*	8	4	70	72	69,00	-3,50	65,50	2,04	-0,50
577*	8	4	75	77	69,05	-3,50	65,55	1,90	-0,07
577*	8	4	80	82	69,10	-3,50	65,60	2,00	-0,31
577*	8	4	85	87	69,15	-3,50	65,65	1,91	-0,18
577*	8	4	90	92	69,20	-3,50	65,70	1,96	-0,53
577*	8	4	95	97	69,25	-3,50	65,75	1,99	-0,37
577*	8	4	100	102	69,30	-3,50	65,80	1,97	-0,48
577*	8	4	105	107	69,35	-3,50	65,85	2,01	-0,38
577*	8	4	110	112	69,40	-3,50	65,90	2,06	-0,54
577*	8	4	115	117	69,45	-3,50	65,95	2,04	-0,25
577*	8	4	120	122	69,50	-3,50	66,00	1,99	-0,54
577*	8	4	125	127	69,55	-3,50	66,05	1,99	-0,21
577*	8	4	130	132	69,60	-3,50	66,10	1,96	-0,35
577*	8	4	135	137	69,65	-3,50	66,15	1,98	-0,26
577*	8	4	140	142	69,70	-3,50	66,20	2,03	-0,38
577*	8	4	145	147	69,75	-3,50	66,25	2,01	-0,09
577*	8	5	5	7	69,85	-3,50	66,35	1,86	-0,19
577*	8	5	15	17	69,95	-3,50	66,45	1,84	-0,31
577*	8	5	25	27	70,05	-3,50	66,55	1,87	-0,29
577*	8	5	35	37	70,15	-3,50	66,65	1,99	-0,26
577*	8	5	45	47	70,25	-3,50	66,75	2,01	-0,37
577*	8	5	55	57	70,35	-3,50	66,85	1,90	-0,36
577*	8	5	65	67	70,45	-3,50	66,95	1,96	-0,15
577*	8	5	70	72	70,50	-3,50	67,00	2,00	-0,47
577*	8	5	75	77	70,55	-3,50	67,05	1,99	-0,49
577*	8	5	80	82	70,60	-3,50	67,10	1,98	-0,32
577*	8	5	85	87	70,65	-3,50	67,15	2,03	-0,42
577*	8	5	90	92	70,70	-3,50	67,20	1,91	-0,59
577*	8	5	95	97	70,75	-3,50	67,25	1,99	-0,15
577*	8	5	100	102	70,80	-3,50	67,30	1,91	-0,56
577*	8	5	105	107	70,85	-3,50	67,35	1,94	-0,43
577*	8	5	115	117	70,95	-3,50	67,45	1,99	-0,13
577*	8	5	125	127	71,05	-3,50	67,55	1,84	-0,18
577*	8	5	135	137	71,15	-3,50	67,65	1,71	-0,17
577*	8	5	145	147	71,25	-3,50	67,75	1,82	-0,23
577*	8	6	5	7	71,35	-3,50	67,85	1,84	-0,27
577*	8	6	15	17	71,45	-3,50	67,95	1,95	-0,31
577*	8	6	20	22	71,50	-3,50	68,00	1,97	-0,60
577*	8	6	25	27	71,55	-3,50	68,05	1,86	-0,33
577*	8	6	28	30	71,58	-3,50	68,08	1,77	-0,50
577*	8	6	32	34	71,62	-3,50	68,12	1,69	-0,49
577*	8	6	35	37	71,65	-3,50	68,15	1,62	-0,55
577*	8	6	37	39	71,67	-3,50	68,17	1,63	-0,55
577*	8	6	45	47	71,75	-3,50	68,25	2,02	-0,44
577*	8	6	50	52	71,80	-3,50	68,30	2,07	-0,21
577*	8	6	55	57	71,85	-3,50	68,35	2,04	-0,18
577*	8	6	60	62	71,90	-3,50	68,40	1,95	-0,25
577*	8	6	67	69	71,97	-3,50	68,47	1,88	-0,23

577*	8	6	75	77	72,05	-3,50	68,55	1,93	-0,16
577*	8	6	85	87	72,15	-3,50	68,65	1,58	-0,27
577*	8	6	95	97	72,25	-3,50	68,75	1,72	-0,10
577*	8	6	105	107	72,35	-3,50	68,85	1,67	-0,21
577*	8	6	108	110	72,38	-3,50	68,88	1,75	-0,28
577*	8	6	112	114	72,42	-3,50	68,92	1,63	-0,25
577*	8	6	115	117	72,45	-3,50	68,95	1,42	-0,55
577*	8	6	118	120	72,48	-3,50	68,98	1,39	-0,62
577*	8	6	122	124	72,52	-3,50	69,02	1,51	-0,66
577*	8	6	125	127	72,55	-3,50	69,05	1,85	-0,31
577*	8	6	135	137	72,65	-3,50	69,15	1,80	-0,34
577*	8	6	145	147	72,75	-3,50	69,25	1,75	-0,30
577*	9	1	5	7	73,35	0,00	73,35	1,48	-0,29
577*	9	1	10	12	73,40	0,00	73,40	1,50	-0,10
577*	9	1	15	17	73,45	0,00	73,45	1,38	-0,08
577*	9	1	20	22	73,50	0,00	73,50	1,48	-0,26
577*	9	1	25	27	73,55	0,00	73,55	1,46	-0,20
577*	9	1	30	32	73,60	0,00	73,60	1,48	-0,41
577*	9	1	35	37	73,65	0,00	73,65	1,47	-0,22
577*	9	1	40	42	73,70	0,00	73,70	1,48	-0,36
577*	9	1	45	47	73,75	0,00	73,75	1,48	-0,35
577*	9	1	50	52	73,80	0,00	73,80	1,46	-0,46
577*	9	1	55	57	73,85	0,00	73,85	1,46	-0,26
577*	9	1	60	62	73,90	0,00	73,90	1,45	-0,19
577*	9	1	65	67	73,95	0,00	73,95	1,46	-0,18
577*	9	1	70	72	74,00	0,00	74,00	1,44	-0,16
577*	9	1	75	77	74,05	0,00	74,05	1,42	-0,11
577*	9	1	80	82	74,10	0,00	74,10	1,28	-0,14
577*	9	1	85	87	74,15	0,00	74,15	1,18	-0,31
577*	9	1	90	92	74,20	0,00	74,20	1,24	-0,20
577*	9	1	95	97	74,25	0,00	74,25	1,20	-0,33
577*	9	1	100	102	74,30	0,00	74,30	1,35	-0,25
577*	9	1	105	107	74,35	0,00	74,35	1,33	-0,16
577*	9	1	115	117	74,45	0,00	74,45	1,27	-0,09
577*	9	1	125	127	74,55	0,00	74,55	1,33	-0,37
577*	9	1	127	129	74,57	0,00	74,57	1,34	-0,19
577*	9	1	130	132	74,60	0,00	74,60	1,37	-0,06
577*	9	1	133	135	74,63	0,00	74,63	1,38	-0,12
577*	9	1	135	137	74,65	0,00	74,65	1,31	-0,13
577*	9	1	145	147	74,75	0,00	74,75	1,30	-0,12
577A	8	1	115	117	67,55	-1,30	66,25	2,03	-0,14
577A	8	1	125	127	67,65	-1,30	66,35	2,04	-0,20
577A	8	1	135	137	67,75	-1,30	66,45	1,93	-0,05
577A	8	2	5	7	67,95	-1,30	66,65	1,87	-0,35
577A	8	2	15	17	68,05	-1,30	66,75	1,93	-0,21
577A	8	2	25	27	68,15	-1,30	66,85	2,02	-0,16
577A	8	2	35	37	68,25	-1,30	66,95	2,01	-0,26
577A	8	2	45	47	68,35	-1,30	67,05	2,06	-0,21

577A	8	2	55	57	68,45	-1,30	67,15	1,62	-0,48
577A	8	2	65	67	68,55	-1,30	67,25	1,97	-0,35
577A	8	2	75	77	68,65	-1,30	67,35	1,96	-0,46
577A	8	2	85	87	68,75	-1,30	67,45	2,01	-0,32
577A	8	2	95	97	68,85	-1,30	67,55	1,86	-0,24
577A	8	2	105	107	68,95	-1,30	67,65	1,61	-0,72
577A	8	2	115	117	69,05	-1,30	67,75	1,93	-0,32
577A	8	2	125	127	69,15	-1,30	67,85	1,96	-0,37
577A	8	2	135	137	69,25	-1,30	67,95	1,90	-0,32
577A	8	2	145	147	69,35	-1,30	68,05	1,80	-0,33
577A	8	3	5	7	69,45	-1,30	68,15	1,97	-0,55
577A	8	3	15	17	69,55	-1,30	68,25	2,09	-0,48
577A	8	3	25	27	69,65	-1,30	68,35	2,06	-0,48
577A	8	3	35	37	69,75	-1,30	68,45	2,08	-0,57
577A	8	3	45	47	69,85	-1,30	68,55	1,96	-0,43
577A	8	3	55	57	69,95	-1,30	68,65	1,68	-0,52
577A	8	3	65	67	70,05	-1,30	68,75	1,76	-0,32
577A	8	3	75	77	70,15	-1,30	68,85	1,67	-0,48
577A	8	3	85	87	70,25	-1,30	68,95	1,72	-0,37
577A	8	3	95	97	70,35	-1,30	69,05	1,34	-0,63
577A	8	3	105	107	70,45	-1,30	69,15	1,81	-0,61
577A	8	3	115	117	70,55	-1,30	69,25	1,73	-0,34
577A	8	3	125	127	70,65	-1,30	69,35	1,67	-0,70
577A	8	3	135	137	70,75	-1,30	69,45	1,94	-0,50
577A	8	3	145	147	70,85	-1,30	69,55	1,93	-0,44
577A	8	4	5	7	70,95	-1,30	69,65	2,02	-0,41
577A	8	4	15	17	71,05	-1,30	69,75	1,87	-0,51
577A	8	4	25	27	71,15	-1,30	69,85	1,73	-0,29
577A	8	4	30	32	71,20	-1,30	69,90	1,40	-0,45
577A	8	4	35	37	71,25	-1,30	69,95	1,42	-0,81
577A	8	4	40	42	71,30	-1,30	70,00	1,59	-0,56
577A	8	4	45	47	71,35	-1,30	70,05	1,78	-0,44
577A	8	4	50	52	71,40	-1,30	70,10	1,77	-0,28
577A	8	4	55	57	71,45	-1,30	70,15	1,72	-0,46
577A	8	4	60	62	71,50	-1,30	70,20	1,62	-0,03
577A	8	4	65	67	71,55	-1,30	70,25	1,48	-0,61
577A	8	4	70	72	71,60	-1,30	70,30	1,44	-0,32
577A	8	4	75	77	71,65	-1,30	70,35	1,16	-1,03
577A	8	4	80	82	71,70	-1,30	70,40	1,49	-0,36
577A	8	4	85	87	71,75	-1,30	70,45	1,55	-0,76
577A	8	4	90	92	71,80	-1,30	70,50	1,47	-0,29
577A	8	4	95	97	71,85	-1,30	70,55	1,42	-0,92
577A	8	4	100	102	71,90	-1,30	70,60	1,41	-0,38
577A	8	4	105	107	71,95	-1,30	70,65	1,49	-0,73
577A	8	4	110	112	72,00	-1,30	70,70	1,46	-0,42
577A	8	4	115	117	72,05	-1,30	70,75	1,40	-1,23
577A	8	4	120	122	72,10	-1,30	70,80	1,51	-0,45
577A	8	4	125	127	72,15	-1,30	70,85	1,40	-0,75

577A	8	4	130	132	72,20	-1,30	70,90	1,34	-0,33
577A	8	4	135	137	72,25	-1,30	70,95	1,09	-1,11
577A	8	4	138	140	72,28	-1,30	70,98	1,21	-0,72
577A	8	5	5	7	72,45	-1,30	71,15	1,40	-1,11
577A	8	5	10	12	72,50	-1,30	71,20	1,42	-0,25
577A	8	5	15	17	72,55	-1,30	71,25	1,32	-0,67
577A	8	5	20	22	72,60	-1,30	71,30	1,22	-0,32
577A	8	5	25	27	72,65	-1,30	71,35	1,38	-0,90
577A	8	5	30	32	72,70	-1,30	71,40	1,34	-0,31
577A	8	5	35	37	72,75	-1,30	71,45	1,34	-0,73
577A	8	5	40	42	72,80	-1,30	71,50	1,27	-0,40
577A	8	5	45	47	72,85	-1,30	71,55	1,27	-0,72
577A	8	5	50	52	72,90	-1,30	71,60	0,94	-0,64
577A	8	5	55	57	72,95	-1,30	71,65	1,26	-0,86
577A	8	5	60	62	73,00	-1,30	71,70	1,26	-0,30
577A	8	5	65	67	73,05	-1,30	71,75	1,40	-0,75
577A	8	5	70	72	73,10	-1,30	71,80	1,36	-0,29
577A	8	5	75	77	73,15	-1,30	71,85	1,39	-0,63
577A	8	5	80	82	73,20	-1,30	71,90	1,37	-0,34
577A	8	5	85	87	73,25	-1,30	71,95	1,40	-0,66
577A	8	5	90	92	73,30	-1,30	72,00	1,33	-0,30
577A	8	5	95	97	73,35	-1,30	72,05	1,33	-0,62
577A	8	5	100	102	73,40	-1,30	72,10	1,39	-0,36
577A	8	5	105	107	73,45	-1,30	72,15	1,33	-0,60
577A	8	5	110	112	73,50	-1,30	72,20	1,32	-0,32
577A	8	5	115	117	73,55	-1,30	72,25	1,41	-0,69
577A	8	5	120	122	73,60	-1,30	72,30	1,37	-0,25
577A	8	5	125	127	73,65	-1,30	72,35	1,28	-0,61
577A	8	5	130	132	73,70	-1,30	72,40	1,33	-0,25
577A	8	5	135	137	73,75	-1,30	72,45	1,26	-0,75
577A	8	6	5	7	73,95	-1,30	72,65	1,13	-0,71
577A	8	6	15	17	74,05	-1,30	72,75	1,36	-0,85
577A	8	6	25	27	74,15	-1,30	72,85	1,47	-0,73
577A	8	6	35	37	74,25	-1,30	72,95	1,66	-0,57

Table S3.1. Abundances of planktic foraminiferal genera at the Carcoselle Quarry (Possagno).

Thickness (m above the PETM)	No. counted specimens	*Morozovelloides*	*Morozovella*	*Acarinina*	Subbotinids	*Turborotalia fontosa*	*Guembelitroides nuttallii*	*Globanomalina australiformis*	*Planoglobanomalina pseudoalgeriana*	*Pseudohastigerina*	*Planorotalites*	*Igorina*	Biserials
0,98	302	0,0	25,4	26,5	41,4	0,0	0,0	1,5	0,0	2,0	1,1	0,3	1,8
3,00	296	0,0	31,3	36,0	27,5	0,0	0,0	1,0	0,0	0,6	1,6	0,0	2,0
5,00	287	0,0	23,5	35,9	34,9	0,0	0,0	1,8	0,0	1,0	1,4	0,5	1,0
6,00	312	0,0	20,9	37,0	39,3	0,0	0,0	1,3	0,0	0,5	1,0	0,0	0,0
6,50	325	0,0	26,0	37,3	33,5	0,0	0,0	1,8	0,0	0,3	0,6	0,0	0,5
7,00	363	0,0	23,7	36,4	33,5	0,0	0,0	3,5	0,0	0,5	0,5	0,0	1,9
7,50	350	0,0	27,0	54,5	15,8	0,0	0,0	1,3	0,0	0,5	0,3	0,3	0,3
8,00	369	0,0	24,0	59,0	11,0	0,0	0,0	3,0	0,0	1,0	1,0	0,5	0,5
8,50	282	0,0	15,3	65,3	15,0	0,0	0,0	1,5	0,0	2,0	0,3	0,3	0,3
9,00	295	0,0	18,5	57,3	22,5	0,0	0,0	1,0	0,0	0,5	0,2	0,0	0,0
9,50	302	0,0	29,6	40,6	27,7	0,0	0,0	0,5	0,0	0,3	1,0	0,0	0,3
10,00	328	0,0	25,7	29,5	30,0	0,0	0,0	5,8	0,0	4,0	4,5	0,0	0,5
10,50	302	0,0	22,0	48,0	26,0	0,0	0,0	1,0	0,0	1,5	1,5	0,0	0,0
11,00	315	0,0	27,3	40,0	29,5	0,0	0,0	1,2	0,0	1,0	0,8	0,2	0,0
11,50	298	0,0	27,0	44,0	27,4	0,0	0,0	0,7	0,0	0,3	0,3	0,0	0,3
12,00	317	0,0	26,4	50,0	22,0	0,0	0,0	0,8	0,0	0,5	0,3	0,0	0,0
12,50	340	0,0	16,5	56,5	18,5	0,0	0,0	4,0	0,0	2,9	0,5	0,8	0,3
13,00	308	0,0	26,2	55,0	15,2	0,0	0,0	1,5	0,0	1,0	0,3	0,3	0,5
13,50	296	0,0	19,0	60,0	17,9	0,0	0,0	1,4	0,0	1,2	0,5	0,0	0,0
14,40	304	0,0	16,0	55,2	27,0	0,0	0,0	0,5	0,0	1,0	0,3	0,0	0,0
14,60	320	0,0	8,4	53,1	30,4	0,0	0,1	2,7	0,0	3,5	1,0	0,5	0,3
15,00	305	0,0	10,6	53,8	29,0	0,0	0,0	2,5	0,0	2,8	1,0	0,0	0,3
15,60	314	0,0	3,5	71,5	19,0	0,0	0,0	1,5	0,0	1,5	2,4	0,3	0,3
16,00	301	0,0	11,0	56,0	24,6	0,0	0,0	5,9	0,0	2,0	0,5	0,0	0,0
16,20	330	0,0	6,7	64,6	23,9	0,0	0,0	1,5	0,3	1,0	2,0	0,0	0,0
16,40	317	0,0	3,4	67,0	22,2	0,0	0,0	0,3	1,5	1,5	3,5	0,6	0,0
16,60	305	0,0	4,2	73,5	19,0	0,0	0,0	1,5	0,0	0,3	0,6	0,3	0,6
16,80	348	0,0	3,2	80,0	8,6	0,0	0,0	3,1	1,5	0,5	2,8	0,0	0,3
17,00	301	0,0	7,2	71,4	17,1	0,0	0,0	0,3	1,0	0,7	2,0	0,3	0,0
17,20	295	0,0	9,0	72,7	10,3	0,0	0,0	5,0	0,5	1,5	1,0	0,0	0,0
17,40	325	0,0	8,3	73,8	8,0	0,0	0,0	6,3	0,6	2,5	0,5	0,0	0,0
17,60	310	0,0	8,0	72,5	10,1	0,0	0,0	5,5	0,3	3,0	0,3	0,3	0,0
17,80	342	0,0	4,0	78,9	8,7	0,0	0,0	1,3	0,0	5,5	1,3	0,0	0,3
18,00	312	0,0	2,7	79,2	8,9	0,0	0,0	1,8	2,3	1,8	2,3	1,0	0,0
18,20	289	0,0	8,5	67,5	11,5	0,0	0,0	6,5	0,3	5,1	0,3	0,0	0,3
18,40	295	0,0	9,5	68,5	12,5	0,0	0,0	6,5	1,0	2,0	0,0	0,0	0,0
18,60	304	0,0	8,5	69,4	14,5	0,0	0,0	5,5	0,3	1,8	0,0	0,0	0,0
18,80	328	0,0	9,0	64,7	16,5	0,0	0,0	4,5	0,5	4,5	0,3	0,0	0,0

19,00	298	0,0	11,5	66,5	14,4	0,0	0,0	3,8	0,0	3,5	0,0	0,3	0,0
19,20	308	0,0	12,0	67,3	12,5	0,0	0,0	3,5	0,3	4,1	0,3	0,0	0,0
19,40	293	0,0	3,8	72,3	11,0	0,0	0,3	3,5	1,5	3,8	3,0	0,5	0,3
19,60	307	0,0	10,5	68,5	10,3	0,0	0,0	3,0	3,5	2,7	1,5	0,0	0,0
19,80	298	0,0	10,1	69,5	13,0	0,0	0,3	2,8	1,0	2,5	0,5	0,3	0,0
20,00	341	0,0	10,0	62,4	20,0	0,0	0,0	2,4	2,0	0,3	2,4	0,5	0,0
20,20	302	0,0	6,3	65,8	19,5	0,0	0,0	3,0	0,3	3,0	1,8	0,3	0,0
20,40	315	0,0	8,5	60,8	23,5	0,0	0,0	2,9	0,5	2,3	1,5	0,0	0,0
20,60	322	0,0	7,0	59,0	23,9	0,0	0,0	2,7	2,5	1,8	2,5	0,6	0,0
20,80	289	0,0	4,0	35,2	41,6	0,0	0,0	5,3	4,8	5,8	2,8	0,5	0,0
21,00	302	0,0	3,8	41,8	38,0	0,0	0,0	2,5	6,0	4,6	3,3	0,0	0,0
21,20	297	0,0	5,0	34,8	49,1	0,0	0,0	3,9	3,3	1,1	2,2	0,6	0,0
21,40	330	0,0	7,5	40,0	38,0	0,0	0,0	4,7	3,0	4,5	2,0	0,3	0,0
21,60	315	0,0	3,8	43,3	40,5	0,0	0,0	3,0	2,7	3,2	2,5	0,0	1,0
21,80	290	0,0	9,0	38,5	33,2	0,0	0,0	2,5	5,5	9,0	2,0	0,3	0,0
22,00	307	0,0	4,7	38,0	36,5	0,0	0,0	3,8	5,0	9,5	2,5	0,0	0,0
22,20	315	0,0	7,5	41,0	38,0	0,0	0,0	3,5	4,5	4,5	1,0	0,0	0,0
22,60	296	0,0	7,3	38,8	37,5	0,0	0,0	4,5	3,8	4,8	2,7	0,6	0,0
23,40	303	0,0	7,0	40,5	38,8	0,0	0,0	3,5	3,2	5,3	1,4	0,3	0,0
23,60	320	0,0	8,3	42,3	37,5	0,0	0,0	2,6	2,5	4,5	1,5	0,8	0,0
23,80	276	0,0	8,0	38,0	43,0	0,0	0,0	1,3	1,0	7,4	1,0	0,3	0,0
24,20	321	0,0	9,8	42,5	42,5	0,0	0,2	1,0	0,0	2,3	0,0	1,7	0,0
24,70	294	0,0	1,3	43,3	42,3	0,0	1,0	1,6	0,0	4,3	1,6	4,3	0,3
25,80	327	0,0	4,0	55,4	32,7	0,0	0,0	0,0	0,0	4,0	1,5	2,4	0,0
26,80	301	0,0	9,5	44,0	39,5	0,0	2,3	0,3	0,0	3,8	0,0	0,3	0,3
27,40	280	0,0	5,0	75,9	15,6	0,0	0,0	0,0	0,0	0,3	1,3	1,9	0,0
27,60	264	0,0	1,1	68,9	22,7	0,0	0,0	0,5	0,3	3,5	1,5	1,5	0,0
28,20	327	0,0	9,5	45,0	33,7	0,0	0,3	0,8	0,0	9,3	0,8	0,3	0,3
29,40	297	0,0	6,1	52,0	29,0	0,0	0,3	1,5	0,0	8,8	2,0	0,0	0,3
30,60	317	0,0	9,3	48,0	31,7	0,0	0,0	0,0	0,0	9,0	2,0	0,0	0,0
31,40	315	0,0	1,5	81,0	10,6	0,0	0,0	0,4	0,0	1,4	1,0	4,1	0,0
32,40	320	0,0	6,4	48,0	32,3	0,0	0,0	0,0	0,0	11,8	1,0	0,5	0,0
33,00	307	0,0	5,6	64,1	21,5	0,0	0,0	0,2	0,0	8,2	0,3	0,1	0,0
33,60	289	0,0	9,7	48,5	31,8	0,0	0,0	1,5	0,0	7,7	0,0	0,5	0,3
34,20	290	0,0	6,0	51,0	32,1	0,0	0,3	1,5	0,0	6,0	2,1	1,0	0,0
35,40	314	0,0	5,0	48,0	32,7	0,0	1,7	1,8	0,0	3,9	3,9	3,0	0,0
36,00	315	0,0	5,2	48,5	30,0	0,0	2,9	1,7	0,0	4,7	2,8	4,2	0,0
36,60	336	0,0	6,9	51,0	29,9	0,0	3,0	2,0	0.0	2,7	1,6	2,6	0,3
36,80	312	0,0	6,3	53,0	28,3	0,0	1,0	4,0	0,0	3,0	0,4	4,0	0,0
37,20	333	0,0	6,2	45,5	39,0	0,0	0,0	2,6	0,0	2,8	0,7	3,1	0,1
37,80	311	0,0	6,8	61,9	22,9	0,0	0,0	2,0	0,0	2,6	1,7	1,8	0,3
38,00	317	0,0	3,6	59,4	31,3	0,0	0,0	1,0	0,0	2,1	1,0	1,3	0,3
38,40	294	0,3	2,0	46,4	37,8	0,0	0,0	4,3	0,0	3,2	3,4	2,6	0,0
39,00	323	0,3	3,3	65,1	24,3	0,0	0,0	1,5	0,0	3,2	1,5	0,5	0,3
39,60	290	0,6	5,3	69,1	19,2	0,0	0,0	1,3	0,0	2,8	1,0	0,5	0,2
40,20	307	0,5	2,4	65,0	26,0	0,3	0,5	1,5	0,0	2,4	0,4	1,0	0,0
40,80	358	1,8	6,3	42,2	43,4	0,0	0,0	1,6	0,0	2,9	0,5	1,3	0,0
42,00	310	1,0	5,4	41,2	39,1	0,5	0,5	3,6	0,3	2,9	2,5	2,7	0,3

43,20	298	3,0	7,5	39,7	40,0	0,3	0,0	2,7	0,3	2,3	1,7	2,5	0,0
45,00	317	1,3	5,0	46,5	35,6	0,5	0,5	5,0	0,0	1,5	2,5	1,6	0,0
47,40	324	1,8	5,0	41,5	38,3	2,8	0,0	2,1	0,0	2,6	4,0	1,9	0,0
49,20	315	2,0	5,6	51,0	36,0	1,0	0,0	0,6	0,0	1,3	1,5	1,0	0,0
49,40	305	1,0	1,4	59,5	28,8	2,0	0,3	1,0	0,2	1,8	2,5	1,5	0,0
49,80	295	1,5	2,0	63,0	27,0	1,5	0,0	1,4	0,0	1,5	1,8	0,3	0,0
50,40	301	1,7	3,0	45,2	36,5	2,3	0,8	0,9	0,0	2,3	5,0	2,3	0,0
51,60	340	2,5	7,5	41,0	40,7	0,8	1,4	1,0	0,0	1,7	1,7	1,7	0,0
52,20	305	1,2	6,0	32,1	50,1	4,2	0,9	0,0	0,0	0,6	3,0	1,9	0,0
53,00	281	1,7	5,0	44,3	42,3	1,8	0,4	0,5	0,0	0,4	1,8	1,8	0,0
53,20	282	2,5	6,0	48,1	34,0	1,4	0,3	0,0	0,5	3,4	3,4	0,2	0,2
53,40	292	2,4	4,0	41,0	37,8	1,1	0,7	1,2	0,5	3,8	3,0	4,5	0,0
54,00	302	3,6	4,3	47,8	38,3	1,2	0,3	1,6	0,0	0,6	2,3	0,0	0,0
55,00	287	2,5	6,0	55,0	27,3	0,0	0,0	1,2	0,0	2,0	3,0	2,7	0,3
55,80	304	1,6	3,0	42,5	44,2	2,3	0,0	1,5	0,3	2,3	1,7	0,6	0,0
56,00	281	2,8	1,3	59,8	23,1	4,2	0,3	1,0	0,0	1,8	4,5	1,2	0,0
56,20	363	3,1	1,5	61,5	23,7	1,3	0,3	0,5	0,0	1,1	5,5	1,5	0,0
56,40	326	3,0	1,8	36,5	44,6	2,9	0,0	1,5	0,0	0,9	5,3	3,5	0,0
57,00	270	0,9	1,7	61,1	25,5	4,0	0,0	1,0	0,3	2,5	2,0	1,0	0,0
57,60	275	1,5	1,7	61,8	26,2	2,5	0,7	0,4	0,0	3,0	1,0	1,2	0,0
58,20	315	2,8	1,0	37,4	48,5	6,5	0,3	1,0	0,0	0,0	1,0	1,5	0,0
60,25	285	3,3	1,5	38,0	46,0	2,8	3,0	1,6	0,0	0,0	2,0	1,8	0,0
62,50	284	2,5	3,7	36,0	44,0	2,0	5,8	0,6	0,0	0,8	1,3	3,3	0,0
64,00	282	2,8	1,5	36,2	44,5	3,0	3,8	0,3	0,0	0,5	2,8	4,6	0,0
66,00	302	1,5	4,5	39,5	41,2	2,5	3,1	0,6	0,0	0,8	3,1	3,2	0,0

Table S3.2. Fragmentation index (%) and weight percent coarse fraction (%) at the Carcoselle Quarry (Possagno).

Thickness (m above the PETM)	Coarse fraction (%)	*F* index (%)	Thickness (m above the PETM)	Coarse fraction (%)	*F* index (%)
0,98	15,81	9,5	17,60	4,27	45,3
2,00	16,81	–	17,80	6,19	–
2,50	10,82	–	18,00	3,53	70,0
3,00	7,37	13,0	18,20	5,44	–
3,50	7,14	–	18,40	6,05	35,5
4,00	8,57	–	18,60	6,59	24,0
4,50	9,05	–	18,80	5,14	–
5,00	8,83	–	19,00	6,07	–
5,50	7,74	–	19,20	5,79	62,0
6,00	9,70	9,0	19,40	5,11	41,5
6,50	9,16	–	19,60	5,44	–
7,00	14,52	–	19,80	5,55	60,1
7,50	10,14	–	20,00	3,54	–
8,00	8,59	62,4	20,20	5,35	–
8,50	8,77	58,5	20,40	5,76	57,9
9,00	9,02	12,3	20,60	7,06	–
9,50	11,62	–	20,80	5,64	–
10,00	11,01	–	21,00	5,11	23,5
10,50	9,42	–	21,20	7,36	–
11,00	11,62	–	21,40	4,53	–
11,50	12,93	–	21,60	8,36	–
12,00	7,43	16,2	21,80	8,57	–
12,50	12,55	57,2	22,00	8,52	–
13,00	13,13	67,1	22,20	7,23	28,5
13,50	11,06	–	22,60	5,83	–
14,20	13,04	–	23,00	7,64	–
14,40	7,05	–	23,40	4,04	–
14,60	8,51	50,0	23,80	7,62	–
14,80	7,32	68,7	24,20	6,90	–
15,00	13,86	–	24,70	7,53	–
15,20	6,65	66,8	25,20	7,96	–
15,40	8,30	–	25,60	6,34	–
15,60	5,31	25,0	25,80	4,79	–
15,80	5,41	60,2	26,00	5,54	–
16,00	5,95	–	26,40	5,75	24,8
16,20	5,37	20,0	26,80	5,08	–
16,40	5,55	34,0	27,20	5,15	12,1
16,60	7,47	60,0	27,40	3,60	50,5
16,80	6,92	62,0	27,60	4,34	50,0
17,00	4,90	31,0	28,20	6,24	17,9
17,20	5,64	–	28,80	4,54	–
17,40	5,85	–	29,40	5,07	–

30,00	4,93	45,8	48,60	4,14	–
30,60	5,58	11,8	49,20	3,60	11,4
31,20	4,65	–	49,40	3,31	16,0
31,40	8,61	42,5	49,80	4,66	12,1
31,80	7,57	–	50,40	4,32	23,2
32,40	3,76	–	51,00	5,39	–
33,00	5,42	31,4	51,60	4,60	12,0
33,60	5,78	–	52,20	4,74	13,5
34,00	4,82	–	52,80	4,53	–
34,20	8,05	–	53,00	4,46	12,0
34,80	5,96	–	53,20	5,26	12,0
35,00	5,70	–	53,40	5,42	15,0
35,20	–	12,0	53,80	–	10,5
35,40	4,32	–	54,00	4,54	12,5
36,00	5,44	–	54,60	4,26	11,0
36,60	5,76	–	55,00	5,57	23,0
37,20	3,76	10,0	55,20	6,04	–
37,80	4,11	52,0	55,80	4,24	10,0
38,00	2,91	–	56,00	4,85	10,0
38,40	3,19	–	56,20	6,62	15,0
39,00	4,44	55,2	56,40	5,71	13,0
39,60	2,49	49,5	56,60	–	11,0
40,20	3,50	48,2	57,00	3,24	18,0
40,80	4,43	15,0	57,60	4,67	35,0
41,40	5,43	18,0	58,20	3,70	6,5
42,00	4,64	15,0	58,80	2,99	–
42,60	3,94	–	59,50	2,16	–
43,20	5,66	11,0	60,25	5,26	11,0
43,80	5,09	–	61,00	4,40	13,8
44,40	5,84	–	61,75	4,42	–
45,00	5,41	10,0	62,50	6,02	7,0
45,60	5,05	9,2	63,25	5,48	–
46,20	3,71	–	64,00	4,35	6,5
46,80	4,26	–	64,75	4,07	–
47,40	5,68	10,0	65,40	4,74	–
48,00	5,14	–	66,00	5,39	7,4

Table S4. Recalibrated depths and abundances for planktic foraminiferal genera at Site 577 (Lu, 1995).

Hole	Core	Section	Interval Top (cm)	Interval Base (cm)	[1] Reported Depth (mbsf)	[2] Core Top Depth (mbsf)	Void correction (m)	[3] Depth Fix (mbsf)	[4] Offset (m)	[5] Adjusted Depth (mcd)	[1] No. counted specimens	Relative abundance (%) of total number of counted specimens			
												Acarinids	Morozovellids	Subbotinids	Other
577*	8	3	13	15	66,94	63,80	0,00	66,94	-3,50	63,44	220	5	0	6	89
577*	8	3	34	36	67,15	63,80	0,00	67,15	-3,50	63,65	319	65	8	9	18
577*	8	3	48	50	67,29	63,80	0,00	67,29	-3,50	63,79	311	83	3	6	8
577*	8	3	76	78	67,57	63,80	0,00	67,57	-3,50	64,07	298	78	3	6	13
577*	8	3	100	102	67,81	63,80	0,00	67,81	-3,50	64,31	321	66	4	7	23
577*	8	3	138	140	68,19	63,80	0,00	68,19	-3,50	64,69	306	77	1	1	21
577*	8	4	18	20	68,49	63,80	0,00	68,49	-3,50	64,99	287	83	5	3	9
577*	8	4	34	36	68,66	63,80	0,00	68,65	-3,50	65,15	332	75	4	3	18
577*	8	4	48	50	68,79	63,80	0,00	68,79	-3,50	65,29	301	84	3	1	12
577*	8	4	78	80	69,09	63,80	0,00	69,09	-3,50	65,59	297	69	2	6	23
577*	8	4	100	102	69,31	63,80	0,00	69,31	-3,50	65,81	319	86	1	6	7
577*	8	4	138	140	69,69	63,80	0,00	69,69	-3,50	66,19	296	68	1	6	25
577*	8	5	17	19	69,98	63,80	0,00	69,98	-3,50	66,48	276	85	3	6	6
577*	8	5	34	36	70,15	63,80	0,00	70,15	-3,50	66,65	323	61	6	12	21
577*	8	5	57	59	70,38	63,80	0,00	70,38	-3,50	66,88	262	78	5	3	14
577*	8	5	86	88	70,67	63,80	0,00	70,67	-3,50	67,17	290	67	9	11	13
577*	8	5	100	102	70,81	63,80	0,00	70,81	-3,50	67,31	311	64	12	7	17
577*	8	5	137	139	71,18	63,80	0,00	71,18	-3,50	67,68	269	55	5	1	39
577*	8	6	18	20	71,49	63,80	0,00	71,49	-3,50	67,99	295	53	9	8	30
577*	8	6	34	36	71,65	63,80	0,00	71,65	-3,50	68,15	309	54	17	7	22
577*	8	6	57	59	71,88	63,80	0,00	71,88	-3,50	68,38	274	59	5	2	34
577*	8	6	81	83	72,12	63,80	0,00	72,12	-3,50	68,62	306	56	9	3	32
577*	8	6	100	102	71,65	63,80	0,00	72,31	-3,50	68,81	314	48	16	4	32
577*	8	6	140	142	72,71	63,80	0,00	72,71	-3,50	69,21	288	64	5	1	30

Hole	Core	Section	Interval Top (cm)	Interval Base (cm)	[1] Reported Depth (mbsf)	[2] Core Top Depth (mbsf)	Void correction (m)	[3] Depth Fix (mbsf)	[4] Offset (m)	[5] Adjusted Depth (mcd)	[1] No. counted specimens	Relative abundance (%) of total number of counted specimens			
												Acarinids	Morozovellids	Subbotinids	Other
577*	9	1	104	106	74,35	73,30	0,00	74,35	0,00	74,35	347	48	14	8	30
577*	8	7	2	4	72,83	63,80	0,00	72,83	-3,50	69,33	303	49	15	13	23
577*	8-CC	8	36	38	73,17	63,80	-1,37	73,30	-3,50	69,80	305	72	8	10	10
577*	9	1	30	32	73,61	73,30	0,00	73,61	0,00	73,61	280	68	8	6	18
577*	9	1	48	50	73,79	73,30	0,00	73,79	0,00	73,79	288	73	7	6	14
577*	9	1	80	82	74,11	73,30	0,00	74,11	0,00	74,11	316	59	3	17	21
577*	9	1	137	139	74,68	73,30	0,00	74,68	0,00	74,68	296	71	2	8	19
577*	9	2	30	32	75,11	73,30	0,00	75,11	0,00	75,11	298	55	13	17	15
577*	9	2	47	49	75,28	73,30	0,00	75,28	0,00	75,28	302	49	4	16	31
577*	9	2	80	82	75,61	73,30	0,00	75,61	0,00	75,61	307	72	6	9	13
577*	9	2	104	106	75,85	73,30	0,00	75,85	0,00	75,85	337	68	4	18	10
577*	9	2	136	138	76,17	73,30	0,00	76,17	0,00	76,17	288	75	2	7	16
577*	9	3	30	32	76,61	73,30	0,00	76,61	0,00	76,61	322	67	10	9	14
577*	9	3	53	55	76,84	73,30	0,00	76,84	0,00	76,84	289	73	2	8	17
577*	9	3	80	82	77,11	73,30	0,00	77,11	0,00	77,11	307	54	14	12	20
577*	9	3	104	106	77,35	73,30	0,00	77,35	0,00	77,35	331	59	16	13	12
577*	9	3	138	140	77,69	73,30	0,00	77,69	0,00	77,69	298	61	11	7	21
577*	9	4	30	32	78,11	73,30	0,00	78,11	0,00	78,11	334	35	41	8	16
577*	9	4	52	54	78,33	73,30	0,00	78,33	0,00	78,33	311	39	23	8	30
577*	9	4	80	82	78,61	73,30	0,00	78,61	0,00	78,61	315	37	27	3	33
577*	9	4	104	106	78,85	73,30	0,00	78,85	0,00	78,85	347	34	30	4	32
577*	9	4	133	135	78,33	73,30	0,00	79,14	0,00	79,14	306	35	32	6	27
577*	9	5	30	32	79,61	73,30	0,00	79,61	0,00	79,61	332	39	35	11	15

Hole	Core	Section	Interval Top (cm)	Interval Base (cm)	[1] Reported Depth (mbsf)	[2] Core Top Depth (mbsf)	Void correction (m)	[3] Depth Fix (mbsf)	[4] Offset (m)	[5] Adjusted Depth (mcd)	[1] No. counted specimens	Relative abundance (%) of total number of counted specimens			
												Acarinids	Morozovellids	Subbotinids	Other
577*	9	5	80	82	80,11	73,30	0,00	80,11	0,00	80,11	310	30	26	8	36
577*	9	5	104	106	80,35	73,30	0,00	80,35	0,00	80,35	324	17	31	7	45
577*	9	6	30	32	81,11	73,30	0,00	81,11	0,00	81,11	339	22	23	15	40
577*	9	6	53	55	81,34	73,30	0,00	81,34	0,00	81,34	303	34	19	11	36
577*	9	6	78	80	81,59	73,30	0,00	81,59	0,00	81,59	298	20	20	11	49
577*	9	6	104	106	81,85	73,30	0,00	81,85	0,00	81,85	322	19	13	11	57
577*	9-CC	7	2	4	82,63	73,30	-0,30	82,03	0,00	82,03	308	28	16	12	44
577*	9-CC	7	9	11	82,70	73,30	-0,30	82,10	0,00	82,10	322	48	10	7	35
577A	8	3	110	112	70,51	66,40	0,00	70,51	-1,30	69,21	302	65	10	3	22
577A	8	3	143	145	70,84	66,40	0,00	70,84	-1,30	69,54	317	61	17	5	17
577A	8	4	10	12	71,01	66,40	0,00	71,01	-1,30	69,71	331	65	7	3	25
577A	8	4	30	32	71,21	66,40	0,00	71,21	-1,30	69,91	304	48	10	7	35
577A	8	3	143	145	70,84	66,40	0,00	70,84	-1,30	69,54	317	65	10	3	22
577A	8	4	10	12	71,01	66,40	0,00	71,01	-1,30	69,71	331	61	17	5	17
577A	8	4	30	32	71,21	66,40	0,00	71,21	-1,30	69,91	304	65	7	3	25
577A	8	4	47	49	71,38	66,40	0,00	71,38	-1,30	70,08	327	81	12	2	5
577A	8	4	72	74	71,63	66,40	0,00	71,63	-1,30	70,33	312	81	9	3	7
577A	8	4	88	90	71,79	66,40	0,00	71,79	-1,30	70,49	326	63	9	3	25
577A	8	4	110	112	72,01	66,40	0,00	72,01	-1,30	70,71	316	56	16	3	25
577A	8	4	130	132	72,21	66,40	0,00	72,21	-1,30	70,91	333	61	4	1	34
577A	8	5	10	12	72,51	66,40	0,00	72,51	-1,30	71,21	365	62	12	2	24
577A	8	5	30	32	72,71	66,40	0,00	72,71	-1,30	71,41	334	59	8	2	31

Notes: [1] depth reported by Lu (1995); [2] depth reported according to drillers table (Shipboard Scientific Party, 1985) and with positions of "CC" intervals from core logs; [3] depth in mbsf assuming average interval distance and the above; [4] offset of cores from Table S3.2.; [5] depth of the sample in floating depth space (meter composite depth-mcd) relative to meter below seafloor (mbsf).

Table S4. Abundances of planktic foraminiferal genera and fragmentation index (%), at ODP Hole 1051A.

Hole	Core	Section	cm ±1	mbsf	No. counted specimens	*Acarinina*	*Morozovella*	*Morozovelloides*	Subbotinids	Other genera	*F* index
1051A	38	2	120	353,10	309	56,3	3,0	1,2	18,8	20,7	2
1051A				356,60	315	52,0	3,8	0,8	22,0	21,4	3
1051A				360,80	305	39,0	4,2	0,5	24,0	32,3	10
1051A				365,30	321	42,5	4,8	1,0	26,5	25,2	3
1051A	40	1	21	369,90	335	46,8	3,0	0,6	28,0	21,6	5
1051A	40	1	121	370,90	311	50,0	7,4	0,3	28,3	14,0	35
1051A	40	3	121	373,90	303	39,6	5,5	0,5	23,1	31,3	10
1051A	40	5	71	376,40	314	54,0	2,6	0,0	25,5	17,9	20
1051A	40	cc	21	377,00	338	45,8	10,5	0,8	23,7	19,2	35
1051A	41	1	21	379,50	301	52,1	9,8	1,5	23,0	13,6	5
1051A	42	1	21	390,10	219	63,3	5,0	0,0	18,3	13,4	53
1051A	42	3	121	394,10	211	57,8	6,2	0,0	23,7	12,3	50
1051A	42	6	26	397,65	385	47,0	9,8	0,0	27,5	15,7	5
1051A	43	2	69	401,68	285	45,3	10,8	0,0	26,7	17,2	15
1051A	43	4	19	404,18	295	59,3	8,5	0,0	21,7	10,5	12
1051A	43	5	69	406,18	336	57,1	7,1	0,0	21,1	14,7	10
1051A	44	1	21	409,30	310	37,0	17,5	0,0	15,0	30,5	15
1051A	44	1	71	409,80	315	57,0	14,5	0,0	15,5	13,0	10
1051A	44	3	21	412,30	332	62,0	12,0	0,0	16,3	9,7	12
1051A	44	4	21	413,80	290	55,0	13,2	0,0	15,5	16,3	15
1051A	44	5	69	415,78	327	62,0	8,5	0,0	21,0	8,5	20
1051A	44	6	121	417,80	375	50,7	14,1	0,0	23,5	11,7	10
1051A	45	1	121	419,90	371	49,5	16,9	0,0	21,3	12,3	12
1051A	45	3	21	421,90	389	58,3	7,8	0,0	23,6	10,3	5
1051A	45	4	23	423,42	350	48,0	15,1	0,0	16,0	20,9	7
1051A	45	5	71	425,40	307	59,2	18,0	0,0	17,2	5,6	5
1051A	45	6	72	426,90	333	51,6	19,5	0,0	19,8	9,1	10
1051A	45	6	121	427,40	263	61,5	13,3	0,0	22,0	3,2	35
1051A	45	7	22	427,91	250	60,0	14,8	0,0	15,2	10,0	64
1051A	46	1	21	428,50	245	27,7	53,5	0,0	13,0	5,8	18
1051A	46	2	21	430,00	315	25,5	54,0	0,0	15,0	5,5	15
1051A	46	2	71	430,50	242	23,5	42,0	0,0	21,5	13,0	38
1051A	46	4	71	433,50	248	33,0	38,3	0,0	16,1	12,6	35
1051A	46	4	119	433,98	247	24,0	43,0	0,0	24,0	9,0	13
1051A	46	5	19	434,48	223	28,0	39,0	0,0	22,4	10,6	15
1051A	47	2	18,5	439,57	293	30,0	45,0	0,0	19,5	5,5	10
1051A	47	3	69	441,58	282	40,7	41,8	0,0	13,1	4,4	50
1051A	47	5	24	444,13	341	35,2	38,7	0,0	13,5	12,6	10
1051A	48	2	70	449,69	322	46,3	31,4	0,0	15,0	7,3	12
1051A	48	4	25	452,24	259	31,3	46,3	0,0	7,0	15,4	10

Follow-Up on TEX_{86} Methods

To extract the isoprenoid GDGTs and valuate their abundances we follow the methods for samples preparations shown in Schouten et al. (2002, 2013). Prior to lipid extraction, samples were freeze-dried for 48 hours and powdered using mortar and pestle. Lipids from the ten preliminary samples were extracted from 8-10 grams of sediment with dichloromethane (DCM):methanol (MeOH) (9:1, v/v) using a Dionex accelerated solvent extractor (ASE 200) at a temperature of 100°C and under a pressure of 7.6-106 Pa. A larger amount of sediments (~60 g) was instead analysed for the multi-sample. In this case compounds were extracted with a soxhlet extractor using the same solvent mixture (DCM:MeOH, 9:1, v/v). The lipid extracts from both the tests were dried under a N2 stream then separated into an apolar, ketone and polar fraction by column chromatography using an activated Al2O3 column. Eluting was done with hexane:DCM (9:1, v/v), hexane:DCM (1:1, v/v) and DCM:MeOH (1:1, v/v), respectively. Ninety-nine nanograms of a synthetic C46 GDGT-standard were added to the polar fraction, containing the GDGTs. After drying under N2 stream, the polar fraction was dissolved in hexane:isopropanol (99:1, v/v) to a concentration of ~3 mg/mL and filtered through a 0.45 μm PTFE (polytetrafluoroethylene) filter. Quantification of GDGTs from the polar fractions was conducted with an HPLC/APCI-MS (high performance liquid chromatography/atmospheric pressure chemical ionization-mass spectrometry) using an Agilent 1100 series LC/MSD SL (liquid chromatography/mass spectrometry) and following methods described by De Jonge et al., (2014).

References

De Jonge, C., E. C. Hopmans, C. I. Zell, J.-H. Kim, S. Schouten, and J. S. Sinninghe Damsté (2014), Occurrence and abundance of 6-methyl branched glycerol dialkyl glycerol tetraethers in soils: Implications for palaeoclimate reconstruction, Geochim. Cosmochim. Acta, 141, 97–112. doi:10.1016/j.gca.2014.06.013

Schouten, S., E. C. Hopmans, E. Schefuss, and J. S. Sinninghe Damsté (2002), Distributional variations in marine crenarchaeotal membrane lipids: A new tool for reconstructing ancient sea water temperatures?, Earth Planet. Sci. Lett., 204, 265–274, doi:10.1016/S0012-821X(02)00979-2.

Schouten, S., E. C. Hopmans, J. S. Sinninghe Damsté (2013), The organic geochemistry of glycerol dialkyl glycerol tetraether lipids: A review, Org. Geochem. 54, 19–61, doi:10.1016/j.orggeochem.2012.09.006.

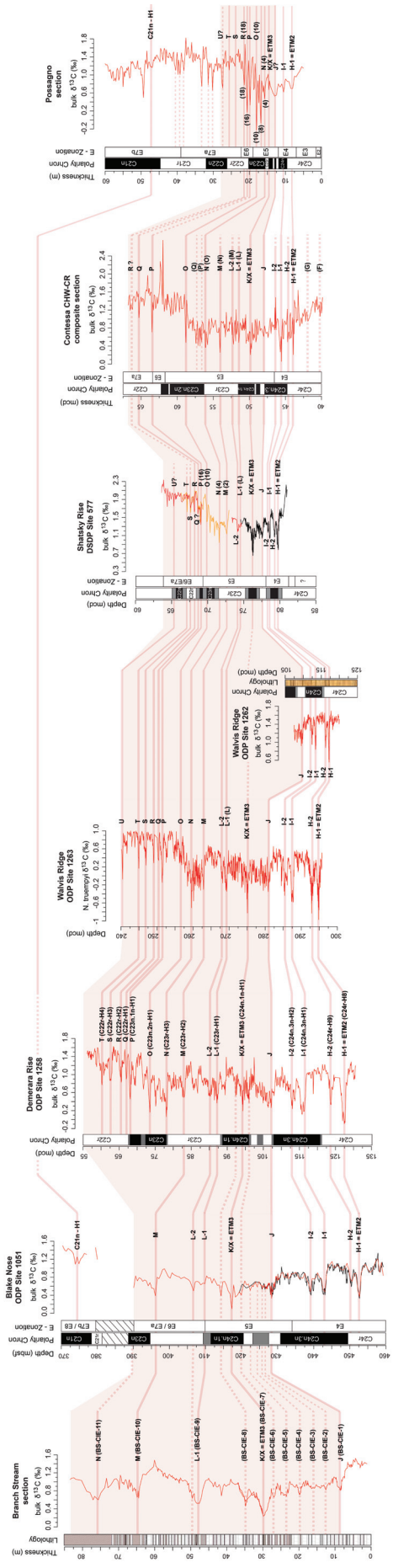

Figure S1. Correlation of carbon isotope records spanning the early Eocene from several Sites worldwide distributed. These are: the Branch Stream (New Zealand, Slotnick et al., 2015), the Possagno (north-eastern Italy, Luciani et al., 2016) and Contessa Road section (central Italy, Coccioni et al., 2012), the ODP Sites 1051 (Blake Nose, this study), 1258 (Demerara Rise, Kirtland-Turner et al., 2014), 1263 (Walvis Ridge, Lauretano et al., 2016), 1262 (Walvis Ridge, Zachos et al., 2010) and the DSDP Site 577 (Shatsky Rise, Cramer et al., 2003; Luciani et al., 2016). Where possible, magnetostratigraphy, lithology and planktic foraminiferal zonation are given. Records from Cramer et al. (2003) at Sites 577 and 1051 are in black colour. At Site 577 $\delta^{13}C$ data are aligned following Dickens and Backman (2013); orange colour refers to hole 577A and red colour to hole 577A. Carbon isotope excursions (CIEs) are highlighted with pink bands and labelled following the alphabetical order of Cramer et al. (2003) and of Kirtland-Turner et al. (2014) for the C21n-H1 event. Original labels used by different authors are shown in brackets. Dashed bands indicate events not consistently correlated. Correlation problems are mainly related to different resolution of $\delta^{13}C$ records and sedimentation rates. A major shift in frequency and amplitude of CIEs appears to have happened during the EECO.

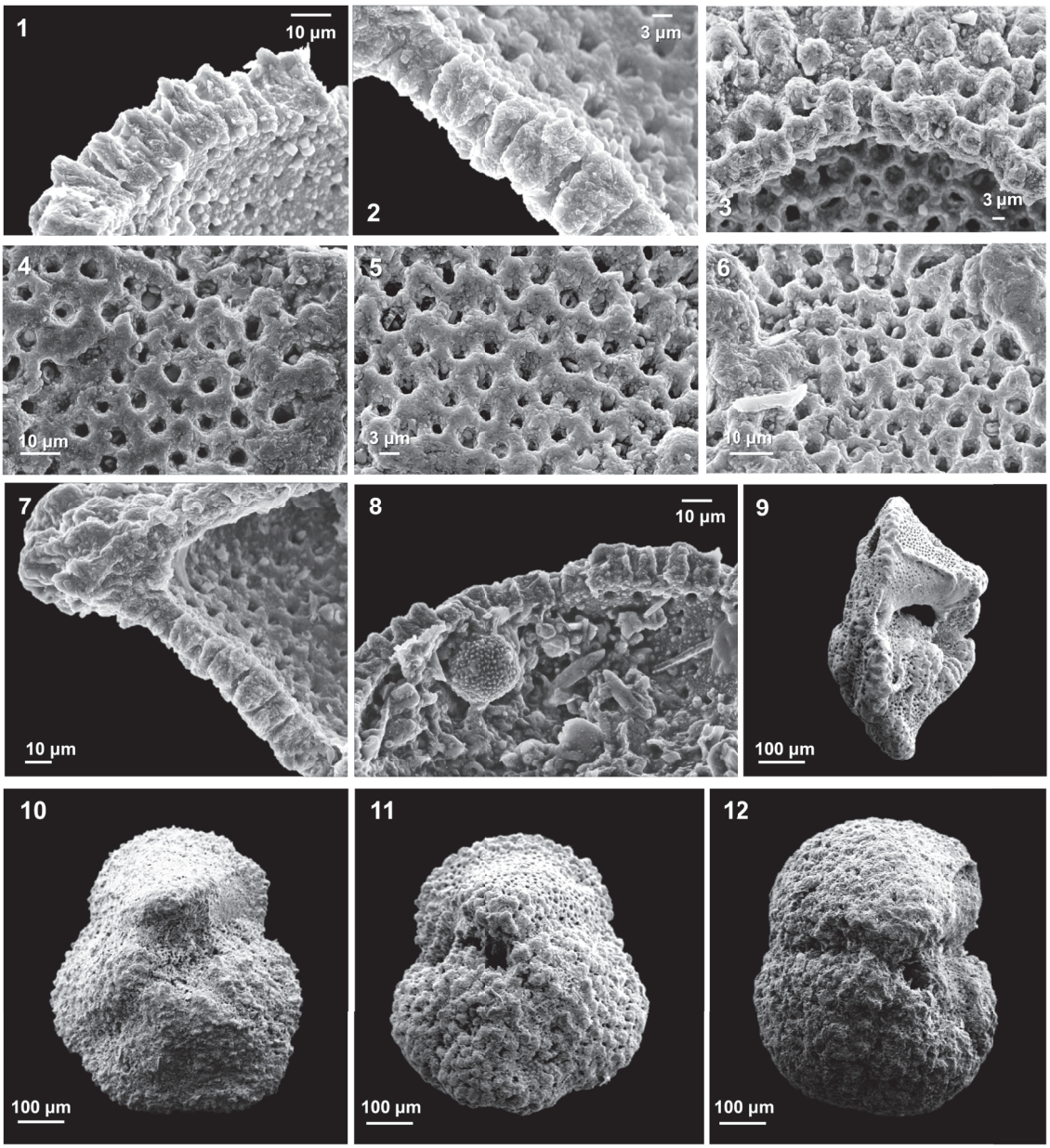

Figure S2. Preservation of early Eocene planktic foraminifera (Zones E4−E6/7a) at the ODP Site 1051. 1−6: SEM images of wall textures showing different degrees of "frosty" preservation, as referred to their appearance at stereomicroscope (Sexton et al., 2006). Broken tests from: (1) *Acarinina soldadoensis* (sample 437 mbsf), (2) *Morozovella formosa* (sample 422.9 mbsf), (3) *Subbotina patagonica* (sample 437 mbsf). Images show micron-scale diagenetic alteration even obscuring the relief of the vertical pore pits in some cases. (4) Wall-textures of *A. soldadoensis* (sample 437 mbsf), (5) *M. formosa* (sample 410.8 mbsf), (6) *S. patagonica* (sample 405.22 mbsf) showing variable amounts of secondary calcite. 7−10: examples of infilled and unfilled specimens. (7) Broken test of unfilled *M. formosa* (sample 422.9 mbsf) (8) broken test of *A. soldadoensis* (sample XX) infilled with large crystals of secondary calcite; (9) entire specimen of *M. formosa* (sample 410.8 mbsf) with a completely clean aperture denoting that test is potentially unfilled; (10) entire specimens of *M. crater* (sample 405.22 mbsf) with sealed aperture denoting that test is completely infilled. 11−12: Examples of significantly recrystallized test of *M. lensiformis* (11, sample 395.10) and *M. aequa* (12, sample 395.10 mbsf) both displaying replacement of surface pustules by coalescent large crystals.

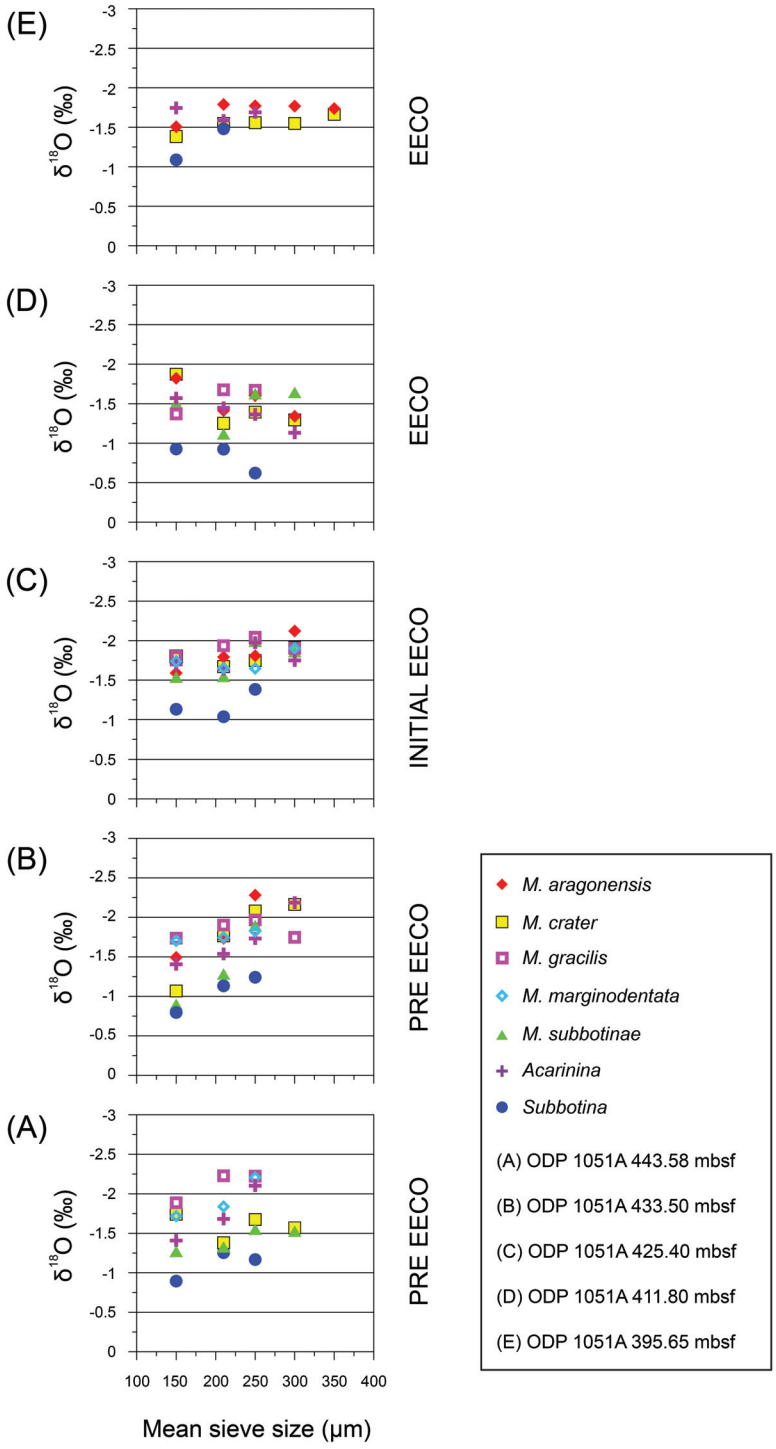

Figure S3. Planktic foraminiferal δ^{13}O-test size trends from five selected samples (A−E) located below and across the EECO at the ODP Sites 1051. Position of the analysed samples is shown in figures 2, 3. The δ^{13}O data were generated using monospecific specimens of the known photosymbiont-bearing species *Morozovella aragonensis* (red solid-diamonds), *M. crater* (yellow solid-squares), *M. gracilis* (pink open-squares), *M. marginodentata* (light-blue open-diamonds) and *M. subbotinae* (green solid-triangles), the *Acarinina* spp. (purple solid-crosses) and of the asymbiotic genus *Subbotina* (blue solid-circles). Data may be affected by recrystallization of plantic foraminiferal test inferred from the "frosty" preservation (sensu Sexton et al. 2006) at Site 1051 (see figure S2).

Table S1. Carbon and oxygen stable-isotope composition of early Eocene bulk carbonate at Site 1051.

Leg	Site	Hole	Core	Section	Interval		Volume	Depth (mbsf)	$\delta^{13}C$ (‰)	$\delta^{18}O$ (‰)
					Top Depth	Bottom Depth				
171	1051	A	40	1	20	22	20	369,9	–	–
171	1051	A	40	1	70	72	20	370,4	1,50	0,21
171	1051	A	40	1	120	122	20	370,9	1,41	-0,02
171	1051	A	40	2	20	22	20	371,4	1,38	0,00
171	1051	A	40	2	70	72	20	371,9	1,44	0,01
171	1051	A	40	2	122	124	20	372,42	1,41	0,06
171	1051	A	40	3	20	22	20	372,9	1,38	-0,01
171	1051	A	40	3	70	72	20	373,4	1,32	0,13
171	1051	A	40	3	120	122	20	373,9	1,09	0,03
171	1051	A	40	4	20	22	20	374,4	1,25	0,17
171	1051	A	40	4	70	72	20	374,9	1,10	-0,16
171	1051	A	40	4	120	122	20	375,4	1,21	-0,91
171	1051	A	40	5	20	22	20	375,9	1,25	-0,46
171	1051	A	40	5	70	72	20	376,4	1,33	-0,07
171	1051	A	40	cc	20	22	20	377	1,31	0,27
171	1051	A	41	1	20	24	20	379,5	1,46	-1,11
171	1051	A	41	1	70	72	20	380	1,20	-0,91
171	1051	A	42	1	20	22	20	390,1	0,57	-0,67
171	1051	A	42	1	70	72	20	390,6	0,83	-0,58
171	1051	A	42	1	120	122	20	391,1	0,72	-0,62
171	1051	A	42	2	20	22	20	391,6	0,79	-0,50
171	1051	A	42	2	70	72	20	392,1	0,77	-0,57
171	1051	A	42	2	120	122	20	392,6	0,71	-0,41
171	1051	A	42	3	20	22	20	393,1	0,74	-0,41
171	1051	A	42	3	70	72	20	393,6	0,72	-0,47
171	1051	A	42	3	120	122	20	394,1	0,61	-0,46
171	1051	A	42	4	20	22	20	394,6	0,68	-0,44
171	1051	A	42	4	70	72	20	395,1	0,56	-0,52
171	1051	A	42	4	125	127	20	395,65	0,55	-0,57
171	1051	A	42	5	20	22	20	396,1	0,39	-0,53
171	1051	A	42	5	70	72	20	396,6	0,80	-0,48
171	1051	A	42	5	120	122	20	397,1	0,77	-0,39
171	1051	A	42	6	25	27	20	397,65	0,87	-0,41
171	1051	A	42	6	70	72	20	398,1	0,97	-0,27
171	1051	A	42	6	120	122	20	398,6	0,99	-0,33
171	1051	A	42	7	20	22	20	399,1	0,91	-0,35
171	1051	A	43	1	22	24	20	399,72	0,81	-0,41
171	1051	A	43	1	70	72	20	400,2	0,78	-0,39
171	1051	A	43	1	122	124	20	400,72	0,90	-0,17
171	1051	A	43	2	20	22	20	401,2	0,86	-0,17
171	1051	A	43	2	68	70	20	401,68	0,84	-0,35
171	1051	A	43	2	120	122	20	402,2	0,82	-0,23
171	1051	A	43	3	20	22	20	402,7	0,81	-0,26

171	1051	A	43	3	69	71	20	403,19	0,77	-0,31
171	1051	A	43	3	118	120	20	403,68	0,79	-0,23
171	1051	A	43	4	18	21	20	404,18	0,80	-0,20
171	1051	A	43	4	70	72	20	404,7	0,77	-0,29
171	1051	A	43	4	122	124	20	405,22	0,75	-0,22
171	1051	A	43	5	20	22	20	405,7	0,71	-0,33
171	1051	A	43	5	68	70	20	406,18	0,61	-0,54
171	1051	A	43	5	120	122	20	406,7	0,50	-0,56
171	1051	A	43	6	17	19	20	407,17	0,70	-0,37
171	1051	A	43	6	68	70	20	407,68	0,71	-0,37
171	1051	A	43	6	122	124	20	408,22	0,69	-0,02
171	1051	A	43	7	18	20	20	408,68	0,63	-0,59
171	1051	A	44	1	20	22	20	409,3	0,67	-0,46
171	1051	A	44	1	70	72	20	409,8	0,66	-0,43
171	1051	A	44	1	120	122	20	410,3	0,83	-0,27
171	1051	A	44	2	20	22	20	410,8	0,78	-0,47
171	1051	A	44	2	70	72	20	411,3	0,79	-0,19
171	1051	A	44	2	120	122	20	411,8	0,67	-0,46
171	1051	A	44	3	20	22	20	412,3	0,77	-0,37
171	1051	A	44	3	70	72	20	412,8	0,70	-0,30
171	1051	A	44	3	120	122	20	413,3	0,62	-0,33
171	1051	A	44	4	20	22	20	413,8	0,63	-0,45
171	1051	A	44	4	70	72	20	414,3	0,39	-0,44
171	1051	A	44	4	120	122	20	414,8	0,70	-0,38
171	1051	A	44	5	18	20	20	415,28	0,71	-0,38
171	1051	A	44	5	68	70	20	415,78	0,63	-0,32
171	1051	A	44	5	118	120	20	416,28	0,50	-0,32
171	1051	A	44	6	20	22	20	416,8	0,43	-0,38
171	1051	A	44	6	70	72	20	417,3	0,10	-0,82
171	1051	A	44	6	120	122	20	417,8	0,63	-0,42
171	1051	A	44	7	20	22	20	418,3	0,36	-0,68
171	1051	A	45	1	20	22	20	418,9	0,41	-0,56
171	1051	A	45	1	70	72	20	419,4	0,48	-0,75
171	1051	A	45	1	120	122	20	419,9	0,41	-0,82
171	1051	A	45	2	20	22	20	420,4	0,58	-0,49
171	1051	A	45	2	69	71	20	420,89	0,72	-0,51
171	1051	A	45	2	120	122	20	421,4	0,63	-0,60
171	1051	A	45	3	20	22	20	421,9	0,65	-0,89
171	1051	A	45	3	70	72	20	422,4	0,51	-0,74
171	1051	A	45	3	120	122	20	422,9	0,62	-0,48
171	1051	A	45	4	3	5	30	423,23	0,59	-0,61
171	1051	A	45	4	22	24	20	423,42	0,65	-0,43
171	1051	A	45	4	47	49	30	423,67	0,65	-0,42
171	1051	A	45	4	68	70	20	423,88	0,70	-0,29
171	1051	A	45	4	98	100	30	424,18	0,61	-0,60
171	1051	A	45	4	120	122	20	424,4	0,59	-0,74
171	1051	A	45	5	1	3	30	424,71	0,69	-0,51
171	1051	A	45	5	18	20	20	424,88	0,70	-0,37

171	1051	A	45	5	48	50	30	425,18	0,64	-0,47
171	1051	A	45	5	70	72	20	425,4	0,63	-0,48
171	1051	A	45	5	72	74	30	425,42	0,61	-0,63
171	1051	A	45	5	89	91	30	425,59	0,62	-0,41
171	1051	A	45	5	109	111	30	425,79	0,54	-0,37
171	1051	A	45	5	120	122	20	425,9	0,61	-0,35
171	1051	A	45	5	128	130	30	425,98	0,61	-0,39
171	1051	A	45	5	138	140	30	426,08	0,58	-0,30
171	1051	A	45	6	4	6	30	426,24	0,58	-0,47
171	1051	A	45	6	9	11	30	426,29	0,62	-0,18
171	1051	A	45	6	18	20	30	426,38	0,64	-0,19
171	1051	A	45	6	20	22	20	426,4	0,62	-0,38
171	1051	A	45	6	29	31	30	426,49	0,58	-0,29
171	1051	A	45	6	39	41	30	426,59	0,56	-0,29
171	1051	A	45	6	47	49	30	426,67	0,55	-0,46
171	1051	A	45	6	61	63	30	426,81	0,58	-0,43
171	1051	A	45	6	71	73	20	426,91	0,54	-0,52
171	1051	A	45	6	73	75	30	426,93	0,58	-0,45
171	1051	A	45	6	80	82	30	427,00	0,59	-0,27
171	1051	A	45	6	120	122	20	427,4	0,66	-0,20
171	1051	A	45	6	84	86	30	427,04	0,56	-0,34
171	1051	A	45	6	89	91	30	427,09	0,58	-0,43
171	1051	A	45	6	94	96	30	427,14	0,54	-0,34
171	1051	A	45	6	99	101	30	427,19	0,62	-0,27
171	1051	A	45	6	104	106	30	427,24	0,62	-0,36
171	1051	A	45	6	107	109	30	427,27	0,61	-0,35
171	1051	A	45	6	114	116	30	427,34	0,61	-0,44
171	1051	A	45	6	118	120	30	427,38	0,63	-0,37
171	1051	A	45	6	124	126	30	427,44	0,67	-0,31
171	1051	A	45	6	128	130	30	427,48	0,63	-0,38
171	1051	A	45	6	134	136	30	427,54	0,64	-0,42
171	1051	A	45	6	141	143	30	427,61	0,67	-0,46
171	1051	A	45	6	144	146	30	427,64	0,64	-0,36
171	1051	A	45	7	0	2	30	427,70	0,66	-0,28
171	1051	A	45	7	6	8	30	427,76	0,67	-0,45
171	1051	A	45	7	9	11	30	427,79	0,66	-0,28
171	1051	A	45	7	14	16	30	427,84	0,61	-0,48
171	1051	A	45	7	19	21	30	427,89	0,58	-0,53
171	1051	A	45	7	21	23	20	427,91	0,60	-0,47
171	1051	A	45	7	26	28	30	427,96	0,55	-0,49
171	1051	A	45	7	29	31	30	427,99	0,42	-0,60
171	1051	A	45	7	36	38	30	428,06	0,42	-0,69
171	1051	A	45	7	38	40	30	428,08	0,48	-0,69
171	1051	A	45	7	45	47	30	428,15	0,58	-0,59
171	1051	A	45	8	2	5	30	428,19	0,59	-0,47
171	1051	A	45	8	7	10	30	428,24	0,61	-0,45
171	1051	A	46	1	4	6	30	428,34	0,33	-0,83
171	1051	A	46	1	10	12	30	428,40	0,42	-0,92

171	1051	A	46	1	14	16	30	428,44	0,41	-0,92
171	1051	A	46	1	18	20	30	428,48	0,51	-0,72
171	1051	A	46	1	20	22	20	428,5	0,55	-0,44
171	1051	A	46	1	22	24	30	428,52	0,54	-0,74
171	1051	A	46	1	29	31	30	428,59	0,49	-0,67
171	1051	A	46	1	34	36	30	428,64	0,49	-0,78
171	1051	A	46	1	38	40	30	428,68	0,48	-0,94
171	1051	A	46	1	44	46	30	428,74	0,58	-0,77
171	1051	A	46	1	48	50	30	428,78	0,58	-0,71
171	1051	A	46	1	54	56	30	428,84	0,65	-0,51
171	1051	A	46	1	58	60	30	428,88	0,65	-0,37
171	1051	A	46	1	64	66	30	428,94	0,63	-0,54
171	1051	A	46	1	68	70	30	428,98	0,59	-0,35
171	1051	A	46	1	71	73	20	429,01	0,65	-0,14
171	1051	A	46	1	77	79	30	429,07	0,69	-0,30
171	1051	A	46	1	89	91	30	429,19	0,56	-0,55
171	1051	A	46	1	98	100	30	429,28	0,64	-0,55
171	1051	A	46	1	108	110	30	429,38	0,71	-0,49
171	1051	A	46	1	119	121	30	429,49	0,82	-0,17
171	1051	A	46	1	120	122	20	429,5	0,75	-0,43
171	1051	A	46	1	129	131	30	429,59	0,82	-0,24
171	1051	A	46	1	140	142	30	429,70	0,82	-0,30
171	1051	A	46	2	1	3	30	429,81	0,76	-0,60
171	1051	A	46	2	9	11	30	429,89	0,72	-0,56
171	1051	A	46	2	20	22	20	430	0,76	-0,47
171	1051	A	46	2	22	24	30	430,02	0,86	-0,75
171	1051	A	46	2	36	38	30	430,16	0,74	-0,53
171	1051	A	46	2	57	59	30	430,37	0,78	-0,69
171	1051	A	46	2	70	72	20	430,5	0,76	-0,48
171	1051	A	46	2	98	100	30	430,78	0,84	-0,56
171	1051	A	46	2	120	122	20	431	0,88	-0,35
171	1051	A	46	3	1	3	30	431,31	0,91	-0,45
171	1051	A	46	3	22	24	20	431,52	0,90	-0,43
171	1051	A	46	3	48	50	30	431,78	0,80	-0,51
171	1051	A	46	3	68	70	20	431,98	0,82	-0,47
171	1051	A	46	3	97	99	30	432,27	0,79	-0,70
171	1051	A	46	3	120	122	20	432,5	0,80	-0,47
171	1051	A	46	4	2	4	30	432,82	0,90	-0,51
171	1051	A	46	4	18	20	20	432,98	0,77	-0,48
171	1051	A	46	4	70	72	20	433,5	0,81	-0,44
171	1051	A	46	4	118	120	20	433,98	0,89	-0,48
171	1051	A	46	5	18	20	20	434,48	0,88	-0,39
171	1051	A	46	5	74	76	20	435,04	0,91	-0,39
171	1051	A	46	5	120	122	20	435,5	0,86	-0,34
171	1051	A	46	6	18	20	20	435,98	0,77	-0,42
171	1051	A	46	6	70	72	20	436,5	0,79	-0,39
171	1051	A	46	6	120	122	20	437	0,78	-0,45
171	1051	A	46	7	22	24	20	437,52	0,89	-0,36

171	1051	A	47	1	18	20	20	438,08	0,75	-0,52
171	1051	A	47	1	74	76	20	438,64	0,65	-0,51
171	1051	A	47	1	118	120	20	439,08	0,48	-0,60
171	1051	A	47	2	17,5	19,5	20	439,575	0,77	-0,38
171	1051	A	47	2	72	74	20	440,12	0,76	-0,41
171	1051	A	47	2	117,5	119,5	20	440,575	0,79	-0,55
171	1051	A	47	3	18	20	20	441,08	0,90	-0,37
171	1051	A	47	3	68	70	20	441,58	0,80	-0,57
171	1051	A	47	3	123	125	20	442,13	0,77	-0,40
171	1051	A	47	4	15,5	17,5	20	442,555	0,53	-0,67
171	1051	A	47	4	73	75	20	443,13	0,48	-0,79
171	1051	A	47	4	118	120	20	443,58	0,91	-0,51
171	1051	A	47	5	23	25	20	444,13	1,06	-0,39
171	1051	A	47	5	68	70	20	444,58	1,09	-0,60
171	1051	A	47	5	117,5	119,5	20	445,075	1,15	-0,61
171	1051	A	47	6	17	19	20	445,57	1,01	-0,50
171	1051	A	47	6	73	75	20	446,13	1,04	-0,65
171	1051	A	47	6	114	116	20	446,54	1,09	-0,49
171	1051	A	47	7	7	9	20	446,97	1,03	-0,47
171	1051	A	48	1	23	25	20	447,73	0,97	-0,52
171	1051	A	48	1	68	70	20	448,18	0,96	-0,74
171	1051	A	48	1	118	120	20	448,68	1,01	-0,72
171	1051	A	48	2	22	24	20	449,22	1,11	-0,45
171	1051	A	48	2	69	72	20	449,69	0,98	-0,64
171	1051	A	48	2	117	119	20	450,17	0,76	-0,81
171	1051	A	48	3	17	19	20	450,67	0,71	-0,43
171	1051	A	48	3	69	73	20	451,19	0,88	-0,36
171	1051	A	48	3	118	120	20	451,68	0,89	-0,30
171	1051	A	48	4	24	26	20	452,24	0,51	-0,67
171	1051	A	48	4	73	75	20	452,73	0,37	-0,73
171	1051	A	48	4	118	120	20	453,18	0,90	-0,43
171	1051	A	48	5	18	20	20	453,68	1,01	-0,28
171	1051	A	48	5	68	70	20	454,18	1,09	-0,54
171	1051	A	48	5	120	124	20	454,7	1,04	-0,35
171	1051	A	48	6	18	20	20	455,18	0,95	-0,22
171	1051	A	48	6	69	73	20	455,69	0,91	-0,56
171	1051	A	48	7	23	25	20	456,25	0,95	-0,14
171	1051	A	48	1	18	20	20	457,28	1,17	-0,42
171	1051	A	49	1	66	70	20	457,76	1,21	-0,70
171	1051	A	49	1	118	120	20	458,28	0,91	-0,87
171	1051	A	49	2	16	20	20	458,76	1,13	-0,09
171	1051	A	49	2	66	68	20	459,26	0,84	-0,90

Table S2. Relative abundances (%) of planktic foraminiferal genera and radiolarians, and the fragmentation index (*F index*, %) at Site 1051A. In Italic data from Lucani et al. (2016) (Chapter III).

Leg	Site	Hole	Core	Section	Interval Top Depth	Interval Bottom Depth	Depth (mbsf)	Total counted specimens	*Morozovella* (%)	Morozovelloides (%)	*Acarinina* (%)	Subbotinids (%)	Chiloguemelinids (%)	*Globanomalina* (%)	*Pseudohastigerina* (%)	*Planorotalites* (%)	*Igorina* (%)	*F index* (%)	Radiolarians
–	–	–	–	–	–	–	*353,10*	*309*	*3*	*1,2*	*56,3*	*18,80*	–	–	–	–	–	*2*	15
–	–	–	–	–	–	–	*356,60*	*315*	*3,8*	*0,8*	*52*	*22,00*	–	–	–	–	–	*3*	10
–	–	–	–	–	–	–	*360,80*	*305*	*4,2*	*0,5*	*39*	*24,00*	–	–	–	–	–	*10*	25
–	–	–	–	–	–	–	*365,30*	*321*	*4,8*	*1*	*42,5*	*26,50*	–	–	–	–	–	*3*	5
171	*1051*	*A*	*40*	*1*	*20*	*22*	*369,90*	*335*	*3*	*0,6*	*46,8*	*28,00*	–	–	–	–	–	*5*	18
171	*1051*	*A*	*40*	*1*	*70*	*72*	*370,40*	*311*	*7,4*	*0,3*	*50*	*28,30*	–	–	–	–	–	*35*	60
171	*1051*	*A*	*40*	*3*	*120*	*122*	*373,90*	*303*	*5,5*	*0,5*	*39,6*	*23,10*	–	–	–	–	–	*10*	23
171	*1051*	*A*	*40*	*5*	*70*	*72*	*376,40*	*314*	*2,6*	*0*	*54*	*25,50*	–	–	–	–	–	*20*	0
171	*1051*	*A*	*40*	*cc*	*20*	*22*	*377,00*	*338*	*10,5*	*0,8*	*45,8*	*23,70*	–	–	–	–	–	*35*	3
171	*1051*	*A*	*41*	*1*	*20*	*24*	*379,50*	*301*	*9,8*	*1,5*	*52,1*	*23,00*	–	–	–	–	–	*5*	0
171	*1051*	*A*	*42*	*1*	*20*	*22*	*390,10*	*219*	*5*	*0,0*	*63,3*	*18,30*	–	–	–	–	–	*53*	78
171	1051	A	42	1	70	72	390,60	356	5,6	0,0	79,2	14,0	0,0	0,0	0,3	0,0	0,8	–	–
171	1051	A	42	2	20	22	391,60	376	3,7	0,0	83,2	12,2	0,3	0,0	0,0	0,0	0,5	–	–
171	1051	A	42	2	120	122	392,60	352	5,4	0,0	79,0	14,5	0,0	0,3	0,0	0,6	0,3	–	–
171	1051	A	42	3	70	72	393,60	391	5,1	0,0	80,3	14,1	0,0	0,5	0,0	0,0	0,0	–	–
171	*1051*	*A*	*42*	*3*	*120*	*122*	*394,10*	*211*	*6,2*	*0,0*	*57,8*	*23,70*	–	–	–	–	–	*50*	75
171	1051	A	42	4	20	22	394,60	369	6,5	0,0	78,6	14,1	0,0	0,8	0,0	0,0	0,0	–	–
171	1051	A	42	4	125	127	395,65	395	6,1	0,0	82,0	9,9	0,0	1,3	0,3	0,0	0,5	–	–
171	1051	A	42	5	70	72	396,60	329	3,6	0,0	86,6	9,7	0,0	0,0	0,0	0,0	0,0	–	–
171	*1051*	*A*	*42*	*6*	*25*	*27*	*397,65*	*385*	*9,8*	*0,0*	*47*	*27,50*	–	–	–	–	–	*5*	45
171	1051	A	42	6	120	122	398,60	338	5,6	0,0	79,3	14,2	0,0	0,0	0,0	0,3	0,6	–	–
171	1051	A	43	1	22	24	399,72	326	5,8	0,0	78,8	13,8	0,0	0,0	0,0	1,5	0,0	–	–
171	1051	A	43	1	122	124	400,72	394	5,1	0,0	67,5	25,6	0,3	0,3	0,5	0,3	0,5	–	–
171	*1051*	*A*	*43*	*2*	*68*	*70*	*401,68*	*285*	*10,8*	*0,0*	*45,3*	*26,70*	–	–	–	–	–	*15*	58
171	1051	A	43	2	120	122	402,20	369	4,6	0,0	82,1	10,6	0,0	0,3	0,8	0,8	0,8	–	–
171	1051	A	43	3	69	71	403,19	372	5,6	0,0	76,6	16,7	0,0	0,0	0,3	0,3	0,5	–	–

Leg	Site	Hole	Core	Section	Interval Top Depth	Interval Bottom Depth	Depth (mbsf)	Total counted specimens	*Morozovella* (%)	Morozovelloides (%)	*Acarinina* (%)	Subbotinids (%)	Chiloguemelinids (%)	*Globanomalina* (%)	*Pseudohastigerina* (%)	*Planorotalites* (%)	*Igorina* (%)	*F index* (%)	Radiolarians
171	*1051*	*A*	*43*	*4*	*18*	*21*	*404,18*	*295*	*8,5*	*0,0*	*59,3*	*21,70*	–	–	–	–	–	*12*	68
171	1051	A	43	4	122	124	405,22	396	10,6	0,0	66,7	21,2	0,0	0,8	0,0	0,5	0,3	–	–
171	*1051*	*A*	*43*	*5*	*68*	*70*	*406,18*	*336*	*7,1*	*0,0*	*57,1*	*21,10*	–	–	–	–	–	*10*	70
171	1051	A	43	6	17	19	407,17	375	7,7	0,0	68,0	20,8	0,3	0,8	0,3	0,8	1,3	–	–
171	1051	A	43	6	122	124	408,22	357	12,9	0,0	65,8	20,7	0,0	0,0	0,0	0,0	0,6	–	–
171	*1051*	*A*	*44*	*1*	*20*	*22*	*409,30*	*310*	*17,5*	*0,0*	*37*	*15,00*	–	–	–	–	–	*15*	65
171	*1051*	*A*	*44*	*1*	*70*	*72*	*409,80*	*315*	*14,5*	*0,0*	*57*	*15,50*	–	–	–	–	–	*10*	20
171	1051	A	44	2	20	22	410,80	403	4,7	0,0	66,3	26,1	0,0	0,2	0,2	0,7	1,7	–	–
171	1051	A	44	2	120	122	411,80	438	6,2	0,0	71,9	20,1	0,0	0,0	0,0	1,4	0,5	–	–
171	*1051*	*A*	*44*	*3*	*20*	*22*	*412,30*	*332*	*12*	*0,0*	*62*	*16,30*	–	–	–	–	–	*12*	18
171	1051	A	44	3	70	72	412,80	377	6,4	0,0	66,6	25,2	0,0	0,5	0,0	0,5	0,8	–	–
171	*1051*	*A*	*44*	*4*	*20*	*22*	*413,80*	*290*	*13,2*	*0,0*	*55*	*15,50*	–	–	–	–	–	*15*	20
171	1051	A	44	4	120	122	414,80	375	6,1	0,0	81,1	9,6	0,3	0,0	0,0	0,8	2,1	–	–
171	*1051*	*A*	*44*	*5*	*68*	*70*	*415,78*	*327*	*8,5*	*0,0*	*62*	*21,00*	–	–	–	–	–	*20*	25
171	1051	A	44	6	20	22	416,80	382	10,2	0,0	64,9	21,7	0,0	1,0	0,5	1,0	0,5	–	–
171	*1051*	*A*	*44*	*6*	*120*	*122*	*417,80*	*375*	*14,1*	*0,0*	*50,7*	*23,50*	–	–	–	–	–	*10*	35
171	1051	A	45	1	20	22	418,90	375	10,1	0,0	66,7	16,5	0,8	0,3	0,0	2,1	3,5	–	–
171	*1051*	*A*	*45*	*1*	*120*	*122*	*419,90*	*371*	*16,9*	*0,0*	*49,5*	*21,30*	–	–	–	–	–	*12*	25
171	1051	A	45	2	69	71	420,89	389	8,2	0,0	72,8	11,8	0,5	0,5	0,5	3,6	2,1	–	–
171	*1051*	*A*	*45*	*3*	*20*	*22*	*421,90*	*389*	*7,8*	*0,0*	*58,3*	*23,60*	–	–	–	–	–	*5*	8
171	1051	A	45	3	70	72	422,40	352	22,2	0,0	57,7	19,3	0,9	0,0	0,0	0,0	0,0	–	–
171	1051	A	45	3	120	122	422,90	186	11,8	0,0	71,5	16,7	0,0	0,0	0,0	0,0	0,0	–	–
171	*1051*	*A*	*45*	*4*	*22*	*24*	*423,42*	*350*	*15,1*	*0,0*	*48*	*16,00*	–	–	–	–	–	*7*	45
171	1051	A	45	4	68	70	423,88	349	9,7	0,0	67,9	20,1	2,3	0,0	0,0	0,0	0,0	–	–
171	1051	A	45	4	120	122	424,40	330	20,9	0,0	63,9	13,6	1,5	0,0	0,0	0,0	0,0	–	–
171	1051	A	45	5	18	20	424,88	343	19,5	0,0	61,5	17,5	1,5	0,0	0,0	0,0	0,0	–	–

Leg	Site	Hole	Core	Section	Interval Top Depth	Interval Bottom Depth	Depth (mbsf)	Total counted specimens	*Morozovella* (%)	Morozovelloides (%)	*Acarinina* (%)	Subbotinids (%)	Chiloguemelinids (%)	*Globanomalina* (%)	*Pseudohastigerina* (%)	*Planorotalites* (%)	*Igorina* (%)	*F index* (%)	Radiolarians
171	1051	A	45	5	120	122	425,90	354	15,0	0,0	64,1	15,5	3,1	0,6	0,0	0,3	1,4	–	10
171	1051	A	45	6	20	22	426,40	395	15,4	0,0	64,6	15,2	1,0	0,8	0,3	1,3	1,5	–	–
171	*1051*	*A*	*45*	*6*	*71*	*73*	*426,91*	*333*	*19,5*	*0,0*	*51,6*	*19,80*	–	–	–	–	–	*10*	30
171	*1051*	*A*	*45*	*6*	*120*	*122*	*427,40*	*263*	*13,3*	*0,0*	*61,5*	*22,00*	–	–	–	–	–	*35*	70
171	*1051*	*A*	*45*	*7*	*21*	*23*	*427,91*	*250*	*14,8*	*0,0*	*60*	*15,20*	–	–	–	–	–	*64*	65
171	1051	A	45	7	29	31	427,99	331	15,4	0,0	64,0	17,5	3,0	0,0	0,0	0,0	0,0	–	74
171	1051	A	45	7	36	38	428,06	347	11,2	0,0	68,0	18,2	2,6	0,0	0,0	0,0	0,0	–	70
171	1051	A	45	7	38	40	428,08	342	14,6	0,0	63,2	20,2	2,0	0,0	0,0	0,0	0,0	–	67
171	1051	A	45	7	45	47	428,15	348	15,5	0,0	64,4	17,2	2,9	0,0	0,0	0,0	0,0	–	77
171	1051	A	45	8	2	5	428,19	384	16,7	0,0	62,8	16,1	4,4	0,0	0,0	0,0	0,0	–	78
171	1051	A	45	8	7	10	428,24	359	12,5	0,0	65,5	20,3	1,7	0,0	0,0	0,0	0,0	–	79
171	1051	A	46	1	4	6	428,34	325	29,2	0,0	55,1	13,2	2,5	0,0	0,0	0,0	0,0	–	82
171	1051	A	46	1	10	12	428,40	340	27,9	0,0	56,5	15,3	0,3	0,0	0,0	0,0	0,0	–	85
171	1051	A	46	1	14	16	428,44	329	34,3	0,0	50,5	14,9	0,3	0,0	0,0	0,0	0,0	–	72
171	1051	A	46	1	18	20	428,48	336	36,9	0,0	46,4	16,1	0,6	0,0	0,0	0,0	0,0	–	76
171	*1051*	*A*	*46*	*1*	*20*	*22*	*428,50*	*245*	*53,5*	*0,0*	*27,7*	*13,00*	–	–	–	–	–	*18*	10
171	1051	A	46	1	71	73	429,01	387	44,4	0,0	35,7	14,5	3,1	0,3	0,5	0,3	1,3	–	–
171	1051	A	46	1	120	122	429,50	399	45,9	0,0	34,8	9,8	2,8	0,8	0,0	1,5	4,5	–	–
171	*1051*	*A*	*46*	*2*	*20*	*22*	*430,00*	*315*	*54*	*0,0*	*25,5*	*15,00*	–	–	–	–	–	*15*	12
171	*1051*	*A*	*46*	*2*	*70*	*72*	*430,50*	*242*	*42*	*0,0*	*23,5*	*21,50*	–	–	–	–	–	*38*	28
171	1051	A	46	3	22	24	431,52	403	46,4	0,0	33,7	13,9	3,5	0,5	0,2	0,0	1,7	–	–
171	1051	A	46	3	120	122	432,50	345	46,4	0,0	34,8	11,9	4,6	0,0	0,0	0,3	2,0	–	–
171	*1051*	*A*	*46*	*4*	*70*	*72*	*433,50*	*248*	*38,3*	*0,0*	*33*	*16,10*	–	–	–	–	–	*35*	15
171	*1051*	*A*	*46*	*4*	*118*	*120*	*433,98*	*247*	*43*	*0,0*	*24*	*24,00*	–	–	–	–	–	*13*	13
171	*1051*	*A*	*46*	*5*	*18*	*20*	*434,48*	*223*	*39*	*0,0*	*28*	*22,40*	–	–	–	–	–	*15*	15
171	1051	A	46	6	18	20	435,98	362	43,1	0,0	37,6	12,7	5,2	0,8	0,0	0,0	0,6	–	–

Leg	Site	Hole	Core	Section	Interval Top Depth	Interval Bottom Depth	Depth (mbsf)	Total counted specimens	*Morozovella* (%)	Morozovelloides (%)	*Acarinina* (%)	Subbotinids (%)	Chiloguemelinids (%)	*Globanomalina* (%)	*Pseudohastigerina* (%)	*Planorotalites* (%)	*Igorina* (%)	*F index* (%)	Radiolarians
171	1051	A	46	6	120	122	437,00	345	43,2	0,0	36,5	8,7	4,6	2,3	1,2	0,9	2,6	–	–
171	1051	A	47	1	18	20	438,08	408	50,0	0,0	32,8	10,8	4,7	0,2	0,0	0,2	1,2	–	–
171	1051	A	47	1	118	120	439,08	360	53,1	0,0	39,7	4,2	0,6	0,6	0,3	0,3	1,4	–	–
171	*1051*	*A*	*47*	*2*	*17,5*	*19,5*	*439,58*	*293*	*45*	*0,0*	*30*	*19,50*	–	–	–	–	–	*10*	5
171	1051	A	47	2	72	74	440,12	364	42,6	0,0	38,5	12,4	3,3	0,8	0,0	0,3	2,2	–	–
171	1051	A	47	3	18	20	441,08	364	43,7	0,0	34,6	13,2	6,0	0,8	0,0	0,3	1,4	–	–
171	*1051*	*A*	*47*	*3*	*68*	*70*	*441,58*	*282*	*41,8*	*0,0*	*40,7*	*13,10*	–	–	–	–	–	*50*	15
171	1051	A	47	4	15,5	17,5	442,56	362	45,6	0,0	43,1	4,4	4,1	1,4	0,3	0,0	1,1	–	–
171	*1051*	*A*	*47*	*4*	*73*	*75*	*443,13*	*341*	*38,7*	*0,0*	*35,2*	*13,50*	–	–	–	–	–	*10*	–
171	1051	A	47	5	68	70	444,58	360	42,2	0,0	37,8	12,8	3,6	2,2	0,0	0,0	1,4	–	7
171	1051	A	47	6	17	19	445,57	378	48,1	0,0	34,7	8,5	4,5	1,9	0,0	0,5	1,9	–	–
171	1051	A	47	6	114	116	446,54	406	46,6	0,0	36,0	9,4	6,4	0,5	0,0	0,2	1,0	–	–
171	1051	A	48	1	23	25	447,73	341	39,6	0,0	40,5	10,3	6,5	2,6	0,0	0,0	0,6	–	–
171	1051	A	48	1	118	120	448,68	356	42,1	0,0	38,8	9,8	6,2	2,5	0,0	0,0	0,6	–	–
171	*1051*	*A*	*48*	*2*	*69*	*72*	*449,69*	*322*	*31,4*	*0,0*	*46,3*	*15,00*	–	–	–	–	–	*12*	8
171	1051	A	48	3	17	19	450,67	378	36,2	0,0	53,4	2,9	1,3	2,4	0,0	0,5	3,2	–	–
171	1051	A	48	3	69	73	451,19	342	43,6	0,0	32,2	11,1	3,5	2,3	0,6	2,3	4,4	–	–
171	1051	A	48	3	118	120	451,68	352	34,1	0,0	54,3	4,0	2,8	3,4	0,0	0,3	1,1	–	–
171	*1051*	*A*	*48*	*4*	*24*	*26*	*452,24*	*259*	*46,3*	*0,0*	*31,3*	*7,00*	–	–	–	–	–	*10*	5
171	1051	A	48	4	118	120	453,18	344	36,0	0,0	54,1	4,1	2,3	0,9	0,0	0,0	2,6	–	–
171	1051	A	48	5	18	20	453,68	409	35,0	0,0	53,3	2,9	2,4	2,7	0,2	0,5	2,9	–	–
171	1051	A	48	5	68	70	454,18	364	35,2	0,0	50,3	6,3	3,3	1,1	0,0	0,3	3,6	–	–
171	1051	A	48	6	18	20	455,18	348	43,1	0,0	39,4	12,6	2,6	0,3	0,0	0,9	1,1	–	–

Table S3. Relative abundances (%) of *Morozovella* species at Site 1051.

Hole	Core	Section	Interval (cm ±1)	Sample Depth (mbsf)	No. Total counted specimens	N. Morozovella	*Morozovella* (%)	*M.aequa* (%)	*M. subbotinae* (%)	*M. gracilis* (%)	*M. marginodentata* (%)	*M. lensiformis* (%)	*M. formosa* (%)	*M. crater* (%)	*M. aragonensis* (%)	*M. caucasica* (%)
1051A	40	1	21	369,9	335	11	3	0,0	0,0	0,0	0,0	0,0	0,0	2,7	0,3	0,0
1051A	40	1	121	370,9	311	27	7,4	0,0	0,0	0,0	0,0	0,0	0,0	6,1	1,3	0,0
1051A	40	3	121	373,9	303	21	5,5	0,0	0,0	0,0	0,0	0,0	0,0	4,2	1,3	0,0
1051A	40	5	71	376,4	314	10	2,6	0,0	0,0	0,0	0,0	0,0	0,0	1,3	1,1	0,2
1051A	40	cc	21	377	338	40	10,5	0,0	0,0	0,0	0,0	0,0	0,0	4,4	6,1	0,0
1051A	41	1	21	379,5	301	37	9,8	0,0	0,0	0,0	0,0	0,0	0,0	3,6	5,2	1,0
1051A	42	1	21	390,1	219	20	6	0,0	0,0	0,0	0,0	0,7	0,0	4,0	1,3	0,0
1051A	42	3	121	394,1	211	24	6,2	0,3	0,0	0,0	0,0	1,3	0,5	3,1	1,0	0,0
1051A	42	6	26	397,65	385	39	9,8	0,0	0,0	0,0	0,0	3,1	0,7	4,5	1,2	0,3
1051A	43	2	69	401,68	285	43	10,8	0,0	0,0	0,3	0,0	2,6	1,4	5,5	1,0	0,0
1051A	43	4	19	404,18	295	34	8,5	0,0	0,0	0,0	0,0	2,2	0,9	4,3	1,1	0,0
1051A	43	5	69	406,18	336	29	7,1	0,0	0,0	0,0	0,0	2,1	0,5	3,2	1,3	0,0
1051A	44	1	21	409,3	310	72	17,5	0,2	0,0	0,8	0,0	2,2	2,0	8,5	3,8	0,0
1051A	44	1	71	409,8	315	59	14,5	0,5	0,5	1,2	0,3	3,1	0,9	4,0	4,0	0,0
1051A	44	3	21	412,3	332	49	12	0,5	0,5	2,0	0,3	3,0	0,2	3,0	2,5	0,0
1051A	44	4	21	413,8	290	27	13,2	0,0	1,1	1,1	0,0	1,6	1,1	5,2	3,1	0,0
1051A	44	5	69	415,78	327	28	8,5	0,9	1,8	0,6	0,0	1,8	0,0	1,8	1,6	0,0
1051A	44	6	121	417,8	375	53	14,1	0,0	1,5	2,4	0,3	1,1	1,3	6,7	0,8	0,0
1051A	45	1	121	419,9	371	63	16,9	2,2	1,6	1,3	1,1	3,1	1,1	3,8	2,7	0,0
1051A	45	3	21	421,9	389	29	7,8	1,0	1,0	0,5	0,6	0,7	1,0	2,4	0,6	0,0
1051A	45	3	71	422,4	352	78	22	1,1	0,0	2,8	1,1	4,0	2,8	7,7	2,5	0,0
1051A	45	3	121	422,9	186	22	11,8	0,0	1,0	1,1	2,2	1,6	1,1	4,8	0,0	0,0
1051A	45	4	23	423,42	350	53	15,1	2,9	1,1	1,7	4,3	1,4	0,3	1,7	1,7	0,0
1051A	45	4	68	423,88	349	34	9,7	0,0	0,3	1,7	2,6	1,4	0,3	3,1	0,3	0,0
1051A	45	4	120	424,4	330	69	20,9	0,0	1,9	5,3	8,4	1,9	0,0	3,4	0,0	0,0
1051A	45	5	18	424,88	343	67	19,5	0,3	2,6	3,8	4,7	2,3	0,3	5,2	0,3	0,0
1051A	45	5	71	425,4	307	55	18	0,3	2,0	2,4	8,1	1,0	0,0	2,9	1,3	0,0
1051A	45	6	72	426,9	333	65	19,5	1,5	3,0	3,3	4,8	2,1	0,6	3,0	1,2	0,0
1051A	45	6	121	427,4	263,0	35	13,3	0,4	2,7	1,9	1,1	1,9	0,8	4,5	0,0	0,0
1051A	45	7	22	427,91	250,0	37	14,8	1,2	2,0	4,4	0,4	1,6	0,4	3,2	1,6	0,0
1051A	45	7	30	427,99	331,0	51	15,4	0,0	1,5	1,8	0,9	1,5	0,3	7,9	1,5	0,0
1051A	45	7	37	428,06	347,0	39	11,2	0,9	1,1	1,1	1,4	0,9	0,6	4,6	0,6	0,0
1051A	45	7	39	428,08	342,0	50	14,6	0,6	2,3	0,6	0,6	1,8	0,9	6,6	1,2	0,0
1051A	45	7	46	428,15	348,0	54	15,5	0,3	2,3	2,6	3,2	0,9	0,0	5,6	0,6	0,0
1051A	45	8	3	428,19	384,0	64	16,7	0,0	1,6	1,6	4,7	0,3	0,5	6,7	1,3	0,0
1051A	45	8	8	428,24	359,0	45	12,5	0,3	1,7	1,9	3,8	0,8	0,6	3,1	0,3	0,0
1051A	46	1	5	428,34	325,0	95	29,2	1,2	5,2	2,8	13,2	1,2	1,0	4,0	0,6	0,0
1051A	46	1	11	428,4	340,0	95	27,9	0,3	2,6	1,2	12,6	1,5	0,6	7,6	1,5	0,0
1051A	46	1	15	428,44	329	113	34,3	1,2	4,9	7,0	10,8	4,0	0,6	5,2	0,6	0,0
1051A	46	1	19	428,48	336	124	36,9	0,6	4,5	9,8	10,7	2,7	1,2	6,5	0,9	0,0

1051A	46	1	21	428,5	245	111	53,5	0,0	8,0	16,1	8,4	6,5	0,6	8,4	5,5	0,0
1051A	46	2	21	430	315	130	54	1,0	7,7	15,6	12,6	3,6	2,9	7,3	3,3	0,0
1051A	46	2	71	430,5	242	101	42	1,2	4,2	7,9	5,4	5,0	2,6	12,4	3,3	0,0
1051A	46	4	71	433,5	248	95	38,3	0,0	4,4	10,2	16,5	1,6	0,0	5,6	0,0	0,0
1051A	46	4	119	433,98	247	98	43	2,5	3,7	9,7	12,5	3,2	1,5	8,5	1,4	0,0
1051A	46	5	19	434,48	223	85	39	2,3	3,3	4,2	13,2	4,1	0,6	11,3	0,0	0,0
1051A	47	2	18,5	439,57	293	132	45	3,5	6,8	7,8	9,2	4,8	1,0	11,9	0,0	0,0
1051A	47	3	69	441,58	282	118	41,8	4,6	6,0	0,7	11,3	2,8	0,4	16,0	0,0	0,0
1051A	47	5	24	444,13	341	132	38,7	2,1	5,0	3,2	19,1	3,8	0,3	5,2	0,0	0,0
1051A	48	2	70	449,69	322	101	31,4	3,1	4,7	2,8	7,8	3,7	0,6	8,7	0,0	0,0
1051A	48	4	25	452,24	259	138	46,3	5,1	9,0	4,0	4,6	5,5	0,0	18,2	0,0	0,0

Table S4. Test-size diameters of *Morozovella* species from the >300 μm fraction at Site 1051 with average values and standard deviations (1σ).

Sample A (443.58 mbsf) – pre EECO interval					
M. subbotinae		*M. aequa*	*M. marginodentata*	*M. gracilis*	*M. crater*
519	438	509	518	519	635
513	425	503	402	421	622
509	411	458	387		563
504	406	442			509
475	405	441			503
472	399	437			462
467	399	436			450
467	392	436			435
466	391	430			424
462	385	398			418
457	384	390			402
455	383	385			340
452	378	362			
449	372	355			
448	369	348			
444	357				
441	355				
438	354				

Sample B (433.5 mbsf) – pre EECO interval								
M. subbotinae		*M. aequa*	*M. marginodentata*	*M. gracilis*	*M. crater*		*M. aragonensis*	*M. lensiformis*
560	427	506	449	451	607	467	499	532
549	425	479	405	448	587	466	498	518
511	424	472		405	586	463	411	455
498	424	470		388	585	459		433
496	423	458			555	457		403
494	422	433			540	455		
492	421	416			538	454		

487	420	415			533	448		
486	420	409			532	447		
468	419	408			524	446		
463	419	404			516	438		
462	418	399			508	438		
458	418	378			506	437		
458	410	376			503	435		
448	410	369			497	429		
448	408				496	429		
442	406				488	418		
440	404				480	409		
435	395				479			
435	392				478			
434	390				476			
431	385				475			
430	381				473			
428					471			

Sample C (425.4 mbsf) – pre J – initial EECO interval

M. subbotinae		*M. aequa*	*M. marginodentata*		*M. gracilis*	*M. crater*		*M. aragonensis*	*M. lensiformis*	*M. formosa*
449	405	425	474	400	453	556	447	504	492	571
440	403	405	460	400	437	530	443	502	478	568
437	399	399	457	396	436	518	433	480	439	567
436	399		452	390	422	516	433	457	428	553
432	396		451	357	419	508	431	444	410	452
429	391		447	355	418	500	429	441	401	427
425	391		439	354	385	496	429	423	397	
424	389		432	347	385	483	423	420	396	
419	386		428	343		483	410	411	395	
417	380		423	340		478	394	403	371	
416	375		421	338		458		403		
413	374		420	337		458				
405	352		418	328		457				
405	352		404			452				

Sample D (411.8 mbsf) – main EECO phase

M. subbotinae	*M. aequa*	*M. gracilis*	*M. crater*		*M. aragonensis*	*M. lensiformis*	*M. formosa*
467	473	457	675	465	537	504	519
454	468	397	622	464	531	501	516
454	460	387	574	457	529	484	
453	459	377	558	457	513	470	
445	425		538	453	505	461	
438	402		531	451	474	456	
439	401		531	450	465	452	
439	401		520	443	462	443	
437	399		515	443	450	438	
431	380		510	442	449	431	
430			504	435	441	424	
428			504	429	420	421	
427			503	424	407	416	

409			501	423	405	410	
404			491	421	383	402	
386			487	416		400	
340			487	411		395	
			482	403		386	
			472			380	
			471			374	
			470			372	
			468			358	
			467			342	

Sample E (395.65 mbsf) – main EECO phase

M. crater			*M. aragonensis*		*M. lensiformis*	*M. formosa*
612	477	441	522	451	489	509
595	475	440	521	451	466	485
593	475	439	519	451	463	478
567	474	439	512	449	458	471
543	473	438	512	449	456	471
540	473	438	509	446	455	445
532	472	438	491	445	455	
525	471	438	486	445	452	
523	471	437	486	445	448	
516	470	433	485	441	435	
515	469	433	483	429	429	
514	466	432	483	420	429	
510	465	432	482	418	428	
507	463	432	482	418	426	
501	461	431	482	415	425	
500	460	430	478	415	419	
498	460	429	477	413	416	
498	459	427	477	413	411	
496	456	427	476	411	410	
495	454	424	474	411	396	
494	453	421	469	406	395	
494	453	419	468	404	395	
492	452	419	466	404	391	
492	451	419	465	402	384	
489	450	416	465	398	373	
487	450	416	465	395	372	
486	450	413	465	395	367	
486	449	413	465	394	359	
485	449	411	460	394	359	
482	448	408	459	384	348	
481	447	406	459	363		
481	443	405	458	343		
478	442		453			

M. formosa max-diameter standard deviation (1σ)	–	–	59,6	1,5	19,2
M. formosa average max-diameter (μm)	–	–	522,8	517,5	477
M. lensiformis max-diameter standard deviation (1σ)	–	49,4	36,8	43,5	36,6
M. lensiformis average max-diameter (μm)	–	468,2	420,7	422,6	417
M. aragonensis max-diameter standard deviation (1σ)	–	41,2	35,6	47,9	39,5
M. aragonensis average max-diameter (μm)	–	469,3	444,4	464,7	449
M. crater max-diameter standard deviation (1σ)	85,8	48,8	40,6	55,3	41,5
M. crater average max-diameter (μm)	480,3	486,4	465,2	482,1	466,63727
M. gracilis max-diameter standard deviation (1σ)	49	27,2	22,6	31,1	–
M. gracilis average max-diameter (μm)	470,0	423,0	419,4	404,5	–
M. marginodentata max-diameter standard deviation (1σ)	58,7	22	44,6	–	–
M. marginodentata average max-diameter (μm)	435,8	427,0	400,4	–	–
M. aequa max-diameter standard deviation (1σ)	47,2	40,4	11,1	33	–
M. aequa average max-diameter (μm)	422,0	426,1	409,7	426,8	–
M. subbotinae max-diameter standard deviation (1σ)	47,2	39,6	24,6	29,4	–
M. subbotinae average max-diameter (μm)	428,9	440,7	405	428,3	–
Sample depth (mbsf)	443,58	433,5	425,4	411,8	395,65
Samples	A	B	C	D	E

Table S5. Carbon and oxygen stable-isotope data from restricted size-fraction monospecific specimens of *Morozovella* and from restricted size-fraction specimens of *Acarinina* spp. and *Subbotina* spp. across the early Eocene at the ODP Sites 1051.

Sample A (443.58 mbsf) – pre EECO interval												
Fraction	*Subbotina* $\delta^{13}C$ (‰)	*Subbotina* $\delta^{18}O$ (‰)	*Acarinina* $\delta^{13}C$ (‰)	*Acarinina* $\delta^{18}O$ (‰)	*M. crater* $\delta^{13}C$ (‰)	*M. crater* $\delta^{18}O$ (‰)	*M. gracilis* $\delta^{13}C$ (‰)	*M. gracilis* $\delta^{18}O$ (‰)	*M. marginodentata* $\delta^{13}C$ (‰)	*M. marginodentata* $\delta^{18}O$ (‰)	*M. subbotinae* $\delta^{13}C$ (‰)	*M. subbotinae* $\delta^{18}O$ (‰)
150	0,61	-0,89	2,05	-1,41	2,09	-1,74	2,11	-1,89	1,98	-1,72	2,14	-1,27
210	1,30	-1,25	2,62	-1,68	2,04	-1,38	2,13	-2,23	2,37	-1,84	2,19	-1,32
250	0,92	-1,17	2,95	-2,10	2,53	-1,67	2,48	-2,22	2,40	-2,21	2,47	-1,55
300	–	–	–	–	2,92	-1,57	–	–	–	–	2,80	-1,52

Sample B (433.5 mbsf) – pre EECO interval														
Fraction	*Subbotina* $\delta^{13}C$ (‰)	*Subbotina* $\delta^{18}O$ (‰)	*Acarinina* $\delta^{13}C$ (‰)	*Acarinina* $\delta^{18}O$ (‰)	*M. aragonensis* $\delta^{13}C$ (‰)	*M. aragonensis* $\delta^{18}O$ (‰)	*M. crater* $\delta^{13}C$ (‰)	*M. crater* $\delta^{18}O$ (‰)	*M. gracilis* $\delta^{13}C$ (‰)	*M. gracilis* $\delta^{18}O$ (‰)	*M. marginodentata* $\delta^{13}C$ (‰)	*M. marginodentata* $\delta^{18}O$ (‰)	*M. subbotinae* $\delta^{13}C$ (‰)	*M. subbotinae* $\delta^{18}O$ (‰)
150	0,76	-0,80	2,32	-1,41	1,96	-1,49	2,33	-1,07	2,01	-1,74	1,96	-1,70	2,23	-0,90
210	0,84	-1,13	2,22	-1,54	2,08	-1,73	2,35	-1,77	2,36	-1,90	2,33	-1,75	2,21	-1,28
250	0,44	-1,24	2,48	-1,73	2,67	-2,28	2,63	-2,08	2,63	-1,97	2,54	-1,82	2,57	-1,89
300	–	–	2,29	-2,19	–	–	2,93	-2,16	2,92	-1,75	–	–	–	–

Sample C (425.4 mbsf) –initial EECO interval														
Fraction	*Subbotina* $\delta^{13}C$ (‰)	*Subbotina* $\delta^{18}O$ (‰)	*Acarinina* $\delta^{13}C$ (‰)	*Acarinina* $\delta^{18}O$ (‰)	*M. aragonensis* $\delta^{13}C$ (‰)	*M. aragonensis* $\delta^{18}O$ (‰)	*M. crater* $\delta^{13}C$ (‰)	*M. crater* $\delta^{18}O$ (‰)	*M. gracilis* $\delta^{13}C$ (‰)	*M. gracilis* $\delta^{18}O$ (‰)	*M. marginodentata* $\delta^{13}C$ (‰)	*M. marginodentata* $\delta^{18}O$ (‰)	*M. subbotinae* $\delta^{13}C$ (‰)	*M. subbotinae* $\delta^{18}O$ (‰)
150	0,49	-1,13	2,06	-1,70	1,61	-1,59	1,60	-1,80	1,74	-1,80	1,54	-1,74	1,67	-1,53
210	0,35	-1,04	2,17	-1,64	1,82	-1,79	1,99	-1,67	1,81	-1,94	1,99	-1,65	1,77	-1,55
250	0,84	-1,38	2,36	-1,97	2,16	-1,81	2,15	-1,75	2,21	-2,04	2,11	-1,65	1,90	-1,99
300	–	–	2,36	-1,75	2,35	-2,12	2,62	-1,91	2,66	-1,90	2,06	-1,90	2,28	-1,86

Sample D (411.8 mbsf) – main EECO phase												
Fraction	*Subbotina* $\delta^{13}C$ (‰)	*Subbotina* $\delta^{18}O$ (‰)	*Acarinina* $\delta^{13}C$ (‰)	*Acarinina* $\delta^{18}O$ (‰)	*M. aragonensis* $\delta^{13}C$ (‰)	*M. aragonensis* $\delta^{18}O$ (‰)	*M. crater* $\delta^{13}C$ (‰)	*M. crater* $\delta^{18}O$ (‰)	*M. gracilis* $\delta^{13}C$ (‰)	*M. gracilis* $\delta^{18}O$ (‰)	*M. subbotinae* $\delta^{13}C$ (‰)	*M. subbotinae* $\delta^{18}O$ (‰)
150	0,73	-0,93	1,75	-1,57	1,52	-1,82	1,43	-1,87	1,25	-1,37	1,24	-1,50
210	0,61	-0,92	2,03	-1,45	1,80	-1,41	1,68	-1,25	1,42	-1,68	1,72	-1,11
250	0,99	-0,62	2,02	-1,36	2,24	-1,60	2,24	-1,39	1,98	-1,67	2,09	-1,62
300	–	–	2,50	-1,13	2,60	-1,34	2,76	-1,29	–	–	2,47	-1,64

Sample E (395.65 mbsf) – main EECO phase								
Fraction	*Subbotina* $\delta^{13}C$ (‰)	*Subbotina* $\delta^{18}O$ (‰)	*Acarinina* $\delta^{13}C$ (‰)	*Acarinina* $\delta^{18}O$ (‰)	*M. aragonensis* $\delta^{13}C$ (‰)	*M. aragonensis* $\delta^{18}O$ (‰)	*M. crater* $\delta^{13}C$ (‰)	*M. crater* $\delta^{18}O$ (‰)
150	0,65	-1,09	0,93	-1,74	0,97	-1,51	0,81	-1,38
210	0,86	-1,48	1,49	-1,59	1,35	-1,79	1,24	-1,55
250	–	–	1,54	-1,69	1,48	-1,77	1,69	-1,56
300	–	–	–	–	1,86	-1,77	1,83	-1,55
350	–	–	–	–	1,95	-1,74	2,31	-1,66

Table S1. Stable isotope composition of early Eocene bulk carbonate at Site 1263B.

Leg	Site	Hole	Core	Section	Interval (cm ±1)	Sample Depth (mbsf)	Sample Depth (rmcd)	$\delta^{13}C$ (‰)	$\delta^{18}O$ (‰)
208	1263	B	20	2	11	206,5	240,21	1,59	-0,13
208	1263	B	20	2	42	206,81	240,52	1,36	-0,39
208	1263	B	20	2	71	207,1	240,81	1,66	-0,27
208	1263	B	20	2	93	207,32	241,03	1,71	-0,17
208	1263	B	20	2	141	207,8	241,51	1,72	-0,21
208	1263	B	20	3	12	208,01	241,81	1,60	-0,26
208	1263	B	20	3	43	208,32	242,03	1,85	-0,11
208	1263	B	20	3	71	208,6	242,31	1,84	-0,19
208	1263	B	20	3	101	208,9	242,61	1,79	-0,19
208	1263	B	20	3	133	209,22	242,93	1,83	-0,20
208	1263	B	20	4	11	209,5	243,21	1,93	-0,15
208	1263	B	20	4	41	209,8	243,51	1,84	-0,14
208	1263	B	20	4	71	210,1	243,81	1,76	-0,26
208	1263	B	20	4	101	210,4	244,11	1,94	-0,23
208	1263	B	20	4	131	210,7	244,41	1,83	-0,17
208	1263	B	20	5	11	211	244,71	1,77	-0,19
208	1263	B	20	5	41	211,3	245,01	1,50	-0,30
208	1263	B	20	5	71	211,6	245,31	1,70	-0,21
208	1263	B	20	5	101	211,9	245,61	1,77	-0,34
208	1263	B	20	5	131	212,2	245,91	1,82	-0,16
208	1263	B	20	6	1,5	212,4	246,11	1,74	-0,32
208	1263	B	20	6	31	212,7	246,41	1,59	-0,19
208	1263	B	20	6	61	213	246,71	1,34	-0,48
208	1263	B	20	6	92	213,31	247,02	1,38	-0,60
208	1263	B	20	6	121	213,6	247,31	1,88	-0,32
208	1263	B	20	7	1	213,9	247,61	1,86	-0,32
208	1263	B	20	7	31	214,2	247,91	1,83	-0,31
208	1263	B	20	7	61	214,5	248,279	1,92	-0,21
208	1263	B	21	1	1	214,4	250,393	1,60	-0,40
208	1263	B	21	1	31	214,7	250,711	1,79	-0,29
208	1263	B	21	1	61	215	251,008	1,64	-0,32
208	1263	B	21	1	91	215,3	251,281	1,44	-0,34
208	1263	B	21	1	121	215,6	251,554	1,43	-0,59
208	1263	B	21	1	149	215,88	251,812	1,26	-0,67
208	1263	B	21	2	31	216,2	252,12	1,61	-0,22
208	1263	B	21	2	61	216,5	252,42	1,57	-0,33
208	1263	B	21	2	91,5	216,8	252,72	1,35	-0,66
208	1263	B	21	2	121	217,1	253,02	1,84	-0,21
208	1263	B	21	3	1	217,4	253,32	1,77	-0,25
208	1263	B	21	3	31	217,7	253,62	1,74	-0,33
208	1263	B	21	3	61	218	253,92	1,73	-0,33
208	1263	B	21	3	91	218,3	254,22	1,76	-0,12
208	1263	B	21	3	121	218,6	254,52	1,56	-0,24
208	1263	B	21	4	1	218,9	254,82	1,74	-0,30

208	1263	B	21	4	31	219,2	255,12	1,23	-0,59
208	1263	B	21	4	61	219,5	255,42	1,53	-0,40
208	1263	B	21	4	91	219,8	255,72	1,54	-0,20
208	1263	B	21	4	121	220,1	256,02	1,49	-0,08
208	1263	B	21	5	1	220,4	256,32	1,22	-0,27
208	1263	B	21	5	31	220,7	256,62	1,37	-0,35
208	1263	B	21	5	61	221	256,92	1,42	-0,12
208	1263	B	21	5	91	221,3	257,22	1,45	-0,29
208	1263	B	21	5	121	221,6	257,512	1,53	-0,24
208	1263	B	21	6	1	221,9	257,797	1,58	-0,13
208	1263	B	21	6	31	222,2	258,086	1,49	-0,20
208	1263	B	21	6	61	222,5	258,372	1,55	-0,35
208	1263	B	21	6	91	222,8	258,659	1,56	-0,26
208	1263	B	21	6	121	223,1	258,946	1,47	-0,13
208	1263	B	21	7	1	223,4	259,230	1,26	-0,41
208	1263	B	21	7	31	223,7	259,519	1,38	-0,13
208	1263	B	21	7	61	224	259,806		-0,28
208	1263	B	21	cc	16	224,3	260,106	1,50	-0,23
208	1263	B	22	1	21	224,1	262,240	1,18	-0,31
208	1263	B	22	1	51	224,4	262,622	1,02	-0,40
208	1263	B	22	1	81,5	224,7	262,986	1,14	-0,59
208	1263	B	22	1	111	225	263,307	1,29	-0,57
208	1263	B	22	1	141	225,3	263,629	1,36	-0,42
208	1263	B	22	2	21	225,6	263,93	1,46	-0,41
208	1263	B	22	2	51	225,9	264,23	1,50	-0,32
208	1263	B	22	2	81	226,2	264,53	1,50	-0,47
208	1263	B	22	2	111	226,5	264,83	1,41	-0,43
208	1263	B	22	2	141	226,8	265,13	1,33	-0,51
208	1263	B	22	3	21	227,1	265,43	1,38	-0,36
208	1263	B	22	3	51	227,4	265,73	1,29	-0,45
208	1263	B	22	3	81	227,7	266,03	1,42	-0,42
208	1263	B	22	3	111	228	266,33	1,32	-0,37
208	1263	B	22	3	141	228,3	266,63	1,30	-0,40
208	1263	B	22	4	21	228,6	266,93	1,38	-0,29
208	1263	B	22	4	51	228,9	267,23	1,39	-0,21
208	1263	B	22	4	81	229,2	267,53	1,32	-0,28
208	1263	B	22	4	111	229,5	267,83	1,06	-0,52
208	1263	B	22	4	141	229,8	268,13	1,00	-0,52
208	1263	B	22	5	21	230,1	268,43	1,19	-0,51
208	1263	B	22	5	51	230,4	268,73	1,20	-0,31
208	1263	B	22	5	81	230,7	269,03	1,02	-0,46
208	1263	B	22	5	111	231	269,33	0,97	-0,64
208	1263	B	22	5	141	231,3	269,63	1,17	-0,47
208	1263	B	22	6	21	231,6	269,93	1,24	-0,34
208	1263	B	22	6	71	232,1	270,43	1,23	-0,38
208	1263	B	22	6	121	232,6	270,93	1,18	-0,41
208	1263	B	22	7	21	233,1	271,43	1,19	-0,37
208	1263	B	22	cc	1	233,61	271,93	1,22	-0,28

208	1263	B	23	1	41	233,8	274,258	1,06	-0,32
208	1263	B	23	1	91	234,3	274,814	0,97	-0,18
208	1263	B	23	1	141	234,8	275,227	0,63	-0,66
208	1263	B	23	2	41	235,3	275,639	0,92	-0,58
208	1263	B	23	2	91	235,8	276,090	0,91	-0,48
208	1263	B	23	2	141	236,3	276,604	0,92	-0,69
208	1263	B	23	3	41	236,8	277,124	1,12	-0,47
208	1263	B	23	3	91	237,3	277,643	0,99	-0,61
208	1263	B	23	3	141	237,8	278,129	1,15	-0,49
208	1263	B	23	4	41	238,3	278,596	1,04	-0,50
208	1263	B	23	4	91	238,8	279,064	1,07	-0,51
208	1263	B	23	4	141	239,3	279,616	0,87	-0,60
208	1263	B	23	5	41	239,8	280,232	0,95	-0,54
208	1263	B	23	5	91	240,3	280,772	0,94	-0,46
208	1263	B	23	6	1	240,9	281,380	0,97	-0,66
208	1263	B	23	6	51	241,4	281,879	1,31	-0,36
208	1263	B	23	6	101	241,9	282,375	1,40	-0,42
208	1263	B	23	7	1	242,4	282,871	1,16	-0,52
208	1263	B	23	7	51	242,9	283,272	1,24	-0,50
208	1263	B	24	1	1	242,9	285,147	1,12	-0,34
208	1263	B	24	1	51	243,4	285,689	1,07	-0,39
208	1263	B	24	1	101	243,9	286,240	1,18	-0,41
208	1263	B	24	2	1	244,4	286,778	1,19	-0,35
208	1263	B	24	2	51	244,9	287,309	0,83	-0,49
208	1263	B	24	2	101	245,4	287,760	0,77	-0,65
208	1263	B	24	3	1	245,9	288,19	1,33	-0,42
208	1263	B	24	3	51	246,4	288,69	1,42	-0,42
208	1263	B	24	3	101,5	246,9	289,19	1,30	-0,50
208	1263	B	24	4	1	247,4	289,69	1,38	-0,31
208	1263	B	24	4	51	247,9	290,19	1,17	-0,40
208	1263	B	24	4	101	248,4	290,69	1,31	-0,42
208	1263	B	24	5	1	248,9	291,19	1,29	-0,38
208	1263	B	24	5	51	249,4	291,69	1,37	-0,33
208	1263	B	24	5	101	249,9	292,19	1,23	-0,36
208	1263	B	24	6	11	250,5	292,79	0,97	-0,52
208	1263	B	24	6	61	251	293,219	1,00	-0,55
208	1263	B	24	6	111	251,5	293,649	1,17	-0,35
208	1263	B	24	7	11	252	294,052	1,28	-0,29
208	1263	B	24	cc	1	252,51	294,479	0,90	-0,44
208	1263	B	25	1	31	252,7	295,808	1,25	-0,34
208	1263	B	25	1	81	253,2	296,325	1,19	-0,40
208	1263	B	25	1	131	253,7	296,827	1,26	-0,41
208	1263	B	25	2	21	254,1	297,168	1,31	-0,35

Table S2. Planktic foraminiferal dissolution and productivity proxies at Site 1263B: the fragmentation index (*F-index*, %), the weight percent coarse fraction (*WPCF*, %) and the plankton benthos ratio (*P/B*, %).

Leg	Site	Hole	Core	Section	Interval (cm ±1)	Sample Depth (mbsf)	Sample Depth (rmcd)	*WPCF* (%)	*F-Index* (%)	*P/B* %
208	1263	B	20	2	11	206,5	240,21	1,18	23,53	98,53
208	1263	B	20	2	42	206,81	240,52	1,25	–	–
208	1263	B	20	2	71	207,1	240,81	0,03	15,30	97,70
208	1263	B	20	2	93	207,32	241,03	1,67	–	–
208	1263	B	20	2	141	207,8	241,51	1,50	–	–
208	1263	B	20	3	12	208,01	241,81	2,09	15,33	99,10
208	1263	B	20	3	43	208,32	242,03	1,51	–	–
208	1263	B	20	3	71	208,6	242,31	1,27	–	–
208	1263	B	20	3	101	208,9	242,61	1,35	36,70	95,70
208	1263	B	20	3	133	209,22	242,93	1,86	–	–
208	1263	B	20	4	11	209,5	243,21	1,12	–	–
208	1263	B	20	4	41	209,8	243,51	1,80	34,70	97,30
208	1263	B	20	4	71	210,1	243,81	1,96	21,90	99,30
208	1263	B	20	4	101	210,4	244,11	2,01	–	–
208	1263	B	20	4	131	210,7	244,41	0,76	–	–
208	1263	B	20	5	11	211	244,71	1,03	33,83	97,00
208	1263	B	20	5	41	211,3	245,01	1,26	36,17	98,46
208	1263	B	20	5	71	211,6	245,31	1,25	26,27	96,99
208	1263	B	20	5	101	211,9	245,61	0,84	–	–
208	1263	B	20	5	131	212,2	245,91	1,38	34,63	98,20
208	1263	B	20	6	1,5	212,4	246,11	0,98	–	–
208	1263	B	20	6	31	212,7	246,41	1,15	40,81	98,74
208	1263	B	20	6	61	213	246,71	0,94	48,74	97,37
208	1263	B	20	6	92	213,31	247,02	0,38	58,00	98,30
208	1263	B	20	6	121	213,6	247,31	1,00	–	–
208	1263	B	20	7	1	213,9	247,61	0,88	–	–
208	1263	B	20	7	31	214,2	247,91	0,80	40,99	95,43
208	1263	B	20	7	61	214,5	248,279	0,79	–	–
208	1263	B	21	1	1	214,4	250,393	0,85	–	–
208	1263	B	21	1	31	214,7	250,711	1,26	16,80	99,10
208	1263	B	21	1	61	215	251,008	1,07	–	–
208	1263	B	21	1	91	215,3	251,281	1,35	–	–
208	1263	B	21	1	121	215,6	251,554	0,87	–	–
208	1263	B	21	1	149	215,88	251,812	2,03	32,95	98,02
208	1263	B	21	2	31	216,2	252,12	2,00	–	–
208	1263	B	21	2	61	216,5	252,42	1,60	27,38	98,53
208	1263	B	21	2	91,5	216,8	252,72	1,28	51,82	95,98
208	1263	B	21	2	121	217,1	253,02	1,03	19,93	98,63
208	1263	B	21	3	1	217,4	253,32	0,91	–	–
208	1263	B	21	3	31	217,7	253,62	1,17	36,61	97,14
208	1263	B	21	3	61	218	253,92	1,05	–	–
208	1263	B	21	3	91	218,3	254,22	0,07	20,34	98,07

208	1263	B	21	3	121	218,6	254,52	0,92	–	–
208	1263	B	21	4	1	218,9	254,82	0,86	–	–
208	1263	B	21	4	31	219,2	255,12	0,46	–	–
208	1263	B	21	4	61	219,5	255,42	1,35	30,14	97,61
208	1263	B	21	4	91	219,8	255,72	1,41	–	–
208	1263	B	21	4	121	220,1	256,02	0,77	37,30	96,82
208	1263	B	21	5	1	220,4	256,32	1,28	35,40	97,77
208	1263	B	21	5	31	220,7	256,62	0,97	–	–
208	1263	B	21	5	61	221	256,92	0,90	–	–
208	1263	B	21	5	91	221,3	257,22	1,08	28,75	96,56
208	1263	B	21	5	121	221,6	257,512	0,94	–	–
208	1263	B	21	6	1	221,9	257,797	0,92	34,63	96,95
208	1263	B	21	6	31	222,2	258,086	1,33	–	–
208	1263	B	21	6	61	222,5	258,372	0,72	–	–
208	1263	B	21	6	91	222,8	258,659	0,95	–	–
208	1263	B	21	6	121	223,1	258,946	0,65	35,04	98,28
208	1263	B	21	7	1	223,4	259,230	1,28	–	–
208	1263	B	21	7	31	223,7	259,519	1,28	–	–
208	1263	B	21	7	61	224	259,806	–	–	–
208	1263	B	21	7	16	224,3	260,106	1,04	–	–
208	1263	B	22	1	21	224,1	262,240	0,42	89,00	88,25
208	1263	B	22	1	51	224,4	262,622	0,63	–	–
208	1263	B	22	1	81,5	224,7	262,986	0,92	–	–
208	1263	B	22	1	111	225	263,307	1,54	18,90	98,40
208	1263	B	22	1	141	225,3	263,629	1,88	–	–
208	1263	B	22	2	21	225,6	263,93	1,29	–	–
208	1263	B	22	2	51	225,9	264,23	1,17	–	–
208	1263	B	22	2	81	226,2	264,53	1,33	18,70	95,00
208	1263	B	22	2	111	226,5	264,83	1,69	–	–
208	1263	B	22	2	141	226,8	265,13	1,06	–	–
208	1263	B	22	3	21	227,1	265,43	0,86	18,98	98,79
208	1263	B	22	3	51	227,4	265,73	0,97	–	–
208	1263	B	22	3	81	227,7	266,03	1,50	–	–
208	1263	B	22	3	111	228	266,33	1,69	–	–
208	1263	B	22	3	141	228,3	266,63	1,26	21,00	98,00
208	1263	B	22	4	21	228,6	266,93	1,32	–	–
208	1263	B	22	4	51	228,9	267,23	1,71	–	–
208	1263	B	22	4	81	229,2	267,53	1,41	16,38	99,11
208	1263	B	22	4	111	229,5	267,83	1,58	43,36	97,59
208	1263	B	22	4	141	229,8	268,13	1,99	28,80	98,80
208	1263	B	22	5	21	230,1	268,43	1,77	16,80	98,80
208	1263	B	22	5	51	230,4	268,73	2,01	19,80	99,00
208	1263	B	22	5	81	230,7	269,03	2,19	–	–
208	1263	B	22	5	111	231	269,33	1,85	37,30	97,38
208	1263	B	22	5	141	231,3	269,63	1,74	–	–
208	1263	B	22	6	21	231,6	269,93	1,81	–	–
208	1263	B	22	6	71	232,1	270,43	1,40	–	–
208	1263	B	22	6	121	232,6	270,93	1,29	–	–

208	1263	B	22	7	21	233,1	271,43	1,23	–	–
208	1263	B	22	7	1	233,61	271,93	0,86	–	–
208	1263	B	23	1	41	233,8	274,258	0,56	26,50	98,30
208	1263	B	23	1	91	234,3	274,814	1,32	39,82	97,23
208	1263	B	23	1	141	234,8	275,227	1,77	34,06	98,08
208	1263	B	23	2	41	235,3	275,639	2,63	45,20	99,70
208	1263	B	23	2	91	235,8	276,090	1,84	–	–
208	1263	B	23	2	141	236,3	276,604	2,27	–	–
208	1263	B	23	3	41	236,8	277,124	1,54	20,20	99,20
208	1263	B	23	3	91	237,3	277,643	1,48	13,10	99,40
208	1263	B	23	3	141	237,8	278,129	1,03	45,00	97,00
208	1263	B	23	4	41	238,3	278,596	0,51	–	–
208	1263	B	23	4	91	238,8	279,064	1,06	49,60	97,00
208	1263	B	23	4	141	239,3	279,616	1,75	21,60	98,30
208	1263	B	23	5	41	239,8	280,232	1,75	24,19	98,29
208	1263	B	23	5	91	240,3	280,772	1,75	26,27	97,58
208	1263	B	23	6	1	240,9	281,380	1,67	63,00	92,60
208	1263	B	23	6	51	241,4	281,879	1,28	–	–
208	1263	B	23	6	101	241,9	282,375	1,00	11,00	95,30
208	1263	B	23	6	1	242,4	282,871	0,84	–	–
208	1263	B	23	7	51	242,9	283,272	1,18	19,57	97,11
208	1263	B	24	1	1	242,9	285,147	1,55	27,10	97,00
208	1263	B	24	1	51	243,4	285,689	1,05	23,30	97,00
208	1263	B	24	1	101	243,9	286,240	1,42	–	–
208	1263	B	24	2	1	244,4	286,778	2,40	–	–
208	1263	B	24	2	51	244,9	287,309	3,59	50,47	96,41
208	1263	B	24	2	101	245,4	287,760	1,45	30,45	97,47
208	1263	B	24	3	1	245,9	288,19	1,61	–	–
208	1263	B	24	3	51	246,4	288,69	1,27	–	–
208	1263	B	24	3	101,5	246,9	289,19	2,29	–	–
208	1263	B	24	4	1	247,4	289,69	2,23	–	–
208	1263	B	24	4	51	247,9	290,19	1,20	–	–
208	1263	B	24	4	101	248,4	290,69	1,55	–	–
208	1263	B	24	5	1	248,9	291,19	2,19	–	–
208	1263	B	24	5	51	249,4	291,69	1,88	22,90	95,40
208	1263	B	24	5	101	249,9	292,19	1,25	28,02	97,34
208	1263	B	24	6	11	250,5	292,79	0,74	37,65	97,98
208	1263	B	24	6	61	251	293,219	0,90	37,60	96,24
208	1263	B	24	6	111	251,5	293,649	0,77	43,54	92,59
208	1263	B	24	7	11	252	294,052	1,29	47,62	93,68
208	1263	B	24	7	1	252,51	294,479	2,16	54,50	95,32
208	1263	B	25	1	31	252,7	295,808	1,15	15,33	98,51
208	1263	B	25	1	81	253,2	296,325	2,25	16,55	96,60
208	1263	B	25	1	131	253,7	296,827	2,06	–	–
208	1263	B	25	2	21	254,1	297,168	2,95	17,80	98,80

Table S3. Relative abundances (%) of planktic foraminiferal genera at Site 1263B.

Leg	Site	Hole	Core	Section	Interval (cm ±1)	Sample Depth (mbsf)	Sample Depth (rmcd)	*Morozovella* (%)	*Acarinina* (%)	*Subbotina* (%)	*S. semni* (%)	Chiloguembelinids (%)	*Igorina* (%)	*Planorotalites* (%)	*Globanomalina* (%)	*Catapsydrax* (%)	*G. nuttalli* (%)	No. Total counted specimens
208	1263	B	20	2	42	206,81	240,52	5,7	77,1	6,3	5,4	0,0	3,0	1,2	1,5	0,0	0,0	336
208	1263	B	20	2	71	207,1	240,81	4,7	68,7	16,6	6,1	0,0	0,0	2,0	0,0	1,6	0,3	342
208	1263	B	20	3	12	208,01	241,81	4,2	69,2	8,8	8,2	0,0	5,1	1,8	2,7	0,0	0,0	331
208	1263	B	20	3	101	208,9	242,61	11,1	68,5	13,5	4,5	0,0	0,0	1,2	0,0	0,9	0,3	333
208	1263	B	20	4	41	209,8	243,51	12,3	69,8	11,4	5,0	0,7	0,0	0,5	0,0	0,3	0,0	397
208	1263	B	20	4	71	210,1	243,81	11,2	73,9	7,4	6,5	0,3	0,0	0,7	0,0	0,0	0,0	456
208	1263	B	20	5	11	211	244,71	4,2	81,7	7,0	5,6	0,0	0,6	0,6	0,3	0,0	0,0	356
208	1263	B	20	5	41	211,3	245,01	3,9	85,2	6,5	2,9	0,0	0,8	0,0	0,0	0,0	0,8	384
208	1263	B	20	5	71	211,6	245,31	14,3	70,8	9,3	4,7	0,0	0,9	0,0	0,0	0,0	0,0	322
208	1263	B	20	5	131	212,2	245,91	8,6	73,7	8,4	3,3	0,0	1,8	0,7	1,5	0,0	0,0	381
208	1263	B	20	6	31	212,7	246,41	6,1	78,4	8,9	2,8	0,0	0,6	0,6	0,3	0,0	0,3	314
208	1263	B	20	6	61	213	246,71	5,4	81,1	6,1	3,7	0,0	1,0	1,0	1,7	0,0	0,0	296
208	1263	B	20	6	92	213,31	247,02	6,3	45,2	35,0	9,5	4,0	0,0	0,0	0,7	0,0	0,0	274
208	1263	B	20	7	31	214,2	247,91	5,1	86,3	5,1	2,2	0,0	0,3	0,0	0,3	0,0	0,6	313
208	1263	B	21	1	31	214,7	250,711	10,5	66,1	13,5	9,3	0,0	0,0	0,6	0,0	0,0	0,0	337
208	1263	B	21	1	149	215,88	251,812	9,8	72,3	7,2	6,3	0,0	2,6	0,0	1,7	0,0	0,0	347
208	1263	B	21	2	61	216,5	252,42	4,8	83,6	4,5	2,1	0,0	1,8	0,6	0,9	0,0	1,8	335
208	1263	B	21	2	91,5	216,8	252,72	5,1	73,1	10,8	4,8	0,0	3,6	0,6	2,1	0,0	0,0	334
208	1263	B	21	2	121,5	217,1	253,02	4,7	82,0	8,9	2,8	0,0	1,1	0,0	0,3	0,0	0,3	361
208	1263	B	21	3	31	217,7	253,62	7,8	77,5	7,5	5,6	0,0	1,3	0,0	0,3	0,0	0,0	306
208	1263	B	21	3	91	218,3	254,22	7,3	80,8	3,4	3,9	0,0	1,7	2,0	0,8	0,0	0,0	355
208	1263	B	21	4	61	219,5	255,42	6,5	82,0	3,8	3,8	0,0	2,2	0,8	0,8	0,0	0,0	367
208	1263	B	21	4	121	220,1	256,02	5,7	85,4	3,9	2,1	0,0	0,6	1,8	0,6	0,0	0,0	335
208	1263	B	21	5	1	220,4	256,32	7,9	82,2	4,6	2,0	0,0	1,8	0,8	0,8	0,0	0,0	394
208	1263	B	21	5	91	221,3	257,22	7,4	79,3	9,4	2,9	0,0	0,6	0,0	0,3	0,0	0,0	309
208	1263	B	21	6	1	221,9	257,797	6,3	81,4	5,8	3,9	0,0	1,8	0,3	0,5	0,0	0,0	381
208	1263	B	21	6	121	223,1	258,946	5,2	85,4	5,5	1,5	0,0	1,5	0,3	0,6	0,0	0,0	343
208	1263	B	21	cc	16	224,3	260,106	10,7	76,9	10,4	0,0	0,0	0,7	0,3	1,0	0,0	0,0	307
208	1263	B	22	1	21	224,1	262,240	4,2	86,7	8,1	1,0	0,0	0,0	0,0	0,0	0,0	0,0	308
208	1263	B	22	1	111	225	263,307	8,8	80,0	9,3	1,1	0,0	0,8	0,0	0,0	0,0	0,0	363
208	1263	B	22	2	81	226,2	264,53	11,9	67,4	14,4	6,3	0,0	0,0	0,0	0,0	0,0	0,0	285
208	1263	B	22	3	21	227,1	265,43	6,7	81,0	10,4	1,8	0,0	0,0	0,0	0,0	0,0	0,0	326
208	1263	B	22	3	141	228,3	266,63	10,2	59,8	28,0	2,0	0,0	0,0	0,0	0,0	0,0	0,0	296
208	1263	B	22	4	21	228,6	266,93	17,5	56,6	24,2	0,0	0,7	1,0	0,0	0,0	0,0	0,0	311
208	1263	B	22	4	81	229,2	267,53	4,2	89,5	5,4	0,9	0,0	0,0	0,0	0,0	0,0	0,0	334
208	1263	B	22	4	111	229,5	267,83	7,4	84,9	7,1	0,0	0,3	0,3	0,0	0,0	0,0	0,0	324

208	1263	B	22	4	141	229,8	268,13	10,9	81,1	4,9	2,1	0,0	0,0	1,0	0,0	0,0	0,0	367
208	1263	B	22	5	21	230,1	268,43	5,9	71,3	21,9	0,0	0,0	0,7	0,2	0,0	0,0	0,0	269
208	1263	B	22	5	51	230,4	268,73	6,8	62,8	29,0	0,6	0,0	0,0	0,8	0,0	0,0	0,0	356
208	1263	B	22	5	81	230,7	269,03	13,3	59,7	23,5	2,6	0,0	0,0	0,3	0,3	0,3	0,0	322
208	1263	B	22	5	111	231	269,33	4,5	88,1	2,4	1,2	0,0	2,1	1,2	0,6	0,0	0,0	335
208	1263	B	22	5	141	231,3	269,63	16,3	58,6	23,6	0,0	0,3	1,2	0,0	0,0	0,0	0,0	331
208	1263	B	22	6	71	232,1	270,43	15,3	54,0	27,7	0,6	0,6	1,8	0,0	0,0	0,0	0,0	332
208	1263	B	22	7	21	233,1	271,43	14,2	58,6	25,4	0,0	0,9	0,9	0,0	0,0	0,0	0,0	338
208	1263	B	23	1	41	233,8	274,258	10,3	65,0	19,3	4,7	0,5	0,2	0,0	0,0	0,0	0,0	380
208	1263	B	23	1	91	234,3	274,814	10,1	76,6	12,7	0,0	0,3	0,0	0,3	0,0	0,0	0,0	316
208	1263	B	23	1	141	234,8	275,227	11,7	81,1	3,3	0,0	1,3	1,6	0,3	0,7	0,0	0,0	307
208	1263	B	23	2	41	235,3	275,639	12,7	60,3	16,3	0,0	2,3	2,2	6,2	0,0	0,0	0,0	345
208	1263	B	23	3	41	236,8	277,124	12,7	42,8	36,7	0,0	7,3	0,0	0,5	0,0	0,0	0,0	392
208	1263	B	23	3	91	237,3	277,643	11,7	59,1	24,4	0,0	3,0	1,2	0,6	0,0	0,0	0,0	332
208	1263	B	23	3	141	237,8	278,129	25,6	36,6	24,2	0,0	12,9	0,0	0,7	0,0	0,0	0,0	281
208	1263	B	23	4	91	238,8	279,064	25,6	41,0	18,8	0,0	14,0	0,6	0,0	0,0	0,0	0,0	320
208	1263	B	23	4	141	239,3	279,616	18,1	52,6	22,0	0,0	6,3	0,7	0,3	0,0	0,0	0,0	325
208	1263	B	23	5	41	239,8	280,232	12,8	79,1	3,5	0,0	4,4	0,0	0,0	0,3	0,0	0,0	344
208	1263	B	23	5	91	240,3	280,772	19,6	71,7	3,4	0,0	3,7	0,6	0,3	0,6	0,0	0,0	322
208	1263	B	23	6	1	240,9	281,380	29,1	45,3	16,3	0,0	7,5	1,2	0,6	0,7	0,0	0,0	319
208	1263	B	23	6	101	241,9	282,375	26,8	41,4	22,5	0,0	9,0	0,0	0,0	0,3	0,0	0,0	328
208	1263	B	23	7	51	242,9	283,272	29,2	51,8	12,5	0,0	5,1	1,2	0,3	0,0	0,0	0,0	336
208	1263	B	24	1	1	242,9	285,147	21,7	49,3	18,5	0,0	10,5	0,0	0,0	0,0	0,0	0,0	286
208	1263	B	24	1	51	243,4	285,689	21,1	40,1	18,8	0,0	20,0	0,0	0,0	0,0	0,0	0,0	325
208	1263	B	24	2	1	244,4	286,778	16,9	46,2	22,3	0,0	12,0	0,0	0,6	2,0	0,0	0,0	302
208	1263	B	24	2	51	244,9	287,309	23,9	54,7	8,4	0,0	12,4	0,3	0,0	0,3	0,0	0,0	322
208	1263	B	24	2	101	245,4	287,760	27,1	59,7	5,8	0,0	5,8	1,2	0,0	0,6	0,0	0,0	347
208	1263	B	24	3	51	246,4	288,69	17,1	43,0	24,5	0,0	15,4	0,0	0,0	0,0	0,0	0,0	345
208	1263	B	24	3	101,5	246,9	289,19	21,0	40,0	16,0	0,0	15,0	0,3	7,2	0,5	0,0	0,0	345
208	1263	B	24	5	51	249,4	291,69	25,3	38,5	19,1	0,0	17,1	0,0	0,0	0,0	0,0	0,0	391
208	1263	B	24	5	101	249,9	292,19	42,2	37,1	7,9	0,0	11,2	0,9	0,0	0,6	0,0	0,0	329
208	1263	B	24	6	11	250,5	292,79	10,6	76,8	4,4	0,0	7,9	0,0	0,3	0,0	0,0	0,0	340
208	1263	B	24	6	61	251	293,219	12,0	69,1	12,9	0,0	5,4	0,6	0,0	0,0	0,0	0,0	333
208	1263	B	24	6	111	251,5	293,649	10,3	67,0	10,0	0,0	12,7	0,0	0,0	0,0	0,0	0,0	300
208	1263	B	24	7	11	252	294,052	6,5	69,8	7,6	0,0	15,5	0,0	0,6	0,0	0,0	0,0	341
208	1263	B	24	cc	1	252,51	294,479	25,8	55,8	5,2	0,0	11,3	0,9	0,3	0,6	0,0	0,0	326
208	1263	B	25	1	31	252,7	295,808	39,0	39,0	13,3	0,0	7,3	1,2	0,3	0,0	0,0	0,0	331
208	1263	B	25	1	81	253,2	296,325	31,8	42,6	17,4	0,0	5,5	1,7	1,0	0,0	0,0	0,0	289
208	1263	B	25	2	21	254,1	297,168	34,9	37,0	17,0	0,0	7,8	0,0	3,3	0,0	0,0	0,0	336

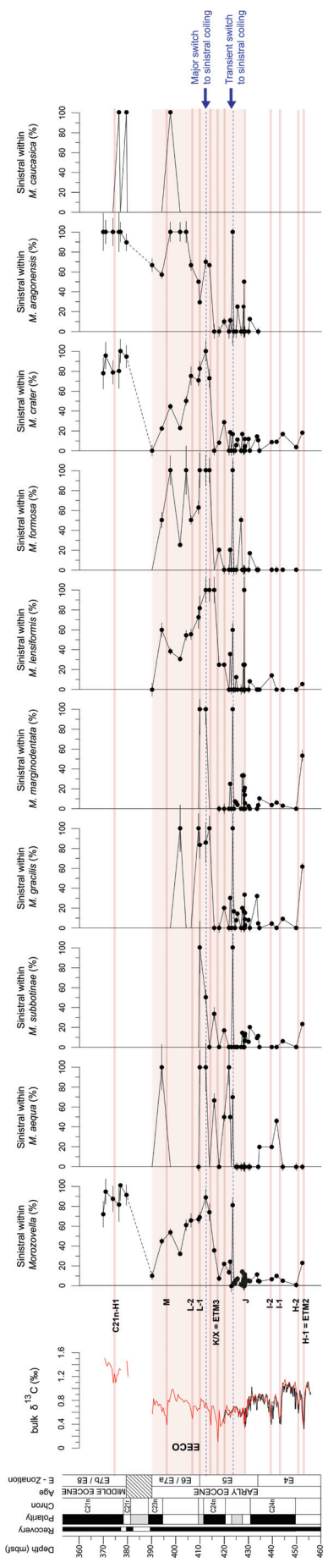

Figure S1. Changes in coiling direction within the Morozovella species (≥63 µm size fraction) at Atlantic Site 1051 across the EECO interval and the earlier middle Eocene. Error bars for coiling data coincide with ±1σ. Stable isotope data is from Chapter IV. Bio-magnetostratigraphy is from Luciani et al. (2016). Note the marked but transitory flip from dominant dextral to dominant sinistral coiling of all the Morozovella species slightly above the J event and the major long-lasted switch slightly above the K/X event. Below the EECO interval the dextral coiling is prevailing in morozovellids with moderate increases of sinistral morphotypes during some of the pre-EECO hyperthermals.

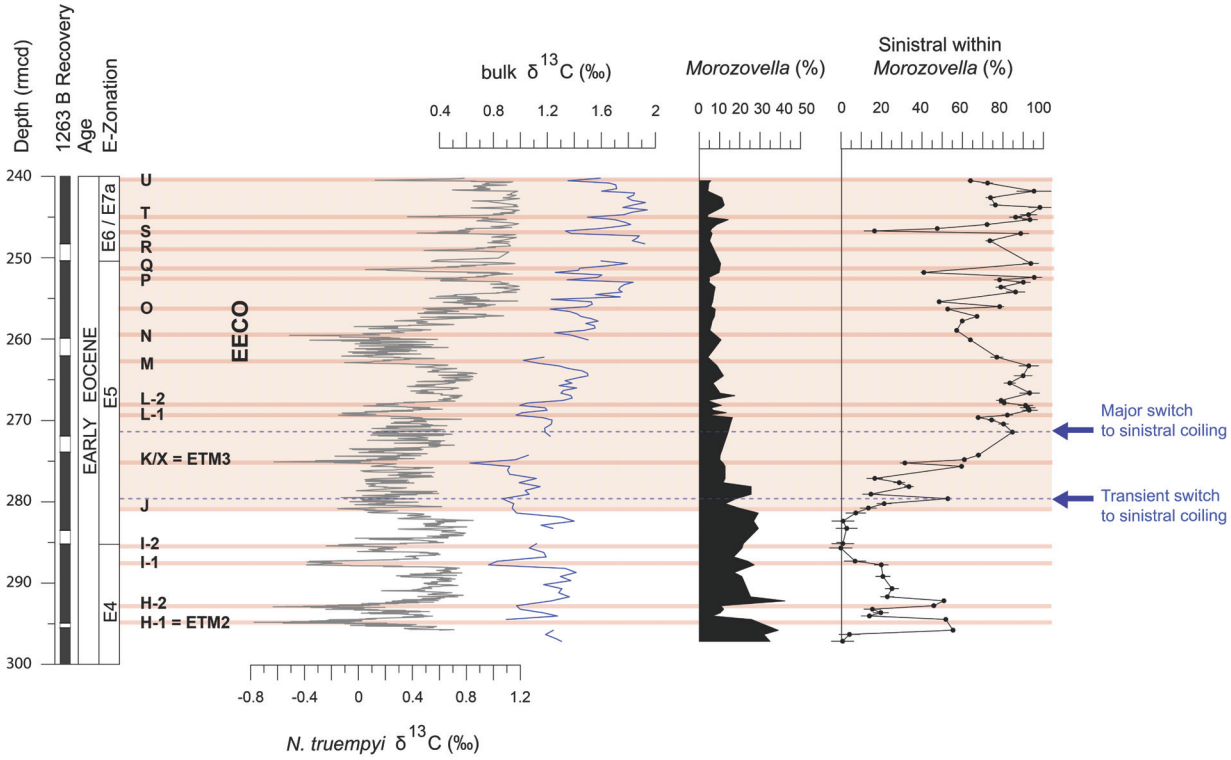

Figure S2. Early Eocene changes in coiling direction within the *Morozovella* genus (≥63 µm size fraction) at the ODP Site 1263 plotted against the benthic foraminifera *Nuttallides truempyi* (Lauretano et al., 2016) and bulk $\delta^{13}C$ (Chapter V) records. Error bars for coiling data coincide with ±1σ. The missing data in the bulk $\delta^{13}C$ curve correspond to unrecovered intervals. The thin light-red bands highlight the main carbon isotope excursions (CIEs) interpreted and labelled according to Lauretano et al. (2016). We consider the onset of the EECO as coinciding with the J event, in agreement to Luciani et al. (2016). The relative *Morozovella* abundance is also shown (data from Chapter V). Note the consistent drop in abundance of morozovellids occurring in the interval between the J and K/X events. Note also the marked but transitory flip from dominant dextral to dominant sinistral coiling of the *Morozovella* genus slightly above the J event and the remarkable change from dominant dextral to dominant sinistral coiling above the K/X event. Below the EECO interval the dextral coiling is prevailing in morozovellids with moderate increases of sinistral morphotypes during some of the pre-EECO hyperthermals.

Table S1. Dextral and sinistral (%) morphotypes of *Morozovella* species at Site 1051A.

M. caucasica Sinistral (%)	0,0	0,0	0,0	100,0	0,0	100,0	0,0	0,0	0,0	0,0	100,0	0,0	0,0	0,0	0,0	0,0	0,0	0,0	0,0	0,0	0,0	0,0	0,0	0,0
M. caucasica Dextral (%)	0,0	0,0	0,0	0,0	0,0	0,0	0,0	0,0	0,0	0,0	0,0	0,0	0,0	0,0	0,0	0,0	0,0	0,0	0,0	0,0	0,0	0,0	0,0	0,0
M. aragonensis Sinistral (%)	100,0	100,0	100,0	100,0	100,0	100,0	89,5	66,7	57,1	100,0	100,0	100,0	100,0	66,7	50,0	29,4	70,0	66,7	0,0	0,0	0,0	0,0	0,0	0,0
M. aragonensis Dextral (%)	0,0	0,0	0,0	0,0	0,0	0,0	10,5	33,3	42,9	0,0	0,0	0,0	0,0	33,3	50,0	70,6	30,0	33,3	100,0	100,0	100,0	100,0	100,0	100,0
M. crater Sinistral (%)	77,8	95,5	78,6	80,0	100,0	94,4	0,0	22,2	44,4	22,7	50,0	75,0	70,6	82,4	100,0	72,7	0,0	8,0	0,0	0,0	0,0	0,0	0,0	0,0
M. crater Dextral (%)	22,2	4,5	21,4	20,0	0,0	5,6	100,0	77,8	55,6	77,3	50,0	25,0	29,4	17,6	0,0	27,3	100,0	92,0	100,0	100,0	100,0	100,0	100,0	100,0
M. formosa Sinistral (%)	0,0	0,0	0,0	0,0	0,0	0,0	0,0	50,0	100,0	25,0	100,0	50,0	62,5	100,0	100,0	100,0	100,0	20,0	0,0	0,0	0,0	0,0	0,0	0,0
M. formosa Dextral (%)	0,0	0,0	0,0	0,0	0,0	0,0	0,0	50,0	0,0	75,0	0,0	50,0	37,5	0,0	0,0	0,0	0,0	80,0	0,0	0,0	0,0	0,0	0,0	0,0
M. lensiformis Sinistral (%)	0,0	0,0	0,0	0,0	0,0	0,0	0,0	60,0	38,5	30,8	54,5	55,6	72,7	81,8	100,0	100,0	100,0	25,0	100,0	100,0	100,0	100,0	100,0	100,0
M. lensiformis Dextral (%)	0,0	0,0	0,0	0,0	0,0	0,0	100,0	40,0	61,5	69,2	45,5	44,4	27,3	18,2	0,0	0,0	0,0	75,0	0,0	0,0	0,0	0,0	0,0	0,0
M. marginodentata Sinistral (%)	0,0	0,0	0,0	0,0	0,0	0,0	0,0	0,0	0,0	0,0	0,0	0,0	0,0	100,0	100,0	100,0	0,0	0,0	0,0	0,0	0,0	0,0	0,0	0,0
M. marginodentata Dextral (%)	0,0	0,0	0,0	0,0	0,0	0,0	0,0	0,0	0,0	0,0	0,0	0,0	0,0	0,0	0,0	0,0	0,0	100,0	0,0	0,0	0,0	0,0	0,0	0,0
M. gracilis Sinistral (%)	0,0	0,0	0,0	0,0	0,0	0,0	0,0	0,0	0,0	100,0	0,0	0,0	100,0	83,3	85,7	100,0	0,0	0,0	0,0	0,0	0,0	0,0	0,0	0,0
M. gracilis Dextral (%)	0,0	0,0	0,0	0,0	0,0	0,0	0,0	0,0	0,0	0,0	0,0	0,0	0,0	16,7	14,3	0,0	100,0	100,0	100,0	100,0	100,0	100,0	100,0	100,0
M. subbotinae Sinistral (%)	0,0	0,0	0,0	0,0	0,0	0,0	0,0	0,0	0,0	0,0	0,0	0,0	0,0	100,0	50,0	0,0	0,0	0,0	33,3	0,0	0,0	0,0	0,0	0,0
M. subbotinae Dextral (%)	0,0	0,0	0,0	0,0	0,0	0,0	0,0	0,0	0,0	0,0	0,0	0,0	0,0	0,0	50,0	100,0	66,7	100,0	66,7	33,3	0,0	0,0	0,0	0,0
M.aequa Sinistral (%)	0,0	0,0	0,0	0,0	0,0	0,0	0,0	100,0	0,0	0,0	0,0	0,0	0,0	100,0	100,0	0,0	66,7	0,0	0,0	0,0	0,0	0,0	0,0	0,0
M.aequa Dextral (%)	0,0	0,0	0,0	0,0	0,0	0,0	0,0	0,0	0,0	0,0	0,0	0,0	100,0	0,0	0,0	0,0	33,3	0,0	0,0	0,0	0,0	0,0	0,0	0,0
Morozovella Sinistral (%)	72,0	93,6	86,4	81,7	100,0	92,0	10,2	47,0	53,8	33,3	62,2	65,3	66,5	69,7	89,9	74,1	35,7	7,5	0,0	0,0	0,0	0,0	0,0	0,0
Morozovella Dextral (%)	28,0	6,4	13,6	18,3	0,0	8,0	89,8	53,0	46,2	66,7	37,8	34,7	33,5	30,3	10,1	25,9	64,3	92,5	0,0	0,0	0,0	0,0	0,0	0,0
Morozovella (%)	3	7,4	5,5	2,6	11	9,8	5	6,2	9,8	11	8,5	7,1	18	15	12	13	8,5	14	0,0	0,0	0,0	0,0	0,0	0,0
No. *Morozovella*	11	27	21	10	40	37	20	24	39	43	34	29	72	59	49	27	28	53	0,0	0,0	0,0	0,0	0,0	0,0
No. counted specimens	335	311	303	314	338	301	219	211	385	285	295	336	310	315	332	290	327	375	0,0	0,0	0,0	0,0	0,0	0,0
Sample depth (mbsf)	369,9	370,9	373,9	376,4	377	379,5	390,1	394,1	397,65	401,68	404,18	406,18	409,3	409,8	412,3	413,8	415,78	417,8	0,0	0,0	0,0	0,0	0,0	0,0
cm ±1	21	121	121	71	21	21	21	121	26	69	19	69	21	71	21	21	69	121	0,0	0,0	0,0	0,0	0,0	0,0
Section	1	1	3	5	cc	1	1	3	6	2	4	5	1	1	3	4	5	6	0,0	0,0	0,0	0,0	0,0	0,0
Core	40	40	40	40	40	41	42	42	42	43	43	43	44	44	44	44	44	44	0,0	0,0	0,0	0,0	0,0	0,0
Hole	1051A	1051A	1051A	1051A	1051A	1051A	1051A	1051A	1051A	1051A	1051A	1051A	1051A	1051A	1051A	1051A	1051A	1051A	0,0	0,0	0,0	0,0	0,0	0,0

Hole	Core	Section	cm ±1	Sample depth (mbsf)	No. counted specimens	No. *Morozovella*	*Morozovella* (%)	*Morozovella* Dextral (%)	*Morozovella* Sinistral (%)	*M.aequa* Dextral (%)	*M.aequa* Sinistral (%)	*M. subbotinae* Dextral (%)	*M. subbotinae* Sinistral (%)	*M. gracilis* Dextral (%)	*M. gracilis* Sinistral (%)	*M. marginodentata* Dextral (%)	*M. marginodentata* Sinistral (%)	*M. lensiformis* Dextral (%)	*M. lensiformis* Sinistral (%)	*M. formosa* Dextral (%)	*M. formosa* Sinistral (%)	*M. crater* Dextral (%)	*M. crater* Sinistral (%)	*M. aragonensis* Dextral (%)	*M. aragonensis* Sinistral (%)	*M. caucasica* Dextral (%)	*M. caucasica* Sinistral (%)
1051A	45	1	121	419,9	371	63	17	77,8	22,2	50,0	50,0	83,3	16,7	80,0	20,0	100,0	0,0	75,0	25,0	100,0	0,0	71,4	28,6	90,0	10,0	0,0	0,0
1051A	45	3	21	421,9	389	29	7,8	86,2	13,8	100,0	0,0	100,0	0,0	100,0	0,0	100,0	0,0	100,0	0,0	100,0	0,0	100,0	0,0	100,0	0,0	0,0	0,0
1051A	45	3	71	422,40	352	78	22	75,6	24,4	50,0	50,0	0,0	100,0	70,0	30,0	75,0	25,0	64,3	35,7	80,0	20,0	81,5	18,5	88,9	11,1	0,0	0,0
1051A	45	3	121	422,90	186	22	12	100,0	0,0	0,0	0,0	100,0	0,0	100,0	0,0	100,0	0,0	100,0	0,0	100,0	0,0	100,0	0,0	0,0	0,0	0,0	0,0
1051A	45	4	23	423,42	350	53	15	18,9	81,1	70,0	30,0	0,0	100,0	0,0	100,0	0,0	100,0	60,0	40,0	0,0	100,0	83,3	16,7	0,0	100,0	0,0	0,0
1051A	45	4	69	423,88	349	34	9,7	97,1	2,9	0,0	0,0	100,0	0,0	83,3	16,7	100,0	0,0	0,0	100,0	100,0	0,0	100,0	0,0	100,0	0,0	0,0	0,0
1051A	45	4	121	424,4	330	69	21	97,1	2,9	0,0	0,0	100,0	0,0	100,0	0,0	92,6	7,4	100,0	0,0	0,0	100,0	100,0	0,0	100,0	0,0	0,0	0,0
1051A	45	5	19	424,88	343	67	20	94,0	6,0	100,0	0,0	100,0	0,0	92,3	7,7	93,8	6,3	87,5	12,5	100,0	0,0	94,4	5,6	100,0	0,0	0,0	0,0
1051A	45	5	71	425,4	307	55	18	92,7	7,3	100,0	0,0	100,0	0,0	85,7	14,3	96,0	4,0	100,0	0,0	0,0	0,0	88,9	11,1	75,0	25,0	0,0	0,0
1051A	45	6	72	426,9	333	65	20	98,5	1,5	100,0	0,0	100,0	0,0	100,0	0,0	100,0	0,0	100,0	0,0	50,0	50,0	100,0	0,0	100,0	0,0	0,0	0,0
1051A	45	6	121	427,4	263	35	13	85,7	14,3	100,0	0,0	100,0	0,0	80,0	20,0	66,7	33,3	100,0	0,0	100,0	0,0	83,3	16,7	0,0	0,0	0,0	0,0
1051A	45	7	22	427,91	250	37	15	94,6	5,4	100,0	0,0	100,0	0,0	100,0	0,0	100,0	0,0	100,0	25,0	100,0	0,0	100,0	0,0	75,0	25,0	0,0	0,0
1051A	45	7	30	427,99	331	51	15	96,1	3,9	0,0	0,0	100,0	0,0	83,3	16,7	66,7	33,3	100,0	0,0	100,0	0,0	100,0	0,0	100,0	0,0	0,0	0,0
1051A	45	7	37	428,06	347	39	11	100,0	0,0	100,0	0,0	100,0	0,0	100,0	0,0	100,0	0,0	100,0	0,0	100,0	0,0	100,0	0,0	100,0	0,0	0,0	0,0
1051A	45	7	39	428,08	342	50	15	98,0	2,0	100,0	0,0	100,0	0,0	100,0	0,0	100,0	0,0	100,0	0,0	100,0	0,0	100,0	0,0	100,0	0,0	0,0	0,0
1051A	45	7	46	428,15	348	54	16	92,6	7,4	100,0	0,0	87,5	12,5	100,0	0,0	81,8	18,2	100,0	0,0	0,0	0,0	100,0	0,0	50,0	50,0	0,0	0,0
1051A	45	8	3,5	428,19	384	64	17	98,4	1,6	0,0	0,0	100,0	0,0	100,0	0,0	100,0	0,0	0,0	100,0	100,0	0,0	100,0	0,0	100,0	0,0	0,0	0,0
1051A	45	8	8,5	428,24	359	45	13	100,0	0,0	100,0	0,0	100,0	0,0	100,0	0,0	100,0	0,0	100,0	0,0	100,0	0,0	100,0	0,0	100,0	0,0	0,0	0,0

Hole	Core	Section	cm ±1	Sample depth (mbsf)	No. counted specimens	No. *Morozovella*	*Morozovella* (%)	*Morozovella* Dextral (%)	*Morozovella* Sinistral (%)	*M.aequa* Dextral (%)	*M.aequa* Sinistral (%)	*M. subbotinae* Dextral (%)	*M. subbotinae* Sinistral (%)	*M. gracilis* Dextral (%)	*M. gracilis* Sinistral (%)	*M. marginodentata* Dextral (%)	*M. marginodentata* Sinistral (%)	*M. lensiformis* Dextral (%)	*M. lensiformis* Sinistral (%)	*M. formosa* Dextral (%)	*M. formosa* Sinistral (%)	*M. crater* Dextral (%)	*M. crater* Sinistral (%)	*M. aragonensis* Dextral (%)	*M. aragonensis* Sinistral (%)	*M. caucasica* Dextral (%)	*M. caucasica* Sinistral (%)
1051A	46	1	5	428,34	325	95	29	88,4	11,6	100,0	0,0	94,1	5,9	66,7	33,3	86,0	14,0	75,0	25,0	100,0	0,0	100,0	0,0	100,0	0,0	0,0	0,0
1051A	46	1	11	428,4	340	95	28	88,4	11,6	100,0	0,0	88,9	11,1	100,0	0,0	79,1	20,9	100,0	0,0	100,0	0,0	96,2	3,8	100,0	0,0	0,0	0,0
1051A	46	1	19	428,44	329	113	34	91,2	8,8	100,0	0,0	93,8	6,3	91,3	8,7	86,1	13,9	100,0	0,0	100,0	0,0	88,2	11,8	100,0	0,0	0,0	0,0
1051A	46	1	15	428,48	336	124	37	92,7	7,3	100,0	0,0	93,3	6,7	84,8	15,2	94,4	5,6	100,0	0,0	100,0	0,0	95,5	4,5	100,0	0,0	0,0	0,0
1051A	46	1	21	428,5	245	111	54	97,3	2,7	0,0	0,0	86,7	13,3	97,3	2,7	100,0	0,0	100,0	0,0	100,0	0,0	100,0	0,0	100,0	0,0	0,0	0,0
1051A	46	2	21	430	315	130	54	94,6	5,4	100,0	0,0	94,7	5,3	92,1	7,9	97,2	2,8	100,0	0,0	100,0	0,0	100,0	0,0	100,0	0,0	0,0	0,0
1051A	46	2	71	430,5	242	101	42	95,0	5,0	100,0	0,0	80,0	20,0	100,0	0,0	100,0	0,0	91,7	8,3	83,3	16,7	100,0	0,0	87,5	12,5	0,0	0,0
1051A	46	4	71	433,5	248	95	38	88,4	11,6	0,0	0,0	90,9	9,1	68,0	32,0	100,0	0,0	100,0	0,0	0,0	0,0	85,7	14,3	0,0	0,0	0,0	0,0
1051A	46	4	119	433,98	247	98	43	94,9	5,1	100,0	0,0	88,9	11,1	95,5	4,5	96,4	3,6	100,0	0,0	100,0	0,0	89,5	10,5	100,0	0,0	0,0	0,0
1051A	46	5	19	434,48	223	85	39	95,3	4,7	80,0	20,0	100,0	0,0	100,0	0,0	89,7	10,3	100,0	0,0	100,0	0,0	100,0	0,0	0,0	0,0	0,0	0,0
1051A	47	2	19	439,57	293	132	45	93,2	6,8	80,0	20,0	100,0	0,0	95,7	4,3	96,3	3,7	85,7	14,3	100,0	0,0	91,4	8,6	0,0	0,0	0,0	0,0
1051A	47	3	69	441,58	282	118	42	89,8	10,2	53,8	46,2	100,0	0,0	100,0	0,0	93,8	6,3	100,0	0,0	100,0	0,0	91,1	8,9	0,0	0,0	0,0	0,0
1051A	47	5	24	444,13	341	132	39	94,7	5,3	100,0	0,0	94,1	5,9	90,9	9,1	96,9	3,1	100,0	0,0	100,0	0,0	83,3	16,7	0,0	0,0	0,0	0,0
1051A	48	2	70	449,69	322	101	31	99,0	1,0	100,0	0,0	100,0	0,0	100,0	0,0	100,0	0,0	100,0	0,0	100,0	0,0	96,4	3,6	0,0	0,0	0,0	0,0
1051A	48	4	25	452,24	259	138	46	76,8	23,2	100,0	0,0	76,9	23,1	38,5	61,5	46,7	53,3	94,4	5,6	0,0	0,0	82,0	18,0	0,0	0,0	0,0	0,0

Table S2. Dextral and sinistral (%) morphotypes of *Morozovella* at Site 1263B.

Leg	Site	Hole	Core	Section	Interval (cm ±1)	Sample Depth (mbsf)	Revised Composite Depth (rmcd)	*Morozovella* (%)	No. Total counted specimens	No. Total counted *Morozovella*	Dextral *Morozovella* (%)	Sinistral *Morozovella* (%)
208	1263	B	20	2	42	206,81	240,52	5,7	336	39	35,90	64,10
208	1263	B	20	2	72	207,1	240,81	4,7	342	–	27,50	72,50
208	1263	B	20	3	12	208,01	241,81	4,2	331	22	4,55	95,45
208	1263	B	20	3	101	208,9	242,61	11,1	333	–	26,00	74,00
208	1263	B	20	4	41	209,8	243,51	12,3	397	–	23,60	76,40
208	1263	B	20	4	71	210,1	243,81	11,2	456	–	1,60	98,40
208	1263	B	20	5	11	211	244,71	4,2	356	83	7,23	92,77
208	1263	B	20	5	41	211,3	245,01	3,9	384	103	13,59	86,41
208	1263	B	20	5	71	211,6	245,31	14,3	322	107	6,54	93,46
208	1263	B	20	5	131	212,2	245,91	8,6	381	101	27,72	72,28
208	1263	B	20	6	31	212,7	246,41	6,1	314	107	52,34	47,66
208	1263	B	20	6	61	213	246,71	5,4	296	60	83,33	16,67
208	1263	B	20	6	92	213,31	247,02	6,3	274	–	11,10	88,90
208	1263	B	20	7	31	214,2	247,91	5,1	313	76	26,32	73,68
208	1263	B	21	1	31	214,7	250,7106	10,5	337	–	6,10	93,90
208	1263	B	21	1	149	215,88	251,8117	9,8	347	117	58,97	41,03
208	1263	B	21	2	61	216,5	252,42	4,8	335	113	4,42	95,58
208	1263	B	21	2	91	216,8	252,72	5,1	334	79	21,52	78,48
208	1263	B	21	2	122	217,1	253,02	4,7	361	102	9,80	90,20
208	1263	B	21	3	31	217,7	253,62	7,8	306	91	20,88	79,12
208	1263	B	21	3	91	218,3	254,22	7,3	355	44	13,64	86,36
208	1263	B	21	4	61	219,5	255,42	6,5	367	109	51,38	48,62
208	1263	B	21	4	121	220,1	256,02	5,7	335	121	21,49	78,51
208	1263	B	21	5	1	220,4	256,32	7,9	394	106	47,17	52,83
208	1263	B	21	5	91	221,3	257,22	7,4	309	110	32,73	67,27
208	1263	B	21	6	1	221,9	257,7966	6,3	381	100	40,00	60,00
208	1263	B	21	6	121	223,1	258,9458	5,2	343	124	42,74	57,26
208	1263	B	21	cc	16	224,3	260,106	10,7	307	114	35,96	64,04
208	1263	B	22	1	21	224,1	262,2402	4,2	308	48	22,92	77,08
208	1263	B	22	1	111	225	263,3075	8,8	363	–	7,10	92,90
208	1263	B	22	2	81	226,2	264,53	11,9	285	–	9,90	90,10
208	1263	B	22	3	21	227,1	265,43	6,7	326	97	16,49	83,51
208	1263	B	22	3	141	228,3	266,63	10,2	296	–	6,70	93,30
208	1263	B	22	4	21	228,6	266,93	17,5	–	–	–	–
208	1263	B	22	4	81	229,2	267,53	4,2	334	101	20,79	79,21
208	1263	B	22	4	111	229,5	267,83	7,4	324	109	19,27	80,73
208	1263	B	22	4	141	229,8	268,13	10,9	367	–	8,70	91,30
208	1263	B	22	5	21	230,1	268,43	5,9	269	–	7,60	92,40
208	1263	B	22	5	51	230,4	268,73	6,8	356	–	6,90	93,10
208	1263	B	22	5	81	230,7	269,03	13,3	322	–	–	–

208	1263	B	22	5	111	231	269,33	4,5	335	96	17,71	82,29
208	1263	B	22	5	141	231,3	269,63	16,3	331	109	32,11	67,89
208	1263	B	22	6	21	231,6	269,93	–	–	106	25,47	74,53
208	1263	B	22	6	71	232,1	270,43	15,3	332	102	19,61	80,39
208	1263	B	22	7	21	233,1	271,43	14,2	338	112	15,18	84,82
208	1263	B	23	1	41	233,8	274,2581	10,3	380	–	32,00	68,00
208	1263	B	23	1	91	234,3	274,8139	10,1	316	113	38,94	61,06
208	1263	B	23	1	141	234,8	275,2266	11,7	307	120	68,33	31,67
208	1263	B	23	2	41	235,3	275,6392	12,7	345	–	40,30	59,70
208	1263	B	23	3	41	236,8	277,1236	12,7	392	–	83,20	16,80
208	1263	B	23	3	91	237,3	277,6433	11,7	332	–	71,10	28,90
208	1263	B	23	3	141	237,8	278,1287	25,6	281	–	66,30	33,70
208	1263	B	23	4	91	238,8	279,0642	25,6	320	–	85,10	14,90
208	1263	B	23	4	141	239,3	279,6163	18,1	325	–	47,10	52,90
208	1263	B	23	5	41	239,8	280,2316	12,8	344	98	78,57	21,43
208	1263	B	23	5	91	240,3	280,7719	19,6	322	110	86,36	13,64
208	1263	B	23	6	1	240,9	281,38	29,1	319	–	92,60	7,40
208	1263	B	23	6	101	241,9	282,3747	26,8	328	–	98,90	1,10
208	1263	B	23	7	51	242,9	283,2724	29,2	336	103	97,09	2,91
208	1263	B	24	1	1	242,9	285,1474	21,7	286	–	99,00	1,00
208	1263	B	24	1	51	243,4	285,6894	21,1	325	–	100,00	0,00
208	1263	B	24	2	51	244,9	287,3093	23,9	322	85	92,94	7,06
208	1263	B	24	2	101	245,4	287,76	27,1	347	110	80,00	20,00
208	1263	B	24	3	102	246,9	289,19	21,0	345	–	79,20	20,80
208	1263	B	24	3	51	246,4	288,69	17,1	345	–	–	–
208	1263	B	24	4	101	248,4	290,69	–	–	87	74,71	25,29
208	1263	B	24	5	51	249,4	291,69	25,3	391	0	77,00	23,00
208	1263	B	24	5	101	249,9	292,19	42,2	329	106	49,06	50,94
208	1263	B	24	6	11	250,5	292,79	10,6	340	74	54,05	45,95
208	1263	B	24	6	61	251	293,2192	12,0	333	96	84,38	15,63
208	1263	B	24	6	111	251,5	293,6493	10,3	300	91	80,22	19,78
208	1263	B	24	7	11	252	294,0519	6,5	341	106	85,85	14,15
208	1263	B	24	cc	1	252,51	294,4792	25,8	326	106	48,11	51,89
208	1263	B	25	1	31	252,7	295,8083	39,0	331	110	44,55	55,45
208	1263	B	25	1	81	253,2	296,3246	31,8	289	–	95,70	4,30
208	1263	B	25	2	20	254,1	297,1678	34,9	336	–	99,10	0,90

Acknowledgements

My first and deepest thanks go to my supervisor Valeria Luciani who gave me the opportunity to work on this project and its intriguing topic. Thanks for believing in me, for your tireless guidance, for the scientific and human support and encouragement. I must also to thank you for never turned off the phone including during the days-off, for the last minute revisions and for always finding time to read my drafts putting aside other commitments. Most of the lessons I've learned from you will be a precious luggage to bring with me in the years to come.

Special thanks go to my co-supervisors Jerry Dickens and Bridget Wade. Jerry, thanks for your valuable suggestions and very meticulous revisions, for the continuous improvements you've made to this work, thanks for the teachings on the best approach to adopt with the ODP materials and, above all, thank you for have providing an outside perspective from micropaleontology so that things have not been given for granted and are much better integrated. As Italians really like to say, I can confidently affirm that this would be "not possible" without you!! Many thanks also to Bridget for her kind, helpful and constructive comments and for the discussion about the paleotemperature proxies.

Sincere thanks to the referee, Paul Pearson and Kirsty Edgar, who were fair and constructive with their comments and suggestions.

I'd like to thanks all the Padua group with whom I shared the joys and the pains of the almost endless Terche paper and the stable isotopes analysis: thanks to Luca Giusberti for the several sampling fields, to Eliana Fornaciari for the interesting conversation on calcareous nannofossils and their ecological preferences, thanks to Flavia Boscolo Galazzo that very patiently made proofreading in order to shorten the Terche text and to Claudia Agnini always available to dedicate her time in helping me with my stable isotope analysis. Thanks to Thomas Westerhold and Edoardo Dallanave for their precious contribute to the Terche paper.

I'm sincerely grateful for the opportunity that Appy Sluijs and the Pal/Pal group of the Utrecht University gave to me in trying to get TEX_{86} paleotemperatures from the basal EECO although they did not work so well at Site 1051. Thanks to Peter Bijl who teaching me all the laboratory techniques behind the TEX_{86} method, to Francien Peterse and Tjerk Veenstra that helped me in reading the MS data, thanks to Dimitra and Marjolein for their help with the laboratory stuff and instruments, to Margot Cramwinckel for the samples, to Francesca Sangiorgi as my Italian support and all the other components of the 5^{th} floor that makes me feel like part of this big family for the time of my stay. Thanks also to Stefanie, my smoker foram friend that I was so happy to meet again in Utrecht.

Special thanks go to all the geopeople I was lucky to meet and with whom I'd got the pleasure to share amazing experiences in the years. Thanks to Michele Morsilli and Piero Gianolla for the stimulating discussions and for constantly conveying to me enthusiasm and passion for the geoscience helping me in keeping fight during some hard times. Immeasurable thanks go to Gloria Ciarapica and Leonsevero Passeri who firstly inspired me to embark on the road of the research...Gloria your absence will be an unspeakable gap.

Thanks to all my Ferrara colleagues since survive to a PhD could be impossible without a great group of supporter. I'd like to thanks all the KazzenGeo, the Geoebeti in Carriera, the Geologatte and the yellow floor components, especially my old bachelor friend Bea, for the coffee breaks, the laughter and the divagation that makes easier get to the end of this journey.

Thanks to my special friend Marica that was not only a flatmates but mainly a great confidant and adviser with whom I shared science, PhD frustration, food, good beer, and TV series.

One of the things I'm most grateful of is to have had the opportunity to participate to prestigious international summer schools, such as the USSP and the ISF in Urbino, that gave to me the chance to enrich myself as a scientist opening my scientific point of view and meeting Professors and PhDs from all over the world. I'm also thankful for the wonderful friendships born in those contexts such as the heterogeneous and wonderful Triple F Pride group.

Un immenso grazie alla mia famiglia che mi ha supportato nonostante le difficoltà e incoraggiato a perseguire i miei interessi. Grazie a mia madre che mi ha sempre stimolato al miglioramento e mi ha insegnato che per raggiungere obiettivi importanti bisogna dotarsi di impegno ma soprattutto tenacia, grazie a mio padre per avermi trasmesso quel senso di calma che spesso mi ha aiutato a rimanere lucida nei momenti di stress e grazie a mia sorella che inconsapevolmente mi ha spronato a fare del mio meglio per essere un buon esempio per lei. Grazie anche alla mia seconda famiglia perugina, a Giulia, Federica, Valentina, Elena, Alessia e le Michele che fin dai tempi dell'Università si sono sempre preoccupate di rendere divertente la mia vita da universitaria-dottoranda…perché di tanto in tanto bisogna creare uno stacco ludico tra una scadenza e l'altra. Grazie per le rimpatriate, le chiacchierate, le mangiate, le bevute, le serate e tutte le risate!

Un grazie di cuore va ai miei amici di sempre, specialmente alla mia migliore amica Giorgia, che mi è rimasta sempre vicina negli anni nonostante la distanza e gli impegni diventando una parte imprescindibile della mia vita, grazie per avermi sempre capita all'istante, per aver sempre creduto in me, per aver ascoltato con pazienza i miei interminabili sfoghi e per aver, a tratti, attenuato le paure di un futuro incerto con le tue parole.

Infine, grazie a te caro Max, che in questi anni mi hai amata nonostante i momenti di panico che sfioravano la follia, che sei stato tollerante quando nei fine settimana e nei periodi di vacanza dovevo rinchiudermi in casa a lavorare, grazie di cuore per aver compreso quanto tutto questo fosse importante per me e soprattutto grazie per i bei momenti insieme.